Gas Dynamics Laboratory
Department of Mechanical and
Industrial Engineering
University of Illinois at
Urbana-Champaign
Urbana, IL 61801

UILU-ENG 90-4001

Final Technical Report

FLUID DYNAMIC MECHANISMS AND INTERACTIONS WITHIN SEPARATED FLOWS

J. C. Dutton and A. L. Addy

February 1990

Supported by
U.S. Army Research Office
Research Contract DAAL03-87-K-0010
and the
Department of Mechanical and Industrial Engineering

UNCLASSIFIED MASTER COPY - FOR REPRODUCTION PURPOSES

SECURITY CLASSIFICATION OF THIS PAGE

REPORT DOCUMENTATION PAGE

1a. REPORT SECURITY CLASSIFICATION Unclassified	1b. RESTRICTIVE MARKINGS
2a. SECURITY CLASSIFICATION AUTHORITY	3. DISTRIBUTION/AVAILABILITY OF REPORT Approved for public release; distribution unlimited.
2b. DECLASSIFICATION/DOWNGRADING SCHEDULE	
4. PERFORMING ORGANIZATION REPORT NUMBER(S) UIUC ENG 90-4001	5. MONITORING ORGANIZATION REPORT NUMBER(S) ARO 24139.12-EG
6a. NAME OF PERFORMING ORGANIZATION Dept. of Mech. and Ind. Eng. University of Illinois at U-C 6b. OFFICE SYMBOL (If applicable) UIUC	7a. NAME OF MONITORING ORGANIZATION U. S. Army Research Office
6c. ADDRESS (City, State, and ZIP Code) 1206 West Green Street Urbana, Illinois 61801	7b. ADDRESS (City, State, and ZIP Code) P. O. Box 12211 Research Triangle Park, NC 27709-2211
8a. NAME OF FUNDING/SPONSORING ORGANIZATION U. S. Army Research Office 8b. OFFICE SYMBOL (If applicable)	9. PROCUREMENT INSTRUMENT IDENTIFICATION NUMBER DAAL03-87-K-0010
8c. ADDRESS (City, State, and ZIP Code) P. O. Box 12211 Research Triangle Park, NC 27709-2211	10. SOURCE OF FUNDING NUMBERS PROGRAM ELEMENT NO. / PROJECT NO. / TASK NO. / WORK UNIT ACCESSION NO

11. TITLE (Include Security Classification)
FLUID DYNAMIC MECHANISMS AND INTERACTIONS WITHIN SEPARATED FLOWS

12. PERSONAL AUTHOR(S) J. C. Dutton and A. L. Addy

13a. TYPE OF REPORT	13b. TIME COVERED	14. DATE OF REPORT (Year, Month, Day)	15. PAGE COUNT
Final Technical	FROM 1 Dec 86 TO 30 Nov 89	1990 February 15	154

16. SUPPLEMENTARY NOTATION The view, opinions and/or findings contained in this report are those of the author(s) and should not be construed as an official Department of the Army position, policy, or decision, unless so designated by other documentation.

17. COSATI CODES		
FIELD	GROUP	SUB-GROUP

18. SUBJECT TERMS (Continue on reverse if necessary and identify by block number)
separated flow, supersonic flow, laser Doppler velocimetry, base flow, transonic flow

19. ABSTRACT (Continue on reverse if necessary and identify by block number)

The significant results of a joint research effort investigating the fundamental fluid dynamic mechanisms and interactions within high-speed separated flows are presented in detail. The results have been obtained through analytical and numerical approaches, but with primary emphasis on experimental investigations of missile and projectile base flow-related configurations. The objectives of the research program focus on understanding the component mechanisms and interactions which establish and maintain high-speed separated flow regions.

The analytical and numerical efforts have centered on unsteady plume-wall interactions in rocket launch tubes and on predictions of the effects of base bleed on transonic and supersonic base flowfields. The experimental efforts have considered the development and use of a state-of-the-art two component laser Doppler velocimeter (LDV) system for experiments with planar, two-dimensional, small-scale models in supersonic flows. The LDV experiments have yielded high quality, well documented mean and turbulence velocity data for a variety of high-speed

20. DISTRIBUTION/AVAILABILITY OF ABSTRACT	21. ABSTRACT SECURITY CLASSIFICATION
☐ UNCLASSIFIED/UNLIMITED ☐ SAME AS RPT. ☐ DTIC USERS	Unclassified
22a. NAME OF RESPONSIBLE INDIVIDUAL	22b. TELEPHONE (Include Area Code) / 22c. OFFICE SYMBOL

DD FORM 1473, 84 MAR 83 APR edition may be used until exhausted. All other editions are obsolete.

SECURITY CLASSIFICATION OF THIS PAGE

separated flows including initial shear layer development, recompression/reattachment processes for two supersonic shear layers, oblique shock wave/turbulent boundary layer interactions in a compression corner, and two-stream, supersonic, near-wake flow behind a finite-thickness base. Other experimental studies have investigated the effects of sudden expansions and compressions on turbulent boundary layer integral properties, unsteady reattachment processes for supersonic back-step flow, and the effects of a base cavity on subsonic and transonic near-wake flowfields. The results of these various studies have been carefully documented in a series of journal articles, conference proceedings papers, and theses. The full text of the papers and thesis abstracts are included as appendices of this report.

Future efforts in this area will be conducted as a follow-on to the results of the research program reported herein. These experimental studies will focus on four major areas: two-stream supersonic, plume-induced separation, particle image velocimetry in high-speed flows, axisymmetric power-on and power-off base flows, and control of high-speed separated flows.

FLUID DYNAMIC MECHANISMS AND INTERACTIONS WITHIN SEPARATED FLOWS

Final Technical Report

by

J. C. Dutton*

A. L. Addy**

February 1990

Supported by

U.S. Army Research Office
Research Contract DAAL03-87-K-0010

and the

Department of Mechanical and Industrial Engineering
University of Illinois at Urbana-Champaign
Urbana, Illinois 61801

---

* Associate Professor of Mechanical Engineering

** Professor and Head of Mechanical Engineering

ABSTRACT

The significant results of a joint research effort investigating the fundamental fluid dynamic mechanisms and interactions within high-speed separated flows are presented in detail. The results have been obtained through analytical and numerical approaches, but with primary emphasis on experimental investigations of missile and projectile base flow-related configurations. The objectives of the research program focus on understanding the component mechanisms and interactions which establish and maintain high-speed separated flow regions.

The analytical and numerical efforts have centered on unsteady plume-wall interactions in rocket launch tubes and on predictions of the effects of base bleed on transonic and supersonic base flowfields. The experimental efforts have considered the development and use of a state-of-the-art two component laser Doppler velocimeter (LDV) system for experiments with planar, two-dimensional, small-scale models in supersonic flows. The LDV experiments have yielded high quality, well documented mean and turbulence velocity data for a variety of high-speed separated flows including initial shear layer development, recompression/reattachment processes for two supersonic shear layers, oblique shock wave/turbulent boundary layer interactions in a compression corner, and two-stream, supersonic, near-wake flow behind a finite-thickness base. Other experimental studies have investigated the effects of sudden expansions and compressions on turbulent boundary layer integral properties, unsteady reattachment processes for supersonic back-step flow, and the effects of a base cavity on subsonic and transonic near-wake flowfields. The results of these various studies have been carefully documented in a series of journal articles, conference proceedings papers, and theses. The full text of the papers and thesis abstracts are included as appendices of this report.

Future efforts in this area will be conducted as a follow-on to the results of the research program reported herein. These experimental studies will focus on four major areas: two-stream, supersonic, plume-induced separation, particle image velocimetry in high-speed flows, axisymmetric power-on and power-off base flows, and control of high-speed separated flows.

TABLE OF CONTENTS

I. INTRODUCTION

A. PROBLEM STATEMENT

An ongoing research effort has been funded by the U.S. Army Research Office to investigate the fundamental fluid dynamic mechanisms and interactions within high-speed separated flows with particular attention to the projectile and missile base flow problem. The overall effort has incorporated analytical, experimental, and computational investigations aimed at gaining a more insightful understanding of the fundamental fluid dynamic mechanisms existing in the near-wake flowfield. The investigations of separated flow problems have been focused on missile afterbody flows and more importantly on the interactions between the base and body flows.

Professors J. C. Dutton and A. L. Addy and their graduate students at the University of Illinois at Urbana–Champaign have conducted successful experiments on two–dimensional base flow configurations utilizing two-component laser Doppler velocimeter (LDV) techniques to obtain mean and fluctuating velocity information about the flowfields in and around the embedded separated flow regions that characterize base flows at supersonic speeds.

Analytical predictions based on component model methodologies have also been refined and improved. In addition, finite difference computational techniques, developed primarily by others, have been implemented and investigated. This has led to a unique collaboration between researchers using experiments, component method analyses, and computations, has led to a logical and systematic approach to the base flow problem, and has yielded valuable insight regarding the fundamental interactions and mechanisms within such flows.

The purpose of this final technical report is to collect and present, in their entirety or by summary and reference, the research findings for the near-wake base flow problem and related problems that have been investigated under the research sponsorship of the U.S. Army Research Office through Research Contract DAAL03–87–K–0010. The Technical Monitor for this research has been Dr. Thomas L. Doligalski, Chief, Fluid Dynamics Branch, Engineering Sciences

Division. We are also deeply indebted to the long-term interest and the technical suggestions and comments of Dr. Robert E. Singleton, Director, Engineering Sciences Division.

In all cases, where analytical, experimental, and/or computational efforts have yielded significant or new results, the information has been presented at professional meetings and/or published in the archival literature by the individual researchers. This final report highlights this work and includes copies of the appropriate publications for completeness. In the case of master's and doctoral degree theses, which are often quite long and detailed, a summary of the theses is provided and the appropriate reference to the full document is given. In many cases, the conference and/or archival publications are based upon the detailed work reported in these theses.

B. FINAL TECHNICAL REPORT ORGANIZATION

The overall organization of this report details the major accomplishments of the research group during the three-year period of ARO sponsorship in a fashion that illustrates the three-pronged effort: analytical, numerical, and experimental. Each research investigation is categorized and described in brief detail and the associated published literature is included in an appendix. The inclusion of a copy of the published literature is intended to ease the burden on the reader for obtaining symposium proceedings and other publications which tend to be difficult to obtain.

The relatively brief "text" of this final technical report has been outlined and organized to provide quick reference to a particular topic of interest. Most of the research results have been made available through organized meetings and publications of the American Institute of Aeronautics and Astronautics (AIAA) and the American Society of Mechanical Engineers (ASME). In those instances when a detailed paper is available, only a brief description is given and the reader is referred to the appropriate appendix for further details.

Once the research topics have been discussed, the continuing and future research activities of the research group are described. The strong commitment of this research group towards developing an understanding of the base flow problem is evidenced by the multi-year development and assembly of advanced experimental equipment that will provide well-documented data for the ongoing analytical and computational work. Although this final technical report summarizes our

current three-year effort, our research group is continuing to investigate the base flow problem and anticipates further significant contributions to the understanding of the fundamental mechanisms and interactions within high-speed separated flows. The emphasis of our ongoing research activities is focused on the following general research tasks:

(1) Two-stream, supersonic, plume-induced separation;

(2) Particle image velocimetry in high-speed flows;

(3) Axisymmetric power-on and power-off base flows; and

(4) Control of high-speed separated flows.

These ongoing research activities are described briefly in the last section of the report.

II. SUMMARY OF RESULTS

This section summarizes the results of the ongoing research program concerned with fluid dynamic mechanisms and interactions occurring in high-speed separated flows. The discussion is divided into two major sections: (1) Component Modeling and Numerical Computations of Base Flows, and (2) Small-Scale Experiments of High-Speed Separated Flow Configurations. In each of these sections the most important results are abstracted from the journal articles, conference proceedings papers, and graduate student theses that have been completed under the support of this research contract.

A. COMPONENT MODELING AND NUMERICAL COMPUTATIONS OF BASE FLOWS

A.1 Nonsteady Plume-Wall Interactions in Rocket Launch Tubes

Strong and potentially destructive pressure amplitudes have been observed during the early stages of rocket launch from canisters. This can be explained by a traveling wave system that is caused by quasiperiodic changes in irreversibility levels between the critical flow conditions in the rocket nozzle and at the exit of the launch tube. The interaction between the wave system and the wake region near the base of the rocket and its controlling flow mechanisms result in the complex nonsteady overall interaction of supersonic and subsonic flow regions. Observations by means of the hydraulic analogy allow the identification of constituent mechanisms, which are subsequently subjected to a highly simplified analysis and finally compared to experimental results under laboratory conditions. General agreement between theoretical and experimental results (pressure amplitudes and frequencies) support the validity of the proposed analytical approach.

The complete text of this paper may be found in Appendix A, Section A.1.

A.2 A Review of the Fluid Dynamic Aspect of the Effect of Base Bleed

The fluid dynamic aspect of the effect of base bleed is briefly reviewed. Earlier understandings on the basis of interaction between the viscous and inviscid streams can adequately explain the three different flow regimes as results of base bleed. The effect of energy addition to

the wake has also been ascertained from this approach. With the detailed numerical computations of the flow by solving the Navier-Stokes equations becoming available, the effect of base bleed can be illustrated by providing appropriate boundary conditions of the bleed at the base.

The complete text of this paper may be found in Appendix A, Section A.2.

B. SMALL-SCALE EXPERIMENTS OF HIGH-SPEED SEPARATED FLOW CONFIGURATIONS

B.1 Interaction Between Two Compressible, Turbulent Free Shear Layers

Experimental results of the interaction between two compressible, two-dimensional, turbulent free shear layers are presented. The shear layers were formed by geometrical separation of two high-Reynolds-number, turbulent boundary-layer flows with freestream Mach numbers of 2.07 and 1.50 from a 25.4-mm-high backward-facing step. A two-component, coincident laser Doppler velocimeter was utilized for a detailed flowfield survey. Both shear flows show general features similar to those of compressible, free shear layers reattaching onto a solid surface, including large-scale turbulence in the recompression and interaction regions and enhanced mixing in the redeveloping region. The free shear layer with the lower freestream Mach number shows high turbulence intensities and a higher rate of increase of turbulence intensities in the streamwise direction. These features appear to be caused by higher entrainment of reversed flow recirculating from the highly turbulent reattachment region.

The complete text of this paper may be found in Appendix B, Section B.1.

B.2 Compressible Separated Flows

An experimental investigation of compressible, two-dimensional, planar turbulent flows with large separated regions is presented. Three backward-facing step flow configurations were investigated to gain a detailed knowledge of the mean flow and turbulent field in developing compressible turbulent free shear layers and the adjacent recirculating flow. Two-channel coincident laser Doppler velocimeter measurements, surface static pressure measurements, Schlieren flow visualization, and surface oil flow visualization were used to study these flows. The recirculating flows stimulated increased mixing layer growth and entrainment rates. The

turbulent field of the compressible mixing layer was considerably more anisotropic than the incompressible counterpart with a decrease in the transverse velocity component turbulence intensity and the Reynolds shear stress. Laser Doppler velocity bias effects and bias corrections are demonstrated and discussed.

The complete text of this paper may be found in Appendix B, Section B.2.

B.3 The Effect of Sudden Expansions and Compressions on Turbulent Boundary Layer Momentum Thickness in Supersonic Flow

An experimental investigation of momentum thickness changes in two-dimensional planar, attached boundary layers in supersonic flow undergoing a sudden compression or sudden expansion is presented. Momentum thickness measurements upstream and downstream of disturbance corners were conducted for nominal freestream Mach numbers of 1.5, 2.0, 2.5, and 3.0.

A simple integral formulation leading to a closed form algebraic solution was successfully employed to model the experimentally measured changes in the momentum thickness across both sudden compressions and sudden expansions. A best fit correlation was used to obtain the appropriate incompressible form factor required by the formulation. The resulting form factor differs for sudden compressions from that of sudden expansions. In both cases, the best fit form factor is essentially independent of Mach number over the range tested, and the test results show excellent qualitative and quantitative agreement with the theory. For sudden expansions, the data suggest that apparent sublayer transition and redevelopment into a reduced turbulence outer rotational layer may require a two-profile velocity description downstream of the disturbance.

The complete text of this paper may be found in Appendix B, Section B.3.

B.4 Turbulent Boundary-Layer Properties Downstream of the Shock-Wave/Boundary-Layer Interaction

An experimental investigation was conducted to study the interaction between a shock wave and a turbulent boundary layer. Compression corner models mounted on a wind tunnel floor were used to generate the oblique shock wave in the Mach 2.94 flowfield. Ramp angles of 8, 12, 16, 20, and 24 deg were used to produce the full range of possible flowfields, including flow with no

separation, flow with incipient separation, and flow with a significant amount of separation. The principal measurement technique used was laser Doppler velocimetry (LDV), which was used to make two-component coincident velocity measurements within the redeveloping boundary layer downstream of the interaction. The results of the LDV measurements indicated that the boundary layer was significantly altered by the interaction. The mean streamwise velocity profiles downstream of the separated compression corners were very wake-like in nature, and the boundary-layer profiles downstream of all the interactions showed an acceleration of the flow nearest the wall as the boundary layers began to return to equilibrium conditions. Significant increases in turbulence intensities and Reynolds stresses were caused by the interactions, and indications of the presence of large-scale turbulent structures were obtained in the redeveloping boundary layers.

The complete text of this paper may be found in Appendix B, Section B.4.

B.5 LDV Measurements in Supersonic Separated Flows

An overview is given of a broad-based, experimental research program whose aim is to study and clarify the detailed interactions occurring in high-speed separated flows. The principal tool used in these investigations is a two-component laser Doppler velocimeter, and the implementation of this instrument in the flows of interest is discussed. In addition, as an example of the results obtained, measurements from a recent study concerning the interaction of two compressible shear layers are presented and discussed.

The complete text of this paper may be found in Appendix B, Section B.5.

B.6 Unsteady Reattachment of Supersonic Flow Past a Backward-Facing Step

An experimental investigation was conducted to study the effect of the initial boundary layer thickness prior to separation on the compressible, two-dimensional reattaching free shear layer formed by geometrical separation of a turbulent boundary layer over a backward-facing step. Two small scale full nozzle configurations were constructed to produce a uniform supersonic flow with a freestream Mach number of 2.0. One nozzle set produced an equilibrium turbulent boundary layer with a visually measured thickness of 5 mm and the other nozzle set produced a 2.5

mm boundary layer thickness prior to the geometric corner. Two operating conditions were studied for each nozzle set, incipient and complete reattachment. The incipient reattachment condition was defined as the condition where the shear layers attached to the wall and a normal shock was present within a few boundary layer thicknesses of the reattachment region, while the complete reattachment condition was defined as the case where the realignment compression waves had coalesced into an oblique shock downstream of the reattachment region. A detailed survey of the flow was made utilizing surface static probes, Schlieren photography, and fast response, flush mounted, piezo-resistive pressure transducers. The fast response pressure transducers were placed at locations upstream of separation, in the separated base region, at the reattachment location, and downstream of the reattachment region.

Surface streak pattern measurements indicated highly three-dimensional flow in the separated base and reattachment regions, while upstream of the separation and downstream of the reattachment region no three-dimensionality effects were present. At the condition of complete reattachment, no significant pressure fluctuations were present in the flowfield over the frequency range of 0 to 40 kHz. The incipient reattachment operating condition produced pressure fluctuations at the separated base region, reattachment region, and downstream of the reattachment region, while only white noise was present upstream of the geometric corner. The oscillating frequency for the incipient reattachment condition at the reattachment region was 60.95 Hz for the 5 mm initial boundary layer and 90.87 Hz for the 2.5 mm initial boundary layer flow. Strong coherence was present between the reattachment region and separated base region flows and the flow downstream of the reattachment region.

Possible sources for the pressure fluctuations are the terminating normal shock in the test section, flapping motion of the shear layers (i.e., reattachment and separation of the shear layers to and from the surface), and back and forth movement of the shear layers across the face of the fast response pressure transducers.

The complete manuscript of this thesis is available from the authors of this report.

B.7 Laser Doppler Velocity Bias in Separated Turbulent Flows

Velocity bias effects on data obtained with a coincident two channel laser Doppler velocimeter in a highly turbulent separated supersonic flow are presented. Probability distributions of the fluctuating velocities were distorted by velocity bias in a manner consistent with theory and a two-dimensional velocity inverse weighting function bias correction produced reasonable appearing velocity probability distributions. The addition of an approximate correction term to account for the effects of the unmeasured third velocity component improved these results but had little effect on the velocity statistics. Experimental factors that could partially compensate or falsely add to the velocity bias, conditions for the bias to occur, and conditions for which the bias may also be observed and corrected for are discussed.

The complete text of this paper may be found in Appendix B, Section B.7.

B.8 An Experimental Investigation of the Effects of a Base Cavity on the Near-Wake Flowfield of a Body at Subsonic and Transonic Speeds

An experimental investigation was conducted to study the effects of a base cavity on the near-wake flowfield of a slender, two-dimensional body in the subsonic and transonic speed ranges. Three base configurations were investigated and compared: a blunt base, a shallow rectangular cavity base of depth equal to one-half the base height, and a deep rectangular cavity base of depth equal to one base height. The models were mounted in a small scale transonic wind tunnel with slotted upper and lower walls to allow testing into the transonic range and to minimize the effects of tunnel wall interference. Each base configuration was tested at three freestream Mach numbers, ranging from the low to high subsonic range, to give a total of nine experimental conditions. The objectives of the investigation were to explain the cavity's drag reducing mechanism, to attain a greater understanding of the phenomena of vortex formation and shedding, and to resolve some of the conflicts that have arisen between the numerical and experimental work on base cavities to date. Schlieren photography, surface oil flow visualization, tuft visualization, and wake static pressure traverses were used to examine the details of the wake vortex structure. Static base pressure measurements were used to measure the drag reduction effect and high-speed

near-wake static pressure measurements were employed to determine the effect of the cavity on the vortex shedding frequency.

Schlieren photographs revealed that the basic qualitative structure of the vortex street was unmodified by the presence of a base cavity. However, the vortex street was weakened by the base cavity, apparently due to fluid mixing occurring at the entrance to the cavity. The weaker vortex street yielded higher pressures in the near-wake for the cavity bases relative to the blunt-based configuration, and the higher pressures caused the vortex formation position to be displaced slightly further downstream for the cavity bases as compared to the blunt base. As a result, no strong recirculatory motion was observed in the cavity at all. The base cavity configurations produced increases in the base pressure coefficients on the order of 10 to 14% relative to the blunt-based configuration, and increases in the shedding frequencies on the order of 4 to 6%. The majority of the changes observed occurred in going from the blunt base to the shallow cavity base, with little additional benefit resulting from increasing the depth of the cavity from one-half to one base height.

The complete manuscript of this thesis is available from the authors of this report.

B.9 An Experimental Investigation of the Effects of a Base Cavity on the Near-Wake Flowfield of a Body at Subsonic and Transonic Speeds

An experimental investigation has been conducted to study the effects of a base cavity on the near-wake flowfield of a slender, two-dimensional body in the subsonic and transonic speed ranges. Three base configurations were investigated and compared: a blunt base, a shallow rectangular cavity base of depth equal to one-half the base height, and a deep rectangular cavity base of depth equal to one base height. Each configuration was studied at three freestream Mach numbers, ranging from the low to high subsonic range. Schlieren photographs revealed that the basic qualitative structure of the vortex street was unmodified by the presence of a base cavity. However, the vortex street was weakened by the base cavity, apparently due to enhanced fluid mixing occurring at the entrance of the cavity. The weaker vortex street yielded higher pressures in the near-wake for the cavity bases, increases in the base pressure coefficients on the order of 10-

14%, and increases in the shedding frequencies on the order of 4-6% relative to the blunt-based configuration. The majority of the observed changes occurred in going from the blunt base to the shallow cavity base.

The complete text of this paper may be found in Appendix B, Section B.9.

B.10 Design of an Axisymmetric Supersonic Wind Tunnel and Experimental Study of Supersonic, Power-Off Base Flow Phenomena

A small-scale, supersonic, axisymmetric wind tunnel has been designed and constructed to realistically investigate the flow field behind a body of revolution. The annular nozzle design consists of three interchangeable diverging nozzles, a common converging nozzle, and two interchangeable central stings. Design Mach numbers of 2.0, 2.0 and 2.5 are produced for stings with diameters of 2.0, 2.5 and 2.5 inches, respectively. Cylindrical and boattailed afterbodies can be connected to the end of the sting. To eliminate disturbances in the flow, the stings are supported upstream of the nozzle and test section, and the pressure tap leads from the base of the sting are accessed through its hollow center. The tunnel operates in the blowdown mode, and for a stagnation pressure of 60 psia, the run time is 20 seconds. For power-on experiments, central nozzles which operate at Mach 1.0 to 3.8, and are fed through the center of the hollow sting, can be attached to the base of the afterbody. Pitot probe traverses demonstrated that the flow produced by the wind tunnel was very uniform. Static pressure measurements around the periphery of the nozzle indicated that the Mach number at the exit plane varied by approximately 1%.

Several investigations were made of the separated flow region behind the base of a cylindrical, 2.5 inch diameter, power-off model at M=2.0. Schlieren photographs of the near-wake region indicated that an expansion fan emanating from the exit lip of the nozzle impinged upon the separated base flow region. A series of experiments, including varying the stagnation pressure and bleeding air into the test section, was performed in an attempt to reduce the interference effects. Although the strength of the expansion fan was reduced, the wake behind the model opened up, i.e. a closed recirculation region was not formed and no recompression occurred. The precise effects of the interference and the cause of the open wake are unknown;

however, limitations of available facilities prevented further study of these phenomena. A mixture of lampblack and oil applied to the base proved to be highly sensitive to sting positioning and is, therefore, suggested as a criterion for the alignment of axisymmetric models in a supersonic stream.

The complete manuscript of this thesis is available from the authors of this report.

B.11 An Experimental Investigation of the Shock Wave-Turbulent Boundary Layer Interaction

An experimental investigation was conducted to study the interaction between a shock wave and a turbulent boundary layer. The boundary layer was formed on the floor of a wind tunnel operating with a freestream Mach number of 2.94 and a Reynolds number based on boundary layer thickness of 3.1×10^5. A compression corner model having a ramp angle of 20 degrees was used to generate the interaction flowfield. Measurement techniques used in this investigation included Schlieren photography, surface static pressure measurement, surface streak pattern measurement, and laser Doppler velocimetry (LDV). The LDV system was the primary tool and was used to make two-color, two-component coincident velocity measurements in the undisturbed upstream boundary layer and within the redeveloping boundary layer downstream of the interaction. The results of the LDV measurements indicated that both the mean and turbulent flow properties of the boundary layer were significantly altered by the interaction. The mean velocity profiles in the redeveloping boundary layer exhibited wake-like properties, experiencing a rapid "filling out" downstream of reattachment due most likely to enhanced turbulent mixing via large scale eddies. Large increases in streamwise and vertical turbulence intensity as well as Reynolds stresses confirm the enhanced mixing and alteration of the flowfield turbulence due to the interaction with the shock wave.

The complete text of this paper may be found in Appendix B, Section B.11.

B.12 An Experimental Investigation of the Two-Stream, Supersonic, Near-Wake Flowfield Behind a Finite-Thickness Base

The complex interaction region generated by the separation of two supersonic streams past a finite-thickness base occurs frequently in high-speed flight and is characteristic of the aft-end

flowfield of a powered missile in the supersonic flight regime. In an effort to examine the fundamental fluid dynamic mechanisms and interactions ongoing in this near-wake region, an experimental investigation was conducted to obtain mean and turbulence data by making measurements in a small-scale wind tunnel. The two-dimensional test section produced a Mach 2.56 upper stream and a Mach 2.05 lower stream which both undergo geometric separation past a finite-thickness splitter plate and experience strong expansion and shear layer mixing processes before eventual recompression, reattachment, and redevelopment of the wake flow. This flowfield immediately behind the base in the near-wake is characterized by strong velocity and density gradients, energetic viscous interactions, high turbulence intensity levels, and a relatively energetic recirculation region with large-magnitude reverse flow.

The experimental data for the near-wake interaction flowfield was obtained using Schlieren photographs, stagnation and sidewall static pressure measurements, and laser Doppler velocimeter (LDV) measurements. The primary tool was a two-color, two-component LDV system which provided instantaneous velocity data from which mean and turbulence quantities were extracted. The qualitative and quantitative information for this flowfield was analyzed in a component style approach consistent with the Chapman-Korst model of the near-wake region. The strong dependence of the component model on empirical coefficients defines a need for detailed experimental data, while more recent computational efforts to predict the near-wake flowfield similarly require turbulence data for validation and improvement of turbulence modeling.

The dynamic interactions in the near-wake of the finite-thickness base after separation of the Mach 2.56 and Mach 2.05 streams correctly modeled the flowfield at the aft-end of a powered missile in supersonic flight. The flow regions included strong Prandtl-Meyer expansions, shear layer mixing and recompression, recirculation, and downstream wake redevelopment. The shear layer mixing regions were characterized by constant-pressure mixing along the initial two-thirds of their length, by an evolution of velocity profiles from truncated forms of the boundary layer shapes to more wake-like profiles farther downstream, and by relatively high levels of turbulence as compared to the levels existing in the turbulent boundary layers prior to separation. While relative

self-similarity of the mean velocity data was achieved, the turbulence field exhibited evidence of progression toward self-similarity but did not reach that state before recompression of the shear layers began. The separated flow region was characterized by vigorous recirculation, large negative velocities reaching 23 percent of the Mach 2.56 freestream value, and strong turbulent interaction with the low-velocity regions of both shear layers. Turbulence intensities, kinematic Reynolds stresses, and turbulent triple products were increased greatly in the latter portions of the two shear layers and in the recompression/reattachment region, seeming to indicate the presence of large-scale turbulent structures. The turbulence field in the region of reattachment was strongly anisotropic, and the transverse diffusion of turbulence energy by exchange of the kinematic Reynolds stress for turbulent kinetic energy seems in agreement with existing correlations. Recovery of the mean velocity field in the redeveloping wake flow occurred relatively quickly, while the turbulence field remained perturbed to the furthest streamwise location in the range of measurements. The data obtained for the two-stream interaction flowfield should prove quite valuable for use in validation and improvement of computational schemes aimed at prediction of the mean and turbulence profiles for the near-wake behind a finite-thickness base.

The complete manuscript of this thesis is available from the authors of this report.

III. LIST OF PUBLICATIONS

A substantial number of journal articles, conference proceedings papers, and graduate student theses have reported the results of this research effort. The following is a list of those publications.

A. JOURNAL ARTICLES

Samimy, M. and Addy, A. L., "Interaction Between Two Compressible, Turbulent Free Shear Layers," AIAA Journal, Vol. 24, No. 12, December 1986, pp. 1918-1923.

Petrie, H. L., Samimy, M., and Addy, A. L., "Compressible Separated Flows," AIAA Journal, Vol. 24, No. 12, December 1986, pp. 1971-1978.

Kuntz, D. W., Amatucci, V. A., and Addy, A. L., "Turbulent Boundary-Layer Properties Downstream of the Shock-Wave/Boundary-Layer Interaction," AIAA Journal, Vol. 25, No. 5, May 1987, pp. 668-675.

Petrie, H. L., Samimy, M., and Addy, A. L., "Laser Doppler Velocity Bias in Separated Turbulent Flows," Experiments in Fluids, Vol. 6, January 1988, pp. 80-88.

Marongiu, M. J., Korst, H. H., and White, R. A., "Nonsteady Plume-Wall Interactions in Rocket Launch Tubes," Journal of Spacecraft and Rockets, Vol. 25, No. 3, May-June 1988, pp. 209-216.

Kuntz, D. W., Amatucci, V. A., and Addy, A. L., "An Experimental Investigation of the Shock Wave-Turbulent Boundary Layer Interaction," manuscript submitted to the ASME Journal of Fluids Engineering, March 1989.

B. CONFERENCE PROCEEDINGS PAPERS

Hampton, L. P. and White, R. A., "The Effect of Sudden Expansions and Compressions on Turbulent Boundary Layer Momentum Thickness in Supersonic Flow," ASME Paper No. 86-WA/FE-11, presented at the 1986 ASME Winter Annual Meeting, Anaheim, California, December 1986.

Dutton, J. C., Addy, A. L., and Samimy, M., "LDV Measurements in Supersonic Separated Flows," invited paper presented and published in the Proceedings of the Optical Methods in Flow and Particle Diagnostics Conference, International Congress on Applications of Lasers and Electro-Optics, San Diego, California, November 1987.

Sahu, J. and Chow, W. L., "A Review of the Fluid Dynamic Aspect of the Effect of Base Bleed," paper published and presented at the First International Symposium on Special Topics in Chemical Propulsion: Base Bleed, Athens, Greece, November 1988.

Kruiswyk, R. W. and Dutton, J. C., "An Experimental Investigation of the Effects of a Base Cavity on the Near-Wake Flowfield of a Body at Subsonic and Transonic Speeds," AIAA Paper No. 89-0210, presented at the AIAA 27th Aerospace Sciences Meeting, Reno, Nevada, January 1989.

C. THESES

Taghavi, K., "Unsteady Reattachment of Supersonic Flow Past a Backward-Facing Step," M.S. thesis, Department of Mechanical and Industrial Engineering, University of Illinois at Urbana-Champaign, December 1987.

Kruiswyk, R. W., "An Experimental Investigation of the Effects of a Base Cavity on the Near-Wake Flowfield of a Body at Subsonic and Transonic Speeds," M.S. thesis, Department of Mechanical and Industrial Engineering, University of Illinois at Urbana-Champaign, August 1988.

Sauter, J. M., "Design of an Axisymmetric Supersonic Wind Tunnel and Experimental Study of Supersonic, Power-Off Base Flow Phenomena," M.S. thesis, Department of Mechanical and Industrial Engineering, University of Illinois at Urbana-Champaign, March 1989.

Amatucci, V. A., "An Experimental Investigation of the Two-Stream, Supersonic, Near-Wake Flowfield Behind a Finite-Thickness Base," Ph.D. thesis, Department of Mechanical and Industrial Engineering, University of Illinois at Urbana-Champaign, December 1989.

IV. LIST OF PARTICIPATING SCIENTIFIC PERSONNEL AND ADVANCED DEGREES EARNED

Following are lists of the faculty and graduate student scientific personnel who have contributed to this research effort and the graduate degrees that have been earned in conjunction with this project.

A. FACULTY

A. L. Addy
Co-Principal Investigator
Professor and Head of Mechanical Engineering

W. L. Chow
Co-Principal Investigator
Emeritus Professor of Mechanical Engineering

J. C. Dutton
Co-Principal Investigator
Associate Professor of Mechanical Engineering

B. GRADUATE STUDENTS

V. A. Amatucci
M.S. 1981
Ph.D. 1989

H. C. Chen
B.S. 1980
M.S. 1988

J. L. Herrin
B.S. 1989
M.S. Candidate

R. W. Kruiswyk
B.S. 1986
M.S. 1988

M. J. Morris
M.S. 1980
Ph.D. 1987

J. M. Sauter
B.S. 1987
M.S. 1989

R. J. Shaw
M.S. 1986
Ph.D. Candidate

K. Taghavi
B.S. 1985
M.S. 1987

A. Ting
B.S. 1962
Ph.D. Candidate

C. ADVANCED DEGREES EARNED

K. Taghavi
M.S., December 1987

R. W. Kruiswyk
M.S., August 1988

J. M. Sauter
M.S., March 1989

V. A. Amatucci
Ph.D., December 1989

V. CONTINUING AND FUTURE RESEARCH ACTIVITIES

As a result of continued funding by the U.S. Army Research Office, the investigation reported on herein will be continued for an additional three-year period. Future studies will build on our experience over the last several years of experimentally investigating several fundamental high-speed flow configurations that have particular relevance to projectile and missile base flows. As discussed earlier in this report, geometries studied in the past include development and reattachment of supersonic shear layers, shock wave/boundary layer interactions, two-stream supersonic base flows, and near-wake flowfield modifications due to the presence of a base cavity. In each case, the flows were nominally two-dimensional planar in order to facilitate instrumentation access. The previous measurements included conventional Schlieren photography, surface streakline visualization, pitot and static pressure measurements, and with major emphasis on two-component, coincident laser Doppler velocimetry (LDV) measurements. These studies, particularly the LDV measurements, have provided accurate and very useful spatially resolved data on the time-mean properties of these complex separated flows. However, because of the pointwise nature of the LDV and pressure measurement methods, any information concerning the instantaneous (i.e., time resolved) structure of these flows is indirect at best. Therefore, a major emphasis of the ongoing work will be the development and implementation of planar diagnostic techniques in order to address such questions as the existence and role of large-scale structures in these flows, mechanisms of entrainment, mixing, reattachment, and redevelopment, three-dimensional structure of these flowfields, etc. In addition, measurements will be made for axisymmetric geometries which better model the projectile and missile afterbody and base flows of direct interest here. An improved understanding of the detailed fluid dynamic mechanisms in high-speed separated flows will result in improved numerical predictive capabilities and the possibility of passive and/or active control of these flows to obtain vehicle performance benefits.

Brief descriptions of the specific experimental studies to be conducted in the ongoing research program are given below.

A. TWO-STREAM, SUPERSONIC, PLUME-INDUCED SEPARATION

An experimental effort is underway to investigate plume-induced, boundary layer separation in a planar, two-stream, supersonic flow using an "angle-induced" separation geometry. This study is being conducted in a small-scale wind tunnel operated in the blowdown mode. In essence, the design consists of a Mach 1.5 inner flow located at a 40° angle with respect to a Mach 2.5 freestream flow and separated by a base thickness of 0.500 inches. Design and fabrication of the test section and instrumentation have been completed and preliminary Schlieren photography and surface oil flow experiments have been performed to verify its operation.

In addition to visualization studies, the static pressure fields are being completely documented using approximately 425 pressure taps that have been located in the axial and spanwise directions along the base centerpiece and in the tunnel sidewalls. These mean measurements will be used to investigate the static pressure rise across the separation shock, pressure variations occurring in the separated region due to the recirculating flow, as well as the recompression pressure rise occurring at reattachment between the two free shear layers. Two flush-mounted, high frequency response, miniaturized pressure transducers have also been located in the wall of the base centerpiece bounding the freestream flow. Measurements from these transducers will quantify the amplitude and spectral content of the wall pressure fluctuations resulting from unsteadiness in the separation location.

In order to document in detail the mean and turbulent velocity fields, two-component, coincident LDV data will also be obtained for the separated flowfield. The turbulent boundary layer and adjacent freestream of the flow approaching separation will be measured and reported as will the entire interaction region. These measurements will be used to determine major mechanisms of the mean and turbulent velocity fields such as turbulence amplification at the separation location and at recompression/reattachment of the free shear layers, the magnitude of the mean velocity in the recirculating region which has been found to be surprisingly large in some of our previous studies, and the existence of large triple product values at boundary layer and shear

layer edges which are indicative of intermittent, large-scale structures that are largely responsible for entrainment.

B. PARTICLE IMAGE VELOCIMETRY IN HIGH-SPEED FLOWS

A research program is being conducted to develop a new particle image velocimeter (PIV) system for use as a non-intrusive laser diagnostic tool in our high-speed separated flow studies. The PIV system will be capable of extracting full two-dimensional instantaneous velocity maps within a flow by recording double images of seed particles on photographic film and then examining the particle separations to determine local velocities. The design is based on the use of two pulsed, high-power Nd:YAG lasers to illuminate seed particles for recording on 35 mm format film, with control of seeders, lasers, camera shutter, etc. performed with a Macintosh II computer. Post-processing to examine the film records is done with a high-speed image processing system based on a Macintosh II 36 MHz workstation, a He-Ne laser film illumination source, and automated positioners to handle the film.

Development of the system is proceeding rapidly with specification and purchase of the transmitting system optical components now complete. The Nd:YAG laser system, assembled on a custom-designed single axis positioning table is being successfully operated under control of a Stanford Research Systems pulse generator. Optics are in place to begin testing on a free jet case to verify operation. Purchase of a high-speed oscilloscope is also planned for use in high accuracy verification of the laser light pulse timing. The post-processing system is partially assembled, with the film positioners currently operating from computer control. Receipt of previously ordered equipment, including a video camera, frame grabber board, and other optical components is expected in the near future to coincide with completion of the free jet tests. Currently, software control and image analysis software problems are being examined.

C. AXISYMMETRIC POWER-ON AND POWER-OFF BASE FLOWS

An experimental program is underway which is investigating the flowfield behind bodies of revolution in supersonic freestreams. A newly designed and constructed axisymmetric wind tunnel capable of producing freestream design Mach numbers of 2.0 and 2.5 is being utilized. Various

sting diameters may be used in both the power-on and power-off configurations with cylindrical as well as boattailed afterbodies. For power-on cases, central jet nozzles can be used to produce Mach numbers ranging from 1.0 to 3.8. The versatility of this wind tunnel will allow for experimental investigations in several different operational modes, but only representative power-on and power-off cases will be chosen for detailed study.

Flow visualization studies and pitot probe traverses have been completed in order to document the uniformity of the freestream nozzle exit flow. An extremely uniform flow was produced with exit plane Mach numbers varying by less than 1% around the periphery of the nozzle. Schlieren photographs have indicated the existence of an expected expansion fan emanating from the freestream nozzle lip that must be eliminated before any quantitative data is obtained.

The primary diagnostic tool to be used in documenting the mean and turbulent velocity fields is a two-component laser Doppler velocimeter (LDV) system. This tool collects instantaneous velocity data at any spatial location in the flowfield. The LDV data will be used to identify the fundamental fluid dynamic mechanisms of importance in these complex flows. Proper seeding of this separated flowfield is a major concern in obtaining the velocity data. New seeding techniques may be needed to counteract the low data rate problems typically encountered in the recirculating region.

D. CONTROL OF HIGH-SPEED SEPARATED FLOWS

Our long-term goals go beyond the study of high-speed flows with embedded separated regions to their manipulation and control, by passive and/or active means, in order to obtain performance benefits. Obviously, this could have tremendous positive impact on current and future systems of technological importance to the U.S. Army depending, of course, on the level of success achieved. Historically, several control techniques have been applied, such as base bleed and passive base geometry alteration methods including the use of splitter plates, serrated trailing edges, base cavities, perforated or "ventilated" cavities, and stepped afterbodies. The effects of base combustion and particles (typically originating in the central jet nozzle flow supplied by a

solid rocket motor) are also known to strongly affect the base drag and near-wake flowfield. Several techniques have also been implemented to enhance the entrainment and mixing in parallel two-stream supersonic shear layers including the use of vortex generators, slanted trip wires, and saw-tooth extensions mounted at the splitter plate tip, impingement of the shear layer with an oblique shock, and placement of a circular or square cylinder in the mixing layer in order to generate a bow shock.

In general, these previous attempts at shear layer and separated flow control have been relatively unsuccessful. However, we believe that there is a fundamental reason for this lack of success: there is simply insufficient current understanding of the detailed fluid dynamic mechanisms of importance, including the role of turbulent large-scale structures and the three-dimensional nature of the flow, to make a knowledgeable attempt at controlling them. Therefore, our approach will be to first learn as much as possible about these mechanisms by pursuing the studies mentioned in the preceding three subsections, and then to formulate and implement passive and/or active control strategies based on this understanding. We expect this work to be initiated in the final year of this three-year research program and to utilize the axisymmetric, supersonic base flow facility whose construction has been completed recently.

APPENDIX A

COMPONENT MODELING AND NUMERICAL COMPUTATIONS OF BASE FLOWS

SECTION A.1

NONSTEADY PLUME-WALL INTERACTIONS IN ROCKET LAUNCH TUBES

Journal of Spacecraft and Rockets

Volume 25, Number 3, May-June 1988

Pages 209-216

by

M. J. Marongiu, H. H. Korst, and R. A. White

Nonsteady Plume-Wall Interactions in Rocket Launch Tubes

M. J. Marongiu,* H. H. Korst,† and R. A. White‡
University of Illinois at Urbana-Champaign, Urbana, Illinois

Strong and potentially destructive pressure amplitudes have been observed during the early stages of rocket launch from canisters. This can be explained by a traveling wave system that is caused by quasiperiodic changes in irreversibility levels between the critical flow conditions in the rocket nozzle and at the exit of the launch tube. The interaction between the wave system and the wake region near the base of the rocket and its controlling flow mechanisms result in the complex nonsteady overall interaction of supersonic and subsonic flow regions. Observations by means of the hydraulic analogy allow the identification of constituent mechanisms, which are subsequently subjected to a highly simplified analysis and finally compared to experimental results under laboratory conditions. General agreement between theoretical and experimental results (pressure amplitudes and frequencies) support the validity of the proposed analytical approach.

Nomenclature

A = area, m
c = acoustic velocity, m-s^{-1}
D = channel height or diameter, m
f = frequency, Hz
H = backstep height, m
L = channel length, m
m = mass flow rate, kg $- s^{-1}$ (per unit width)
P = absolute pressure, N-m^{-2}
R = gas constant, N-m-K^{-1} kg^{-1}; radius, m
S = moving shock velocity, m-s^{-1}
t = time, s
t_o = base time constant, $t_o = h/c_{01}$, s
T = absolute temperature, K
v_R = velocity of rocket
W = test-section width, m
x, X = streamwise coordinate or distance, m
θ = streamline angle, radians
ρ = density, kg-m^{-3}
ω = Prandtl-Meyer expansion angle, radians

Dimensionless Quantities

C = Crocco number, U/U_{max}
C_e = effective area ratio coefficient
k = specific heat ratio
M = Mach number
ϕ = velocity ratio (further specified in text)
σ = jet spread rate parameter
τ = dimensionless time

Subscripts

I = conditions in primary nozzle
II = conditions in secondary nozzle
b = base region
c = channel region
d = discriminating or stagnating streamline
e = nozzle exit plane
j = zero streamline or jet streamline
v = wake travel time
w = conditions prevailing in the wave region
x = normal shock wave conditions before wave
y = normal shock wave conditions after wave
0 = stagnation conditions

Superscript

$*$ = critical conditions

I. Introduction

PROPULSIVE jets emerging from underexpanded convergent or convergent-divergent nozzles form plumes that commonly interfere with solid or hydrodynamic (slipstream) boundaries.[1,2] For certain configurations, impingements between the slipstream and solid boundaries can produce nonsteady flowfields characterized by the appearance of transient, large-amplitude pressure wave systems.[3] The study of wake regions bounded by mixing layers and controlled by their mass entrainment and reattachment mechanisms have been the subject of intensive research for several decades. Such work has included experimental, analytical, and computational approaches in attempts to explain and predict the characteristics of these complex flowfields. Flow component models[1] have been particularly useful in delineating the controlling mechanisms for such complex flows under steady, or quasisteady, operating conditions.

Nonsteady flowfields may occur when the jet flow encounters a constriction downstream in which critical flow conditions have to be satisfied leading to temporary mass storage requirements between critical cross sections. Rockwell[4] has enumerated and classified a variety of these cases exhibiting nonsteady phenomena, some of which had been previously investigated experimentally.[5-8] Such nonsteady interactions have been observed during the early phases of in-tube launch of rockets or missiles, often accompanied by strong, and possibly destructive, pressure wave buildup in the canister.

This paper develops criteria for the appearance of such nonsteady operational modes and their analysis by 1) delineation of flow components, and 2) their subsequent synthesis into an overall model for cyclic performance. Because of the complex nature of the various flow components and their interaction, the analysis of the problem, by necessity, requires far-reaching simplifications in treatment. Support for the validity of such abstractions is furnished by experimental evidence of two kinds, namely, 1) qualitative observations of the overall systems performance by means of the hydraulic analogy (water table), and 2) quantitative studies with high-velocity air flows of both component mechanisms[9] and entire systems in cyclic modes of operation. The experimental evidence, although validating the basic analysis, also points to the difficulties in separating individual flow mechanisms with respect to their exact location in space and time.

Presented as Paper 87-1601 at the AIAA 22nd Thermophysics Conference, Honolulu, HI, June 8-10, 1987; received June 25, 1987; revision received Jan. 19, 1988.

*Visiting Research Associate.
†Professor Emeritus. Fellow AIAA.
‡Professor. Associate Fellow AIAA.

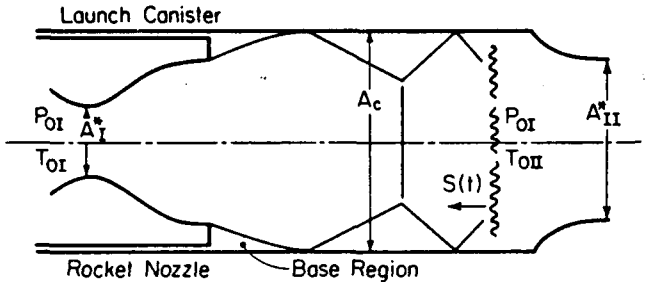

Fig. 1 Typical plume-wall interactions during the initial launch phases of rockets [$S(t)$ is needed to account for mass storage between the moving shock system and second critical cross section].

II. Flow Model

A simple but representative configuration that lends itself to a study of the phenomenon is shown in Fig. 1. It is composed of a converging-diverging nozzle, operating with critical flow in the first throat A^*_I, which discharges into a smooth channel of larger but uniform cross section. The channel (launch tube) may end with a constrictor nozzle A^*_{II}, or without an area reduction. Either type of exit condition can give rise to critical flow conditions, depending on the geometry, rocket-chamber to ambient-pressure ratio, and the dissipative mechanisms occurring in the system. If critical flow rates in the first (rocket nozzle) throat and the (effective) second throat do not match, mass discharge or storage will be required in the launch tube. In the absence of sufficiently high missile velocity in the early launch phases but sufficient distance between the nozzle exit and the launcher exit to allow plume impingement on the wall, a nonsteady wave system may appear and interfere with the dissipative mechanism in the base region, along the tube walls, and within the tube itself. This can change the dissipative flow components sufficiently to produce a cyclic mode of operation.

Because of the complex nature of the problem it was necessary to seek guidance in the form of preliminary experiments by using the hydraulic analogy (water table). Diagnostic experiments with high-velocity airflow in channels representing individual flow mechanisms and overall system behavior were also undertaken to provide understanding and support for the theoretical analysis.

Preliminary Water Table Experiments

Use of the hydraulic analogy in the study of nonsteady flow processes takes advantage of the vastly extended time scale, which in the present case is of the order of 5000:1, as compared to air-channel flow experiments. This coupled with the ease of flow visualization makes the hydraulic analogy a very attractive and useful tool. Figure 2 is a sequence of photographs showing flow patterns referring to the instantaneous flow conditions, as indicated in Fig. 3.

Based on the observations of the water table experiments (again see Figs. 2 and 3), the following mechanisms can be identified:

1) The fully developed wake (base pressure) establishes supersonic flow in the channel. The presence of a second critical cross section requires a shock system to satisfy subsonic approaching flow

2) If the strength of such a shock system together with the wall friction in the channel produces irreversibilities sufficiently strong that the second throat is not large enough to discharge the mass rate supplied by the primary nozzle, then mass has to be stored in the channel, forcing the shock system to move upstream.

3) During the upstream motion of the shock system, the rate of dissipation is modified as the supersonic region of the channel flow is decreasing. This is reflected by a change in strength and speed of the wave.

4) As the wave system approaches and interferes with the wake at the primary nozzle exit, the shear layer bounding the

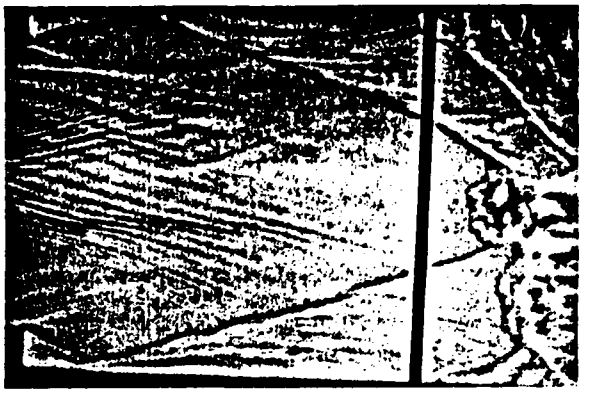

a) At instant C

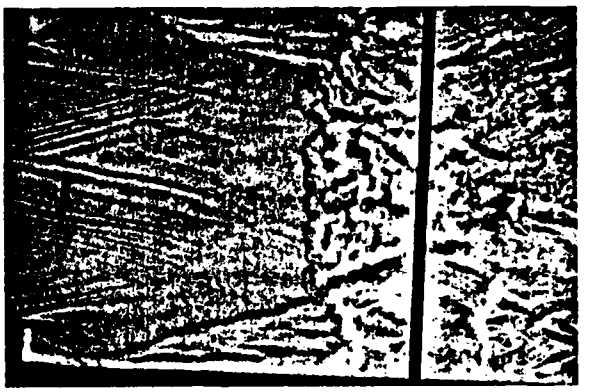

b) After instant C

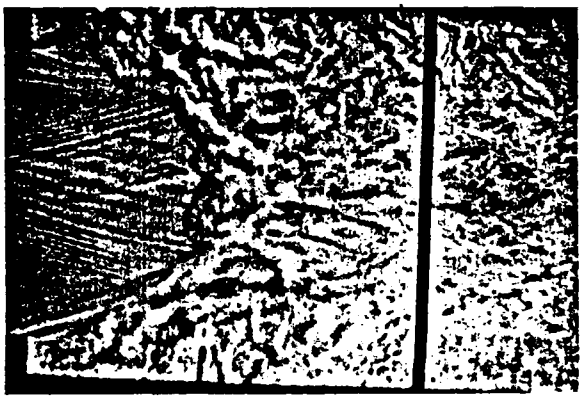

c) At instant D

Fig. 2 Water table photographs showing the instantaneous flowfield at various times in a typical cycle (instants refer to time markers in Fig. 3).

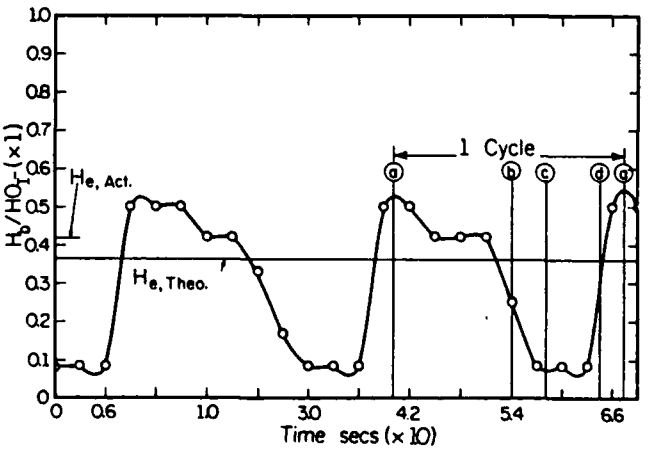

Fig. 3 Base area water height (H_b) vs time on the water table model during nonsteady operation (all H values in this figure refer to water heights).

Dimensions Tested:
H = 4, 5, 6, 7, [8], 9, 10 mm
$H_{e_{II}}$ = 18, 19, 20, 21, [22], 23, 24, 25 mm
L = 76, [101] mm
M_{e_I} = 1.611 Nominal (Folsch nozzle)

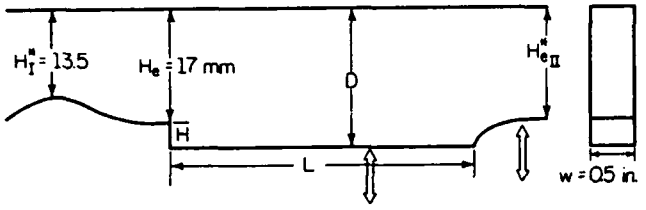

Fig. 4 Two-dimensional configuration for diagnostic experiments showing the dimensions tested.

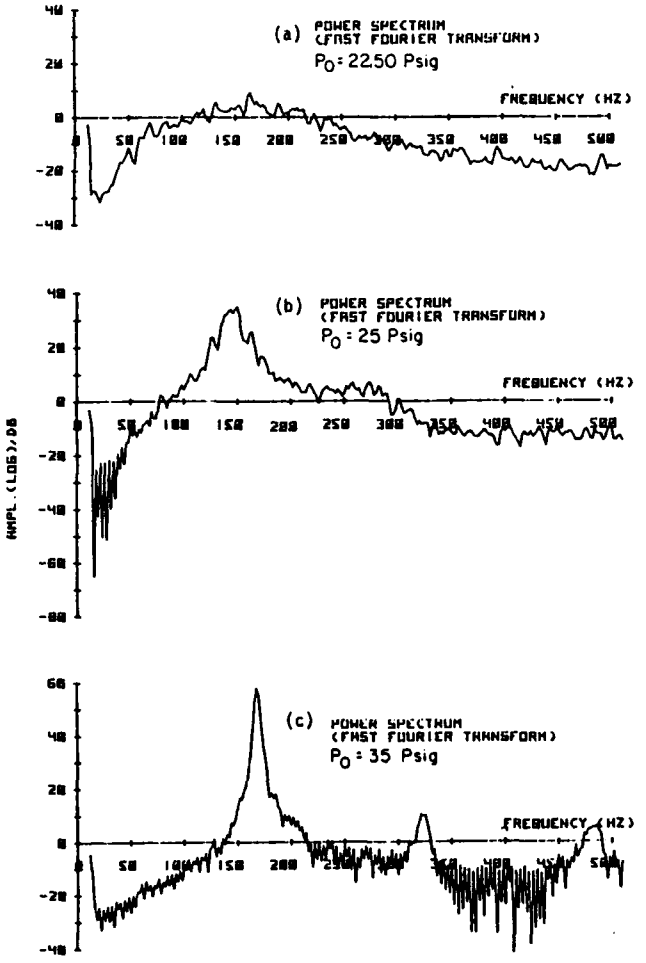

Fig. 5 Power spectra of base pressure oscillations for: a) L = 101 mm, P_{o_I} = 22.5 psig; b) L = 101 mm, P_{o_I} = 25 psig; and c) L = 101 mm, P_{o_I} = 35 psig.

wake will detach from the wall, and the base pressure will increase toward the exit pressure of the nozzle. Under these conditions the level of irreversibilities in the channel is drastically reduced, and the rate of outflow through the second critical cross section increases so that the stored mass may be discharged.

5) The free-mixing layer along the surface of the jet discharging from the nozzle begins to entrain mass so that a new wake will be generated, and the original base pressure is restored.

Although this sequence of events can be conveniently observed with the help of the hydraulic analogy, a theoretical analysis is, in view of the complexity of the flow patterns, dependent on sweeping simplifications.

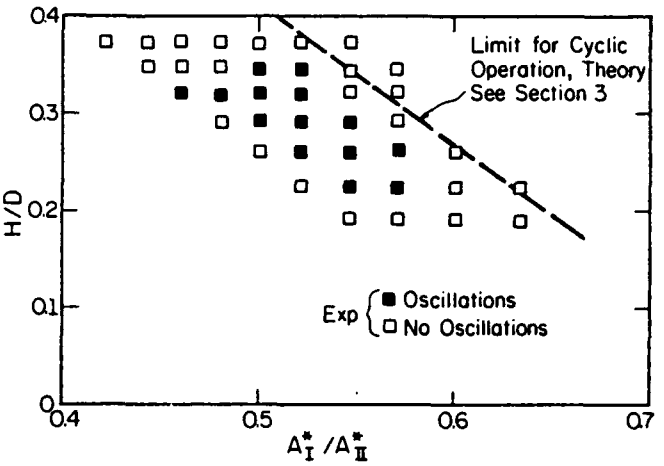

Fig. 6 Influence of geometrical parameters on the base pressure oscillations in two-dimensional channels of the type shown in Fig. 4.

Table 1 Analytical concepts as applied to the flow components

No. components	Analytical concepts: Steady 1-D	Quasisteady 1-D	Quasisteady 2-D	Nonsteady 1-D
1) Primary nozzle flow	X			
2) Viscous entrainment along wake			X	
3) Sudden expansion and frictional channel flow		X		
4) Choking in second throat		X		
5) Time-dependent mass storage				X
6) Shock (wave) kinematics and dynamics				X
7) Shock-wave interaction			X	
8) Mass discharge at second throat		X		
9) Wake pumpdown at nozzle base			X	

Diagnostic Experiments in Air Channels

In order to establish conditions producing nonsteady operation, a two-dimensional channel of constant width was constructed with provisions for varying the pertinent geometries (base-step height, second-throat height, and channel length) while leaving the primary nozzle exit height constant (see Fig. 4). Shown in Fig. 5 (power spectrum of base pressure) is the gradual onset of cyclic oscillations as the primary nozzle pressure is increased, and critical flow conditions are produced in the second throat. Similar results have been obtained for other geometries. The effect of the critical area ratios A_I^*/A_{II}^* and the base-to-channel height ratio on the occurrence of oscillations is demonstrated in Fig. 6. Based on the above observations, it is possible to propose a theoretical flow model as described below.

Flow Model Components

Here, flow components are delineated for subsequent synthesis into an overall operational model. The components are identified as follows: 1) the primary nozzle flow, 2) viscous entrainment along the separated flow (base) region, 3) the abrupt expansion at the nozzle base and frictional channel flow, 4) choking in the second throat, 5) a time-dependent mass storage mechanism, 6) shock system (wave kinematics

and dynamics, 7) shock interaction with the wake and resulting reduction in level of downstream dissipation, 8) mass discharge through the second throat, and 9) pump-down of the wake at the base of the nozzle. The treatment of these flow processes fall into four categories, each of which may be applicable to one or more components, as shown in Table 1. Since the nonsteady nature of the problem is linked to the modification of the dissipation levels due to shock-wake interaction, the analysis of the shock kinematics and dynamics is of utmost importance.

Although the wave system is of a highly complicated structure, it is fortuitous that the Mach number level of the supersonic flow over which the compression waves have to travel is high enough so that the subsonic flowfield behind the shock system can be treated as effectively one-dimensional.[10] In the following section, the major flow components are discussed individually.

III. Theoretical Analysis

Sudden Expansion to Supersonic Channel Flow

The jet discharging from the nozzle undergoes an adjustment to channel flow that is treated as producing one-dimensional, supersonic flow at the end of the wake. Because of the sudden enlargement in cross section and a prevailing base pressure P_b, this process will be irreversible and results in an increase in entropy, and being adiabatic, a decrease in stagnation pressure. (It must be noted that this requirement of the second law imposes an upper limit on the value of the base pressure). Utilizing the fundamental conservation principles for mass and momentum, together with simple adiabatic conditions, the one-dimensional supersonic flow downstream of the wake is determined.

Channel Flow

Fanno-type flow starts at the end of the wake, and the friction coefficient is determined on the basis of an equivalent diameter concept (considering Reynolds number and absolute wall roughness). This friction coefficient is subsequently adopted for the subsonic portion of the channel flow, which is permissible because of the relatively small changes in entropy downstream of the moving shock.

Wave System

A left-running normal shock is needed to allow for mass storage in the channel if the flow irreversibilities cause the second critical cross section to choke at a lesser mass rate than that delivered by the primary nozzle. Denoting the absolute velocity of the shock front by S, the mass storage condition is expressed by

$$m_I^* - m_{II}^* = S(\rho_y - \rho_x)A_c \tag{1}$$

where ρ_y and ρ_x are the densities downstream and upstream, respectively, of the (moving) normal shock.

In terms of the geometrical and flow parameters, one now expresses the dimensionless shock speed as

$$\frac{S}{c_o} = \left(\frac{2}{k+1}\right)^{k+1/2(k-1)} \left\{ A_I^* \frac{P_{o_I}}{T_{o_I}} \left[1 - \frac{AII}{A_I^*} \frac{P_{o_{II}}}{T_{o_I}} \times \left(\frac{T_{o_I}}{T_{o_{II}}}\right)^{1/4} \right] \Big/ \frac{P_x}{T_x}\left(\frac{P_y T_x}{P_x T_y} - 1\right) A_c \right\} \tag{2}$$

where $P_{o_{II}}$ and $T_{o_{II}}$ refer to the stagnation state just upstream of the secondary critical cross section, and P_x, T_x, P_y, T_y are determined by the strength of the moving shock M_x. One notes that

$$M_x = M(X) - S/c_x \tag{3}$$

and $M(X)$ is the local (supersonic) Mach number in the

Table 2 I/O for analysis of components 3 and 6 of Table 1

```
Fanno line, supersonic/subsonic flow with moving shock
After sudden enlargement in cross section, HHK 04/01/82
2-D geometry, linear area ratios
Equivalent pipe diameter = 4*H*B/(2H + 2B), channel
Adiabatic compressible channel flow
Airflow

Stagnation temperature (deg C) = 20
Gas constant = 286.9175 Gamma = 1.4 Abs. temp. (deg R) = 273
H, throat = 0.0135 H0, Exit = 0.017 H1, channel = 0.025 H2,
  Width = 0.0127 Length, ch. = 0.101

Effective second-throat height (m) = 0.02
Stagnation pressure P0 (Pa) = 325000
Primary nozzle area ratio = 1.259259
Channel: equivalent diameter = 0.0168435 Length (m) = 0.101
Absolute roughness (mm) = 0.002
Relative roughness = 1.187402E-04

Base pressure ratio P,b/P,e = 0.55
Note that the Second Law imposes an upper limit on the
  one-dimensional interpretation of a supersonic flow
  adjustment after an abrupt expansion

Supersonic solution
Gamma = 1.4 A/A* = 1.259259
M = 1.611092
P/P0, exit = 0.2314324
Base pressure ratio P,b/P,0 = 0.1272878
M1 = 2.013775 P1 = 0.1153115 P1(Pa) = 37476.25
  P1, SUP/P0 = 0.9217989
Theta, E = 0.265088 Theta, 8 = 0.4616662
Expansion angle (deg) = 11.2631
Attachment distance = 1.607957E-02
Reynolds no. = 6962126 Friction factor = 0.0126567

Next shock location
Shock location at x = 6.698183E-02
  L = 5.090226E-02 MF = 1.88895 Local pressure P/P0 = 0.126378
Local stagnation pressure ratio P0,L/P0 = 0.8324878
Wave Mach number ( + if upstream) = 5.050253E-02
Subsonic Fanno line after normal (moving) shock
After normal shock, P/P,0 = 0.5330178 M,Y = 0.5882898
  M2 = 0.5495359
Stagnation pressure ratio = 0.6544596
Stagnation temp. ratio = 1.013727
At the end of the channel, Mach no. = 0.5539867
Stagnation pressure ratio = 0.6510074
```

of sound $c_x = c_o(T_x/T_{o_I})^{1/4}$. Also, although the entire flow system is adiabatic, $T_{o_{II}} \neq T_{o_I}$ due to the motion of the shock.

An iterative procedure is required for solving the system of Eqs. (2) and (3), and the normal shock relations. Since the absolute shock speed S is much smaller than the speed of sound, a computer-based numerical solution rapidly converges.

Shown in Table 2 is the input-output (I/O) printout of an IBM-PC program for the geometric and flow parameters listed. It should be noted that the selection of a flow coefficient for the second throat is required (here $c_e \sim 0.9$). Inspection of the subsonic approach Mach number to the second throat, together with the geometric contraction ratio A_{II}^*/A_c, is in direct support of the chosen value and which accounts for the nonuniformities of the flow in the second throat. Shown in Fig. 7 are the dimensionless shock velocities S/c_o for the test-section configuration, as highlighted in Fig. 4, for parametric values of P_b/P_e. A decrease in the absolute shock velocity is noted as the shock proceeds upstream. The relationship between momentary shock location and stagnation pressure distribution in the channel is shown in Fig. 8.

These computer results are obtained for nominal theoretical conditions as would be resulting from the channel geometry and stagnation conditions upstream of the primary nozzle. It

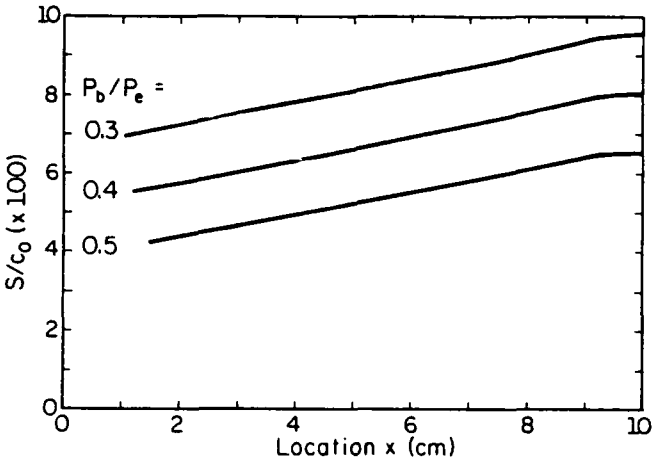

Fig. 7 Upstream dimensionless shock wave velocity.

served between these underlying assumptions and the actual processes involved.

Wake Pressure History

The process of shock wave formation and upstream motion is started by selection of a base pressure ratio P_b/P_e (used as a parameter in Fig. 7) for the closed wake. Considering the base pressure development as the result of mass entrainment by the mixing region between the jet boundary and the wall, one can determine both the steady-state base pressure and the pulldown time. For the present case, a quasisteady treatment[11] is acceptable. Although calculations were originally carried out with computer programs capable of dealing with transitional, nonsimilar mixing profiles to allow the assessment of the approaching shear layer influence,[9] a simplified approach was found to be sufficient for estimating this effect. The wake evacuation process relates the rate of change of mass contained in the base region (due to change in pressure P_w and wake shape (see Fig. 9a), which can be expressed as

$$\frac{dm_w}{dt} = \frac{H^2}{2}\left[\frac{d\rho_w}{dt}\cot\theta + \rho_w \frac{d(\cos\theta)}{dt}\right] \tag{4}$$

where $\rho_w = P_w(t)/RT_{o_f}$ and $P_w/P_{o_f} = [1 + (k-1)M^2(t)/2]^{k/1-k}$ and $\theta = \omega[M(t)] - \omega(M_E)$ with $\omega = \omega(M)$ the Prandtl-Meyer angle. The outflow of mass from the wake due to viscous entrainment along the wake boundary mixing region (approximated by a linear similarity profile, Fig. 9b) is given by

$$\frac{dm_w}{dt} = -\left(\frac{1}{2C^2}\right)\ell_n\left(\frac{1-\phi_j^2C^2}{1-\phi_d^2C^2}\right)(1-C^2) \times M(t)\left(1+\frac{k-1}{2}M^2\right)^{1/2}\left(\frac{k}{RT_{o_f}}\right)^{1/2} P_w \frac{H}{\sigma \sin\theta} \tag{5}$$

where $C^2 = M^2/[[2/(k-1)] + M^2]$, $M = M(t)$, and σ is the empirical mixing spread parameter related to $M(t)$ by $\sigma \simeq 12 + 2.76\,M(t)$. The velocity ratio for the zero streamline is

$$\phi_j = \left\{1 - (1-C^2)\exp\left[\log\left(\frac{1+C}{1-C}\right)/C - 2\right]\right\}^{1/2}/C \tag{6}$$

The velocity ratio for the stagnating streamline (neglecting the correction for incomplete turning of the freestream near reattachment[12,13]), which here compensates for neglecting the effects of finite boundary-layer thickness and sublayer transition,[14] will be

$$\phi_d = [1 - (M_e/M)^2]^{1/2} \tag{7}$$

Since all variables can be expressed in terms of the Prandtl-Meyer angle $\omega(t)$, the system of Eqs. (4–7) can be solved for

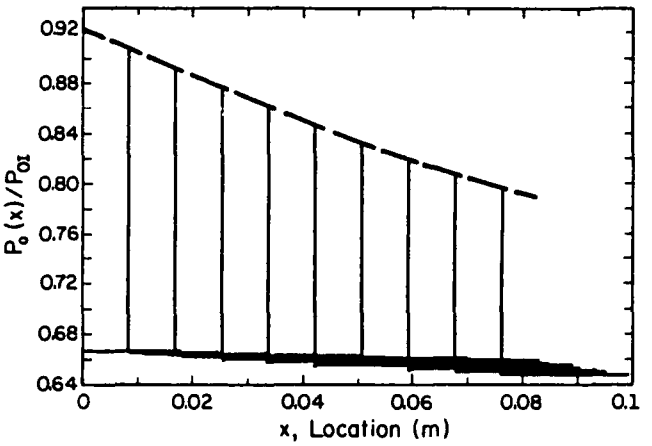

Fig. 8 Dissipation levels in channel as a function of shock wave position in channel.

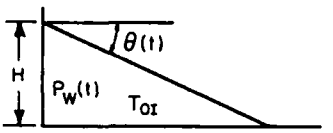

Fig. 9a Wake evacuation components.

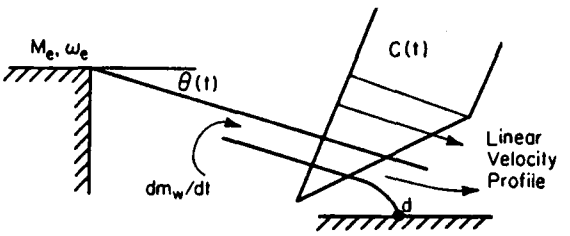

Fig. 9b Base pressure history during wake pumpdown (same operating conditions as Fig. 5).

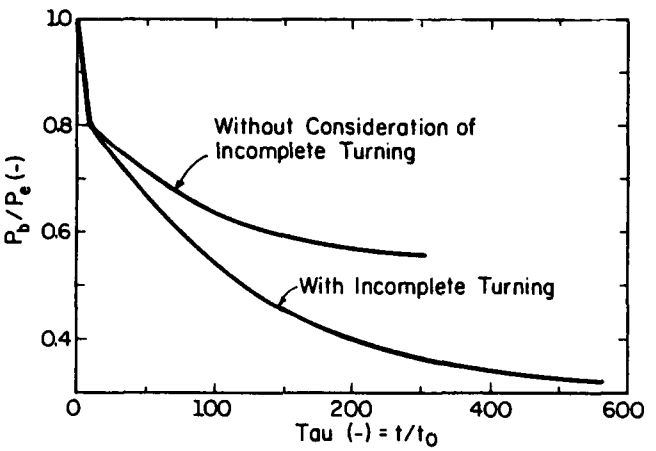

Fig. 10 Wake evacuation history using linear similarity profiles.

given values of k and M_e as a function of the dimensionless independent variable $\tau = t/t_o$ where the reference time is

$$t_o = H/(kRT_{o_f})^{1/2} \tag{8}$$

Shown in Fig. 10 is the solution for $k = 1.4$, $M_{1_e} = 1.611$ and for conditions consistent with the shock wave motion analysis, air, $H = 0.008$ m, $T_{o_f} = 293$ K. It is of interest to note that an asymptotic value of $P_w/P_e = 0.55$ is reached, which agrees well with the measured level of the lowest base pressure. Also

shown is the wake evacuation history for similarity profile mixing, but with consideration of incomplete turning of the freestream. Both the more detailed theoretical calculations[9] and the experimental evidence confirm the expectation that the wake evacuation will be characterized in the present case where $c_o \approx 343$ m/s, and $H = 0.008$ m, by a value of $\tau = 100$.

Component Synthesis

The different flow mechanisms that have been treated separately can actually occur within overlapping time spans. This will be reflected by discrepancies between theoretical and experimental results, as will be discussed later.

Of importance, however, are some observations made based on the hydraulic analogy studies:

1) Within a full cycle, the time requirements for upstream motion of the wave system together with the wake pulldown appear to dominate.

2) The wave system forms somewhat upstream of the second throat (a distance approximately equal to A_{II}^* [see Eq. (9)]), as should be expected considering the pattern of streamlines ahead of a constriction.

3) Pulldown of the wake in its final stages is simultaneous with the expulsion of the stored mass, so that the latter process seemingly does not have to be allowed specific time within the cycle.

4) When the wave system reaches the end of the wake, the penetration of the high pressure behind the shock into the wake is rapid and produces nearly parallel outflow from the primary nozzle, so that a new pulldown of the wake will again start.

In addition, the analytical treatment of the dissipation mechanisms leading to imbalance between critical mass flow rates in the primary and secondary throats has shown that: 1) the nonacoustic nature of the wave system kinematics exemplified by large pressure amplitudes and high relative shock front velocities capable of traveling upstream against the supersonic flowfield, 2) the low absolute shock wave velocities during the upstream travel together with evacuation times establish representative time scales for the cyclic operation, and 3) the slow absolute propagation velocity of the shock wave allows the prediction of the geometrical and operational parameters for which cyclic system performance can be expected (Fig. 6). As can be expected by inspection of the schematic flow pattern of Fig. 1, the component treatment must have serious shortcomings with respect to channel length scales. Indeed, the treatment of the shock system by lumping its dissipative mechanisms into a normal shock front, although representative for flow conditions produced near the end of the channel, lacks realism as increasing mass storage pushes the entire pattern upstream.

Because of these factors, the analysis can only provide reasonable information on peak pressures, but remains somewhat speculative with respect to cycle frequencies even though it establishes a plausible time scale. It is here suggested that a reasonable estimate for cycle frequencies can be based on the following scheme: 1) one selects an effective channel length

$$L_{\text{eff}} = L_c - H\cot\theta - A_{II}^* \tag{9}$$

for determining a dimensionless wave travel time

$$\Delta\tau_V = \Delta t_V / c_o = L_{\text{eff}}/(S/c_o) \tag{10}$$

(from Wave System section), 2) using the dimensionless wake evacuation time $\Delta\tau_w = \Delta t_w c_o / H$ (from Wake Pressure History section), and 3) considering only these two contributing time increments, the cycle frequency should be of the order of

$$f = c_o/[[L_{\text{eff}}/(S/c_o)] + H\,\Delta\tau_w] \tag{11}$$

IV. Experimental Program

The experimental program had several purposes. First, it was necessary to determine those geometrical and operational parameters that clearly cause unsteady operation. In all the experiments, unsteady flow means the occurrence of large, periodical pressure changes in the system, characterized and accompanied by base pressure oscillations. Second, it was important to have channel and base time-dependent static and stagnation pressure data to allow for corroboration of the theoretical models and a deeper understanding of the unsteady phenomena. Finally, one needed base pressure pulldown times data in order to obtain time and pressure scales of the important item-dependent fluidic entrainment mechanisms.

Diagnostic Experiments – Water Table

The most useful information resulted from detailed, exhaustive observations of the cyclic operations at different parametric conditions. These observations were recorded in the form of comments, drawings, sketches, still photographs, moving pictures, and videotapes.

Two-Dimensional Airflow Experiments

The geometrical parameters studied were (see Fig. 4) backstep height H, channel length L, channel height D, the secondary nozzle throat A_{II}^*, and the primary nozzle throat A_I^*. The operational parameters included only plenum stagnation pressure because facilities for back-pressure variation were neither needed nor provided. Static pressure taps for time-averaged measurements were placed along the line of symmetry for the two-dimensional system, and along the external walls for both axisymmetric[9] and two-dimensional channels.

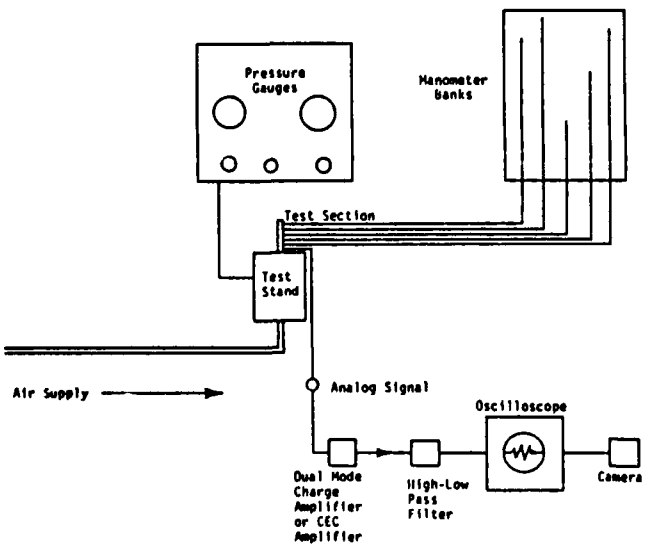

Fig. 11 Data acquisition flow diagram for channel pressure history experiments.

Table 3 Configurations tested for diagnostic two-dimensional data acquisition[a]

$N_{c_{II}}^*/H$	4, mm	5, mm	6, mm	7, mm	8, mm	9, mm	10, mm
18 (mm)	1[b]	5					
19	2	6	10				
20	3	7	11	15	20	25	
21	4	8	12	16	21	26	30
22		9	13	17	22	27	31
23			14	18	23	28	32
24				19	24	29	33
25							34
Open[c]	35	36	37	38	39	40	41

[a]All configurations tested at $L = 76$ mm, 101 mm, $M_{e_I} = 1.61$ (nominal); all configurations tested at $P_{o_I} = 15, 25, 35, 45, 55$ psig.
[b]Number assigned for the configuration case.

All of the experiments were carried out at the continuous-flow facilities of the Department of Mechanical and Industrial Engineering Gas Dynamics Laboratory. These continuous-flow stands allow for accurate control over a wide range of stagnation chamber pressures. The test stands include attachments to an illuminated manometer bank where static pressures are displayed for photographic recording.

A high-frequency transducer was placed in the base region where the pressure fluctuations are most significant, as is emphasized in the analysis. Fast Fourier analysis of the transducer signals on selected parametric combinations was performed to obtain power spectra information. Base pressure spectral analysis permitted the detection of weak or incipient wave formations, whose traces on the oscilloscope do not show clearly strict periodicity. A data acquisition flow diagram is presented in Fig. 11. The computer systems used for data processing and reduction included HP 9800, Cyber 175, and PDP 11-34 systems. Table 3 lists the test cases for the two-dimensional experiments.

Channel and Base Pressure History Experiments

Figure 12 offers an overall view of the two-dimensional test section in which one can see the configuration and the transducer tap locations. A single transducer tap is used for the permanent placement of the base area transducer. The transducer taps are 0.25 in. apart and the "zero-volume" transducer mount is bolted onto this plate at the desired test location.

The locations of pressure taps used are marked on the figure by a letter code. Only one set of geometrical and operational parameters was tested. Table 4 presents the actual transducer locations along with the rest of the pertinent information.

An oscilloscope coupled with an amplifier and transducer excitation voltage supply displayed the pressure signals. Simultaneous recording of more than two transducers was not possible, which led to the placement of one transducer permanently at the base region to serve as phase reference in the cycle. The signals were then photographed for further digitization and data processing. Data reduction and plotting was achieved by computer programs based on the Cyber 175 and HP 9800 systems. The results from these tests are presented in Tables 5 and 6.

V. Comparison of Theoretical and Experimental Results

A large body of experimental data[9] is available for examination with the main objective of finding whether a highly simplified theory can provide useful information on the following practical questions: 1) under what conditions will nonsteady near-cyclic operation be expected, 2) if nonsteady operation is occurring, what pressure peaks will be anticipated, and 3) can cyclic frequencies be predicted.

Although the development of computer programs has made it possible to deal in principle with all of the geometrical and operational parameters germaine to the problem, only a few, but typical cases have been selected here for the purpose of comparison.

In addressing item 1 above, Fig. 6 shows that the geometrical parameters for producing nonsteady operation can be predicted (additional restrictions are low-speed motion of the rocket $V_R < S$ and L large enough to allow plume attachment ahead of the channel exit restriction).

With respect to item 2, Fig. 13a indicates that the static pressure peaks predicted by the theory are verified to occur in a region slightly upstream of the channel restriction (see Fig.

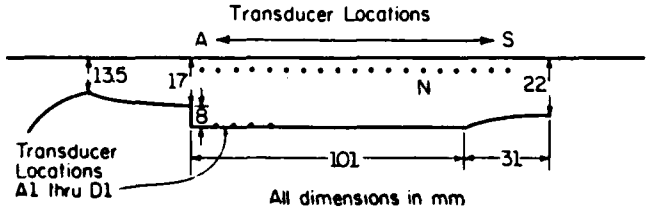

Fig. 12 Two-dimensional configuration for channel pressure history acquisition showing dimensions and transducer locations.

Table 4 Transducer locations in the two-dimensional test configuration[a]

Transducer location	Distance from nozzle exit, mm	Transducer location	Distance from nozzle exit, mm
Locations 5 mm from symmetry line			
A	4.0	K	67.5
B	10.35	L	73.85
C	16.7	M	80.2
D	23.05	N	86.55
E	29.14	O	92.9
F	37.75	P	99.25
G	42.1	Q	105.6
H	48.25	R	111.95
I	54.8	S	118.3
J	61.15		

Locations along backstep wall

Transducer location	Distance from backstep (mm)
A1	8.4
B1	15.4
C1	22.5
D1	30.1

[a]Test configuration: $M_{e_I} = 1.585$ (nominal 1.611), $h = 8$ mm, $H^*_{e_{II}} = 22$ mm, $L = 101$ mm, $P_{o_I} = 74.5$ psia, $H_{e_I} = 19$ mm.

Table 5 Experimental results for test configurations where nonsteady operation occurred in two-dimensional diagnostic experiments; $L = 76$ mm (see Fig. 4)

H, mm	A_I^*/A_{II}^*	$H^*_{e_{II}}/D$	P_{Atm}/P_{o_I}	P_b/P_{e_I}/Avg[a]	f, Hz
10	0.587	0.85	0.3	0.963	230
	0.587	0.85	0.25	0.90	234
	0.587	0.85	0.215	0.96	213
	0.614	0.815	0.25	1.02	165
	0.614	0.815	0.215	0.99	160
9	0.587	0.885	0.3	0.796	235
	0.587	0.885	0.25	0.776	250
	0.587	0.885	0.215	0.765	245
	0.614	0.846	0.3	0.83	240
	0.614	0.846	0.25	0.83	222
	0.614	0.846	0.215	0.813	217
8	0.587	0.92	0.375	1.03	210
	0.587	0.92	0.3	0.535	180
	0.587	0.92	0.25	0.507	166
	0.587	0.92	0.215	0.498	178
	0.614	0.88	0.3	0.601	188
	0.614	0.88	0.25	0.573	182
	0.614	0.88	0.215	0.570	190
7	0.587	0.96	0.375	0.605	177
	0.614	0.916	0.3	0.553	205
	0.614	0.916	0.25	0.516	195
	0.614	0.916	0.215	0.508	208
6	0.614	0.956	0.3	0.535	181
	0.614	0.956	0.25	0.507	181
	0.614	0.956	0.215	0.488	200
5	0.643	0.9546	0.375	– –	185
	0.675	0.909	0.25	– –	186
	0.675	0.909	0.215	– –	166

[a]As obtained from manometer readings.

Table 6 Experimental results for test configurations where nonsteady operation occurred in two-dimensional diagnostic experiments; L = 101 mm (see Fig. 5)

H, mm	A_i'/A_{ii}'	H_{ii}^*/D	P_{Atm}/P_{o_1}	P_b/P_{e_1}/Avg[a]	f, Hz
10	0.587	0.85	0.3	0.7278	143
	0.614	0.815	0.3	0.87	156
	0.614	0.815	0.25	0.839	161
	0.614	0.815	0.215	0.838	173
9	0.587	0.885	0.375	0.7638	142
	0.614	0.846	0.3	0.7695	156
	0.614	0.846	0.25	0.7465	166
	0.614	0.846	0.215	0.7408	166
	0.614	0.846	0.1875	0.7317	166
8	0.563	0.96	0.375	0.624	278
	0.587	0.92	0.375	0.745	172
	0.614	0.88	0.3	0.782	162
	0.614	0.88	0.25	0.776	160
	0.614	0.88	0.215	0.761	166
7	0.643	0.875	0.375	0.971	125
	0.643	0.875	0.3	0.779	155
	0.643	0.875	0.25	0.7604	155
	0.643	0.875	0.215	0.7540	160
	0.643	0.875	0.1875	0.743	155
6	0.614	0.913	0.375	0.7378	155
	0.653	0.956	0.3	0.882	133
	0.643	0.913	0.25	0.879	123
	0.643	0.913	0.215	0.866	120
5	0.643	0.9545	0.375	0.904	108
	0.643	0.9545	0.3	0.868	136
	0.643	0.9545	0.25	0.841	138
	0.643	0.9545	0.215	0.845	142

[a]As obtained from manometer readings.

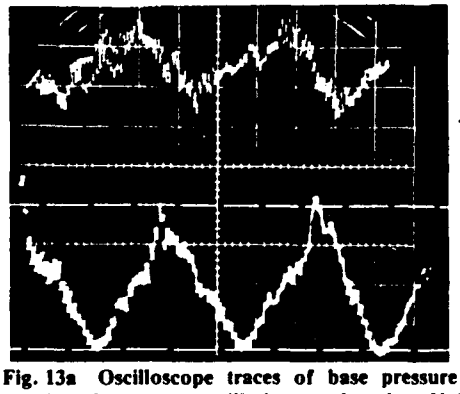

Fig. 13a Oscilloscope traces of base pressure oscillations (lower trace) and pressure oscillations at location N (upper trace) in the two-dimensional channel (see Fig. 7).

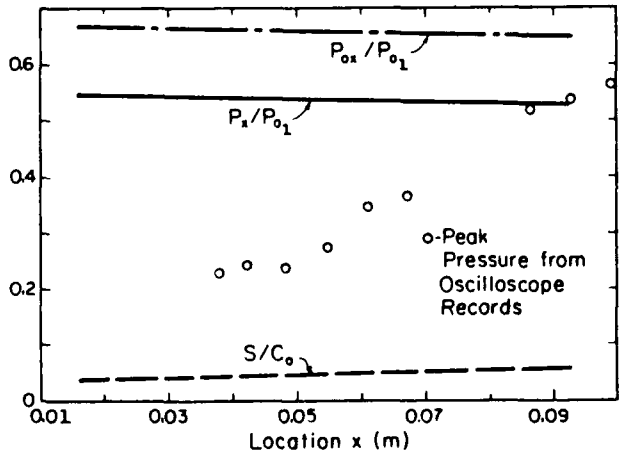

Fig. 13b Traveling shock wave characteristics as a function of location in channel.

13b). With reference to Fig. 1, it is easy to understand why the theoretical assumption of a single normal shock wave does not hold for the region of complex oblique-wave interactions in the upstream portion of the channel, yet produces reasonable results once the flow pattern becomes nearly uniform and entirely subsonic. The prediction of cyclic frequencies (item no. 3) is rendered difficult by the overlapping nature of events treated separately by the theory. Yet, for the selected cases (L_1 = 0.10 m and L_2 = 0.076 m, Tables 5 and 6), it is gratifying to observe that an estimate based on Eq. (11) yields the reasonable results shown below:

	Theory	Measured
$L_1 = 0.101$	167.6	162.7 ± 2.5
$L_2 = 0.076$	193.53	186.7 ± 3.4

VI. Conclusions

Supported by qualitative studies using the hydraulic analogy and high-speed air experiments with two-dimensional (and axisymmetric) channel models, component flows mechanisms have been delineated subjected to theoretical analysis and synthesized into an overall operational model. It has been shown that the problem of nonsteady rocket plume-wall interactions during initial launch phases can be attacked by highly simplified theoretical concepts to yield useful information on peak pressures and cycle frequencies.

Acknowledgment

This work was supported in part by the U.S. Army Research Office, Research Grant DAAG 29-79-C-0184.

References

[1]Page, R. H., "A Review of Component Analysis of Base Pressure for Turbulent Flow," *Proceedings of the Tenth International Symposium on Space Technology and Science*, Tokyo, Japan, Sept. 1974.

[2]Alpinieri, L. J. and Adams, R. M., "Flow Separation Due to Jet Pluming," *AIAA Journal*, Vol. 4, Oct. 1966, pp. 1865-1866.

[3]Batson, J. L. and Bertin, J. J., "Rocket Exhaust Flow in Tube Launchers," *Journal of Spacecraft and Rockets*, Vol. 11, Nov. 1974, pp. 739-790.

[4]Rockwell, O., "Oscillations of Impinging Shear Layers," *AIAA Journal*, Vol. 21, May 1983, pp. 645-664.

[5]Meier, G. E. A., Grabitz, G., Jungowski, W. M., Witczak, K. J., and Anderson, J. S., "Oscillations of the Supersonic Flow Downstream of an Abrupt Increase in Duct Cross-Section," Max-Planck Inst., Goettingen, Federal Republic of Germany, Rept. 65, 1978.

[6]Jungowski, W. M., "Some Self-Induced Supersonic Flow Oscillation," *Progress in Aerospace Science*, Vol. 18, Jan. 1978, pp. 151-176.

[7]Chen, C. P., Sajben, M., and Kroutil, J. C., "Shock-Wave Oscillations in a Transonic Diffuser Flow," *AIAA Journal*, Vol. 17, Oct. 1979, pp. 1076-1083.

[8]Bogar, T. J., Sajben, M., and Kroutil, J. C., "Characteristic Frequencies of Transonic Diffuser Flow Oscillations," *AIAA Journal*, Vol. 21, Sept. 1983, pp. 1232-1240.

[9]Marongiu, M., "Mechanisms Controlling Non-Steady Plumes-Wall Interactions in Rocket Launch Tubes," Ph.D. Dissertation, Dept. of Mechanical and Industrial Engineering, Univ. of Illinois at Urbana-Champaign, IL, July 1985.

[10]Korst, H. H. and Bertin, J. J., "The Analysis of Secondary Flows for Tube-Launched Rocket Configurations," *Journal of Spacecraft and Rockets*, Vol. 20, Jan.-Feb. 1983, pp. 35-42.

[11]Ihrig, H. K. Jr. and Korst, H. H., "Quasi-Steady Aspects of the Adjustment of Separated Flow Regions to Transient External Flows," *AIAA Journal*, Vol. 1, 1963, pp. 934-936.

[12]Carriere, P., Sirieix, M., and Delery, J., "Methodes de Calcule des Ecoulements Turbulents Decolles en Supersonique," *Progress in Aerospace Sciences*, Vol. 16, 1975, pp. 385-429.

[13]Page, R. H., Hill, W. G., Jr., and Kessler, T. J., "Reattachment of Two-Dimensional Supersonic Turbulent Flows," American Society of Mechanical Engineers Paper 67-FE-20, May 1967.

[14]Chapman, D. R. and Korst, H. H., "Theory of Base Pressures in Transonic and Supersonic Flow," *Journal of Applied Mechanics*, Vol. 24, 1957, p. 484.

SECTION A.2

A REVIEW OF THE FLUID DYNAMIC ASPECT OF THE EFFECT OF BASE BLEED

Presented at the First International Symposium on Special Topics in Chemical Propulsion: Base Bleed

Athens, Greece

November 1988

by

J. Sahu and W. L. Chow

A REVIEW OF THE FLUID DYNAMIC ASPECT OF THE EFFECT OF BASE BLEED

J. Sahu
Aerospace Engineer
Computational Aerodynamics Branch
U.S. Army Ballistic Research Laboratory
Aberdeen Proving Ground, MD 21105

and

W. L. Chow*
Professor of Mechanical Engineering
Department of Mechanical and Industrial Engineering
University of Illinois at Urbana-Champaign
1206 West Green Street
Urbana, IL 61801

ABSTRACT

The fluid dynamic aspect of the effect of base bleed is briefly reviewed. Earlier understandings on the basis of interaction between the viscous and inviscid streams can adequately explain the three different flow regimes as results of base bleed. The effect of energy addition to the wake has also been ascertained from this approach. With the detailed numerical computations of the flow by solving the Navier-Stokes Equations becoming available, the effect of base bleed can be illustrated by providing appropriately boundary conditions of the bleed at the base.

INTRODUCTION

Flow studies on the pressure prevailing behind the blunt based bodies in flight have been prompted by the considerable importance in its practical applications. Since this pressure--the base pressure, is usually much lower than that of the free stream, it constitutes a major portion of the overall drag experienced by the body. Although early studies of low speed flow around blunt based bodies tended to be overshadowed by the phenomenon of vortex shedding, research initiated since the advent of high speed flight resulted in a slow unraveling of the processes and mechanisms which control and establish these flows. The essentially inviscid external stream establishes and determines the overall flow pattern including the low pressure prevailing within the major portion of the wake. On the other hand the viscous flow processes, such as the jet mixing along the wake boundary, recompression at the end of the wake and the ensuing process of flow redevelopment, establish and determine the "corresponding inviscid body geometry." Thus, a low base pressure is the result of the strong interaction between the inviscid and viscous flows; the latter being attached to the inviscid flow in the sense of the boundary layer concept. Naturally the method of controlling and reducing the base drag becomes also part of these investigations.

*Present Address: Department of Mechanical Engineering, Florida Atlantic University, Boca Raton, FL 33431

interactions. It may also be conjectured that similar phenomenon also exists for other flow regimes of the slip stream.

Through a similar consideration, the effect of heat addition into the wake through conducting walls on the base pressure has also been examined [7]. Figure 6 presents a set of results for a flow past a backward facing step showing the influence of heat addition (or exaction) on the base pressure ratio without any mass addition, while Fig. 7 shows the effect of both mass and heat addition for the same problem. Experimental verification on the effect of heat addition is also presented in Fig. 8 [7]. Obviously heat addition provides the same favorable influence as the mass bleed.

The methods of analysis on viscous flow recompression and redevelopment were improved and developed later [8-12]. These more refined analyses have been employed to study base pressure problems in supersonic, incompressible and transonic flow regimes. specifically, the study of transonic flow past a projectile based on an equivalent body concept yielded the detailed breakdown of the fore-body drag, the skin friction, and the base drag. Indeed, the base drag is always a major portion of the total drag experienced by the projectile (see Fig. 9). The merit of boattailing has also been substantiated and explained [12]. It is conceivable that the effect of base bleed may be examined with these improved analyses. Since the schemes of large scaled numerical computations have been developed, this effort has not been pursued.

STUDIES THROUGH SOLVING THE NAVIER-STOKES EQUATIONS

As more powerful (both in speed and memory space) digital computers become available, it is quite popular to examine flow problems by solving the Navier-Stokes equations with adequate turbulence modeling. Indeed one of the major research activities of the first author has been the study of base pressure problems with or without bleed, by solving the Navier-Stokes equations in the transformed coordinates. Upon adopting a thin-layer approximation of the transformed Navier-Stokes equation, the phenomena of base bleed in any of the foregoingly described flow regimes can be completely predicted from this approach by simply providing the appropriate boundary conditions in the base region (conditions of the bleeding jet). Results obtained by the first author and his colleagues [13-17] have supported the observed influences of the base bleed throughout all three flow regimes. Figure 10 shows the detailed streamline pattern of the flow within the regime I, where all mass of bleed has been entrained into the mixing region. It can be easily observed from this figure that i) the horizontal bleed core flow persists farther downstream within the wake for a larger mass bleed parameter (I) before it is completely entrained into the mixing region, and ii) judging from the shade simulating the Prandtl-Meyer expansion at the corner, larger mass bleed parameter corresponds to a higher base pressure ratio. Indeed, this increase in pressure is also observed in the early phase of the bleed for the case shown in Fig. 11. Figure 11 also shows a drop in the base pressure ratio for a higher stagnation pressure of the bleeding jet (or a larger bleed parameter) which corresponds to the flow conditions within the Regime II. A detailed streamline plot does indicate that some of the bleed flow can penetrate the downstream region of a higher pressure (see Fig. 12). Figure 13 shows the case of higher jet stagnation pressure ratios, where the bleed

stream becomes a plumming jet. This is obviously the flow condition in Regime III. The base pressure increases as the stagnation pressure (or the static pressure) of the jet is increased. A detailed streamline flow pattern of the plumming jet is shown in Fig. 14. The interaction between the jet and the free stream results in a pair of recirculating bubbles in the near wake. Many other investigators have also computed the popular MICOM problem [18-20] within this flow regime.

For all these numerical computations, there is only the effect of mass bleed if the stagnation temperature of the jet, T_{oj}, equals to that of the free stream, $T_{o\infty}$. Should $T_{oj} > T_{o\infty}$, the results corresponds to the combined influences of both the mass and energy additions. Such a simulation can easily be produced by simply changing the temperature boundary condition at the bleed exit.

CONCLUSIONS

A short review of the fluid dynamic aspect of the effect of base bleed is given. From the interactive study, it was observed that depending upon the relative level of the stagnation pressure of the bleed stream, its influence to the base pressure ratio can be classified into three distinctively different flow regimes. The effect of energy addition to the wake can also be extracted from a simple component analysis. However, since the schemes of large scaled numerical computation of the Navier-stokes equation became available, it has been shown that the effect of base bleed can be effectively simulated by providing the appropriate boundary conditions of the bleeding stream at the base. It may be anticipated that the effect of combustion by bleeding fuel into the wake may be interpreted in terms of the effects of mass and energy additions. Again, when chemical reactive computer code is incorporated into the present Navier-Stokes solver, this phenomenon can be simulated by simply specifying the concentration of various reactive species at the bleed exit.

ACKNOWLEDGMENT

The authors are grateful to Dr. W. B. Sturek and Mr. C. J. Nietubicz at the Ballistic Research Laboratory for their continued interest and guidance on the numerical computations of the base pressure problems. The second author wishes to acknowledge the support of the U.S. Army Grant DAAL03-87-K-0010, and NSF Grant No. MSM-8603985 so that large scaled numerical computations are possible.

REFERENCES

1. Chow, W. L., "On the Base Pressure Resulting from the Interaction of a Supersonic External Stream with a Sonic or Subsonic Jet," J. Aero. Sci., Vol. 26, No. 3, pp. 176-180, 1959.

2. Fuller, L., and Reid J., "Experiments on Two-Dimensional Base Flow at M = 2.4," Brit. RAE Report Aero, 2569, 1956.

3. Wimbrow, W. R., Effect of Base Bleed on the Base Pressure of Blunt-Trailing-Edge Airfoils at Supersonic Speeds, NACA RM A54A 07, 1954.

4. Bowman, J. E., Clayden, W. A., "Cylindrical Afterbodies in Supersonic Flow with Gas Ejection," AIAA Journal, Vol. 5, pp. 1524-1525, 1967; "Cylindrical Afterbodies at M_∞ = 2 with Hot Gas Ejection," AIAA Journal, Vol. 6, pp. 2429-2431, 1968.

5. Schilling, H. (1984), "Experimental Investigation on the Base-Bleed-Effect for Body-Tail-Combinations. Proc., 8th Intern. Symp. Ballistics, Amsterdam.

6. Korst, H. H., "A Theory for Base Pressures in Transonic and Supersonic Flow, Journal of Applied Mechanics, Vol. 23, pp. 593-600, 1956.

7. Page, R. H., and Korst, H. H., "Non-Isoenergetic Compressible Jet Mixing with Consideration of its Influence on the Base Pressure Problem," Proc., Fourth Midwestern Conference on Fluid Mechanics, Purdue Univ., pp. 45-68, Sept. 1955.

8. Chow, W. L., "Recompression of a Two-Dimensional Supersonic Turbulent Free Shear Layer," Devlopment of Mech., Vol. 6, Proc., 12th Midwestern Mech. Conf., University of Notre Dame Press, 1971, pp. 319-332.

9. Chow, W. L., and Spring, D. J., "The Viscous Interaction of Flow Redevelopment after Reattachment with Supersonic External Streams," AIAA Journal, Vol. 13, No. 12, pp. 1576-1584, 1975.

10. Chow, W. L., and Spring, D. J., "Viscid-Inviscid Interaction of Two-Dimensional Incompressible Separated Flows," J. Applied Mech., Vol. 43, Series E, Sept. 1976, pp. 387-395.

11. Chow, W. L., "Base Pressure of a Projectile within the Transonic Flight Regime," AIAA Paper 84-230, presented in the AIAA 22nd Aerospace Sciences Meeting, Reno, Nevada, Jan. 1984, also AIAA J., Vol. 23, No. 3, 1985, pp. 388-395.

12. Chow, W. L., "The Effect of Boattailing of a Projectile in Transonic Flow," Proc., of the Third Symposium on Numerical and Physical Aspects of Aerodynamic Flows, California State University, Long Beach, CA, Jan. 1985, 9-15 to 9-23.

13. Sahu, J., Nietubicz, C. J., and Steger, J. L., "Numerical Computation of Base Flow for a Projectile at Transonic Speeds," U.S. Army Ballistic Research Laboratory, Aberdeen Proving Ground, MD, ARBRL-TR-02495, June 1983. (AD A130293) (See also, AIAA Paper No. 82-1358, August 1982.)

14. Sahu, J., Neitubicz, C. J., and Steger, J. L., "Navier-Stokes Computations of Projectile Base Flow at Transonic Speeds With and Without Mass-Injection," ARBRL-TR-02532, U.S. Army Ballistic Research Laboratory, Aberdeen Proving Ground, MD. Nov. 1983 (see also AIAA Journal, Vol. 23, No. 9, Sept. 1985, pp. 1348-1355).

15. Sahu, J., and Nietubicz, C. J., "Numerical Computation of Base Flow for a Missile in the Presence of a Centered Jet," ARBRL-MR-3397, U.S. Army Ballistic Research Laboratory, Aberdeen Proving Ground, MD, October 1984. (AD A148784) (See also, AIAA Paper No. 84-0527, January 1984.)

16. Sahu, J., "Supersonic Flow over Cylindrical Afterbodies with Base Bleed," U.S. Army Ballistic Research Laboratory, ARRADCOM, Tech. Report BRL-TR-2742, June 1986 (see also Computational Mechanics, No. 2, 1987, pp. 176-184).

17. Sahu, J., "Computations of Supersonic Flow over a Missile Afterbody Containing an Exhaust Jet," J. of Spacecraft and Rockets, Vol. 24, No. 25, Sept.-Oct., 1987, pp. 403-410.

18. Petrie, H. L., and B. J. Walter, "Comparisons of Experiment and Computations for a Missile Base Region Flow Field with a Centered-Propulsive Jet," AIAA Paper 85-1618, 1985.

19. Venkatapathy, E., C. K. Lombard, and C. C. Luh, "Accurate Numerical Simulation of Supersonic Jet Exhaust Flow with CSCM on Adaptive Overlapping Grids," AIAA Paper 87-0465.

20. Hoffman, J. J., Birch, S. F., Hopcroft, R. G., and Holcomb, J. E., "Navier-Stokes Calculations of Rocket Base Flows," AIAA-Paper 87-0466.

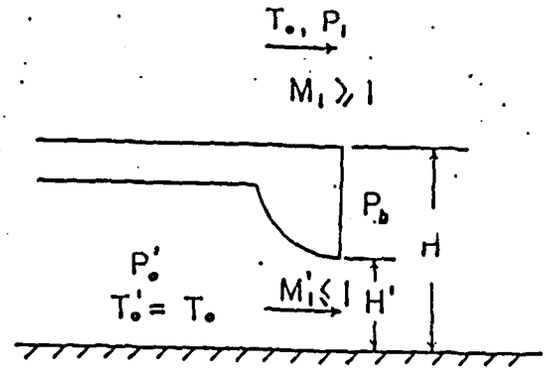

Fig. 1 Two-dimensional model

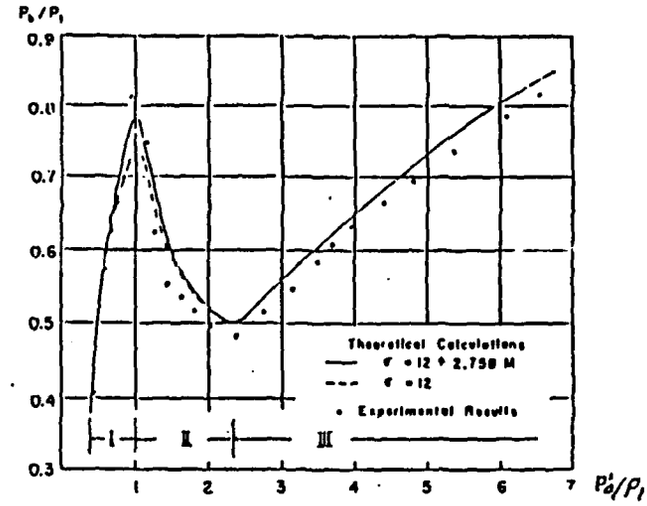

Fig. 2 The relation between P_b/P_1 and P_0'/P_1 for $M_1 = 1.92$, $H/H' = 1.94$

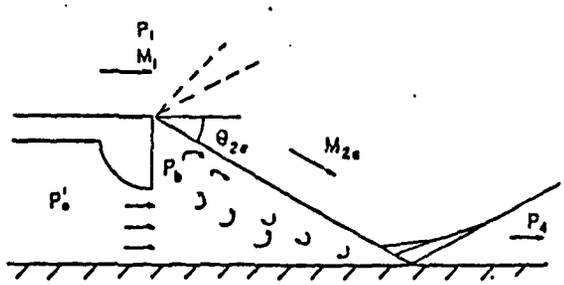

Fig. 3 Flow model for Regime 1

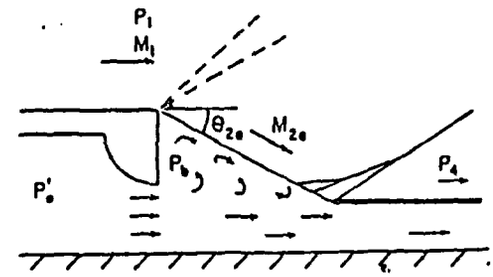

Fig. 4 Flow model for Regime 2

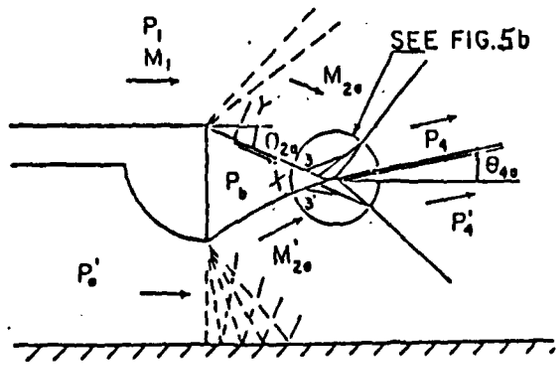

Fig. 5 Inviscid flow model for Regime III

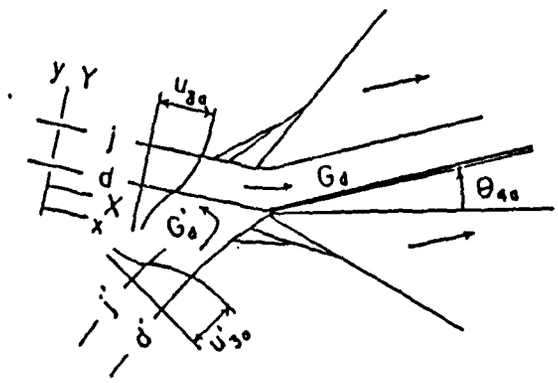

Fig. 5b Details in dissipative flow near the end of the wake

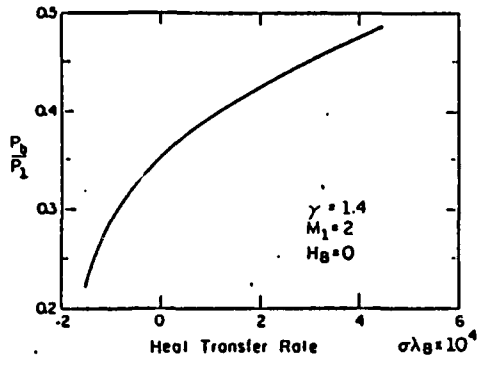

Fig. 6 The effect of heat addition on base pressure

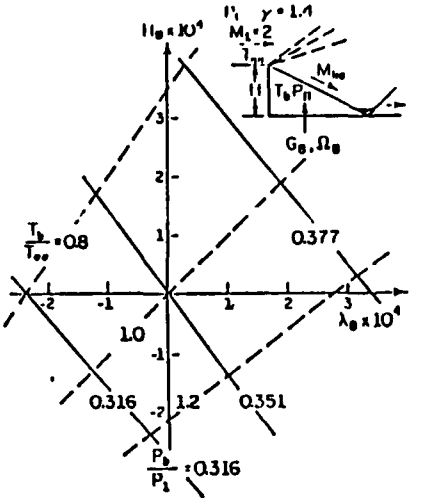

Fig. 7 The effect of both mass and heat addition

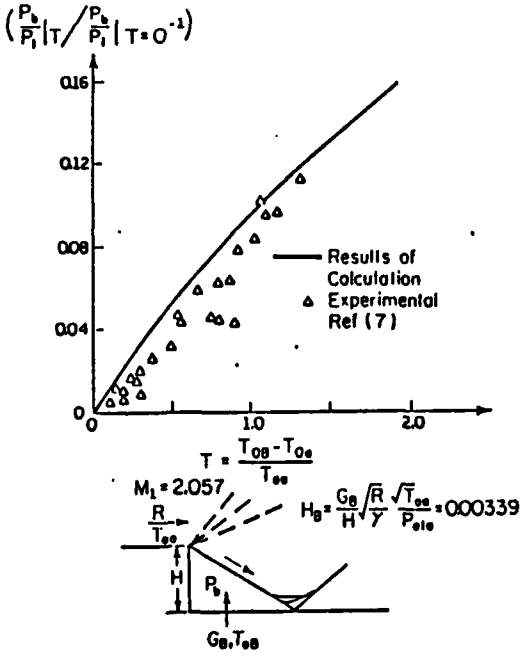

Fig. 8 Base pressure as influenced by both mass and energy additions

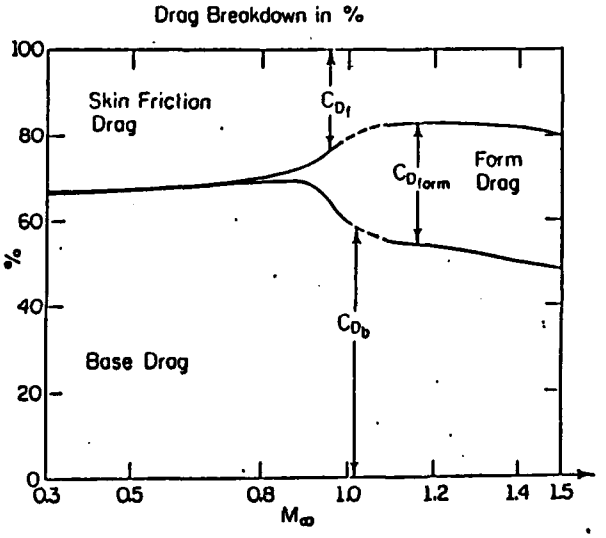

Fig. 9 Breakdown of drag characteristics of a SOC-6 projectile (based on the results obtained from Ref. [11])

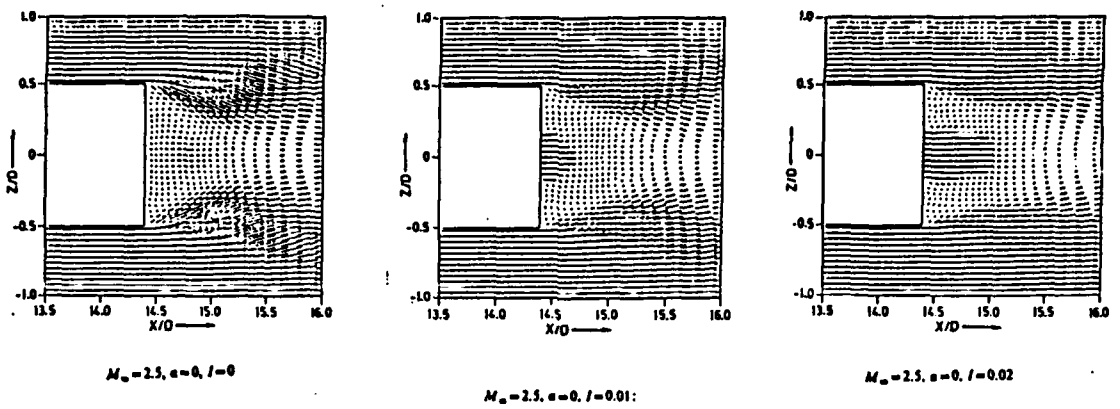

Fig. 10 Velocity vectors in the base region (from Ref. [16])

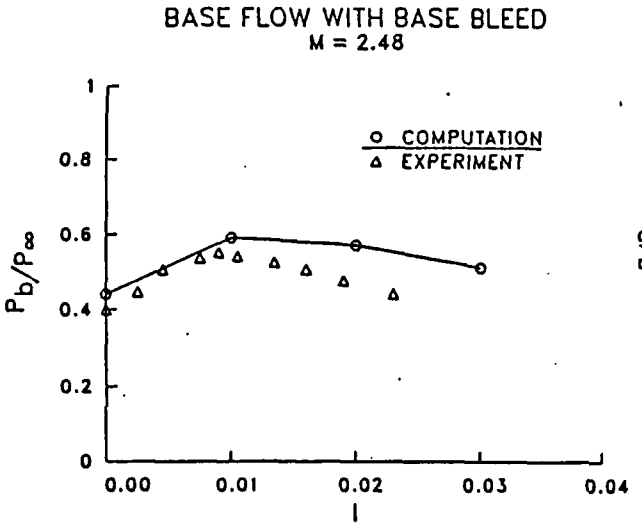

Fig. 11 Base pressure as influenced by the bleed parameter I (showing both regimes I and II)

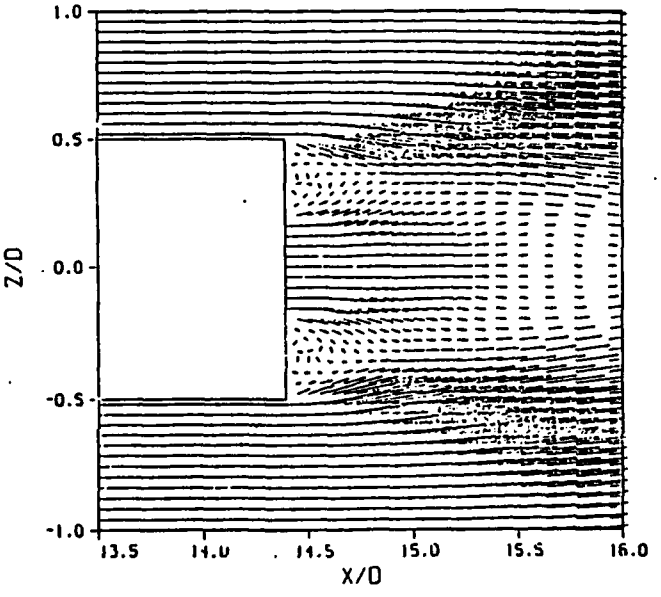

Fig. 12 Detailed velocity vectors diagram in Regime II

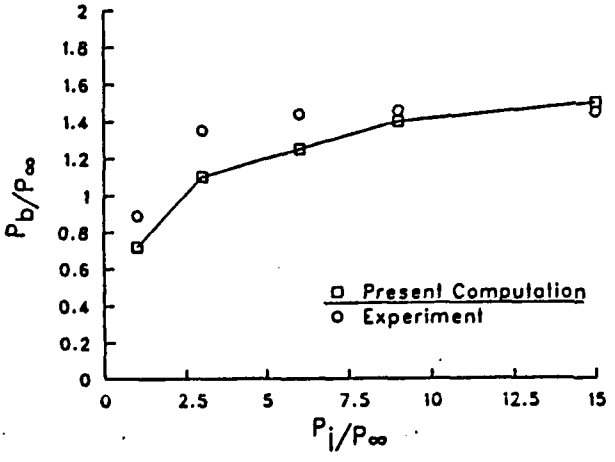

Fig. 13 Base pressure as influenced by the jet pressure ratio -- Regime III

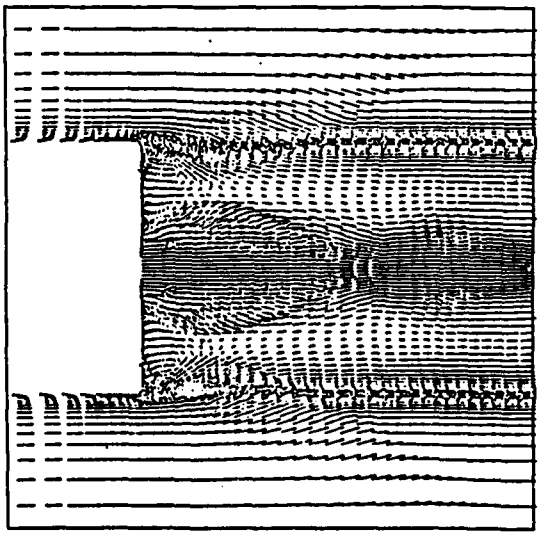

Fig. 14 Detailed velocity vectors diagram-- Regime III (M_∞ = 1.4)

APPENDIX B

SMALL-SCALE EXPERIMENTS OF HIGH-SPEED SEPARATED FLOW CONFIGURATIONS

Interaction Between Two Compressible, Turbulent Free Shear Layers

M. Samimy*
The Ohio State University, Columbus, Ohio
and
A. L. Addy†
University of Illinois, Urbana, Illinois

Experimental results of the interaction between two compressible, two-dimensional, turbulent free shear layers are presented. The shear layers were formed by geometrical separation of two high-Reynolds-number, turbulent boundary-layer flows with freestream Mach numbers of 2.07 and 1.50 from a 25.4-mm-high backward-facing step. A two-component, coincident laser Doppler velocimeter was utilized for a detailed flowfield survey. Both shear flows show general features similar to those of compressible, free shear layers reattaching onto a solid surface, including large-scale turbulence in the recompression and interaction regions and enhanced mixing in the redeveloping region. The free shear layer with the lower freestream Mach number shows high turbulence intensities and a higher rate of increase of turbulence intensities in the streamwise direction. These features appear to be caused by higher entrainment of reversed flow recirculating from the highly turbulent reattachment region.

Introduction

THE work presented herein is part of an extensive research program to investigate recompression and reattachment of compressible, turbulent free shear layers and subsequent redeveloping boundary layers. The experimental efforts of this research have focused on simple, two-dimensional, backward-facing step geometries. These types of simple models, which have fixed separation points and contain all of the features of more general separated flows, have been widely used for many years in the investigation of subsonic and supersonic separated flows.[1-9]

Three different configurations were investigated in this research program in order to gain some basic knowledge about high-velocity separated flows. In the first configuration,[6] a Mach 2.46 flow with a turbulent boundary layer separated at a 25.4-mm step and formed a free shear layer that attached onto a ramp. The position and angle of the ramp were adjusted so that the incoming boundary layer separated at the step without any pressure change. The detailed turbulence results showed a gradual increase of turbulence intensities and shear stresses through the constant-pressure shear layer, a strong increase through the recompression and reattachment zone, and a gradual decrease after reattachment. This is in sharp contrast to incompressible shear-flow results, which show a sharp decay of turbulence intensity and shear stress upstream of the reattachment location. The maximum local turbulence intensities and shear stresses occurred around the sonic line in each transverse survey in disagreement with earlier hot-wire results,[5] which showed that these parameters peaked in the supersonic region of the shear layer. Large-scale turbulence near the lower edge of the shear layer in the reattachment region and enhanced mixing in the redeveloping boundary layer were detected, which confirmed earlier observations.[4]

In the second configuration,[7] a Mach 2.07 flow with a turbulent boundary layer separated at the step and subsequently formed a free shear layer that attached onto a flat plate parallel to the incoming boundary-layer flow direction (classic backstep geometry). The general trends of turbulence intensities and shear stresses were similar to those obtained in the first configuration with the exception of much higher fluctuation levels and higher anisotropy ratios. The differences appear to be caused by smaller size of the recirculating bubble and as a result a greater influence of the highly turbulent flow recirculating from the reattachment region. Also, the streamwise turbulence intensity increase through the separation at the step for the backstep experiment was a factor of approximately 1.3 higher than the ramp results. These results were in sharp contrast to the earlier observations by the schlieren technique[10,11] and measurements made by the hot-wire technique,[12] all of which showed a decay of the turbulence level through the expansion at the step. Some systematic experiments are needed to clarify this discrepancy.

The contributors to the measured fluctuations are the actual random turbulence fluctuations and the coherent large-scale oscillations. Since the time and length scales of the large-scale structures would be different for the two configurations, this could be another contributing factor to the observed different fluctuation levels in the ramp and backstep configurations.

In the third configuration, which is the subject of this paper, the interaction between two shear flows was investigated; see Fig. 1. The objective was the further exploration of compressible shear flows, specifically the effects of the interaction of shear flows with solid walls at reattachment on the turbulence scale and structure.

Experimental Program

A series of dry, cold air experiments was conducted in a small-scale blowdown wind-tunnel facility. The wind-tunnel test-section width and height were 50.8 and 101.6 mm, respectively, and the step height was 25.4 mm; see Fig. 1. The approach Mach number, Reynolds number, stagnation pressure, and stagnation temperature were 2.07, 5.85×10^7/m, 457.3 kPa, and 295 K, respectively, for the upper boundary layer, and 1.50, 3.37×10^7/m, 233.8 kPa, and 295 K, respec-

Received Dec. 26, 1985; presented as Paper 86-0443 at the AIAA 24th Aerospace Sciences Meeting, Reno, NV, Jan. 6-9, 1986; revision received May 15, 1986.

*Assistant Professor, Department of Mechanical Engineering. Member AIAA.

†Professor and Associate Head, Department of Mechanical and Industrial Engineering. Associate Fellow AIAA.

tively, for the lower boundary layer. The freestream Mach and Reynolds numbers after expansion at the step were 2.56 and 3.98×10^7/m, respectively, for the upper shear flow, and 2.23 and 2.72×10^7/m, respectively, for the lower shear flow. The Mach and Reynolds numbers of the upper free shear flow and two earlier configurations[6,7] were designed to be comparable for comparison of data.

For ease of presentation of the results, the dashed line in Fig. 1 is used to separate the upper and lower flows. The u velocity component direction was defined to correspond to the local freestream flow direction; parallel to the x coordinate for the incoming boundary-layer flows, rotated 12.4 deg relative to the x coordinate in a clockwise direction for the shear flow with higher M, and rotated 18.5 deg in the counterclockwise direction for the shear flow with lower M. The v velocity component is orthogonal to the corresponding u component in all cases.

A two-component, coincident laser Doppler velocimeter (LDV) system was used to make the velocity measurements. The details of data acquisition, reduction, and the errors involved have been reported earlier[6,7] and will not be repeated here. The LDV results reported here are corrected for velocity bias by using the two-dimensional velocity inverse weighting factor. The fringe bias correction was found to be unnecessary because a large focal-length lens was used in the highly turbulent region of the flowfield. Silicone oil particles with a mean diameter of approximately 1 μm were used for seeding the flow. The errors due to the spatial resolution were less than 1% for the mean flow and 1.8% for the second-order fluctuation measurements. The statistical uncertainty due to a limited number of samples was better than $\pm 2.8\%$ for the mean flow and $\pm 3.2\%$ for the turbulence-intensity measurements.

Experimental Results

The Approach Boundary Layer

Two- and one-component velocity measurements were made to within 1 and 0.25 mm of the wall, respectively. The approach boundary-layer and momentum thicknesses for the Mach 2.07 and 1.5 boundary-layer flows were measured to be (2.26 and 0.18 mm) and (1.50 and 0.14 mm), respectively. The ratio of momentum thickness to boundary-layer thickness for the upper and lower flows was approximately 5 and 1%, respectively, higher than the values predicted by the method of Maise and McDonald.[13] Based on these and earlier results,[6,7] it appears that Maise and McDonald's prediction of the ratio of momentum to boundary-layer thickness for compressible turbulent boundary layers is in better agreement with experimental results at lower Mach numbers.

Figure 2 shows the boundary-layer, mean-velocity data of the present study in comparison with the Maise and McDonald curve.[13] The Mach 1.50 boundary-layer results show better agreement with the curve than the Mach 2.07 results. The skin-friction coefficients C_f used in Fig. 2 were determined from the wall-wake law and were 0.00176 and 0.00247 for the upper and lower flows, respectively. These friction factors are in the range of values reported by Laderman[14] for comparable Mach and Reynolds numbers.

The boundary-layer, streamwise turbulence-intensity results for both flows show consistently higher values than those for the incompressible flow of Klebanoff,[15] but are in relatively good agreement with the data of Dimotakis et al.[16] at comparable Mach numbers. The boundary-layer, shear-stress results follow closely Sandborn's[17] "best estimate" for equilibrium compressible boundary layers.[6] The streamwise component of the skewness and flatness factors peak sharply at the outer edge of the boundary layers for both flows, then decline rapidly for the upper boundary layer and gradually for the lower boundary-layer flow. The Mach 2.85 turbulent boundary layers of Hayakawa et al.[18] and the Mach 2.43 results of Petrie et al.[8] showed skewness profiles similar to those of the Mach 2.07 flow of the present study.

Two-Dimensionality of the Flowfield

All of the LDV data presented herein correspond to the centerline location of the wind tunnel. The uniformity of the mean flow and turbulence field across the tunnel was checked by additional LDV measurements at ± 10 mm on either side of the wind-tunnel centerline at $x = 28$, 38, and 46 mm. The deviation of the data from the centerline values was the largest near the sonic line at $x = 28$ and 38 mm, where turbulence fluctuations were high as was the statistical uncertainty.[6-8] The maximum spanwise variation of the data for

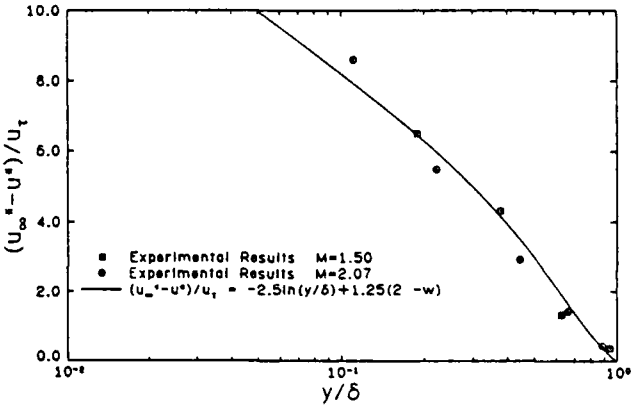

Fig. 2 Boundary-layer mean-velocity profiles and generalized curve of Maise and McDonald.[13]

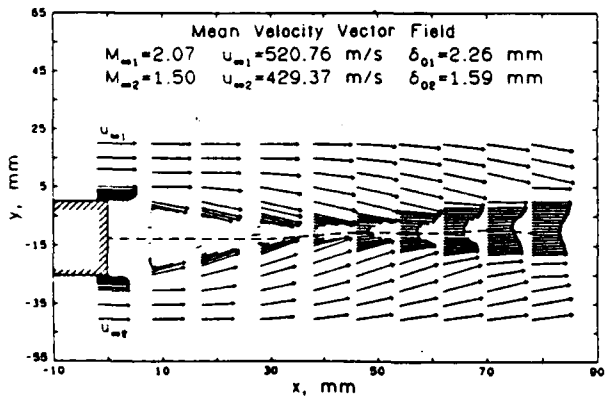

Fig. 1 Mean-velocity vector field.

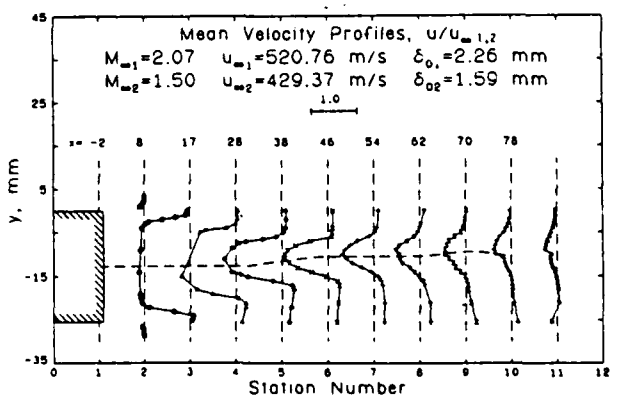

Fig. 3 Streamwise mean-velocity profiles ($u_{\infty 1,2}$ means $u_{\infty 1}$ for the higher-Mach-number flow and $u_{\infty 2}$ for the lower-Mach-number flow).

the mean-velocity, streamwise turbulence intensity, and shear stress were ±1.9, ±2.8, and ±2.5%, respectively. These variations were within the statistical uncertainty for the finite sample size of the present experiments.[6-8] Since further off-center LDV measurements were not possible due to reflections of the laser light from the glass windows of the wind tunnel, it can only be concluded that the flow was two-dimensional within ±10 mm of the centerline.

Mean Flow Results

The mean-velocity profiles for all measurement stations, including boundary-layer profiles, are shown in Fig. 3. The abscissa shows the station numbers, the vertical dashed lines indicate the location of zero velocity for each station, the numbers above the dashed lines give the x locations of the stations, and the horizontal dashed line chosen to separate the two shear flows for ease of presentation of the experimental results is also shown. The u velocity component direction was defined to correspond to the local freestream flow direction: parallel to the x coordinate, see Fig. 1, at station 1 for the incoming boundary-layer flows, rotated 12.4 deg in the clockwise direction for the higher-Mach-number shear flow, and 18.5 deg in the counterclockwise direction for the lower-Mach-number shear flow. The v velocity component is orthogonal to the corresponding u component. The velocities of higher and lower Mach number flows were nondimensionalized by $u_{\infty 1}$ and $u_{\infty 2}$, respectively, where $u_{\infty 1}$ and $u_{\infty 2}$ are the higher- and lower-Mach-number boundary-layer freestream velocities, respectively.

The mean-velocity results for both flows show similar trends up to the last three stations, where the velocity profiles exhibit a rapid "filling out." At the last three stations, the rate of profile development seems to be faster for the lower-Mach-number flow. This rapid development in the mean-velocity profiles has also been observed in redeveloping boundary layers.[4,7] Schlieren photographs of the present flowfield and earlier experiments[7] have shown the existence of large eddies stretched in the streamwise direction that seem to cause enhanced mixing in the redeveloping regions. This matter will be discussed further in the presentation of the turbulence field results.

Turbulence Field

The streamwise turbulence intensities for all stations are shown in Fig. 4. The maximum turbulence intensity at each station occurs near the sonic line for both shear flows. This is consistent with earlier LDV results[6-8] and disagrees with hot-wire results[5] that located the maximum in the supersonic region. For stations 3-7, the absolute maximum turbulence intensity at each station for the lower M flow is higher than that for the higher M flow and shows a faster streamwise growth. This could possibly be a Mach number effect, which means larger entrainment of recirculating flow coming from the highly turbulent interaction region, and/or due to the changes in the scales of coherent large-scale motions, which are one of the contributors of the measured fluctuations. The approximate location of the line separating forward and backward flows was determined to be at $x = 35$ mm from oil streaks on the glass windows. For stations 8-10, the maximum turbulence intensity at each station for both flows spreads across the shear layer and also decays in the streamwise direction. An almost uniform turbulence-intensity profile across both shear layers at the last station confirms the existence of enhanced mixing in the redeveloping region, which was also observed by the rapid development of the mean-velocity profiles in Fig. 3.

The transverse turbulence-intensity profiles are shown in Fig. 5. For the first two stations after the expansion at the step, the maximum turbulence intensity occurs around the sonic line, which is similar to the streamwise turbulence intensity. Around the onset of interaction of the two shear flows and afterwards, the peak turbulence intensity occurs at

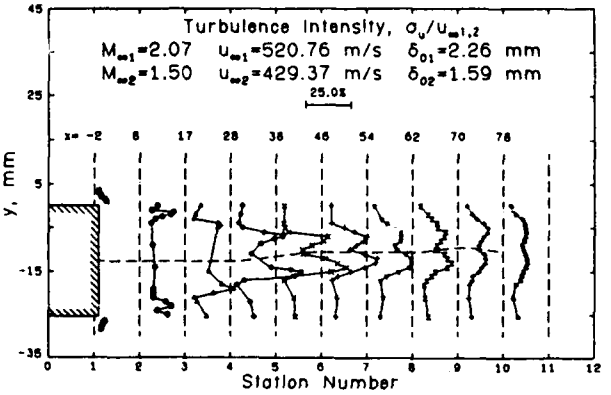

Fig. 4 Streamwise turbulence-intensity profiles.

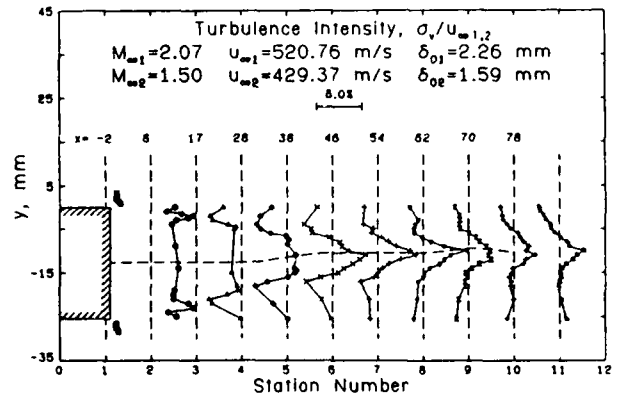

Fig. 5 Transverse turbulence-intensity profiles.

the interface region between the two flows, which shows high turbulence momentum exchange near the two flows. The anisotropy ratio σ_u/σ_v peaks near the sonic line for both flows and decays rapidly toward the interface between the two flows. As shown in Figs. 4-6, at the interface between the shear flows at the interaction region, the Reynolds shear stress is small and the anisotropy ratio is nearly unity. This type of turbulence is called isotropic turbulence in a crude sense.[19]

The evolutionary kinematic shear-stress profiles are shown in Fig. 6. The general trend, to some extent, is similar to the streamwise turbulence-intensity evolution; maximum stresses occur near the sonic line, very high shear stresses occur in the recompression and reattachment regions, and the absolute shear-stress level in the lower M flow is higher than in the higher M flow. The shear stress at the interface of the two shear flows is small, which is similar to the results for subsonic flows behind airfoils[20] and blunt bodies.[21] Growth of the maximum shear stress in both free shear layers in the streamwise direction and the existence of very large shear stresses near the onset of interaction of two shear flows in this study are consistent with earlier results where free shear layers attached onto solid surfaces.[6,7] This seems to indicate that imposition of the $v = 0$ boundary condition by the solid wall in the reattachment region does not affect turbulence intensity or scale in compressible reattaching shear flows. In contrast, for incompressible reattaching shear flows,[1,22] the $v = 0$ restriction is believed to be the cause of significant turbulence intensity and scale decay in the reattachment region. The convective velocity of large-scale motions in supersonic flows is higher than the local speed of sound.[9] Therefore, the large-scale structures are unaware of the existence of the solid walls. Thus, the breaking up process of the eddies perhaps would occur at or after reattachment. This could be a cause for the differences between subsonic and supersonic reattaching shear flows.

The axial distributions of the maximum turbulence intensities and kinematic shear stresses are shown in Fig. 7. The general trends are the same for both shear flows and similar to earlier results.[6,7] The plateau in maximum turbulence intensities in compressible flows occurs in the reattachment region, while the same type of plateau has been observed in incompressible flow about one step height before reattachment. The rate of increase of the turbulence intensity and shear stress is higher for the shear flow with the lower freestream Mach number. The growth rate of those compressible shear layers is approximately a factor of 2 or more less than the average incompressible results.[6-8] For compressible shear flows, previous work has shown that the growth rate is inversely proportional to Mach number,[23,24] which is consistent with the present results in that the lower-Mach-number shear-layer growth and entrainment rate are higher. The entrained recirculating flow coming from the highly turbulent reattachment region could be "charging up" the turbulence field of the lower shear flow, thus causing higher turbulence intensity and shear stress. Another possible cause could be the larger distortion of the turbulence field passing through the 18.5-deg expansion at the step for the lower M flow in comparison to the higher M flow with only a 12.4-deg expansion.

The ratio of the kinematic shear stress to the estimated turbulent kinetic energy is shown in Fig. 8, where k is estimated to be equal to $\frac{1}{4}(\sigma_u^2 + \sigma_v^2)$. Harsha and Lee[25] examined this parameter for boundary layers, two-dimensional and circular jets, and wakes in incompressible flow. They concluded that a value of 0.3 for this parameter is reasonable for computational purposes. Bradshaw and Ferriss[26] and Bradshaw[27] also assumed a value of 0.3 for this parameter in their compressible boundary-layer calculations. This parameter, which is often called the turbulence "structure parameter," generally does not vary significantly but, as is seen in Fig. 8, the variation in this flowfield is significant. Another turbulence "structure parameter," the shear-stress correlation coefficient defined as $u'v'/\sigma_u\sigma_v$, showed a similar trend thus confirming significant turbulence structural changes in the flowfield.

Figures 9 and 10 show two components of the turbulence triple products The results show significant increases in the triple products, which most probably means an increase in turbulence scale in the recompression and interaction regions. This is similar to results obtained in free shear layers reattaching to a solid wall, and it may be interpreted that solid boundaries in the reattachment region do not have a significant impact on the turbulence scale and turbulence intensities, Fig. 7. This is in contrast to speculation about the significant effects of solid walls at reattachment on turbulence characteristics in subsonic flows.[1,22] As discussed

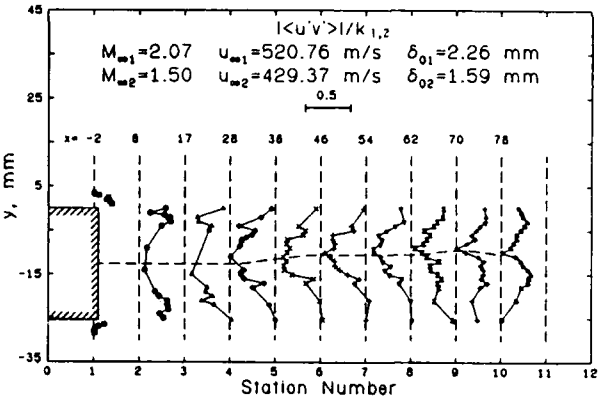

Fig. 8 Turbulence "structure parameter" profiles.

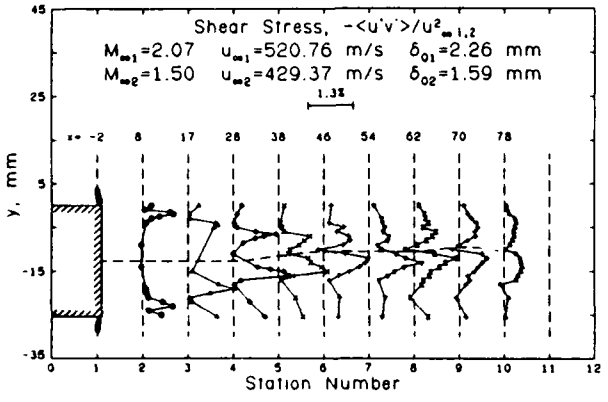

Fig. 6 Evolutionary shear-stress profiles.

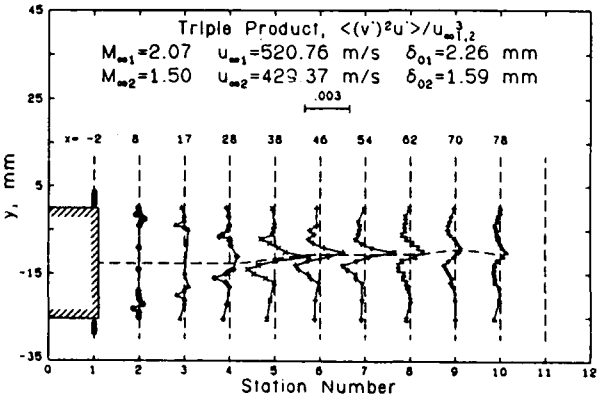

Fig. 9 Turbulent triple product.

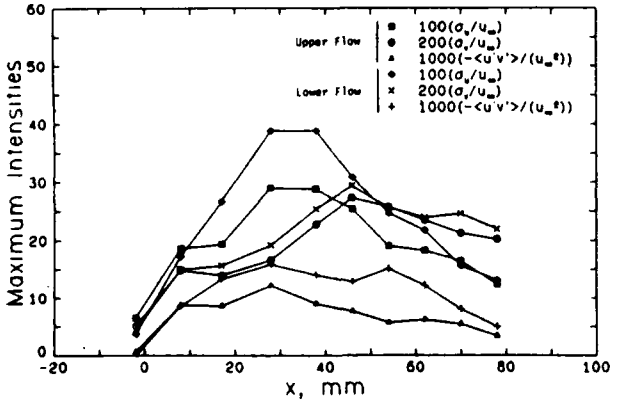

Fig. 7 Maximum turbulence fluctuations and shear stresses.

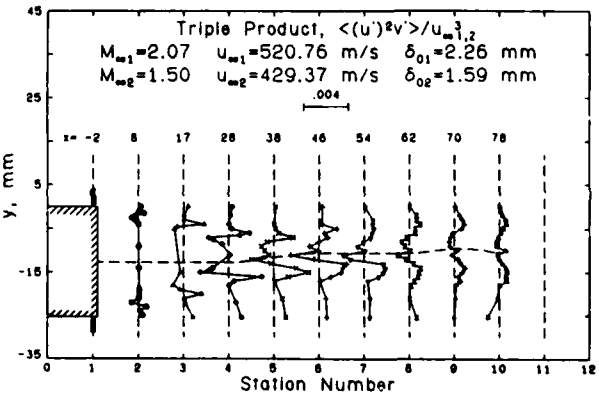

Fig. 10 Another component of the turbulent triple product.

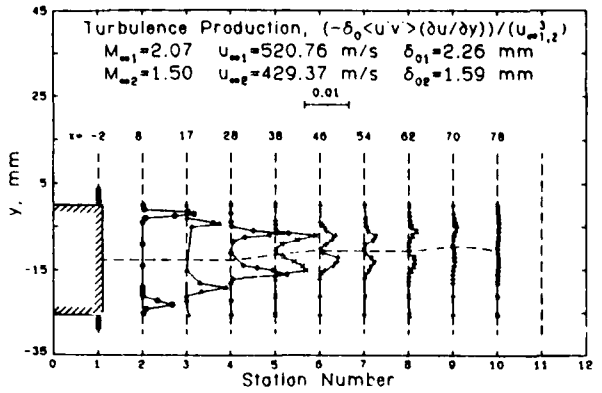

Fig. 11 Turbulence production.

earlier, the high convective velocity of large-scale eddies in supersonic shear flows could be a cause for these differences.

Two components of the triple products—namely, $\langle(v')^2u'\rangle$, Fig. 9, and $\langle(u')^3\rangle$—show behavior in the transverse direction similar to that of incompressible shear flows.[1,22] This suggests similar streamwise turbulence diffusion characteristics in incompressible and compressible shear layers. The significant difference between incompressible and compressible shear flows occurs in the $\langle(u')^2v'\rangle$ and $\langle(v')^3\rangle$ components of the triple products, which is related to the diffusion of turbulence in the transverse direction. In compressible shear flows, see Fig. 10, in the lower edge of both shear flows and also in the interaction region, turbulence diffusion is inward (toward the wind-tunnel centerline) and in the upper edges of the shear flow it is outward (away from the wind-tunnel centerline). This is opposite to incompressible shear-flow cases and seems to be a significant structural difference.

Figure 11 shows kinematic turbulence production, which excludes significant density changes through the recompression and interaction regions. Turbulence production is high in developing shear flows, which is similar to subsonic reattaching shear flows[22] and other compressible reattaching shear flows.[6,28] However, this high level of production in the recompression and onset of interaction regions have not been observed in incompressible flows. The dramatic decay of turbulence production in the redeveloping region is obviously caused by the rapid development of the mean-velocity profiles in this region, which confirms the existence of enhanced mixing and is consistent with earlier results.[28]

Conclusions

Detailed experimental results of the interaction between two free shear layers utilizing a two-component, coincident laser Doppler velocimeter have been documented. The general trends for both shear layers are the same and similar to those of compressible shear layers reattaching to solid surfaces. Therefore, in contrast to incompressible reattaching shear layers, where imposition of the $v=0$ restriction by the solid surface at the reattachment location is believed to decrease significantly the turbulence scale and intensities, this does not appear to be the case for compressible shear flows. In addition, the results have confirmed earlier findings of essential structural difference between compressible and incompressible shear flows, especially in terms of the diffusion of turbulence energy in the transverse direction. The turbulence-intensity levels and rate of increase in the streamwise direction in the shear layer with the lower Mach number were higher. This could be caused by a higher entrainment rate of highly turbulent recirculating flow, and/or by contribution from the large-scale structures.

Acknowledgment

This research was supported by the U.S. Army Research Office, Dr. Robert E. Singleton, Contract Monitor.

References

[1]Eaton, J.K. and Johnston, J.P., "A Review of Research on Subsonic Turbulent Flow Reattachment," *AIAA Journal*, Vol. 19, Sept. 1981, pp. 1093-1100.

[2]Chapman, D.R., "An Analysis of Base Pressure at Supersonic Velocities and Comparison with Experiment," NACA TN 2137, 1950.

[3]Roshko, A. and Thomke, G.J., "Observations of Turbulent Reattachment Behind an Axisymmetric Downstream-Facing Step in Supersonic Flow," *AIAA Journal*, Vol. 4, June 1966, pp. 975-980.

[4]Settles, G.S., Baca, B.K., Williams, D.R., and Bogdonoff, S.M., "A Steady of Reattachment of a Free Shear Layer in Compressible, Turbulent Flow," *AIAA Journal*, Vol. 20, Jan. 1982, pp. 60-67.

[5]Hayakawa, K., Smits, A.J., and Bogdonoff, S.M., "Turbulence Measurements in a Compressible Reattaching Shear Layer," *AIAA Journal*, Vol. 22, July 1984, pp. 889-895.

[6]Samimy, M., Petrie H.L., and Addy, A.L., "A Study of Compressible Turbulent Reattaching Free Shear Layers," *AIAA Journal*, Vol. 24, Feb. 1986, pp. 261-267.

[7]Samimy, M., Petrie, H.L., and Addy, A.L., "Reattachment and Redevelopment of Turbulent Free Shear Layers," *International Symposium on Laser Anemometry*, ASME, New York, FED Vol. 33, 1985, pp. 159-166.

[8]Petrie, H.L., Samimy, M., and Addy, A.L., "A Study of Compressible Turbulent Free Shear Layers Using Laser Doppler Velocimetry," AIAA Paper 85-0177, 1985; also, to appear in *AIAA Journal*.

[9]Ikawa, H. and Kubota, T., "Investigation of Supersonic Turbulent Mixing Layer with Zero Pressure Gradient," *AIAA Journal*, Vol. 13, May 1975, pp. 566-572.

[10]Page, R.H. and Sernas, V., "Apparent Reverse Transition in an Expansion Fan," *AIAA Journal*, Vol. 8, Jan. 1970, pp. 189-190.

[11]Small, R.D. and Page, R.H., "Turbulent Supersonic Boundary Layer Flow in the Neighborhood of a 90° Corner," *Astronautica Acta*, Vol. 18, Feb. 1973, pp. 99-107.

[12]Lewis, J.E. and Behrens, W., "Fluctuation Measurements in the Wake With and Without Base Injection," *AIAA Journal*, Vol. 7, April 1969, pp. 664-670.

[13]Maise, G. and McDonald, H., "Mixing Length and Kinematic Eddy Viscosity in a Compressible Boundary Layer," *AIAA Journal*, Vol. 6, Jan. 1968, pp. 73-80.

[14]Laderman, A.J., "Adverse Pressure Gradient on Supersonic Boundary Layer Turbulence," *AIAA Journal*, Vol. 18, Oct. 1980, pp. 1186-1195.

[15]Klebanoff, D.S., "Characteristics of Turbulence in a Boundary Layer with Zero Pressure Gradient," NACA Rept. 1247, 1955.

[16]Dimotakis, P.E., Collins, D.J., and Lang, D.B., "Laser Doppler Measurements in Subsonic, Transonic, and Supersonic Turbulent Layers," *Laser Velocimetry and Particle Sizing*, edited by H.D. Thompson and W.H. Stevenson, Hemisphere Publishing Co., New York, 1979, pp. 208-219.

[17]Sandborn, V.A., "A Review of Turbulence Measurements in Compressible Flow," NASA TM X-62-337, March 1974.

[18]Hayakawa, K., Smits, A.J., and Bogdonoff, S.M., "Hot-Wire Investigation of an Unseparated Shock-Wave/Turbulent Boundary-Layer Interaction," *A'4A Journal*, Vol. 22, May 1984, pp. 579-585.

[19]Townsend, A.A., *The Structure of Turbulent Shear Flow*, 2nd Ed., Cambridge University Press, New York, 1976.

[20]Andreopoulos, J. and Bradshaw, P., "Measurements of Interacting Turbulent Shear Layers in the Near Wake of a Flat Plate," *Journal of Fluid Mechanics*, Vol. 100, Pt. 3, 1980, pp. 639-668.

[21]Palmer, M.D. and Keffer, J.F., "An Experimental Investigation of an Asymmetrical Turbulent Wake," *Journal of Fluid Mechanics*, Vol. 53, Pt. 4, 1972, pp. 593-610.

[22]Chandrsuda, C. and Bradshaw, P., "Turbulence Structure of a Reattaching Mixing Layer," *Journal of Fluid Mechanics*, Vol. 110, 1981, pp. 171-194.

[23]Channapragada, R.S., "Compressible Jet Spread Parameter for Mixing Zone Analysis," *AIAA Journal*, Vol. 1, Sept. 1963, pp. 2188-2190.

[24]Birch, S.F. and Eggers, J.M., "A Critical Review of the Experimental Data for Developed Free Turbulent Shear Layers," *Free Turbulent Shear Flows*, Vol. 1, NASA SP-321, 1972.

[25]Harsha, P.T. and Lee, S.C., "Correlation Between Turbulent Shear Stress and Turbulent Kinetic Energy," *AIAA Journal*, Vol. 8, Aug. 1970, pp. 1508-1510.

[26]Bradshaw, P. and Ferriss, D.H., "Calculation of Boundary Layer Development Using the Turbulent Energy Equation: Compressible Flow on Adiabatic Walls," *Journal of Fluid Mechanics*, Vol. 46, Pt. 1, 1971, pp. 83-110.

[27]Bradshaw, P., "Mean Compression Effects in Turbulent Boundary Layers," *Journal of Fluid Mechanics*, Vol. 63, Pt. 3, 1974, pp. 449-464.

[28]Gaviglio, J., Dussauge, J.P., Debieve, J.F., and Favre, A., "Behavior of a Turbulent Flow Strongly Out of Equilibrium at Supersonic Speeds," *The Physics of Fluids*, Vol. 20, No. 10, Pt. 2, 1977, pp. 5179-5192.

SECTION B.2

COMPRESSIBLE SEPARATED FLOWS

AIAA Journal

Volume 24, Number 12, December 1986

Pages 1971-1978

by

H. L. Petrie, M. Samimy, and A. L. Addy

Compressible Separated Flows

H. L. Petrie*
Pennsylvania State University, State College, Pennsylvania
M. Samimy†
The Ohio State University, Columbus, Ohio
and
A. L. Addy‡
University of Illinois at Urbana-Champaign, Urbana, Illinois

An experimental investigation of compressible, two-dimensional, planar turbulent flows with large separated regions is presented. Three backward-facing step-flow configurations were investigated to gain a detailed knowledge of the mean flow and turbulent field in developing compressible turbulent free shear layers and the adjacent recirculating flow. Two-channel coincident laser Doppler velocimeter measurements, surface static pressure measurements, Schlieren flow visualization, and surface oil flow visualization were used to study these flows. The recirculating flows stimulated increased mixing layer growth and entrainment rates. The turbulent field of the compressible mixing layer was considerably more anisotropic than the incompressible counterpart with a decrease in the transverse velocity component turbulence intensity and the Reynolds shear stress. Laser Doppler velocity bias effects and bias corrections are demonstrated and discussed.

Introduction

THE near wake base region of blunt-based missile-type bodies at supersonic freestream Mach numbers presents challenges to experimentalists, analytical modelers, and computationalists alike. These base flows contain a large separated region bounded by the freestream and propulsive jet flow free shear layers. The bounding shear layers merge and change direction in a highly turbulent recompression zone. Although base flow modeling methods like the Chapman-Korst component analysis[1,2] have seen extensive attention and development, and Navier-Stokes finite-difference codes have been applied to such flowfields,[3-5] an accurate and general predictive capability for base flows with large separated regions does not exist.[6]

Knowledge of the physics of these flowfields, gained through simple model experiments, has guided the development of Chapman-Korst component analyses but these past experimental efforts have provided little turbulent field or recirculating flow information. The purpose of this study was to gain a detailed knowledge of the fundamental nature of such separated compressible flows. Specifically, the turbulent mixing layers, the adjacent recirculating flow, and flowfield interactions are discussed. A related study of shear layer reattachment by Samimy et al.[7] considers other important aspects of these flows not presented herein.

Experimental Program

The flowfield configurations and experimental apparatus are discussed in the following sections. Important aspects of the laser Doppler velocimeter (LDV) instrumentation and considerations for the current flowfields are presented. The experimental results are then compared with existing data and incompressible flow results where possible.

Experimental Configurations

Three backward-facing step flowfields were investigated and the flowfield configuration of primary interest in this study is shown in Fig. 1. Constant pressure separation at the backward-facing step in Fig. 1 was achieved by adjusting the angle of the inclined ramp onto which the free shear layer reattached downstream of the step. For the second configuration investigated, the wind tunnel floor downstream of the step and the ramp were removed and replaced with a flat porous plate assembly through which low-momentum flow could be bled. The flowrate of the porous plate mass bleed through the wind tunnel floor downstream of the step was matched to the free shear layer entrainment rate to achieve constant pressure separation of the shear layer at the step. These two configurations allowed study of the developing mixing layer after separation without the complications of an expansion or compression at the separation point. The purpose of the porous plate mass bleed was to remove the recirculating flow and its possible effects on the adjacent shear layer by simulating a quiescent semi-infinite fluid boundary condition in a small-scale wind tunnel. The reattachment and redevelopment of the mixing layer was a primary concern of Samimy et al.[8] in studying a simple backward-facing step flowfield, but mixing layer and recirculating flow data also were obtained. This is the third configuration discussed below.

A ramp configuration geometry at Mach 2.92 was used previously in studies[9,10] of shear layer reattachment and redevelopment using pressure probes and hot-wire anemometry. Samimy et al.[7] have also studied the reattachment and redevelopment process for a ramp configuration at Mach 2.46 using laser Doppler velocimetry. Ikawa and Kubota[11] examined a similar porous plate flowfield in a study of the compressible mixing layer at Mach 2.46 using hot-wire anemometry and pressure probes.

The ramp and porous plate experiments were conducted in a 101.6-mm span blow-down wind tunnel and the simple backstep experiments were conducted in a 50.8-mm span wind tunnel. Step heights were 25.4 mm for the ramp and simple backstep and 44.45 mm for the porous plate. The leading apex of the ramp was approximately 101 mm, or 3.98 step heights downstream of the base of the step. The porous plate had an

Presented as Paper 85-0177 at the AIAA 23rd Aerospace Sciences Meeting, Reno, NV, Jan. 14-17, 1985; received July 17, 1985; revision received March 18, 1986.

*Research Associate, Applied Research Laboratory. Member AIAA.
†Assistant Professor, Department of Mechanical Engineering. Member AIAA.
‡Professor and Associate Head, Department of Mechanical and Industrial Engineering. Associate Fellow AIAA.

open area 240 mm in length by 101.6 mm in span and consisted of a baffled subplenum followed by a series of six drilled 1.59-mm-thick plates 0.51 mm apart and positioned below two stacked sintered steel plates. These plates, with a combined thickness of 6.35 mm, were the wind tunnel floor.

The ramp angle and the porous plate mass bleed were adjusted for constant pressure separation by viewing the flow with a Schlieren system. Side wall static pressure measurements were also made to determine that the constant pressure separation had been achieved. A 19.4 deg ramp angle was used.

Experimental Flow Conditions

The approach flow to the ramp and porous plate test sections was at Mach 2.43 with a stagnation temperature of 298 ± 4 K and a stagnation pressure of 551.6 kPa. This produced a freestream velocity of approximately 570 m/s with a unit Reynolds number of 5.57×10^7/m. For the simple backward-facing step flowfield, a Mach 2.07 approach flow expanded to Mach 2.74 at the step. The freestream velocity adjacent to free shear layer after the expansion and separation at the step was approximately 594 m/s with a unit Reynolds number of 6.69×10^7/m.

The mixing layer reattached onto the ramp 4.5 mm below the level of the step (see Fig. 2). Although the reattachment line was straight and horizontal, the flow was not two-dimensional but developed spanwise cells. Measurements made 19.05 mm off the wind tunnel centerplane showed that the variation of the mean streamwise velocity with center plane values was 2.2–2.7% of the freestream velocity in the region of maximum velocity gradient in the mixing layer and less elsewhere. The standard deviations of the corresponding streamwise component velocity fluctuations were 0.2–0.5% of the freestream velocity greater that the centerplane values. These differences are comparable to those that would result from a shift of the mixing layer of approximately 0.13 mm transverse to the freestream direction. This is twice the estimated limit of the precision with which the LDV measurement volume could be repositioned in the transverse direction after rezeroing, as was done for these off-center measurements. The 50.8-mm span wind tunnel results were similar.[7,8]

The LDV System

A two-channel coincident LDV system with forward scatter light collection at 10 deg off axis was used. The measurement volume diameter was approximately 0.13 mm for the ramp and porous plate experiments. The effective length of the measurement volume was approximately 0.9 mm. A longer focal length lens producing a 0.30-mm-diam measurement volume and a correspondingly larger fringe spacing was used in the simple backstep experiments.

One laser beam in each LDV channel was frequency shifted at 40 MHz to allow determination of the velocity direction and to reduce fringe bias. The fringes were oriented at ± 45 deg to the freestream direction to minimize any fringe bias.[12] Approach flow boundary-layer data near the wall were taken with only the streamwise velocity component measured due to beam blockage.

The small scale of the experiments and the large velocity gradients across shear layers could have led to errors due to poor spatial resolution. Estimates of the effects of the spatial resolution, after Karpuk and Tiederman,[13] were made. The worst-case error occurred initially after separation. For the ramp, this error was 1.1% in the mean streamwise velocity and 2.8% in the standard deviation of the streamwise component velocity fluctuations. The resultant increase in the streamwise component turbulent intensity was 0.41%. These errors decreased substantially downstream of the separation point as the gradients diminished.

All flows were artificially seeded with atomizers using a 50-cP silicone oil. The wind tunnel plenum and the porous plate mass bleed were seeded but the recirculating flows of the ramp and simple backstep were not directly seeded. The plenum seed was passed through a 1-μm oil mist filter prior to injection. The ratio of the LDV data rate to the local mass flowrate was nearly the same in the ramp recirculating and freestream flows. This indicates that particles were transported across the streamline discriminating between the flow in the mixing layer that escapes from the base at reattachment and that which is returned to the base sufficiently well such that the particle concentration did not change significantly across the mixing layer.

An estimate was made of the mean diameter of the seed particles by examining the velocity relaxation of the particles downstream of an oblique shock wave. Comparison of the results with calculations using the empirical drag coefficient correlation of Walsh[14] indicated a 1-μm mean aerodynamic diameter was seen by the LDV.[15] The expected frequency response of such particles is 25–30 kHz.[15-17] From the moving frame of the particles, this should have been sufficient for response to the energy-containing eddies and for accurate estimation of the turbulent stresses.

The number of samples taken at a data location was determined by the data rate and the local turbulence intensity. Only 1024 samples were taken in the freestream flow due to the low turbulence levels there but 4096 samples were taken in the mixing layer. Either 1024 or 2048 samples were taken in the low-

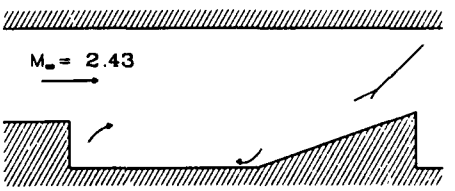

Fig. 1 Ramp configuration backward-facing step flowfield.

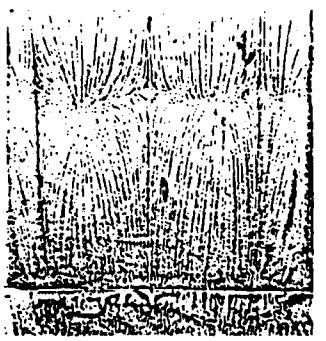

Fig. 2 Surface oil flow visualization of the free shear layer reattachment onto the ramp. The freestream flow moves from the bottom to the top.

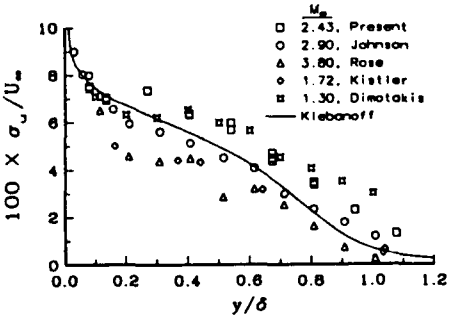

Fig. 3 Streamwise component boundary-layer turbulence intensity profiles taken by various researchers with hot-wire anemometers and LDV and the present data.

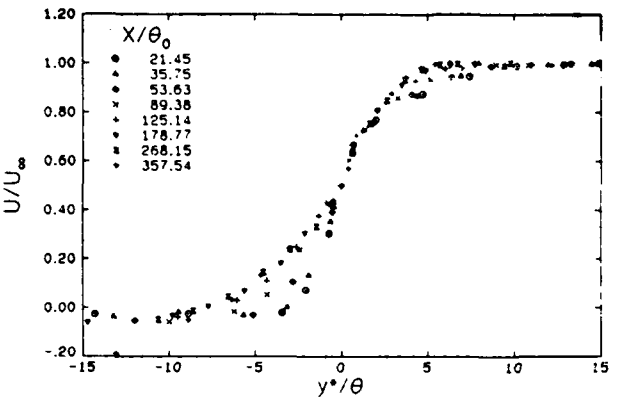

Fig. 4 Mean U component velocity profiles in similarity coordinates for the ramp mixing layer.

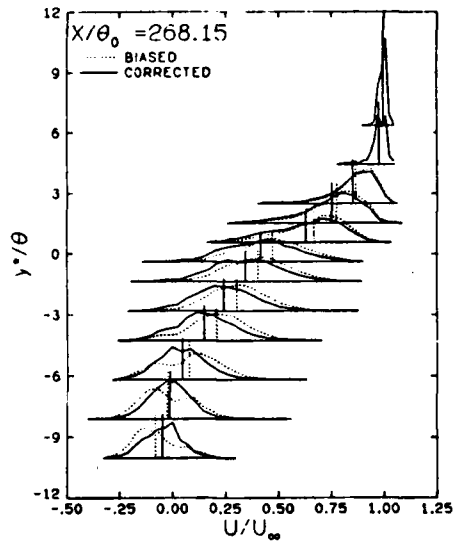

Fig. 5 U component velocity-biased and two-dimensional velocity bias-corrected PDF's across the mixing layer in the ramp flowfield.

velocity, low-data rate recirculating flow. Mixing layer and recirculating flow data were sampled in two sequential wind tunnel runs per location due to the 90 s maximum run times in the larger blow-down wind tunnel.

The Approach Boundary Layer

The 99% and momentum thicknesses of the approach boundary layer for the ramp and porous plate test sections at the step, δ_0 and θ_0, were 3.71 mm and 0.28 mm, respectively. This agrees with pressure probe results, to within 2.5%, obtained by Hampton and White.[18] The momentum-to-boundary-layer-thickness ratio was 0.075, which is approximately 12% larger than the result of the formulation of Maise and McDonald.[19]

A one-sixth power-law profile fit the mean streamwise component boundary-layer velocity profile well. A modified law of the wall (see Maise and McDonald[19]) with the Van Driest compressibility transformation was also fit to the velocity profile. This allowed estimation of the skin friction coefficient, $C_f = 0.00142$, for the ramp and porous plate boundary layers. This value is comparable with the results of others.[7,9]

The boundary-layer streamwise-component turbulent intensity profile of the present study generally agrees with other data, as shown in Fig. 3. The LDV data of Johnson[20] and Dimotakis et al.,[21] and the hot-wire data of Kistler[22] and Rose,[23] are shown with a curve for Klebanoff's incompressible result.[24] The data of the current study follow Klebanoff's curve but is above it through most of the boundary layer. LDV boundary-layer data by Yanta and Lee[25] at Mach 3 and by Johnson and Rose[26] at Mach 2.9, not shown in Fig. 3, follow along but above this curve. Although the hot-wire data of Kistler[22] and Rose[23] fall below the other data in the lower half of the boundary layer, the later hot-wire results in Ref. 26 do not. The high freestream levels of turbulence intensity in Fig. 3 were the result of the clock count resolution of the Doppler signal processors. In the current study, the freestream turbulence is estimated as less than 0.5%.

The boundary-layer profiles of the Reynolds shear stress fluctuation term, $\langle u'v' \rangle$, are similar to those of others.[7,20,25] These boundary-layer shear stress results follow Sanborn's[27] "best estimate" for equilibrium boundary layers closely (see Samimy et al.[7]).

The Mean Flow

The mean streamwise velocity profile data for the ramp configuration indicated that the mixing layer had spread across the approach boundary-layer remnant by $X/\theta_0 = 179$. For $y < 0$ and $X/\theta_0 > 179$, the ramp velocity profiles were noticeably fuller than the porous plate profiles, thus indicating greater entrainment into the mixing layer. The mixing layer momentum thickness was estimated at each X station by assuming constant pressure isoenergetic flow in the integration and by using a curve fit to the mean velocity data. For a mixing layer with a semi-infinite quiescent fluid boundary condition at negative infinity

$$\frac{d\theta}{dX} = \frac{d}{dX}\int_{-\infty}^{y_j} \frac{\rho U}{\rho_\infty U_\infty} dy$$

where y_j is the location of the dividing streamline. The mixing layer entrainment rate can be estimated, in the presence of a reverse flow, by changing the lower limit of integration to include only entrained flow. In this case the lower limit was the location where the mean streamwise velocity was $\tilde{U} = 0$. The entrainment rate, $d\theta/dX$, was 0.0088 for the ramp and 0.0072 for the porous plate. The Mach 2.46 porous plate result of Ikawa and Kubota[11] was $d\theta/dX = 0.0073$, or 23% less than the current ramp configuration result. The incompressible result of Liepmann and Laufer[28] is $d\theta/dX = 0.035$, which is approximately a factor of 5 greater than these porous plate entrainment rates.

The mixing layer width b, defined as the distance between the $\tilde{U}/U_\infty = 0.9$ to $\tilde{U}/U_\infty = 0.1$ locations was also determined at each X station. The mixing layer growth rate, db/dX, was 0.078 for the ramp mixing layer. This is 22% greater than the porous plate value of Ikawa and Kubota,[11] which is $db/dX = 0.064$. The current porous plate result was $db/dX = 0.064$. Samimy et al.[7] observed a ramp flowfield growth rate, $db/dX = 0.093$, which is 19% larger than the current ramp result. The results discussed below indicate that this difference in the two-ramp flowfield growth rates may in part be the result of the relative position of the ramp, which was 1.23 step heights closer to the backstep in the geometry studied by Samimy et al.[7]

The y coordinate has been scaled with the local shear layer momentum thickness, θ, in Fig. 4 and y^* is the distance from the $\tilde{U}/U_\infty = 0.5$ location. Mean profile similarity is indicated by the collapse of the velocity profiles at the two most downstream X stations, which was also the case for the porous plate data. In the current study, mean flow similarity was observed for $X/\theta_0 > 250$ or $X/\delta_0 > 18.8$. Ikawa and Kubota[11] observed similarity for $X/\theta_0 > 275$ and Settles et al.[9] and Hayakawa et al.[10] observed similarity for $X/\delta_0 > 18$ and 17, respectively, at Mach 2.92 in a ramp flowfield. Samimy et al.[7] observed for $X/\delta_0 > 16$.

Sidewall static pressure measurements were made for all three flow configurations. The porous plate static pressures were constant with X for a distance greater than $X/\theta_0 = 600$

from the step. The ramp mixing layer static pressures were constant with X for the first two-step heights downstream of separation, through $X/\theta_0 = 90$. These mixing layer static pressures then decreased approximately 4% to a minimum at 3.5–4.0 step heights after separation; the leading edge of the ramp was at 3.98 step heights. Pressures increased downstream of this minimum but LDV data were not taken downstream of 3.94 step heights. A larger static pressure drop, 6%, was observed with the simple backward-facing step flowfield prior to the pressure rise to reattachment. The maximum reverse flow velocity was also larger in the simple backward-facing step recirculating flow—26% of the adjacent freestream velocity compared to 19% for the ramp.

The Turbulent Field

A qualitative knowledge of the turbulent field was obtained by observation of the velocity probability distribution functions (PDF). Figure 5 shows the PDF's for the U velocity component across the mixing layer at $X/\theta_0 = 268$. The horizontal lines locate the ordinate of the data and the short vertical lines mark the mean velocity. The bias referred to in Fig. 5 is the statistical sampling or velocity bias inherent to individual realization LDV. A sampling bias toward higher velocities results because the probability of obtaining a sample is dependent on the velocity magnitude, among other factors.[29] The biased distributions in Fig. 5 were obtained by adding a weighting factor of one to the histogram bin accumulator if an individual velocity realization fell within the range of the bin. All bins were of equal size. The normalized distribution was obtained by dividing the bin accumulator sums by the total sum of the weights. This is the total number of realizations in this case. The velocity-biased corrected distributions were obtained by adding a two-dimensional velocity inverse weight to the bin accumulator, w_i, where $w_i = (U_i^2 + V_i^2)^{-1/2}$ for the ith realization. Normalization was achieved by division by the total sum of these weights. The effects of any weighting function correction, such as transit time or time between data point weights on the PDF, can be visualized by this approach.

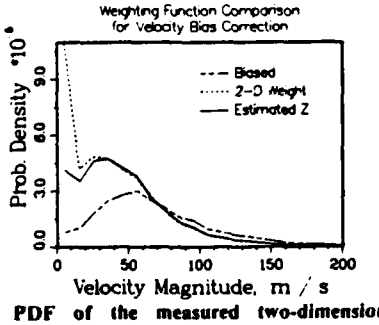

Fig. 6 The PDF of the measured two-dimensional velocity magnitude with no bias correction, with the two-dimensional velocity bias correction, and with the two-dimensional correction with the estimated Z term included, $y^*/\theta_0 = -6.56$, $X/\theta_0 = 268.15$.

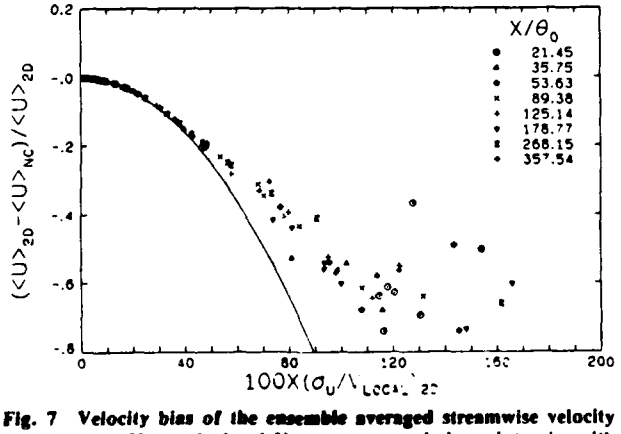

Fig. 7 Velocity bias of the ensemble averaged streamwise velocity component, $\langle U \rangle$, vs the local U component turbulence intensity with the statistical prediction of the bias by Erdmann and Tropea.[33,34]

Velocity Bias in Turbulent Flows

If velocity bias occurs in a turbulent flow as hypothesized, a distinct decrease in the probability of obtaining a sample should be observed when the total velocity magnitude is small. The mixing-layer flow of the present study is dominated by the U or streamwise velocity component such that a small magnitude U velocity correlates well with small magnitude total velocity realization. Because of this, appreciable decreases in the U component PDF's were observed at $U = 0$ in all cases where the probability at $U = 0$ was large enough to discern such details (see Fig. 5). The V component PDF's exhibit no such decrease at $V = 0$ because the transverse velocity magnitude correlates poorly with the total velocity magnitude. However, the bias is still present.

The above results indicate that velocity bias can substantially affect the velocity PDF's in these highly turbulent flows, therefore the two-dimensional velocity inverse bias correction has been used to reduce all of the data presented in this paper. This two-dimensional weighting function correction produced reasonable results but does appear to have overweighted near $U = 0$ in some cases (see Fig. 5). Recent work has found that the addition of a simple estimate of the average unmeasured Z component contribution to the velocity magnitude based on the turbulence intensities in the measured U and V components reduces the tendency of the bias correction to overweight realizations with small U and V velocities.[12] This approach has been used previously by Nakayama[30] and is discussed by Johnson et al.[31] However, the effect of this Z term on the mean velocity was less than 2% of the simple two-dimensional velocity-inverse-corrected value, which indicates overweighting was not a significant problem. Figure 6 shows the effect this estimated Z term has on the probability distribution of the measured two-dimensional velocity magnitude for the data at $y^*/\theta = -6.56$ in Fig. 5. Also, Fig. 6 indicates no noticeable compensation for velocity bias due to improved signal quality at low-velocity magnitudes.[32] Such a compensation may be effective over only a small fraction of the current velocity range and is likely to have a signal-to-noise ratio dependence.

The velocity bias effect on the mean U component as a function of the streamwise turbulence intensity, based on the magnitude of the local mean velocity, is shown in Fig. 7. The NC subscript refers to the result with no correction and 2D refers to the bias corrected result. The curve in Fig. 7 is the predicted form of the bias obtained by the statistical analysis of Erdmann and Tropea.[33,34] The current LDV sampling process was at low burst and data density with a free-running processor. The bias in the mean velocity is predicted to equal the turbulence intensity squared. The analysis is consistent with the two-dimensional corrected results, and the low-speed mixing-layer data of Johnson et al.[31] show a similar trend. Turbulence intensities based on the local mean velocity for $y^*/\theta < 0.0$ were 30% or larger.

Examination of the effects of the bias on flowfield statistics has shown that the biased standard deviations of the velocity distributions differ by less than ±10% with the bias-corrected values in most of the flowfield, but this difference may be as large as −20%.[12] The differences between the biased and corrected Reynolds shear stress term, $\langle u'v' \rangle$, were twice as large as for the normal stresses. This indicates that the largest deviations from the mean contribute most significantly to the shear stress.

Turbulent Field Characteristics

The velocity PDF's in Fig. 5 skew out at the freestream edge of the mixing layer, developing a long flat tail on the low-speed side of the mean of the distribution. The dynamic range

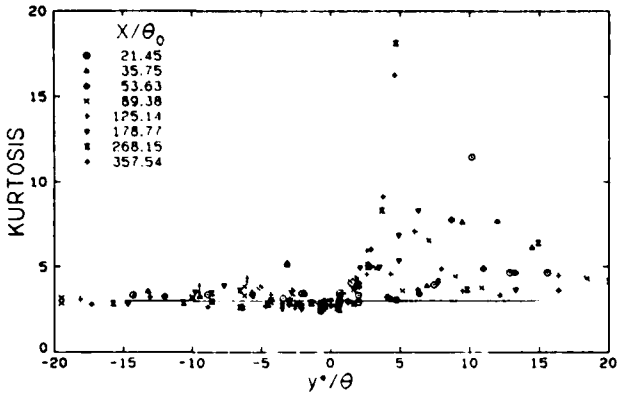

Fig. 8 Profiles of the U velocity component kurtosis factor for the ramp configuration flowfield.

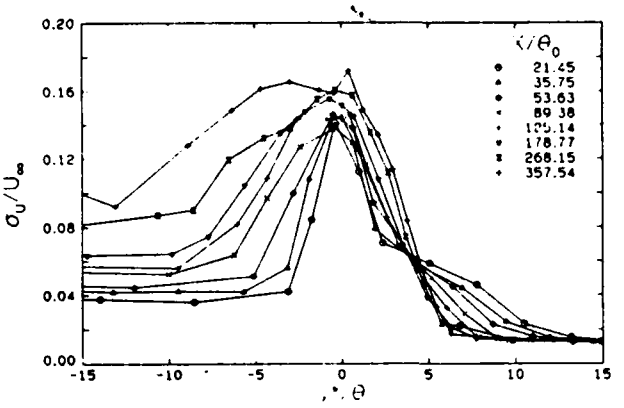

Fig. 9 Streamwise component turbulence intensity profiles for the ramp flowfield.

of velocity fluctuations increased to a maximum at $y^*/\theta = 0.0$ and the distribution filled out, taking on a Gaussian form. The dynamic range decreased as the low-speed edge or recirculating flow side of the mixing layer was approached, and skewing of the PDF in an opposite sense to that at the freestream side occurred. The observed behavior is similar to what Davies[35] observed in a low-speed round jet traversing from the potential core across the jet into a quiescent ambient fluid.

These features of the PDF's are also seen in the higher-order central moments of the distributions. Figure 8 shows the normalized fourth-order central moment or kurtosis factor results for the U component in the ramp flowfield. The porous plate results are similar. A higher-order moment is most affected by and weights most heavily the larger excursions from the mean of the distribution. The large kurtosis factors at the high-speed side of the mixing layer correspond to the long, flat tails in the PDF's of Fig. 5. A few kurtosis values on this side of the mixing layer were too large to be shown in Fig. 8 as it is scaled. The kurtosis values in the core of the mixing layer were actually slightly less than the indicated Gaussian value of 3. A subtle kurtosis peak occurred at the low-speed edge of the mixing layer. These kurtosis factor results are similar to incompressible mixing-layer results with one exception. The incompressible mixing layer exhibits a peak value at the low-speed edge that is as large or larger than on the high-speed side.[36,37] This indicates that comparatively fewer large-scale fluctuations and entraining motions occur on the low-speed side of the compressible mixing layer. The observed factor of 5 decrease of the entrainment rates, relative to incompressible flow, support that this should be the case. However, Hayakawa et al.[10] observed mass flowrate kurtosis profiles in a Mach 2.92 mixing layer similar to the incompressible result. The skewness factor or third-order normalized central moment results also differed with the incompressible mixing-layer behavior in that the peak values on the low-speed side were typically less than half of those on the high-speed side, opposite to the incompressible case.[36,37]

Turbulence intensity profiles for the ramp configuration flowfield are shown in Fig. 9 for the U velocity component. These profiles did not collapse together as the mean profiles did in Fig. 4. However, scaling with the local maximum intensity did collapse the data for $y^*/\theta > 0.0$. The turbulence intensities on the low-speed side of the mixing layer were noticeably higher in the ramp flow than in the porous plate flow for $X/\theta_0 > 178$ where the ramp recirculating flow velocities were largest. The maximum U component intensities occurred at $y^*/\theta = 0$, which is the same as observed in the incompressible mixing layer.[36,37] The V component intensity profiles peaked on the low-speed side of the mixing layer. This is opposite to the incompressible mixing layer for which the shift is toward the high-speed side.

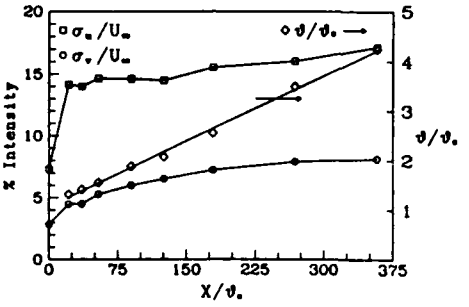

Fig. 10 Local maximum turbulence intensities and momentum thicknesses for the ramp flowfield mixing layer. The linear least-squares fit to the momentum thickness data, used to estimate the entrainment rate, is shown.

The local maximum turbulence intensities vs X/θ_0 for the ramp are shown in Fig. 10. Also, the ramp mixing layer momentum thicknesses with a linear least-squares fit are included in Fig. 10. The initial boundary layer intensity values shown are less than the true maximum values because beam blockage limited the proximity to which the wall could be approached (see Fig. 3). The U component intensity remained nearly constant initially but increased from 14.6% after separation to 17.2% at the base of the ramp. An increase in mass flowrate intensities with increasing X was observed previously.[9,10] Porous plate maximum intensities remained near the 15% level, indicating that the interaction between the mixing layer and the recirculating flow leads to the downstream intensity increase. However, the V component maximum turbulence intensity asymptotically approached 8.2% and does not appear to have been affected by the recirculating flow since the porous plate results were nearly the same. Such an increase in the U component intensity with no increase in the V component values would be observed if the mixing layer were subject to small transverse oscillations as the ramp and the reattachment were approached. The velocity-biased corrected U component PDF at $X/\theta_0 = 357.54$, $y^*/\theta = -6.36$ (see Fig. 4) was slightly bimodal about $U = 0$. This indicates that this stagnant measurement location was alternately in the entrained mixing-layer flow or the reversed recirculating flow and that some larger scale motion and unsteadiness was present at the base of the ramp.

The turbulent intensities in incompressible mixing layers are larger than observed in the present compressible flow. Champagne et al.[6] observed 17.1% and 11.7% values for the U and V component maximum turbulence intensities, respectively, in an incompressible mixing layer. The current V component maximum intensities were one-third to one-half of the U com-

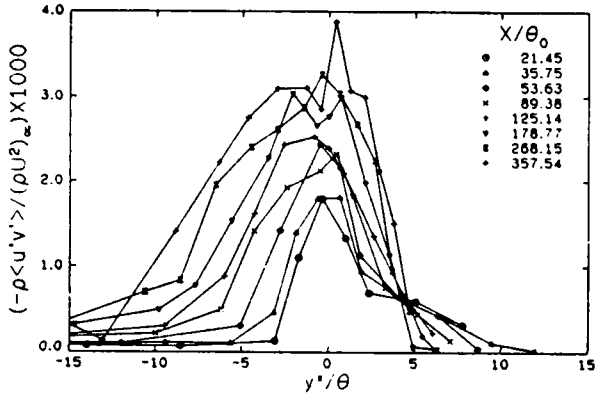

Fig. 11 Reynolds shear stress profiles for the ramp flowfield.

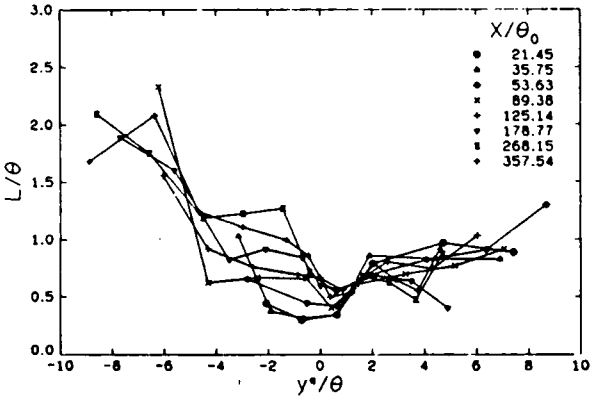

Fig. 12 Mixing length profiles for the ramp flowfield, $L = |\langle u'v'\rangle|^{1/2}/(d\bar{U}/dy)$.

ponent values but this ratio is approximately two-thirds for the incompressible mixing layer. An order-of-magnitude analysis by Brown and Roshko[38] indicates that the transverse component intensity should decrease as Mach number increases in supersonic flow.

The available hot-wire turbulence data differ with the current results. Wagner[39] did not make measurements in the transonic core of a Mach 5.0 mixing layer. This was because of the reported difficulties with the hot-wire calibration at transonic Mach numbers.[39,40] An extrapolated estimate of the maximum streamwise turbulent intensity was 9%. Ikawa and Kubota[11] observed a maximum streamwise component turbulent intensity of 5–6%. This is much less than the current result of approximately 15% after separation and significantly less than in the approach boundary layer. Ikawa and Kubota also observed the peak streamwise intensity occurring decidedly on the high-speed side of the mixing layer, where the mean density gradient is large, and away from the maximum gradient of the U velocity component. The hot-wire results of Hayakawa et al.[10] were presented in terms of mass flowrate fluctuation level and were similar to the mass flowrate results of Ikawa and Kubota.[11] The velocity fluctuation intensity profiles of Ikawa and Kubota, reduced from hot-wire mass flowrate fluctuation data, resemble the mass flowrate profiles in form. However, the boundary-layer mass flowrate fluctuation intensity profiles of Hayakawa et al.[41] do not resemble the velocity fluctuation profiles of Fig. 3, and no sharp peak is observed in the mixing-layer mass flowrate intensity near $y^* = 0$ where the maximum velocity gradients occur.[9,10]

The current maximum intensity estimates are subject to error sources that would falsely increase the turbulence level. The combined effect of the spatial resolution and processor clock count resolution is estimated to increase these maximum intensities by as much as 1.0% near the step and 0.65% at downstream locations. Electronic noise also increases the turbulence intensity falsely but no procedure for accurately estimating the noise effect was carried out. Particle dynamics could also have a potential effect on the turbulence statistics.

Reynolds shear stress results for the ramp flowfield are given in Fig. 11. The density was estimated by assuming constant pressure isoenergetic flow across the mixing layer. The local maximum Reynolds stress occurs on the low-velocity side of the mixing layer. The shift to the low-velocity side is more pronounced for the $\langle u'v'\rangle$ term alone; approximately 85% of the factor of 2.2 density decrease across the mixing layer occurred above the $y^*/\theta = 0$ location. This shift is opposite to that observed in an incompressible mixing layer which is toward the high-speed side.[36,37] The maximum shear stresses Ikawa and Kubota[11] determined from their mean profile data, $\tau_{max}/(\rho_\infty U_\infty^2) = 0.0028$, are comparable to the values measured directly with the LDV in the current study. The incompressible mixing-layer result of Wygnanski and Fiedler[37] is approximately triple the current result, $\tau_{max}/(\rho_\infty U_\infty^2) = 0.0092$. The decrease of the density from the high- to the low-speed side of the mixing layer accounts for half of the reduction of the compressible flow shear stress relative to incompressible results. The reduced V component turbulence intensity and, therefore, transverse transport capability in the compressible mixing layer also reduces the shear stress. The correlation coefficient, $R_{uv} = \langle u'v'\rangle/\sigma_u\sigma_v$, was typically -0.5 to -0.58 in the ramp and porous plate mixing layers. This is similar to the incompressible results of Patel[42] (-0.54), and of Liepmann and Laufer[28] (-0.57).

Relative to the local maximum value, the shear stresses in the recirculating flow were much smaller than the normal stresses were in Fig. 9. These large normal stresses and relatively small shear stresses suggest that a pulsation or unsteadiness is a feature of the recirculating flow.

Samimy et al.[7] have observed that the reattachment region of these separated flowfields exhibit large increases in the turbulent triple product terms, indicating the development of large-scale structures and motions. Settles et al.[9] have also observed the development of large eddies at reattachment. The reattachment region appears to be a potential source for the unsteadiness observed in the present flow.

The normal stress results in the simple backward-facing step flowfield differed from the ramp flow. The U component direction is defined as parallel to the shear layer after the expansion at the separation corner. The U component turbulence intensities in the free shear layer reached 21% prior to the beginning of the pressure rise preceding reattachment. The V component intensities, which were slightly less than the ramp and porous plate values, reached 7.3% before the beginning of the pressure rise. The normal stresses in the recirculating flow were slightly higher than those observed in the ramp flowfield. Reynolds shear stresses reached values nearly double those in the ramp mixing layer and the maximum local correlation coefficient values were -0.6 to -0.8. The shear layer reattached only 2.76 step heights downstream of the step. The unsteady reattachment process appears to contaminate the entire recirculating flow and the adjoining shear layer in this simple backward-facing step flowfield.

An estimate of the turbulent kinetic energy, k, was made by assuming

$$k = \tfrac{1}{2}[\overline{u'^2} + \overline{v'^2} + \tfrac{1}{2}(\overline{u'^2} + \overline{v'^2})] = \tfrac{3}{4}(\overline{v'^2} + \overline{u'^2})$$

The ratio of the Reynolds shear term, $-\langle u'v'\rangle$, to the estimated TKE was examined. The often-cited value for this correlation for a variety of shear flows is 0.3,[43] and this was a typical value on the subsonic side of the mixing layer. However, a decrease to lower values was observed in the transonic and supersonic regions of the mixing layer where typical values were 0.23–0.25.

The apparent kinematic viscosity, $|\langle u'v' \rangle / d\bar{U}/dy)|$, increased dramatically on the low-speed side of the ramp flow mixing layer for $X/\theta_0 > 178$. This increase in the shear stresses relative to the local mean flow gradient is indicative of an increase in larger scale fluctuations.

The turbulent mixing length, $|\langle u'v' \rangle|^{1/2}/(d\bar{U}/dy)$, is shown in Fig. 12 for the ramp flowfield nondimensionalized with the mixing layer momentum thickness. Mixing-layer momentum thickness growth was nearly linear with the distance from the separation point (see Fig. 10), therefore the mixing length growth with X was nearly linear. The porous plate results were similar but values of the mixing length were smaller at the low-speed edge of the mixing layer by 25-50%. The ratio of the shear layer width, b, to the mixing length is $1/32 < L/b < 1/4$ across the mixing layer.

Conclusions

An experimental study of compressible separated flows using a two-channel LDV system and three backward-facing step flowfield configurations was conducted. Mixing-layer growth and entrainment rates were much less than those observed in incompressible flow, as expected. The profiles of turbulence intensity, shear stress, and the kurtosis and skewness factors indicate that the compressible mixing layer is structured differently from the incompressible counterpart. Transverse component turbulent intensities and Reynolds shear stresses in compressible mixing layers are substantially less and the turbulence field substantially more anisotropic than in the incompressible counterpart. In the presence of a recirculating flow, increased mixing-layer growth and entrainment rates were observed. This appears to be the result of the unsteady character of the free shear layer reattachment process and how these disturbances propagate into the recirculating flow. LDV velocity bias was observed and two-dimensional velocity inverse correction worked reasonably well. This correction was improved by the inclusion of an estimated Z component term to the corrective weight.

Acknowledgments

This research was supported by the U.S. Army Research Office under Contracts DAAG 29-79-C-0184 and DAAG 29-83-K-0043. Dr. Robert E. Singleton served as contract monitor.

References

[1]Chapman, D. R., "An Analysis of Base Pressure at Supersonic Velocities and Comparison with Experiment," NACA TN 2137, 1950.

[2]Korst, H. H., "A Theory for Base Pressure in Transonic and Supersonic Flow," *Journal of Applied Mechanics*, Vol. 23, 1956, pp. 593-600.

[3]Hasen, G. A., "Navier-Stokes Solutions for an Axisymmetric Nozzle in a Supersonic External Stream," AFWAL-TR-3161, March 1982.

[4]Horstmann, C. C., Settles, G. S., Bogdonoff, S. M., and Williams, D. R., "A Reattaching Free Shear Layer in Compressible Turbulent Flow—A Comparison of Numerical and Experimental Results," *AIAA Journal*, Vol. 20, Jan. 1984, pp. 79-85.

[5]Weinberg, B. C., McDonald, H., and Shamroth, S. J., "Navier-Stokes Computations of Aft End Flow Fields," U.S. Army Research Office Final Report Contract DAAG 29-79-C-0003, Scientific Research Associates, Inc., Glastonbury, CT, May 1982.

[6]Petrie, H. L. and Walker, B. J., "Comparison of Experiment and Computation for a Missile Base Region Flow with a Centered Propulsive Jet," AIAA Paper 85-1618, July 1985.

[7]Samimy, M., Petrie, H. L., and Addy, A. L., "A Study of Compressible Turbulent Reattaching Free Shear Layers," *AIAA Journal*, Vol. 24, Feb. 1986, pp. 261-267.

[8]Samimy, M., Petrie, H. L., and Addy, A. L., "Reattachment and Redevelopment of Turbulent Free Shear Layers," *International Symposium on Laser Anemometry*, FED-Vol. 33, 1985, pp. 159-166; also presented at the ASME Winter Annual Meeting, Nov. 1985.

[9]Settles, G. S., Baca, B. K., Williams, D. R., and Bogdonoff, S. M., "A Study of Reattachment of a Free Shear Layer in Compressible Turbulent Flow," *AIAA Journal*, Vol. 20, Jan. 1984, pp. 60-67.

[10]Hayakawa, K., Smits, A. J., and Bogdonoff, S. M., "Turbulence Measurements in a Compressible Reattaching Shear Layer," *AIAA Journal*, Vol. 22, July 1984, pp. 889-895.

[11]Ikawa, H. and Kubota, T., "Investigation of Supersonic Turbulent Mixing Layer with Zero Pressure Gradient," *AIAA Journal*, Vol. 13, May 1975, pp. 566-572.

[12]Petrie, H. L., Samimy, M., and Addy, A. L., "An Evaluation of LDV Velocity and Fringe Bias Effects in Separated High Speed Turbulent Flow," *ICIASF Record '85*, edited by F. K. Owen, IEEE, New York, Aug. 1985, pp. 297-308.

[13]Karpuk, M. E. and Tiederman, W. G. Jr., "Effect of Finite Size Probe Upon Laser Doppler Anemometer Measurements," *AIAA Journal*, Vol. 14, Aug. 1976, pp. 1099-1105.

[14]Walsh, M. J., "Influence of Particle Drag Coefficient on Particle Motion in High-Speed Flow with Typical Laser Velocimetry Applications," NASA TN D8120, 1976.

[15]Petrie, H. L., "A Study of Compressible Turbulent Free Shear Layers Using Laser Doppler Velocimetry," Ph.D. Dissertation, Dept. of Mechanical and Industrial Engineering, Univ. of Illinois at Urbana-Champaign, Urbana, IL, April 1984.

[16]Sommerscales, E. F. C., "The Dynamic Characteristics of Flow Tracing Particles," *Proceedings of the 2nd International Workshop on Laser Velocimetry*, Vol. 1, Purdue University, West Lafayette, IN, March 1974, pp. 216-233.

[17]Mazumder, M. K. and Kirsch, K. J., "The Flow Tracing Fidelity of Scattering Aerosol in Laser Doppler Velocimetry," *Applied Optics*, Vol. 14, No. 4, April 1975, pp. 884-901.

[18]Hampton, L. P. and White, R. A., "The Effect of Sudden Expansions and Compressions on Turbulent Boundary Layer Momentum Thickness in Supersonic Flow," University of Illinois at Urbana-Champaign, Urbana, IL, Rept. UILU-ENG-83-4004, 1983.

[19]Maise, G. and McDonald, H., "Mixing Length and Kinematic Eddy Viscosity in a Compressible Boundary Layer," *AIAA Journal*, Vol. 6, Jan. 1968, pp. 73-80.

[20]Johnson, D. A., "Turbulence Measurements in a Mach 2.9 Boundary Layer Using Laser Velocimetry," *AIAA Journal*, Vol. 12, May 1974, pp. 711-714.

[21]Dimotakis, P. E., Collins, D. J., and Lang, D. B., "Laser Doppler Velocity Measurement in Subsonic, Transonic, and Supersonic Turbulent Layers," *Laser Velocimetry and Particle Sizing*, edited by H. D. Thompson and W. H. Stevenson, Hemisphere, New York, 1979, pp. 208-219.

[22]Kistler, A. L., "Fluctuation Measurements in a Supersonic Turbulent Boundary Layer," *The Physics of Fluids*, Vol. 2, No. 3, March 1959, pp. 290-297.

[23]Rose, W. C., "Turbulence Measurements in a Compressible Boundary Layer Subject to a Shock-Wave Induced Adverse Pressure Gradient," AIAA Paper 73-167, 1973.

[24]Klebanoff, D. S., "Characteristics of Turbulence in a Boundary Layer with Zero Pressure Gradient," NACA Rept. 1247, 1955.

[25]Yanta, W. J. and Lee, R. E., "Measurements of Mach 3 Turbulence Transport Properties on a Nozzle Wall," *AIAA Journal*, Vol. 14, June 1976, pp. 725-729.

[26]Johnson, D. A. and Rose, W. C., "Laser Velocimeter and Hot-Wire Anemometer Comparison in a Supersonic Boundary Layer," *AIAA Journal*, Vol. 13, April 1975, pp. 512-515.

[27]Sanborn, V. A., "A Review of Turbulence Measurements in Compressible Flow," NASA TM X-62-337, March 1974.

[28]Liepmann, H. W. and Laufer, J., "Investigation of Free Turbulent Mixing," NACA TN 1257, 1947.

[29]McLaughlin, D. K. and Tiederman, W. G. Jr., "Biasing Correction for Individual Realization of Laser Anemometer Measurements in Turbulent Flow," *The Physics of Fluids*, Vol. 16, No. 12, Dec. 1973, pp. 2082-2088.

[30]Nakayama, A., "Measurements of a Separating Boundary Layer and Wake of an Airfoil Using Laser Doppler Velocimetry," AIAA Paper 85-0181, Jan. 1985.

[31]Johnson, D. A., Modarress, D., and Owen, F. K., "An Experimental Verification of Laser Velocimeter Sampling Bias and Its Correction," *Engineering Applications of Laser Velocimetry*, ASME, New York, 1982, pp. 153-162.

[32]Durao, D. F. G. and Whitelaw, J. H., "Relationship Between Velocity and Signal Quality in Laser Doppler Anemometry," *Journal of Physics, E: Scientific Instruments*, Vol. 12, No. 1, Jan. 1979, pp. 47-50.

[33]Erdmann, J. C. and Tropea, C., "Statistical Bias of the Velocity Distribution Function in Laser Anemometry," International Symposium on Applications of Laser Doppler Anemometry to Fluid Mechanics, Lisbon, Portugal, July 1982, Paper 16.2.

[34]Erdmann, J. C. and Tropea, C., "Turbulence Induced Statistical Bias in Laser Anemometry," *Proceedings of the Seventh Symposium on Turbulence*, University of Missouri-Rolla, Sept. 1981, pp. 129-138.

[35]Davies, P.O.A.L., "Turbulence Structure in Free Shear Layers," *AIAA Journal*, Vol. 4, Nov. 1966, pp. 1971-1978.

[36]Champagne, F. H., Pao, Y. H., and Wygnanski, I. J., "On the Two-Dimensional Mixing Region," *Journal of Fluid Mechanics*, Vol. 74, Pt. 2, 1976, pp. 209-250.

[37]Wygnanski, I. J. and Fiedler, H. E., "The Two-Dimensional Mixing Region," *Journal of Fluid Mechanics*, Vol. 41, 1970, pp. 327-361.

[38]Brown, G. L. and Roshko, A., "On Density Effects and Large Structure in Turbulent Mixing Layers," *Journal of Fluid Mechanics*, Vol. 64, Pt. 4, 1974, pp. 775-816.

[39]Wagner, R. D., "Mean Flow and Turbulence Measurements in a Mach 5 Free Shear Layer," NASA TN D7366, 1973.

[40]Smits, A. J., Hayakawa, K., and Muck, K. C., "Constant Temperature Hot-Wire Anemometer Practice in Supersonic Flows—Part 1-The Normal Wire," AIAA Paper 83-0050, Jan. 1983.

[41]Hayakawa, K., Smits, A. J., and Bogdonoff, S. M., "Hot-Wire Investigation of an Unseparated Shock-Wave/Turbulent Boundary Layer Interaction," *AIAA Journal*, Vol. 22, May 1984, pp. 579-585.

[42]Patel, R. P., "An Experimental Study of a Plane Mixing Layer," *AIAA Journal*, Vol. 11, Jan. 1973, pp. 67-71.

[43]Harsha, P. T. and Lee, S. C., "Correlation Between Turbulent Shear Stress and Turbulent Kinetic Energy," *AIAA Journal*, Vol. 8, Aug. 1970, pp. 1508-1510.

SECTION B.3

THE EFFECT OF SUDDEN EXPANSIONS AND COMPRESSIONS ON TURBULENT BOUNDARY LAYER MOMENTUM THICKNESS IN SUPERSONIC FLOW

ASME Paper No. 86-WA/FE-11

Presented at the 1986 ASME Winter Annual Meeting

Anaheim, California

December 1986

by

L. P. Hampton and R. A. White

THE AMERICAN SOCIETY OF MECHANICAL ENGINEERS
345 E. 47 St., New York, N.Y. 10017

86-WA/FE-11

24139 -EG

The Effect of Sudden Expansions and Compressions on Turbulent Boundary Layer Momentum Thickness in Supersonic Flow

L. P. HAMPTON
R. A. WHITE
Department of Mechanical
and Industrial Engineering
University of Illinois at Urbana-Champaign
Urbana, IL 61801

ABSTRACT

An experimental investigation of momentum thickness changes in two-dimensional planar, attached boundary layers in supersonic flow undergoing a sudden compression or sudden expansion is presented. Momentum thickness measurements upstream and downstream of disturbance corners were conducted for nominal free-stream Mach numbers of 1.5, 2.0, 2.5, and 3.0.

A simple integral formulation leading to a closed Form Algebraic solution was successfully employed to model the experimentally measured changes in the momentum thickness across both sudden compressions and sudden expansions. A best fit correlation was used to obtain the appropriate incompressible form factor required by the formulation. The resulting form factor difrers for sudden compressions from that of sudden expansions. In both cases, the best fit form factor is essentially independent of Mach number over the range tested, and the test results show excellent qualitative and quantitative agreement with the theory. For sudden expansions, the data suggest that apparent sublayer transition and redevelopment into a reduced turbulence outer rotational layer may require a two-profile velocity description downstream of the disturbance.

NOMENCLATURE

C	Crocco Number $u/(2c_{p_o}T_o)^{1/2}$
H	Boundary Layer Form Factor, δ^*/θ
M	Mach Number
P	Absolute Pressure
U	Velocity in Streamwise Direction
X	Length in Streamwise Direction
θ	Boundary Layer Momentum Thickness
δ	Boundary Layer Thickness
δ^*	Boundary Layer Displacement Thickness
ρ	Density

Subscripts

F	Refers to Conditions Downstream of Disturbance
I	Refers to Conditions Upstream of Disturbance
i	Incompressible
o	Stagnation Conditions
∞	Refers to Conditions Adjacent to the Boundary Layer

1. INTPODUCTION

Aerodynamic stability and drag for rocket-type vehicles may be significantly affected by the afterbody boundary layer and the near wake spanning shear layer(s) (1,2). Boundary layer development along the vehicle body establishes the velocity and energy distributions which directly influence both flow separation conditions on the body and at the base plane (3) and the initial characteristics of any separated shear layer. The separated shear layers which are formed from the afterbody boundary layer and external flow in conjunction with the jet plume determine the level of wake mass entrainment, momentum and energy distribution, and the recompression closure conditions that determine base pressures and temperatures (1-4).

Since the supersonic external flowfield over typical rocket-propelled vehicles contains both expansions (Prandtl-Meyer) and compressions (shocks) in the vicinity of the afterbody and base plane, it is important to be able to determine the effects of these sudden pressure gradients on the boundary layer approaching the base plane and the resulting near wake conditions. In particular, for wake solution techniques such as the widely used component approach (2-4), it can be shown that the approaching boundary layer can be treated as an equivalent mass bleed into the wake, directly effecting the base pressure and energy and thus vehicle drag. This effective mass bleed is a function of the boundary layer momentum thickness. Consequently, an investigation has been made of the effects of both Prandtl-Meyer expansions and sudden compressions (not reflected shocks) on the change in a turbulent boundary layer with adjacent supersonic stream.

Presented at the Winter Annual Meeting
Anaheim, California — December 7-12, 1986

2. ANALYSIS

While the effects of sudden expansions and compressions on shear layers are important in a number of problems, no systematic data correlating both types of effects have appeared in the literature. A number of studies (5-8) have considered the effects of sudden or rapid pressure gradients on boundary layer parameters, with the primary emphasis limited to reflected shocks in supersonic flow, and embedded shocks in the transonic case. Similarly, fairly broad success has been achieved in predicting effects of sudden expansions using the stream tube expansion method (7) but this method is also limited, since it is inapplicable to the compression case. Supersonic flow over missiles, of course, may involve either an expansion or compression (not reflected or embedded shocks) at separation, depending on the engine to free stream pressure ratio and body geometry, see Fig. 1.

While the numerical solution of flow fields for rockets with plume slip stream interactions have made significant advances (9) they are not as widely used in the design stage as the component approach (2-4) due to the time required and their inability, at this time, to treat the complex flow fields associated with angle of attack and control surfaces (10,11). Similarly numerical approaches to turbulent shear layer-shock wave interactions have made substantial progress (12), however, complete agreement is still lacking in many cases. This appears to be true of both k-ε models and mixing length models particularly with respect in the factor shape (12). Consequently, an empirical study was undertaken of the change in momentum thickness across sudden compressions and expansions and its correlation with a simple model of this process for use in jet-slipstream interaction problems.

Some years ago a simplified and unified approach to the rapid compression or expansion of boundary layers was proposed (13) which indicated that gross features such as the momentum thickness could be found by integrating the integral momentum equation subject to appropriate assumptions. Such an approach is attractive, and its confirmation or possible modification was one of the goals of the current study.

Although turbulent boundary layer calculations are capable of predicting boundary layer parameters with good accuracy, sudden expansions or compressions involve discontinuities in pressure, transverse pressure gradients, and loss of an appropriate length scale. Thus, the basic boundary layer assumptions no longer hold, and other computational schemes must be sought. Boundary layer calculations which approximate the effects of a sudden discontinuity may be made by using continuous expansions with systematic reductions in the length coordinate. Nevertheless, the limiting case must be treated in some other fashion. In the approach suggested by White (13) it was reasoned that by assuming the effects of friction to be negligible compared with those of the pressure gradient in the immediate vicinity of a sudden pressure change, the compressible momentum integral equation could be written as

$$d\theta/dx + (\theta/u_\infty)\,(du_\infty/dx)\,[2 + H - M_\infty^2] = 0 \quad (1)$$

Introducing the Crocco number for expressing compressibility effects and incorporating Culick and Hill's representation for relating the compressible and incompressible form factors (14), a simple integration across the boundary layer disturbance could be carried out and yielded

$$\frac{\theta_F}{\theta_I} = \left(\frac{C_I}{C_F}\right)^{(2+H_i)} \left(\frac{C_F^2 - 1}{C_I^2 - 1}\right)^{(H_i+1 - 2/(\gamma-1))/2} \quad (2)$$

This formulation is appropriate for both sudden expansions and sudden compressions and thus has potential for wide application, with the only limiting assumption being that momentum changes in the direction normal to the main flow are small enough to be neglected.

A reasonable choice of the incompressible form factor for sudden expansions has been suggested as 1.2 (15), a value representative of a full turbulent velocity shear layer profile (16). A comparison of results, based on boundary layer theory for increasingly rapid expansions and Eq. (2) shows that the former approaches the latter as the pressure gradient tends toward a discontinuity. However, the agreement is only moderately good; and it is clear that the value of H_i is open for clarification. Further, for the compression case, the value of H_i is not likely to be identical with that for expansions; and the correct H_i value must be determined.

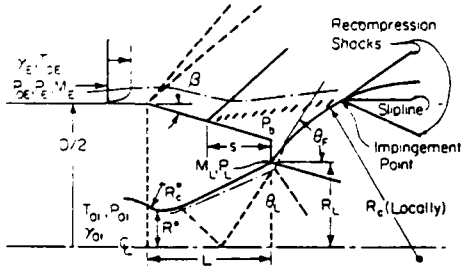

Fig. 1 Flow Configuration for Plume Induced Separation from a Conical Afterbody and Identification of Geometric and Operational Parameters

3. EXPERIMENTAL PROGRAM

An experimental investigation was undertaken to determine the change in boundary layer momentum thickness across sudden compressions and expansions in the Mach number range of 1.5 to 3.0. While the initial intent was to study changes across separations at a rearward facing step, the difficulties in separating mass entrainment and laminar sublayer effects made it more attractive to examine attached boundary layers by utilizing slope discontinuities such as in boattails and flares.

The Department of Mechanical Engineering's Gas Dynamics Laboratory blow down wind-tunnel with fixed interchangeable nozzles provided nominal free stream Mach number conditions of 1.5, 2.0, 2.5, and 3.0. Extensive static pressure tap distributions over the model surfaces were used to obtain a clear determination of the pressure field. The shear layer was probed using a 0.018 in. (.046 cm height) diameter flattened probe. The probe was manually adjusted in increments of 0.005 in. (.013 cm). Consequently, 40 to 50 points were obtained in each profile.

The probe could be located in both upstream and downstream positions in fixed steps with finer divisions being obtained by changing the model slope discontinously with respect to the probe position. Pressure data was obtained using a Scanivalve system and Fluke Data Logger. Boundary layer expansion data was taken at nominal Mach numbers of 1.5, 2.0, 2.5, and 3.0 for integer expansion corner angles between 1° and 13°, inclusive. Compression data was taken at nominal Mach numbers 2.0, 2.5, and 3.0 for compression corner angles of 11°, 13°, and 15°. (Compression data at Mach 1.5 was not obtainable with the existing wind tunnel configuration for these corner angles). The flow Reynolds numbers were 18×10^6, 25.5×10^6, 30×10^6, and 43.4×10^6 per foot (5.9×10^7, 8.4×10^7, 9.8×10^7, and 14.2×10^7 per meter), respectively, for the nominal free stream Mach numbers of 1.5, 2.0, 2.5, and 3.0.

The upstream profiles were well-developed and in terms of the power profile approximation had values in the range of 7.7 to 5.8., with approach boundary layer thickness values ranging between .121 and .178 in. (.307 and .452 cm). Typical expansion and compression disturbed downstream profiles are shown in Fig. 2. The unusual shape of the expansion profile was found to be typical and to have an increasingly distinct knee near the sublayer portion for increasing expansion ratios. A close check of both schlieren photographs, oil flow patterns, and probing nearer the corner showed no indication of a separation bubble; nor were the velocity profiles indicative of a reattaching or redeveloping flow.

The inner and outer profile nature of the expanded profiles suggests that over-expansion of the laminar sublayer may be occurring, followed by redevelopment of this new near wall layer into a quenched lower turbulence outer rotational flow. Such over-expansion has been suggested by previous investigators for separating flows (17) and in association with the lip shock problem. Thus, the boundary layer on afterbodies and its separation characteristics may require a new look at the actual boundary layer profile and description when the flow has experienced a strong and rapid expansion such as occurs at boattail body junctions or for the base pressure problem.

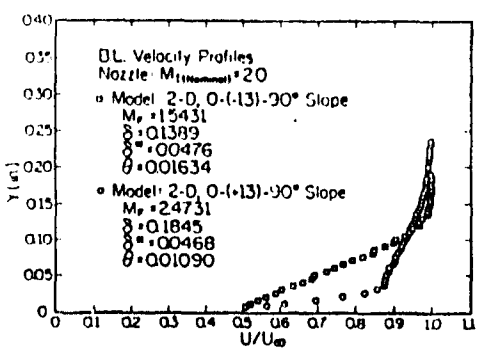

Fig. 2 Typical Profiles Downstream of a Sudden Expansion and Compression for Nominal Mach 2.0 Freestream

4. RESULTS AND ANALYSIS

The correlation of the sudden expansion and compression experimental results to the momentum integral solution (Eq. (2)) is shown in Figs. 3 through 5. Extraction of the best fit H_1 for the measured changes in the momentum thickness at a given free stream Mach number was accomplished using the method of parameter identification by optimization. Starting with the equation

$$\partial/\partial H_1 \left[\left(\theta_F/\theta_I\right)_{experimental} - \left(\theta_F/\theta_I\right)_{theoretical}\right]^2 = 0 \qquad (3)$$

where $(\theta_F/\theta_I)_{theoretical}$ was replaced by its description in Eq. (2), differentiation of both sides with respect to H_1 yielded a nonlinear equation in which H_1 was the only unknown and represented the best fit between the data and theoretical description.

As can be seen in Figs. 3 through 5, Eq. (2) accurately models and predicts momentum thickness changes for both expansion and compression corners. Even for measurements taken with moderately large turning angles (13° for expansions, 15° for compressions), the agreement is remarkably good. For expansion corners, the best fit values of H_1 are $H_1 = 1.10$ for $M = 1.5$, $H_1 = 0.99$ for $M = 2.0$, $H_1 = 1.06$ for $M = 2.5$, and $H_1 = 0.87$ for $M = 3.0$. These have an average value of 1.0, see Fig. 6, which is below the value of 1.2 previously suggested as representative of attached full turbulent velocity layer profiles. Turbulent boundary layer calculations were performed for continuous expansions with systematic reductions in the length coordinate; and in the limiting case, the boundary layer calculation results were found essentially to match results of Eq. (2) with a choice of $H_1 = 1.0$. For expansions the downstream velocity profiles are more full than upstream, which would have the effect of reducing the required H_1 below 1.2. In contrast, the sensitivity of Eq. (2) to H_1 selection is such that $H_1 = 1.2$ gives only qualitative agreement.

For compression corners, the best fit values as shown in the figures are $H_1 = 2.10$ for $M = 2.0$, $H_1 = 1.85$ for $M = 2.5$, and $H_1 = 1.97$ for $M = 3.0$. Fig. 2 shows that the nature of the profiles downstream of a sudden compression, while not indicating separation, does approach that of a separating profile, and the corresponding experimental form factor values again consistently fall within the expected range. In this latter case, it should be mentioned concerning the determination of H_1, that the measured post-compression Mach numbers were typically several hundredths (0.07 ± 0.04) less than the expected theoretical values. It was desirable to measure the downstream Mach number close to the flow disturbance to reduce the possibility of errors from momentum thickness growth and to accommodate wind-tunnel startup limitations. Consequently, the expected pressure rise was generally not fully achieved (ranging between 87 percent and 96 percent) at the location at which the downstream static pressure measurement was taken. The probable effect was an enlargement of the H_1 value.

Determination of the best fit H_1 using the theoretical final Mach number results in values of $H_1 = 1.72$ for $M = 2.0$, $H_1 = 1.73$ for $M = 2.5$, and $H_1 = 1.84$ for $M = 3.0$. The average value of 1.76 agrees well with the proposal of $H_1 = 1.8$ for separating flows. In both types of corner flows, the best fit shape parameter clearly appears to be independent of the approach Mach number (Fig. 6), and to be well-

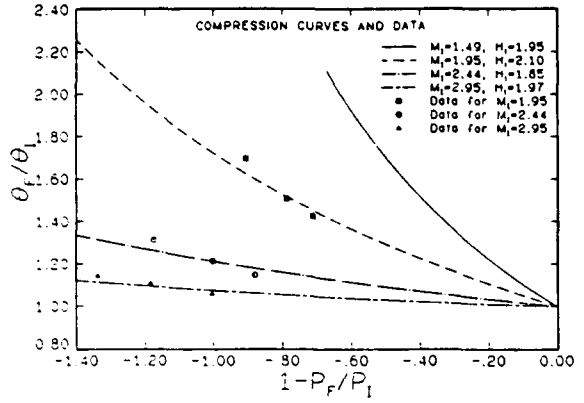

Fig. 3 Theoretical and Experimental Momentum Thickness Ratios for Sudden Compressions

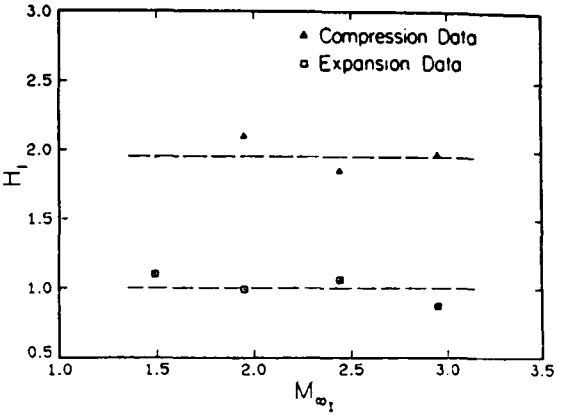

Fig. 6 Best Fit H_i for Eq. (2) to Experimental Data as a Function of Initial Mach Number

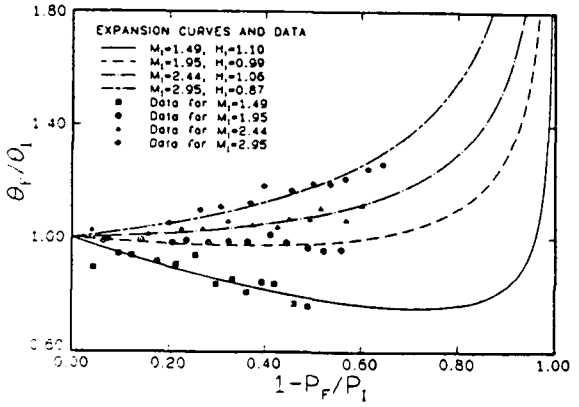

Fig. 4 Theoretical and Experimental Momentum Thickness Ratios for Sudden Expansions

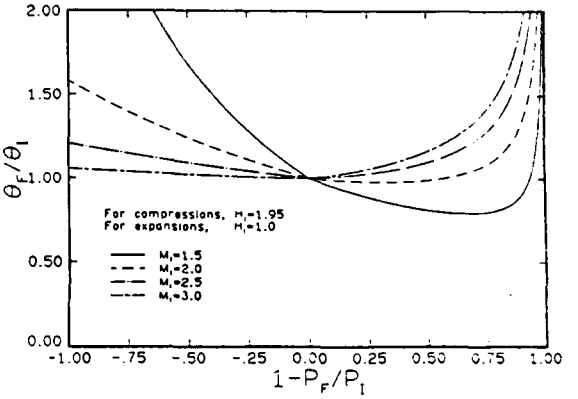

Fig. 7 Effects of Sudden Expansions and Compressions on Momentum Thickness Ratio Before and After the Interaction

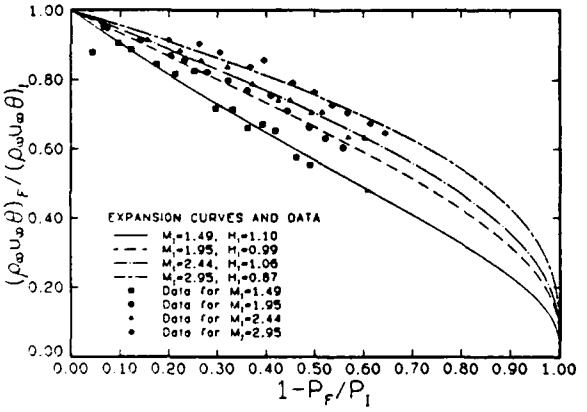

Fig. 5 Theoretical and Experimental Momentum Thickness Ratios for Sudden Expansions; Modified Form

modeled by Eq. (2) with the appropriate choice of H_i. Figure 7 shows the relation between momentum thickness ratio and pressure ratio presented by Eq. (2) using the best fit form factors from Fig. 6.

As indicated by White (13), and others (7), there is an inversion region across which the effects of expansion and compression corners upon the momentum thickness ratio (θ_F/θ_I) are reversed. Earlier results (13,15) using Eq. (2) were plotted in the absence of experimentally determined values of the shape parameter H_i; and the H_i value used was identical, i.e., 1.2, for both expansions and compressions. The inversion region appeared to span a small range of approach Mach numbers between approximately 2.2 and 2.7. The use of distinct values of H_i for expansions and compressions based on the experimental data allows for further discussion of inversion.

Figure 8 shows that the "inversion region" can more clearly be described in terms of an "expansion inversion region" centered approximately at an approach Mach number of 2.1, and a "compression inversion region" centered approximately at Mach 3.4. For a given degree of expansion or compression, there is an inversion point, i.e., a specific approach Mach number at which the value of the momentum thickness remains unchanged as the flow turns and across which the effects on the magnitude of the momentum thickness are essentially reversed. Thus, for an expansion corner of 15°, the expansion inversion point is located at Mach 1.97. For the same corner and for a smaller approach Mach number of 1.5, there results a

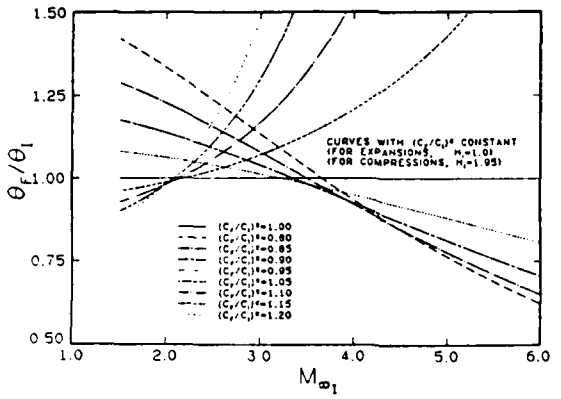

Fig. 8 Eq. (2), Plotted for Lines of Constant Degree of Expansion or Compression, using Best Fit H_i Values as shown

reduction in momentum thickness of 20 percent; for a larger approach Mach number of 2.5, there results an increase in momentum thickness of 20 percent. That this reversal of effects exists has been demonstrated experimentally (Fig. 4).

Similarly, for a compression corner of 15°, the compression inversion point is located at Mach 3.65. A similar reversal of effects upon the momentum thickness exists for higher and lower approach Mach numbers, although now the momentum thickness increase results from the lower Mach numbers instead of from the higher ones, as in the case of the expansion corner. Thus for the 15° compression corner and for an approach Mach number of 3.0, there results an increase in momentum thickness of 16 percent; while for a larger approach Mach number of 4.0, the effect upon the momentum thickness is projected as a 7 percent reduction. Further, the inversion point locations (i.e., the approach Mach numbers at these intersections) are found to vary almost linearly with turning angles for both expansion and compression corners of moderate angles (up to about 15° to good approximation).

Thus, the compression and expansion solutions divide Fig. 8 into three distinct regions. Below the expansion inversion region, for low supersonic flow, expansion corners reduce the momentum thickness while compression corners increase it. Above the compression inversion region, for high supersonic and low hypersonic flow, the reverse is true. Between these two regions is a region of overlap, spanning Mach numbers 2.23 to 3.16 for most small turning angles and for which both sudden expansions and compressions may be expected to result in an increase in the momentum thickness. Additionally, for the range of turning angles considered above, the expansion and compression inversion regions enclose a small range of Mach numbers (of widths 0.26 and 0.28, respectively) for which as the degree of expansion or compression increases, the ratio θ_F/θ_I drops below 1.0 before increasing monotonically with further changes.

For expansions, the estimated levels of uncertainty in the experiments for the ratio θ_F/θ_I, computed for a 95% confidence interval, are 3.38%, 2.36%, and 6.22%, for nominal approach Mach numbers of 1.5, 2.0, 2.5, and 3.0, respectively. For compressions, these are 1.08%, .73%, and .28%, for nominal approach Mach numbers of 2.0, 2.5, and 3.0, respectively. If it is assumed, conservatively, that for the compression case the difference between the measured and the theoretical values of the post-compression Mach numbers strongly affects the uncertainty of θ_F then the estimated levels of uncertainty for the ratio θ_F/θ_I, again for a 95% confidence interval, are increased to 6.4%, 7.6%, and 10.3%, respectively.

5. CONCLUSIONS

Since no assumptions were made in the formulation of Eq. (2) which would restrict its applicability merely to approach shear layer flows with simple power profiles, it would not be unreasonable to employ the momentum integral solution in predicting momentum thickness changes for attached approach shear flows having other velocity profiles, (e.g., those already disturbed) if one uses an appropriate shape parameter. The experimentally determined H_i values were found to be in the range anticipated in that they are representative of fully developed and separating profiles, respectively. They also point out that the expansion process and compression process lie along different legs of Eq. (2). Agreement between test data and theory is seen to be excellent both qualitatively and quantitatively. Thus, the integration of the momentum equation represented by Eq. (2) appears to adequately describe the effects of sudden pressure gradients on attached turbulent boundary layers.

Additionally, boundary layer profile shapes indicate that apparent sublayer over-expansion occurs for rapid expansions imposed from the outer flow, which suggests a need for a two profile velocity description downstream of the disturbance. The effects of rapid expansions on the boundary layer may lead to changes in boundary layer development and separation characterization on boattails. A detailed Laser Doppler Velocimeter study of rapidly expanding shear layers is necessary to confirm the effects of sublayer expansion at the corner and in the redevelopment process.

ACKNOWLEDGEMENTS

This study was partially sponsored by the U.S. Army Research Office under Contract DAAG 29-83-K-0043.

REFERENCES

1. Deep, R. A., Henderson, J. H., and Brazzel, C. E., "Thrust Effects on Missile Aerodynamics," U.S. Army Missile Command, RD-TR-71-9, May 1971.
2. Addy, A. L., H. H. Korst, B. J. Walker, and R. A. White, "A Study of Flow Separation in the Base Region and Its Effects during Powered Flight," AGARD-CP-124, AGARD Conf. Proc., No. 124 on Aerodynamic Drag, Specialists' Meeting, April 10-13, 1973 (available from NASA Langley Field, VA 23365, ATTN: Report Distribution and Storage Unit).
3. White, R. A., and Wagner, B., "Influence of Fundamental Parameters on the Supersonic Base Flow Problem in Presence of an Exhaust Jet," AIAA 17th Aerospace Sciences Meeting, New Orleans, LA, 15-17 Jan. 1979, AIAA J., Vol. 18, No. 8, 1980, pp. 876-882.
4. Korst, H. H., W. L. Chow, and G. W. Zumwalt, "Research on Transonic Flow of a Real Fluid at Abrupt Increases in Cross Section (with Special Consideration of Base Drag Problems)--Final Report," University of Illinois, ME-TN-392-5, Dec. 1959.

5. Weinbaum, S. "Rapid Expansion of a Supersonic Boundary Layer and Its Application to the Near Wake," AIAA J., Vol. 4, pp. 217-226, 1966.
6. Holden, M. S., "Theoretical and Experimental Studies of Separated Flows Induced by Shock Wave Boundary Layer Interaction," Proc., AGARD Meeting on Separated Flows, AGARD Fluid Dynamics Panel, AGARD CP4 (1966) (May 1966); also available as Cornell Aeronautical Lab. Report AL-1972-A-3, Dec. 1965.
7. Reshotko, E., and M. Tucker, "Effect of a Discontinuity on Turbulent Boundary Layer Thickness Parameters with Application to Shock Induced Separation," NACA TN 3454, May 1955.
8. Nash, J. F., "An Analysis of Two-Dimensional Turbulent Base Flow, including the Effect of the Approaching Boundary Layer," Aeronautical Res. Council R&M 3344, 1963.
9. Diewert, G. S., "Numerical Simulation of Three-Dimensional Boattail Afterbody Flow Field," AIAA Paper 80-1347, AIAA 13th Fluid and Plasma Dynamics Conference, July 14-16, 1980, Snowmass, CO.
10. Agrell, Johan, "An Experimental Investigation of Supersonic Flow over Axisymmetric Afterbodies with a Centered Propulsive Jet at Angles of Attack," Aeronautical Research Institute of Sweden, Technical Report, FFA-TA-1985-10, Stockholm 1985.
11. Agrell, Johan, "A Wind Tunnel Investigation of the Effect of a Propulsive Jet on Controls Located on a Conical Afterbody in Subsonic and Supersonic Free Streams," Aeronautical Research Institute and Supersonic Free Streams," Aeronautical Research Institute of Sweden, Technical Report, FFA-TN-1985-11, Stockholm, 1985.
12. Proceedings, "International Union of Theoretical and Applied Mechanics (IUTAM) Symposium on Turbulent Shear-Layer/Shockwave Interactions," Ecole Polytechnique, Palaiseau, France, Sept. 9-12, 1985.
13. White, R. A., "Effect of Sudden Expansions or Compressions on the Turbulent Boundary Layer," AIAA Journal, Vol. 4, 1966, pp. 2232-2234.
14. Culick, R. E. C., and J. A. F. Hill, "A Turbulent Analog of the Stewartson-Illingworth Transformation," J. Aeronaut. Sci., 25, 259-262, April 1958.
15. White, R. A., "Turbulent Boundary Layer Separation from Smooth-Convex Surfaces in Supersonic Two-Dimensional Flow," Ph.D. Thesis, University of Illinois, 1963.
16. Schlichting, H., Boundary Layer Theory, McGraw-Hill Book Company, Inc., Seventh Edition, 1979.
17. Gaviglio, J., J.-P. Dussauge, J.-F. DeBieve, and A. Favre, "Behavior of a Turbulent Flow, Strongly out of Equilibrium at Supersonic Speeds," The Physics of Fluids, Vol. 20, No. 10, Pt 11, pp. 179-181, Oct. 1977.

SECTION B.4

TURBULENT BOUNDARY-LAYER PROPERTIES DOWNSTREAM OF THE SHOCK-WAVE/BOUNDARY-LAYER INTERACTION

AIAA Journal

Volume 25, Number 5, May 1987

Pages 668-675

by

D. W. Kuntz, V. A. Amatucci, and A. L. Addy

24139-E6

Turbulent Boundary-Layer Properties Downstream of the Shock-Wave / Boundary-Layer Interaction

D. W. Kuntz*
Sandia National Laboratories, Albuquerque, New Mexico
V. A. Amatucci† and A. L. Addy‡
University of Illinois at Urbana-Champaign, Urbana, Illinois

An experimental investigation was conducted to study the interaction between a shock wave and a turbulent boundary layer. Compression corner models mounted on a wind tunnel floor were used to generate the oblique shock wave in the Mach 2.94 flowfield. Ramp angles of 8, 12, 16, 20, and 24 deg were used to produce the full range of possible flowfields, including flow with no separation, flow with incipient separation, and flow with a significant amount of separation. The principal measurement technique used was laser Doppler velocimetry (LDV), which was used to make two-component coincident velocity measurements within the redeveloping boundary layer downstream of the interaction. The results of the LDV measurements indicated that the boundary layer was significantly altered by the interaction. The mean streamwise velocity profiles downstream of the separated compression corners were very wake-like in nature, and the boundary-layer profiles downstream of all the interactions showed an acceleration of the flow nearest the wall as the boundary layers began to return to equilibrium conditions. Significant increases in turbulence intensities and Reynolds stresses were caused by the interactions, and indications of the presence of large-scale turbulent structures were obtained in the redeveloping boundary layers.

Nomenclature

C_f = skin friction coefficient
M = Mach number
P = pressure
Re_δ = Reynolds number based on boundary-layer thickness
u = mean velocity component parallel to the wind tunnel floor or ramp surface
u_τ = friction velocity, $(\tau_w/\rho_w)^{1/2}$
u^* = Van Driest generalized velocity
v = mean velocity component perpendicular to the wind-tunnel floor or ramp surface
X = longitudinal coordinate
X^+ = longitudinal coordinate parallel to the ramp surface
Y = vertical coordinate
Y^* = displaced vertical coordinate
α = ramp angle
δ = boundary-layer thickness
δ^* = boundary-layer displacement thickness, $\delta^* = \int_0^\delta (1 - \rho u/\rho_e u_e)\,dY$
δ_0 = undisturbed boundary-layer thickness at $X = 0$
θ = boundary-layer momentum thickness, $\theta = \int_0^\delta [\rho u/\rho_e u_e](1 - u/u_e)\,dY$
ν = kinematic viscosity
Π = wake strength parameter
ρ = density
τ = shear stress
$\langle\ \rangle$ = root-mean-square quantity

Subscripts

e = boundary-layer edge
MAX = maximum
R = reattachment
S = separation
w = wall
∞ = freestream condition, upstream of the shock wave

Superscripts

$\bar{(\ )}$ = ensemble average
$(\ )'$ = fluctuation from the mean value

Introduction

THE interaction between a shock wave and a turbulent boundary layer has been a topic of interest to researchers for many years. Flowfields of this type occur frequently in high-speed flight, and a thorough knowledge of the effects of the shock wave on the boundary-layer properties is necessary for accurate flowfield prediction. The investigation described in this report was conducted in order to provide detailed mean and turbulent flowfield properties within boundary layers downstream of shock-wave/turbulent-boundary-layer interactions of various strengths.

A review of the literature published in this area indicates that there is a need for additional measurements within shock-wave/boundary-layer interaction flowfields.[1] A great deal of effort has been dedicated to determining mean properties within these flowfields,[2-5] and some investigations have measured turbulent flowfield properties.[6-12] Unfortunately, the few investigations which have used hot-wire or laser Doppler velocimeter (LDV) systems to study these flowfields have been limited to single-component measurements, and thus have presented a rather limited amount of information. The numerical simulations of these flowfields have achieved some degree of success, but shortcomings exist in the available turbulence models. Advances in turbulence modeling await a better understanding of the nature of turbulence itself. The current investigation was conducted with a two-component

Presented as Paper 86-0348 at the AIAA 24th Aerospace Sciences Meeting, Reno, NV, Jan. 6-9, 1986; received March 18, 1986; revision received Aug. 27, 1986.

*Member of Technical Staff, Aerothermodynamics Division. Member AIAA.
†Graduate Research Assistant, Department of Mechanical and Industrial Engineering. Student Member AIAA.
‡Professor and Associate Head, Department of Mechanical and Industrial Engineering. Associate Fellow AIAA.

LDV system, and thus has produced new information concerning the nature of the turbulence downstream of the shock-wave/turbulent-boundary-layer interaction.

Compression corner models, or ramps mounted on the wind tunnel floor, were used to generate the oblique shock waves for this study. Ramp angles of 8, 12, 16, 20, and 24 deg were used to produce the full range of possible flowfields, including flow with no separation, flow with incipient separation, and flow with a significant amount of separation. In this manner, the effects of increasing shock strength on the turbulent properties of the boundary layer were studied systematically.

Measurement techniques used in this investigation included schlieren photography, surface static pressure measurement, surface streak pattern measurement, and laser Doppler velocimetry. The LDV system was used to make two-component coincident velocity measurements within the upstream boundary layer and within the redeveloping boundary layers downstream of the interactions. The two-component nature of the LDV system allowed direct measurement of the two instantaneous velocity components. These data then enabled calculation of the two mean velocity components, as well as various turbulent properties, such as turbulence intensities, Reynolds stress, turbulence structure parameters, skewness and flatness factors, and turbulence triple products. Space limitations prevent the presentation of all the data obtained, but a complete presentation of these data can be found in Ref. 1. The purpose of this paper is to present an overview of the data obtained in this investigation, with specific emphasis on the effects of increasing shock strength on the various flowfield parameters.

Experimental Facilities

The experiments described in this paper were conducted in the Mechanical Engineering Laboratory of the University of Illinois at Urbana-Champaign. The wind tunnel used in this investigation operated in the blow-down mode and had a 10.2×10.2 cm test section. A solid aluminum nozzle produced a Mach number of 2.94 within the test section. Transparent windows within the wind tunnel sidewalls provided the optical access necessary for schlieren photography and laser Doppler velocimetry. Additional details of the wind tunnel facility can be found in Ref. 1.

The data of this investigation were obtained with a wind-tunnel stagnation pressure of approximately 483 kPa (70 psia). This pressure level was high enough to ensure proper supersonic operation of the wind tunnel, yet was low enough to permit relatively long run times of approximately 90 s. The stagnation temperature was near the ambient temperature in the laboratory facility, and thus the wind tunnel operated with nearly adiabatic conditions within the wall boundary layers.

A diagram of a typical compression corner model is shown in Fig. 1 with the coordinate system used in the presentation of the experimental data. A complete compression corner model consisted of a ramp mounted on a ramp support. The forward part of the ramp support formed the lower wind-tunnel wall upstream of the corner. The section of the model downstream of the end of the ramp sloped gradually down to the floor level of the wind tunnel to reduce the disturbances caused by the models during the wind-tunnel startup process.

The five ramp models and the ramp support were made of aluminum and anodized flat black to reduce laser light reflections during the LDV measurements. The model support was sealed along the sidewalls and upstream of the corner where the support mated with the wind-tunnel floor with linear O-ring material. The junction between the ramp and the ramp support which formed the compression corner was sealed with gasket-sealing compound. Static pressure taps 0.57 mm in diameter were located every 2.54 mm longitudinally on the surface of the ramps and on the model support upstream of the corner.

The models used in this study spanned the full 10.2-cm width of the test section. It may have proven beneficial to have used narrower ramp models with splitter plates located along the sides to eliminate the effects of the sidewall boundary layers on the shock-wave/boundary-layer interaction, similar to those used in other studies.[2-9] However, the sidewall splitter plates would have denied optical access to the interaction region, and thus would have made LDV measurements impossible. As a result, it was decided to use full span models and to experimentally determine the extent of the sidewall boundary-layer interference using surface flow pattern measurements.

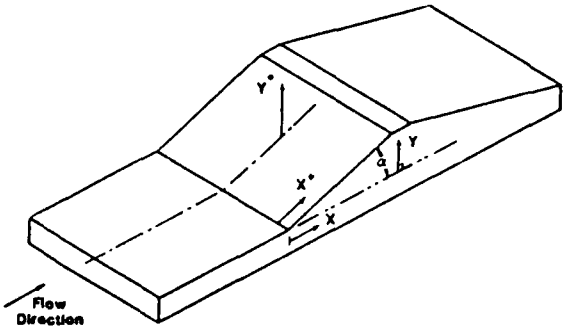

Fig. 1 Compression corner coordinate system.

Measurement Techniques

The primary measurement tool used in this investigation was a two-color laser Doppler velocimeter system. This system was used to obtain two-component mean velocity and turbulent property measurements in both the upstream and redeveloping downstream boundary layers within the five compression corner flowfields. In addition to the LDV measurements, surface static pressure measurements, surface streak pattern measurements, and high-speed schlieren photographs were also taken. The pressure measurements were used to determine the location of the beginning of the interaction, and to ensure that the ramp models were long enough to achieve a complete pressure rise. The surface streak patterns were used to check for flowfield three-dimensionality, to determine the existence of separation, and to determine the separation and reattachment locations. The schlieren photographs were used to map the flowfield and to look for any gross flowfield unsteadiness.

The LDV system used in this investigation was a two-color, two-component system utilizing optical and electronic components manufactured by Thermal Systems Inc. (TSI). A Spectra-Physics 5-W argon-ion laser operating in the multiline mode produced the necessary laser light. The beam from the laser was split into its principal components with a dispersion prism, and the green beam, with a wavelength of 514.5 nm, and the blue beam, with a wavelength of 488 nm, were used by the system. Each of these two beams was reflected down the optical axis with plane surface mirrors, and split into two equal-intensity parallel beams with beam-splitting optics. One beam of each of the two sets of parallel beams was then passed through a Bragg cell in order to shift the frequency by 40 MHz. The four parallel beams were then passed through a 350-mm focal-length lens, which caused the four beams to cross at a single point. This produced the measurement volume containing the two orthogonal fringe patterns necessary for two-component velocity measurements.

The beam spacing and 350-mm lens used in this investigation produced a measurement volume diameter of approximately 0.18 mm and a measurement volume length of approximately 6 mm. The fringe spacing was approximately 8.5 μm, and the fringe velocity due to the frequency shifting was approximately 340 m/s. The laser and transmitting optics were mounted on a traversing table which could be moved manually in three directions by means of threaded rod arrangements with an accuracy of approximately 0.1 mm. In

this manner the measurement volume could be positioned at any location within the wind-tunnel test section.

The collection optics were located on the opposite side of the wind-tunnel test section, and consisted of a 250-mm focal-length lens to collect the scattered light and a dichroic mirror and filter arrangement to separate the two color signals. These optical components were oriented 10 deg off the optical axis in order to simplify alignment procedures, and to reduce the effective measurement volume length to less than 2 mm. Photomultipliers converted the scattered light signals to analog voltage signals, and TSI frequency counters were used to determine the frequencies of the signals, and to perform validation checks to remove erroneous data. The output from the counters was stored directly in the memory of a Digital Equipment Corp. PDP 11-03 minicomputer, which converted the output into velocities and stored the data on floppy disks. The data were then transferred to a Hewlett-Packard 9000 series computer for thorough analysis.

The seed particles used in this investigation consisted of silicone oil droplets which were introduced into the wind-tunnel stagnation chamber. A series of experiments was conducted with the LDV system to determine the mean particle size, in which two-component velocity measurements were made immediately downstream of the oblique shock wave generated by the 8-deg compression corner in the Mach 2.94 flowfield. The mean velocity measurements were then compared to predicted velocities of particles of various sizes in the same flowfield conditions. The results of this series of experiments indicated that the silicone oil droplets had a mean effective diameter of between 1.5 and 2. μm. Particles of this size have been shown to have a sufficient frequency response to track the large-scale velocity fluctuations that exist downstream of shock-wave/turbulent-boundary-layer interactions.[1] The effects of particle lag were seen to some extent in the mean velocity measurements in the regions immediately downstream of the oblique shock waves due to the large velocity gradients in these regions. The influence that particle lag had on the data obtained in this investigation will be discussed during the presentation of the experimental results.

LDV measurements obtained at a particular location involve inherent uncertainties due to the finite sample size. A statistical analysis can be used to determine the level of certainty which can be attained when using the mean of a finite sample size to represent an overall population mean. The statistical uncertainty involved in determining mean velocities from individual velocity measurements is a function of the sample size and the local turbulence intensity. The sample size in this investigation was increased as local turbulence intensity increased, with 1024 samples taken when the local turbulence intensity was less than 15%, 2048 samples taken when the local turbulence intensity was between 15 and 25%, 3072 samples taken when the turbulence intensity was between 25 and 30%, and 4096 samples taken when the local turbulence intensity exceeded 30%. From a statistical analysis which assumes a normal velocity distribution, the uncertainty in mean velocity was found to be less than 2% for all velocity profiles with the exception of the two profiles nearest the compression corner in the 24-deg flowfield, in which local turbulence intensities reached values greater than 100% and the statistical uncertainty in mean velocity is of the order of 3%. The statistical uncertainty in turbulence intensity can be shown to be a function of sample size only, and for the current investigation was everywhere less than 3.6%.

Mean and turbulent flow properties computed from LDV data obtained with counter-type signal processors have been shown in the literature to be affected by biasing errors, most significantly velocity biasing[13] and fringe biasing.[14] Velocity biasing results from the fact that in a turbulent flow with uniformly distributed particles, a larger volume of fluid passes through the measurement volume during periods when the velocity is higher than the mean than when the velocity is lower than the mean. Thus, a simple average of the individual velocity measurements is biased toward higher velocities. Fringe biasing results from the fact that a particle must pass through a given number of fringes within the measurement volume for its velocity to be measured. Thus, particles traveling in a direction parallel to the fringe plane are not "seen" by the LDV, and this results in a bias in favor of particles traveling perpendicular to the fringe plane. The measurements of this investigation were corrected for the effects of velocity biasing by weighting each measurement with the two-dimensional bias correction factor $1/(u^2+v^2)^{1/2}$. The extent to which the effects of velocity biasing are removed with this correction factor is uncertain, and further research into the effects of velocity biasing and the quality of the two-dimensional correction is necessary before this issue can be completely resolved. The effects of fringe biasing were significantly reduced by the frequency shifting, which caused the fringes to move in the upstream direction, and by orienting the fringes at ± 45 deg relation to the wind-tunnel floor for the upstream boundary-layer measurements, and at ± 45 deg relative to the ramp surface for the 12-, 16-, 20-, and 24-deg compression corner redeveloping boundary-layer measurements. It was not necessary to rotate the fringes at ± 45 deg relative to the 8-deg ramp surface due to the small flow angle and low turbulence intensities in this flowfield. A comparison between the two-dimensional velocity bias corrected mean velocities, and mean velocities corrected with both the velocity bias correction and a fringe bias correction based on the analysis of Buchhave[14] yielded differences of less than 2.4%, with only six measurement differences out of nearly 800 exceeding 2%. Thus the effects of fringe bias were not significant in comparison to the effects of velocity bias, and the results presented here were corrected with the velocity bias correction only.

The particle lag, statistical uncertainty, and biasing effects described above constitute the major sources of errors in this investigation. Other less significant sources of errors include alignment accuracy, inaccuracies due to counter clock resolution, and inaccuracies in the frequency shifting components. Alignment accuracy with the LDV is believed to be quite good due to the ability to project the beams over large distances and thus make accurate measurements of small angles. The largest source of alignment error is in the orientation of the two fringe planes perpendicular to each other. This alignment is done by projecting the fringes onto a grid and aligning the beam-splitting optics. Using this procedure, the fringes were aligned within 1 deg of perpendicularity, and thus the error in velocity as a result of alignment errors is of the order of 1%. The counter-clock resolution errors result from the 1-ns resolution of the clock which measures the time required for a particle to pass through eight fringes. The amount of this error is a function of velocity, and decreases from 1.2% at a velocity measurement of 630 m/s to 0.6% at a velocity of 100 m/s. Thus, this source of error is most significant in the high-velocity regions of the flowfield, in which the turbulence intensity is low and the other sources of error such as statistical uncertainty and biasing effects are at a minimum. Errors caused by the frequency shifting components include slight changes in beam angles caused by the necessary optics, and small inaccuracies in the 40-MHz shifting frequency. A comparison between measurements made with and without frequency shifting in flowfields which were similar, but not necessarily identical, indicates that these errors are of the order of 1.5%, although one point indicated a difference of 2.3%.

Experimental Results

Undisturbed Boundary Layer

Detailed boundary-layer surveys were made with the LDV system in the turbulent boundary layer which formed on the floor of the wind tunnel in the absence of the compression corner model. These surveys were made on the wind-tunnel centerline at four stations within the test section. Two-component velocity measurements were made within the boundary

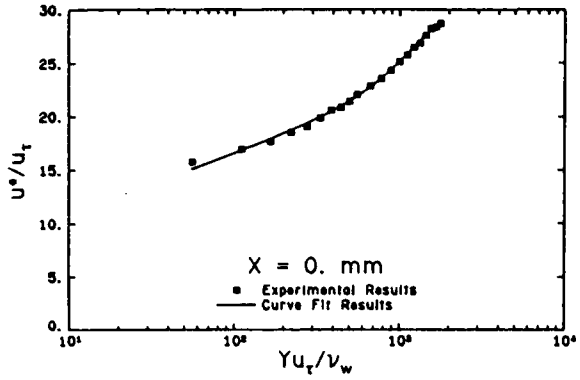

Fig. 2 Undisturbed boundary-layer profile in wall-wake law coordinates.

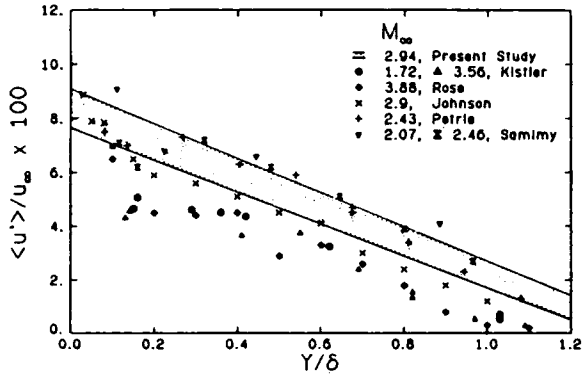

Fig. 3 Undisturbed boundary-layer turbulence intensity measurements.

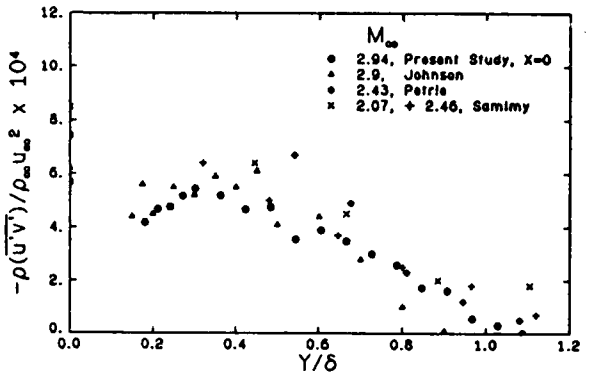

Fig. 4 Undisturbed boundary-layer shear stress measurements.

layer to a point 1.5 mm ($Y/\delta_0 = 0.18$) above the wind-tunnel floor at which point blockage of the two lower laser beams began to occur. The boundary-layer surveys were completed with single-component LDV measurements down to a point 0.25 mm ($Y/\delta_0 = 0.03$) above the surface. In these measurements of the undisturbed boundary layer, frequency shifting proved unnecessary due to the relatively low turbulence intensities.

The boundary-layer thickness at $X = 0$ in the center of the test section was determined to be 8.27 mm ($u_e = 0.99u_\infty$). The displacement and momentum thicknesses were determined by numerical integration of the velocity profiles, accounting for compressibility effects, and had values of $\delta^* = 3.11$ mm and $\theta = 0.57$ mm. The Reynolds number within the test section based on boundary-layer thickness, Re_δ, was 3.1×10^5. The freestream velocity measured at $X = 0$ was within 0.2% of the velocity predicted from the measured pressure distribution.

Further details of the undisturbed boundary layer can be obtained using the transformed wall-wake law of Maise and McDonald.[15] A curve fit of the data of the current investigation to the wall-wake law can be used to obtain estimates of the wake strength parameter, Π, and the skin friction coefficient, C_f. The profile of the undisturbed boundary layer in wall-wake coordinates is shown in Fig. 2 for both the measured LDV data and the least-squares curve fit. The quantity u^+ is the Van Driest generalized velocity[15] and the quantity u_τ is the friction velocity, defined as $(\tau_w/\rho_w)^{1/2}$. From this curve fit, the wake strength parameter, Π, was determined to be equal to 0.98 and the skin friction coefficient, C_f, was found to be 0.00114. Although the wake strength parameter value of 0.98 is somewhat higher than the values reported in much of the literature, Samimy[16] and Sturek and Danberg[17,18] report comparable results. The value for the skin friction coefficient agrees well with the data of Settles[2] and Sturek and Danberg.[17,18]

The streamwise component turbulence intensity measured with the LDV system for the undisturbed boundary layer is shown in Fig. 3. The data measured at four stations within the test section fall within a very narrow band and compare well with other experimental data. The measured turbulence intensities at the edge of the boundary layer and the freestream are probably higher than the actual levels which occur within the flowfield due to the 1 ns counter-clock resolution problem previously discussed. The turbulence intensities of this investigation are somewhat higher than the hot-wire data of Kistler[19] and Rose.[20] This difference can be attributed to the counter-clock resolution in the outer regions of the boundary layer, and possibly to difficulties in hot-wire calibration and interpretation in the lower-velocity regions of the inner boundary layer. The turbulence intensities of this investigation compare well with the LDV data of Petrie,[21] Samimy,[16] and Johnson,[22] as seen in Fig. 3.

The turbulent shear stress distribution determined from the LDV measurements within the undisturbed boundary layer at $X = 0$ is shown in Fig. 4, along with the data of Samimy,[16] Petrie,[21] and Johnson.[22] The density at each measurement location was calculated assuming adiabatic conditions within the boundary layer. Although there is a good deal of scatter in the data, the data of the current investigation agree reasonably well with those of the other three investigations. There is a tendency for the shear stress of the current investigation to reach a peak within the boundary layer and then decrease as the wall is approached. Similar shear stress behavior can be seen in data reported in other boundary-layer studies using both LDV systems[23-25] and slanted hot-wire systems.[8,9] Yanta and Lee[23] and Johnson and Rose[24] have suggested that this is the result of other turbulent shear stress terms, such as $\overline{\rho' u' v'}$, becoming significant in the lower regions of the boundary layer. However, Dimotakis, Collins, and Lang[25] suggest that this is the result of particle dynamics near solid walls which influence LDV measurements. This latter theory does not explain the decrease in shear stress near the wall that has been measured by hot-wire probes, and further study of this phenomenon is necessary.

Compression Corner Flowfields

The schlieren system was used to view the five compression corner flowfields during the initial phase of this investigation. The freestream flow was observed to be completely supersonic, and some unsteadiness was observed in the shock structures, particularly in the large ramp angle configurations, similar to the unsteadiness reported by Dolling and Murphy[26] in a 24-deg compression corner flowfield. The presence of separation near the corner was clearly visible in the schlieren photographs of the 16-, 20-, and 24-deg flowfields.

Surface streak patterns were obtained with two techniques, one using an extremely viscous oil, and a second using a kerosene-zinc oxide mixture. These techniques indicated the presence of separation in the 16-, 20-, and 24-deg compression

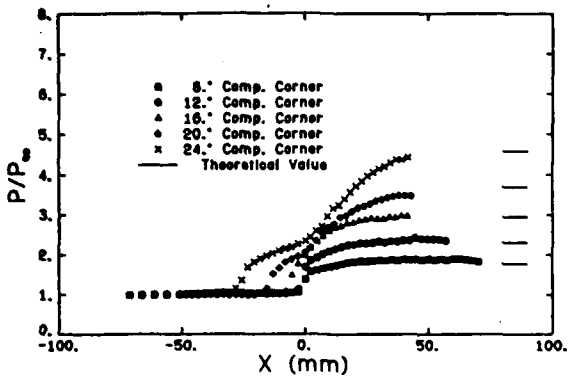

Fig. 5 Surface static pressure distributions.

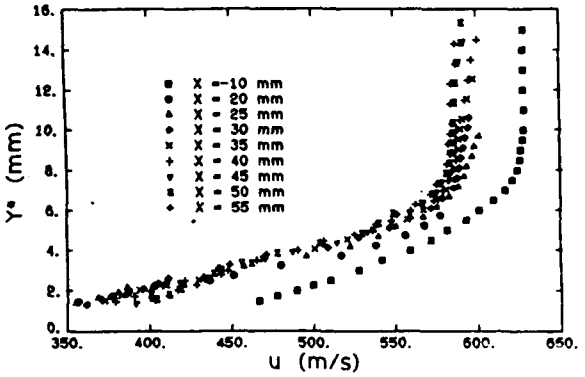

Fig. 6 Streamwise velocity profiles for the 12-deg compression corner flowfield.

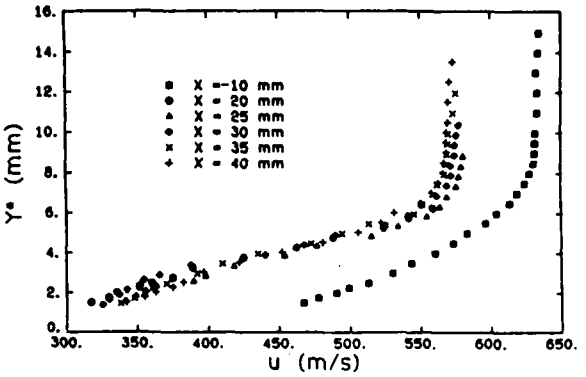

Fig. 7 Streamwise velocity profiles for the 16-deg compression corner flowfield.

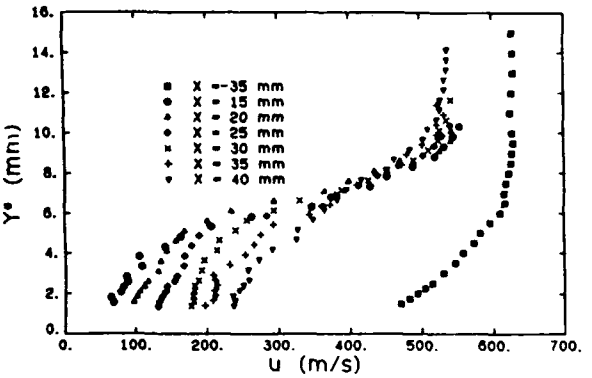

Fig. 8 Streamwise velocity profiles for the 24-deg compression corner flowfield.

corner flowfields, as well as the presence of an extremely small amount of separation in the 12-deg compression corner flowfield. This result is consistent with the results of Settles,[2] who found a very small separated region in a Mach 3, 10-deg compression corner flowfield using a similar surface flow pattern technique. From the results of these surface streak patterns, the dimensionless separation locations at the wind-tunnel centerline, X_S/δ_0, were found to be -0.12, -0.71, -1.63, and -2.95, for the 12-, 16-, 20-, and 24-deg flowfields, respectively. The dimensionless reattachment locations at the wind-tunnel centerline, X_R^+/δ_0, were found to be 0.09, 0.15, 0.52, and 1.11, for the 12-, 16-, 20-, and 24-deg flowfields, respectively. The surface streak patterns indicated some three dimensionality in the 16-, 20-, and 24-deg compression corner flowfields due to the presence of the sidewall boundary layers. As mentioned previously, this could have been significantly reduced with the use of sidewall splitter plates to reduce the effects of the wind-tunnel walls. However, the optical access necessary for the LDV measurements made the use of splitter plates impossible. In all configurations, the reattachment line was found to be very straight and free of three-dimensional effects for at least the center of 7 cm of the 10.2-cm test section width. The LDV measurements were limited to the regions upstream of separation and downstream of reattachment, and thus it is believed that the three-dimensional effects within the separated regions had a negligible effect on the LDV measurements.

The surface static pressure distributions for the five compression corners are presented in Fig. 5. The solid lines on the right side of the figure are the theoretical downstream static pressures calculated with two-dimensional oblique shock wave theory. The pressure distributions on the surface of the ramps indicate that, with the possible exception of the 24-deg configuration, the ramps were long enough to achieve full pressure recovery within the boundary layer. The 24-deg ramp was approximately 14% shorter than the critical ramp length according to the theory of Hunter and Reeves.[27] However, the reattachment point was over four boundary-layer thicknesses upstream of the end of the ramp, and the pressure near the end of the ramp was only 3% less than the theoretical value. Thus it appears that the 24-deg model was very close to the length required for full pressure recovery, and any effects of the less than optimum length were essentially negligible.

The boundary-layer velocity profiles for the 12-, 16-, and 24-deg compression corners are shown in Figs. 6, 7, and 8. The profiles for the 12- and 24-deg corners were chosen for presentation because they best illustrate the effects of large separation regions on the mean velocity profiles. The profiles for the 16-deg configuration are presented such that, with the remaining figures that will be discussed, a complete set of data for this configuration is included in this paper. The horizontal axis in these figures is the velocity component parallel to the wind-tunnel floor for the upstream boundary-layer data, and parallel to the ramp surface for the downstream data. The vertical axis is the distance from the wind-tunnel floor, or ramp surface, measured perpendicular to the upstream flow direction. The surveys were made down to a point approximately 1.5 mm above the wind-tunnel floor or ramp surface. Below this point, blockage of the two lower laser beams began to occur, making two-component measurements impossible. Single-component measurements were not made within these flowfields.

The effects of particle lag can be seen in the velocity profiles of the 12- and 16-deg configurations, in which the velocity just outside the boundary layer is relaxing toward the correct downstream value. Within the boundary layer the effects of particle lag diminish as the distance from the measurement position to the shock wave increases. The velocity in the regions nearest the wall downstream of the corners can be seen increasing with X. This results from the steeper shock wave in the lower Mach number regions of the boundary layer, which causes a larger fractional decrease in the velocity than the shock wave in the outer regions of the boundary

layer. Thus downstream of the interaction, the flow nearest the wall must accelerate as the boundary layer begins to return to an equilibrium state. This behavior was also seen in the 8-deg compression corner redeveloping boundary layer, due to the similarity of the fully attached flow and flows with only small amounts of separation.

The velocity profiles downstream of the 24-deg compression corner exhibit wake-like properties, similar to those observed by other investigators downstream of separated compression corners.[2,4,5] These wake-like profiles are the result of the redeveloping downstream boundary layer having a shear layer velocity profile as its initial condition at reattachment. The shear layer velocity profiles develop over the length of the separated region starting at the separation point of the upstream boundary layer. The velocity profiles downstream of reattachment experience a rapid "filling out," as can be seen in Fig. 8. This rapid change in the boundary-layer profiles is most likely caused by enhanced turbulent mixing, due to the formation of large-scale eddies. The decrease in the measured streamwise velocity with X, which can be seen in the outer regions of the boundary layer downstream of the 24-deg compression corner, is caused by a combination of two effects. The surface static pressure distributions, shown in Fig. 5, indicate that the pressure was still rising at the longitudinal locations where the velocity profiles shown in Fig. 8 were measured. Thus, the flow in these regions was still turning and decelerating in the final stages of the compression process. Also, the effects of particle lag may be contributing to the decrease in u with X. The rather complicated two-stage compression process caused by the presence of the separation and reattachment shock structures makes it not feasible to predict the particle lag in these regions. Thus the extent to which particle lag is contributing to this effect is uncertain.

The streamwise turbulence intensity, $\langle u' \rangle$, nondimensionalized by the freestream velocity upstream of the interaction, u_∞, is plotted for the 16-deg compression corner flowfield in Fig. 9. The turbulence intensity in the upstream boundary layer is also included for comparison. These data were chosen for presentation because they illustrate the trends of the turbulence intensity profiles seen in the data of all five flowfield configurations. In each of the redeveloping boundary layers, the level of the turbulence intensity was significantly increased by the interaction, with the amount of increase directly related to ramp angle, and thus shock strength. The turbulence intensity was found to reach a peak within the central regions of the boundary layers, and then decrease as the wall was approached, as illustrated by the data of Fig. 9. The turbulence intensity in each configuration could be seen spreading vertically with the intensity profiles becoming flatter at the downstream stations. This vertical diffusion can also be seen in the data of Ardonceau[12] downstream of a Mach 2.25 compression corner. A gradual decrease in the peak turbulence intensity accompanied this diffusion process as the boundary layer recovered from the effects of the interaction.

The maximum streamwise turbulence intensities for each measurement station are presented in Fig. 10. The maximum values plotted in this figure clearly show the increase in maximum turbulence intensity with ramp angle, and the gradual decrease of this quantity with X. Further analysis of the data from this investigation indicated that the location of the maximum turbulence intensity in each profile was also directly related to ramp angle, with the maximum values of turbulence intensity occurring further from the ramp surface for the larger shock strength interactions. A comparison of these data with the mean velocity profiles indicated that the maximum values of turbulence intensity occurred in the regions of maximum $\partial u/\partial Y^*$, due to the higher values of turbulence production in these regions of the boundary layers. It was also found that, in spite of the vertical diffusion of the turbulence within the boundary layers, the location of the maximum values remained essentially constant as the flow proceeded downstream.

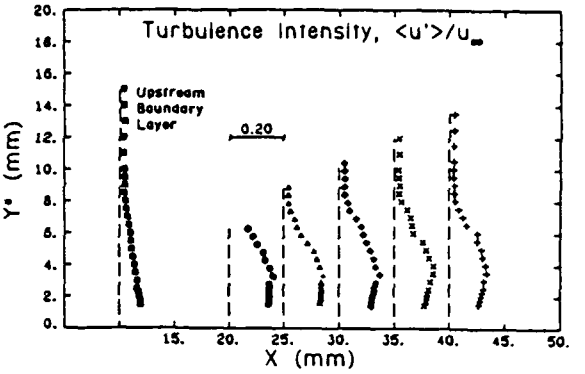

Fig. 9 Streamwise turbulence intensity profiles for the 16-deg compression corner flowfield.

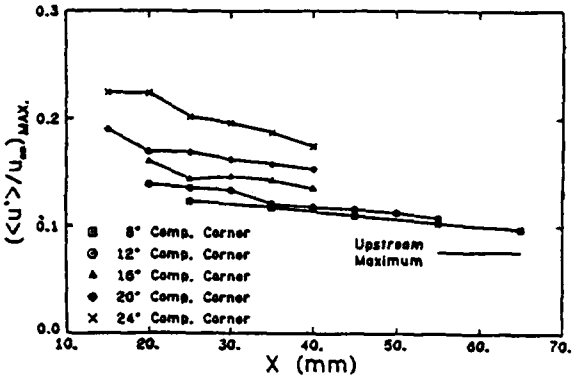

Fig. 10 Maximum streamwise turbulence intensities for the five compression corner flowfields.

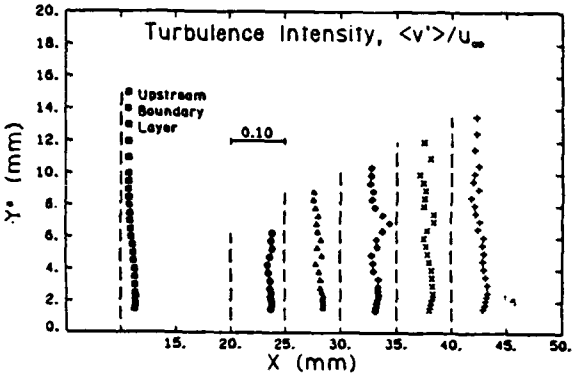

Fig. 11 Vertical turbulence intensity profiles for the 16-deg compression corner flowfield.

Vertical turbulence intensity profiles, $\langle v' \rangle/u_\infty$, are shown in Fig. 11 for the 16-deg compression corner flowfield. The data obtained in this configuration are considered representative of the data obtained for all five configurations in this investigation. It can be seen in this figure that the effect of the shock wave was to increase the vertical turbulence intensity through the interaction. A comparison of the $\langle v' \rangle$ profiles from the five configurations indicates that, similar to the $\langle u' \rangle$ data, the amount of increase in this quantity was directly related to ramp angle, and thus shock strength. However, unlike the $\langle u' \rangle$ data, the $\langle v' \rangle$ profiles show little or no dependence on the distance from the ramp surface, Y^*. There is a tendency for $\langle v' \rangle$ to reach a local maximum near the edge of the boundary layer, but this characteristic is found in only a few of the profiles measured in this investigation. It can also be seen in Fig. 11 that the vertical turbulence intensity was significantly increased in the regions outside the boundary layer. These data, in conjunction with other turbulence statis-

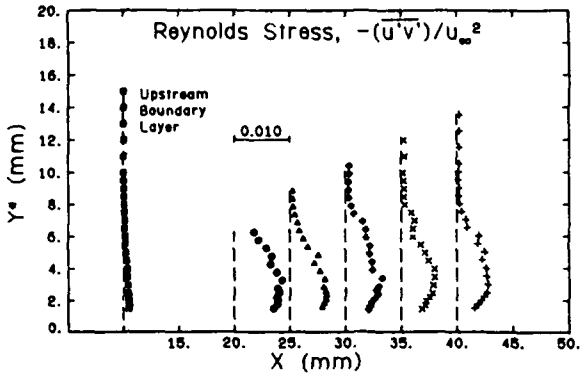

Fig. 12 Reynolds stress profiles for the 16-deg compression corner flowfield.

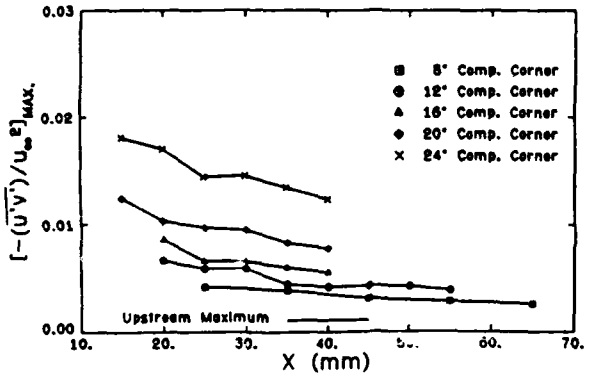

Fig. 13 Maximum Reynolds stresses for the five compression corner flowfields.

tics obtained in this investigation, such as turbulence triple products and skewness and flatness factors, indicated that there was a significant alteration of the freestream turbulence structure caused by the presence of the oblique shock wave. While it is possible that this effect is caused by particle lag, this is considered unlikely by the authors because the effects of lag diminish rapidly as the distance from the shock wave to the measuring point increases, while the large freestream values of $\langle v' \rangle$ persist to the most downstream measurement stations with very little sign of dissipation. Further studies are necessary to determine the exact nature of the effects of the oblique shock waves on the turbulence structure within the freestream flowfield.

The effects of particle lag on the mean velocity measurements can be seen in Fig. 6 in the outer regions of the boundary layer immediately downstream of the 12-deg compression corner shock wave. Some influence of this particle lag was expected in the measured turbulence intensities. In regions of significant particle lag, a false turbulence was expected due to different-sized particles decelerating at different rates, and thus producing a broad velocity histogram. However, no indications of the effects of particle lag were observed in any of the turbulence intensity profiles. The streamwise and vertical turbulence intensities in the freestream regions with significant particle lag were very similar to the values measured in the freestream regions with no significant lag. This is indicative of a relatively uniform particle size distribution, such that the false turbulence generated by the lag was insignificant in comparison to the magnitude of the turbulence within the boundary layers.

The Reynolds stress profiles for the 16-deg compression corner flowfield, nondimensionalized with u_∞^2, are presented in Fig. 12. It can be seen in this figure that the magnitude of the Reynolds stress was significantly increased by the shock wave. In all configurations the Reynolds stress reached a peak within the boundary layer and then decreased as the wall was approached. The tendency for the Reynolds stress to reach a maximum within the central regions of the boundary layer has been reported by other investigators in compression corner flowfields,[7-9] as well as in reattaching free shear layers.[16]

The maximum Reynolds stresses for each boundary-layer profile are shown in Fig. 13. Like the turbulence intensity, the maximum Reynolds stress is a strong function of ramp angle, with very large values associated with the 20- and 24-deg compression corner flowfields. These large Reynolds stresses imply the existence of large-scale eddies, which were also indicated by the rapid "filling out" of the wake-like boundary layers downstream of the 20- and 24-deg compression corner shock waves. A steady decrease in Reynolds stress with X can be seen in this figure, as the turbulence began to dissipate and diffuse through the boundary layers. The dissipation of the turbulence, however, was an extremely gradual process, and even in the weakest interaction, the ramp was of insufficient length to allow the turbulence to completely return to equilibrium conditions.

The trends in the Reynolds stresses of this investigation agree quite well with those found by researchers working with similar flowfields.[7-9] The dependency of the increase in Reynolds stress on α, the gradual decay in Reynolds stress with X downstream of the interaction, and the vertical diffusion of the Reynolds stress in the boundary layer can all be seen in the data of Muck and Smits,[8,9] for 16- and 20-deg compression corners. However, the magnitudes of $-\overline{u'v'}/u_\infty^2$ reported by these authors are significantly lower than the results of the current investigation, with the maximum values differing by factors of 2 to 4 depending on ramp angle. This discrepancy is most likely caused to a large extent by calibration problems associated with the slanted hot-wire technique used in these investigations. These authors state that the hot-wire calibration is only valid in regions in which the Mach number component normal to the wire exceeds 1.2. Taking into account the 30-deg yaw angle of the slanted hot wires, this yields a lower Mach number limit of 1.39. The local mean Mach numbers at the regions of maximum Reynolds stress in the current investigation are all below 1.39 for the 16-, 20-, and 24-deg configurations, and are close to this value for much of the data of the 8- and 12-deg configurations. In addition to these low mean Mach numbers, the high turbulence intensities in these regions indicate that the instantaneous local Mach number frequently drops far below the calibration limits, and these periods of low Mach number contribute significantly to the magnitude of $-\overline{u'v'}$. Considering these factors, it is not surprising that a large discrepancy exists between Reynolds stresses measured with slanted hot wires and those measured with two-component LDV systems in highly turbulent flowfields. An investigation in which both techniques are used to make measurements in the same flowfield would be extremely useful in resolving these discrepancies.

Conclusions

The interaction between an oblique shock wave and a turbulent boundary layer results in significant changes in both the mean and turbulent structure of the boundary-layer flowfield. The mean velocity profiles measured in this investigation indicated that the inner regions of the boundary layer were decelerated to a greater degree than the outer regions by the interaction. The profiles downstream of interactions with large amounts of separation were very wake-like in nature, with the inner regions accelerating rapidly as the boundary layers began to return to equilibrium states. Turbulence intensities and Reynolds stress values were significantly increased by the interaction, with the amount of increase directly related to ramp angle, and thus shock strength. The measured profiles of longitudinal turbulence intensity and Reynolds stress reached peak values within the central regions of the boundary layers, with the distance from the peak values to the ramp

surface also directly related to shock strength. The Reynolds stress values obtained in this investigation were significantly higher than values which have been measured in similar flowfields with slanted hot wires, and this discrepancy is believed to be due to the calibration problems associated with hot-wire systems in highly turbulent supersonic flows. The turbulent structure within the redeveloping boundary layer relaxed very gradually, such that the size limitations imposed by the wind tunnel used in this investigation prohibited the use of ramps of sufficient length to allow a complete return of the turbulent properties to upstream equilibrium values. The rapid "filling out" of the mean velocity profiles, and the large values of the measured Reynolds stresses indicated the presence of large scale turbulent structures in the flow downstream of the shock-wave/turbulent-boundary-layer interactions.

Acknowledgment

Support for this research was provided by the U.S. Army Research Office through contract monitor Dr. Robert E. Singleton under Research Contract DAAG 29-79-C-0184 and Research Contract DAAG 29-83-K-0043; and the Department of Mechanical and Industrial Engineering at the University of Illinois at Urbana-Champaign.

References

[1]Kuntz, D.W., "An Experimental Investigation of the Shock Wave-Turbulent Boundary Layer Interaction," Ph.D. Thesis, Dept. of Mechanical and Industrial Engineering, Univ. of Illinois at Urbana-Champaign, Urbana, 1985.

[2]Settles, G.S., "An Experimental Study of Compressible Turbulent Boundary Layer Separation at High Reynolds Numbers," Ph.D. Thesis, Princeton Univ., Princeton, New Jersey, 1975.

[3]Settles, G.S., Bogdonoff, S.M., and Vas, I.E., "Incipient Separation of a Supersonic Turbulent Boundary Layer at High Reynolds Numbers," *AIAA Journal*, Vol. 14, Jan. 1976, pp. 50–56.

[4]Settles, G.S., Vas, I.E., and Bogdonoff, S.M., "Details of a Shock-Separated Turbulent Boundary Layer at a Compression Corner," *AIAA Journal*, Vol. 14, Dec. 1976, pp. 1709–1715.

[5]Settles, G.S., Fitzpatrick, T.J., and Bogdonoff, S.M., "Detailed Study of Attached and Separated Compression Corner Flowfields in High Reynolds Number Supersonic Flow," *AIAA Journal*, Vol. 17, June 1979, pp. 579–585.

[6]Hayakawa, K., Smits, A.J., and Bogdonoff, S.M., "Hot-wire Investigation of an Unseparated Shock-Wave/Turbulent Boundary Layer Interaction" AIAA Paper 82-0985, June 1982.

[7]Jayaram, M. and Smits, A.J., "The Distortion of a Supersonic Turbulent Boundary Layer by Bulk Compression and Surface Curvature," AIAA Paper 85-0299, Jan. 1985.

[8]Muck, K.C. and Smits, A.J., "The Behavior of a Compressible Turbulent Boundary Layer Under Incipient Separation Conditions," 4th Symposium on Turbulent Shear Flows, Karlsruhe, West Germany, Sept. 1983.

[9]Muck, K.C. and Smits, A.J., "Behavior of a Turbulent Boundary Layer Subjected to a Shock-Induced Separation," AIAA Paper 84-0097, Jan. 1984.

[10]Rose, W.C. and Johnson, D.A., "Turbulence in a Shock-Wave Boundary-Layer Interaction," *AIAA Journal*, Vol. 13, July 1975, pp. 884–889.

[11]Modarress, D. and Johnson, D.A., "Investigation of Turbulent Boundary-Layer Separation Using Laser Velocimetry," *AIAA Journal*, Vol. 17, July 1979, pp. 747–752.

[12]Ardonceau, P.L., "The Structure of Turbulence in a Supersonic Shock-Wave/Boundary-Layer Interaction," *AIAA Journal*, Vol. 22, Sept. 1984, pp. 1254–1262.

[13]McLaughlin, D.K. and Tiederman, W.G., "Biasing Correction for Individual Realization of Laser Anemometer Measurements in Turbulent Flows," *The Physics of Fluids*, Vol. 16, No. 12, 1973, pp. 2082–2088.

[14]Buchhave, P., "Biasing Errors in Individual Particle Measurements with the LDA-Counter Signal Processor," *Proceedings of the LDA-Symposium*, Copenhagen, Denmark, 1975, pp. 258–278.

[15]Maise, G. and McDonald, H., "Mixing Length and Kinematic Eddy Viscosity in a Compressible Boundary Layer," *AIAA Journal*, Vol. 6, Jan. 1968, pp. 73–80.

[16]Samimy, M., "An Experimental Study of Compressible Turbulent Reattaching Free Shear Layers," Ph.D. Thesis, Dept. of Mechanical and Industrial Engineering, Univ. of Illinois at Urbana-Champaign, Urbana, 1984.

[17]Sturek, W.B. and Danberg, J.E., "Supersonic Turbulent Boundary Layer in Adverse Pressure Gradient. Part I: The Experiment," *AIAA Journal*, Vol. 10, April 1972, pp. 475–480.

[18]Sturek, W.B. and Danberg, J.E., "Supersonic Turbulent Boundary Layer in Adverse Pressure Gradient. Part II: Data Analysis," *AIAA Journal*, Vol. 10, May 1972, pp. 630–635.

[19]Kistler, A.L., "Fluctuation Measurements in a Supersonic Turbulent Boundary Layer," *The Physics of Fluids*, Vol. 2, No. 3, May-June 1959, pp. 290–296.

[20]Rose, W.C., "Turbulence Measurements in a Compressible Boundary Layer," *AIAA Journal*, Vol. 12, Aug. 1974, pp. 1060–1064.

[21]Petrie, H.L., "A Study of Compressible Turbulent Free Shear Layers Using Laser Doppler Velocimetry," Ph.D. Thesis, Dept. of Mechanical and Industrial Engineering, Univ. of Illinois at Urbana-Champaign, Urbana, 1984.

[22]Johnson, D.A., "Turbulence Measurements in a Mach 2.9 Boundary Layer Using Laser Velocimetry," *AIAA Journal*, Vol. 12, May 1974, pp. 711–714.

[23]Yanta, W.J. and Lee, R.E., "Measurements of Mach 3 Turbulent Transport Properties on a Nozzle Wall," *AIAA Journal*, Vol. 14, June 1976, pp. 725–729.

[24]Johnson, D.A. and Rose, W.C., "Turbulence Measurements in Supersonic Boundary Layer Flows Using Laser Velocimetry," *Proceedings of the Second International Workshop on Laser Velocimetry*, Vol. 2, Purdue Univ., West Lafayette, IN, March 1974.

[25]Dimotakis, P.E., Collins, D.J., and Lang, D.B., "Laser Doppler Velocity Measurements in Subsonic, Transonic, and Supersonic Turbulent Boundary Layers," *Laser Velocimetry and Particle Sizing*, edited by H.D. Thompson and W.H. Stevenson, Hemisphere Publishing, New York, 1979, pp. 208–219.

[26]Dolling, D.S. and Murphy, M., "Wall Pressure Fluctuations in a Supersonic Separated Compression Ramp Flowfield," AIAA Paper 82-0986, June 1982.

[27]Hunter, Jr., L.G. and Reeves, B.L., "Results of a Strong Interaction, Wake-Like Model of Supersonic Separated and Reattaching Turbulent Flows," *AIAA Journal*, Vol. 9, April 1971, pp. 703–712.

SECTION B.5

LDV MEASUREMENTS IN SUPERSONIC SEPARATED FLOWS

Invited Paper Presented at the Optical Methods in Flow and Particle Diagnostics Conference,
International Congress on Applications of Lasers and Electro-Optics

San Diego, California

November 1987

by

J. C. Dutton, A. L. Addy, and M. Samimy

LDV MEASUREMENTS IN SUPERSONIC SEPARATED FLOWS

J. C. DUTTON
Associate Professor

A. L. ADDY
Professor and Head

M. SAMIMY
Assistant Professor

Department of Mechanical and Industrial Engineering
University of Illinois at Urbana-Champaign
Urbana, Illinois 61801 USA

Mechanical Engineering Department
Ohio State University
Columbus, Ohio 43210 USA

Abstract

An overview is given of a broad-based experimental research program whose aim is to study and clarify the detailed interactions occurring in high-speed separated flows. The principal tool used in these investigations is a two-component laser Doppler velocimeter, and the implementation of this instrument in the flows of interest is discussed. In addition, as an example of the results obtained, measurements from a recent study concerning the interaction of two compressible shear layers are presented and discussed.

Introduction

The research to be discussed herein is part of a long-term investigation of the fundamental fluid dynamic mechanisms and interactions that occur in high-speed flowfields with embedded separated regions. The motivation for these studies is to develop experimental, computational, and analytical tools which will yield an improved understanding of these mechanisms as they relate to missile base flow phenomena. Figure 1 presents schematic diagrams of the flowfields for typical power-on and power-off base flows. In the power-on case of Fig. 1(a), the supersonic freestream and propulsive nozzle flows in the missile afterbody region approach the base where they separate, expand or compress to the common base pressure, and form free shear layers and a recirculating, separated flow region. The free shear layers then must recompress and redevelop in the reattachment region as they are turned to a common flow direction. For the power-off case of Fig. 1(b), a single shear layer is formed by the separation of the supersonic freestream flow at the base with recompression and redevelopment of this mixing layer occurring in the reattachment zone along the missile axis of symmetry.

The physical understanding of the flow mechanisms associated with these problems was originally begun at the University of Illinois in the 1950's by studying the phenomena theoretically on the basis of the component modeling approach. In parallel with the theoretical analysis of high-speed separated flows, experiments have been conducted over the years to examine fundamental aspects of separated flowfields; these experiments have been instrumental in providing guidance to the theoretical formulation of the problems and have been used to verify the theoretical predictions whenever possible. Previous experiments have relied upon our small-scale continuous flow or blow-down facilities in conjunction with conventional pressure instrumentation and Schlieren/shadowgraph photography for surface pressure measurements and flow visualization, respectively. Most recently, however, our experimental efforts have been directed at obtaining two-color, two-component, coincident laser Doppler velocimeter (LDV) measurements of the mean and turbulent velocity fields in high-speed separated flows. It is these measurements that are the focus of this paper.

Research Program Overview

Detailed flowfield data have been obtained for several planar, two-dimensional, supersonic separated flows that contain the fundamental mechanisms and interactions of the base flow configurations sketched in Fig. 1. In the initial series of experiments[1,2], Fig. 2, a supersonic M=2.5 flow with an equilibrium turbulent boundary layer was separated from a backstep. For the flow sketched in Fig. 2(a), the reattachment ramp angle was adjusted to produce a constant pressure separation, i.e. with no expansions or compressions at the backstep, and in conjunction with a solid lower wall, a recirculating flow was thereby formed below the shear layer. For the flow of Fig. 2(b), the lower wall was replaced with a porous plate and an attempt was made to match the mass bleed through the plate with that entrained by the shear layer, thereby modeling a free shear layer in a semi-infinite medium with no recirculation. In both cases, the experimental measurements were focused on the initial shear layer development region immediately downstream from the backstep. In a second series of experiments[3-6], Fig. 3, shear layer reattachment onto a solid surface was investigated. The flow configuration of Fig. 3(a) is similar to that of Fig. 2(a), but the emphasis of the measurements in this case was on the reattachment/redevelopment region as the developed free shear layer is constrained to turn parallel to the ramp, resulting in the formation of an oblique shock near the reattachment point. The classical supersonic backstep flowfield with an approach Mach number of M=2.0, Fig. 3(b), has also been investigated in this series of experiments. The reattachment processes for this flow are qualitatively similar to those of the flow of Fig. 3(a), with the added complication of the expansion waves occurring at the backstep separation point. As might be expected, these expansion waves alter the initial development of the shear layer as compared to the constant pressure separation of the flow of Fig. 3(a). The approach Mach number for the backstep flow, M=2.0, was also chosen so that after expansion at the step, the Mach number of the external inviscid flow was similar to that of the ramp reattachment experiment shown in Fig. 3(a). The third experimental series[7-9], Fig. 4, investigated oblique shock wave/turbulent boundary layer interactions in a compression corner with an upstream Mach number of M=3.0. Ramp angles of 8°, 12°, 16°, 20°, and 24° allowed investigation of the full range of flow conditions possible for this configuration, including flow with no separation, flow with incipient separation, and flow with a significant amount of separation (the case shown in Fig. 4). A fourth, ongoing experimental series[10,11], Fig. 5, concerns a planar, two-dimensional analog of the power-on base flow problem sketched in Fig. 1(a), with separation of two supersonic streams ($M_{\infty 1}$=2.0, $M_{\infty 2}$=1.5 for the first case studied[10]) from a finite thickness base, formation of two free shear layers and a recirculating flow region, and growth, recompression, reattachment, and redevelopment of these shear layers in the downstream region. Clearly, these experimental series contain, in varying degrees of complexity, all of the important flow mechanisms and interactions occurring in the supersonic missile base flows of Fig. 1.

As will be discussed further, the two-component, coincident LDV data obtained in each case have encompassed the mean flow properties, turbulence intensities, kinematic turbulent shear stresses, higher order turbulence moments including the triple products and skewness and flatness factors, and other derived quantities such as the turbulence production, mixing length scale, and eddy viscosity. These measurements, in turn, have been used to discern and explain important features of each of these flows.

Invited Paper presented and published in the Proceedings of the Optical Methods in Flow and Particle Diagnostics Conference, International Congress on Applications of Lasers and Electro-Optics, San Diego, California, November, 1987.

Briefly, key results of these detailed experimental investigations include the finding of maximum turbulence intensities and shear stresses near the sonic line in the shear layers (in disagreement with intrusive hot-wire measurements), large values of these turbulence quantities near recompression/reattachment points with decay through the redevelopment regions, and the existence of large recirculating velocities in the separated regions. This latter observation clearly leads to the conclusion that the recirculating regions in high-speed separated flows may be much more dynamic than previously thought. Further details concerning these measurements may be found in the references cited above.

The following section contains a brief description of the LDV system setup and procedures used in the experiments.

LDV System and Measurement Techniques

The LDV system used in these experiments is a TSI, Inc. two-color, two-component system utilizing the green beam, λ=514.5 nm, and the blue beam, λ=488 nm, from a Spectra-Physics 5 W argon-ion laser operating in the multiline mode. After beam splitting, one beam of each pair is passed through a Bragg cell in order to shift the frequency by 40 MHz. Frequency shifting allows the determination of flow direction in separated regions and, together with orientation of the fringes at ±45° to the mean flow direction, reduces the effects of fringe bias. The four parallel beams are then passed through a focusing lens to produce the measurement volume containing the two orthogonal fringe patterns necessary for the two-component velocity measurements. Depending on the local flow conditions, focusing lenses with 250 mm, 350 mm, and 600 mm focal lengths have been used in these experiments. The collecting optics are located on the opposite side of the test section from the transmitting optics (i.e., forward scatter) and consist of a 250 mm focal length collection lens, dichroic mirrors and filters to separate the scattered light signals for the two colors, and photomultipliers (PMTs) to convert these light signals to analog voltage signals. The collection optics are oriented at 10° off-axis to simplify alignment procedures, to optimize signal strength of the scattered light, and to reduce the effective measurement volume length. With a typical transmitting optical arrangement consisting of 22 mm beam spacing and the 350 mm focal length focusing lens, the green beam measurement volume diameter is approximately 0.18 mm, its effective length is approximately 1.8 mm, and it contains approximately 22 fringes spaced at about 8.5 µm, based on the e^{-2} intensity level. The 40 MHz frequency shifting produces a fringe velocity of approximately 340 m/s in this case. These quantities are all slightly smaller for the blue beam measurement volume. The laser, transmitting optics, and collection optics are mounted on a traversing table which allows movement in the three coordinate directions with an accuracy of approximately ±0.1 mm.

TSI frequency counters, operated in the single measurement per burst mode with high- and low-pass filtering, are used to determine the Doppler shift frequencies of the signals from the PMTs and to perform validation checks to remove erroneous data. The counters used for these studies have a ±1 ns clock resolution in each channel and also perform coincidence interval checks to ensure that both channels have measured the velocity of the same particle. The maximum Doppler signal frequency has been limited to approximately 100 MHz in these experiments, and the uncertainty due to counter clock resolution in a 5-to-8 cycle frequency comparison could reach 3.1% at this maximum frequency. Thus, the comparison level has been set at 4% to avoid discarding data because of clock resolution. The output from the counters is stored in the memory of a DEC PDP 11/73 minicomputer by means of a direct memory access board, and the data are then transferred serially to an HP 9000 computer system for reduction, analysis, and plotting.

The seed particles used in these studies are generated using a commercially available six-jet atomizer to atomize 50 cP silicone oil. The effective mean diameter of these seed particles has been estimated by measuring the relaxation of the velocity downstream of an oblique shock wave[1,7] and comparing the results to analytical predictions which use the empirical drag law of Walsh[12]. Using this procedure, the seed particle diameter has been found to be approximately 1.0 µm. Particles of this diameter have been shown[1,3,7] to have sufficient frequency response to follow the velocity fluctuations of the energy-containing eddies and for accurate estimation of the turbulent stresses in these compressible separated flows.

LDV measurements taken at a particular location involve uncertainties due to the finite sample size of the individual velocity realizations. The statistical uncertainty involved in determining mean velocities from individual measurements is a function both of the sample size and the local turbulent intensity, while the uncertainty for the turbulent intensity is a function only of the sample size[13]. To control these uncertainties, the sample size in these investigations has been increased from 1024 in low turbulence, freestream regions to 2048 or 4096 realizations in highly turbulent regions. As a result, the statistical uncertainty due to finite sample size is a maximum of approximately ±3% for the mean velocity and ±3.5% for the turbulence intensity in the highly turbulent regions of these flows. Elsewhere in the flowfields, these uncertainties are much less.

Another possible source of error in these experiments is that because of the small scale of the experimental models, large velocity gradients exist in some regions of the flow, thereby leading to errors in the velocity statistics due to poor spatial resolution. This is particularly true near the backstep separation points where the shear layers are quite thin. Estimates of the effects of these errors have been made following the method of Karpuk and Tiederman[14]. The spatial resolution errors have been found to be maximum near separation points and of the order of 1% for the mean velocity and 2% for the turbulence intensity. In downstream regions where the shear layers are thicker and the velocity gradients smaller, these errors diminish substantially.

Mean and turbulent flow properties computed from LDV data obtained with counter-type signal processors are also subject to biasing errors, most significantly velocity biasing and fringe biasing. Velocity biasing results from the fact that in a turbulent flow with uniformly distributed particles, a larger volume of fluid is swept through the measurement volume during periods when the velocity is higher than the mean than during periods when it is lower than the mean, thereby biasing the results toward the higher velocities. The individual velocity realization-type counters used in these experiments have the capability of measuring and storing 83,300 coincident samples per second. However, the maximum coincident data rates achieved in these studies range from several thousand per second in the freestream to less than 100 per second in the separated flow regions. Therefore, the sampling process is totally controlled by the flow in these experiments. According to Erdmann and Tropea[15,16], this "free-running processor" condition is completely velocity biased. For this reason, a two-dimensional velocity inverse weighting factor, $1/(u^2+v^2)^{1/2}$, similar to that proposed by McLaughlin and Tiederman[17], has been employed to correct for velocity bias in these studies. This method has also recently been extended[18] to include the effects of the unmeasured third velocity component (w) which may become significant when the (u,v) measured velocity components are both nearly zero. The extent to which the effects of velocity biasing are removed with this technique is somewhat uncertain, and further study is needed before this issue is completely resolved. In general, the topic of LDV velocity biasing is a controversial and active area of current research, as evidenced by the many and varied recent contributions on the subject[19].

Fringe biasing results from the fact that a particle must pass through a specified number of fringes within the measurement volume (8 in these experiments) for its velocity to be measured. Thus, particles traveling in a direction parallel to the fringe plane are not "seen" by the LDV, resulting in a bias in favor of particles traveling perpendicular to the fringe plane. The effects of fringe bias have been significantly reduced in these experiments by the previously mentioned 40 MHz frequency shifting, which causes the fringes to move in the upstream direction, and by orienting the fringes at ±45° to the mean flow direction. The fringe bias analysis of Buchave[20] has been modified to incorporate frequency shifting and has been used to correct for possible fringe bias in these studies. The largest difference between two-dimensional velocity bias-corrected mean velocities and mean velocities corrected for both velocity bias and fringe bias was approximately 3% in these experiments. Therefore, the effects of fringe bias are not significant in comparison to those of velocity bias, and the results presented here are corrected for velocity bias only.

More extensive discussions of the LDV system and the associated experimental techniques used in these studies may be found in Refs. 1, 3, and 7. In the following sections, results from an ongoing experimental series are presented and discussed.

Experimental Results for the Interaction Between Two Compressible, Turbulent Free Shear Layers[10]

Experimental Conditions

A series of cold flow experiments has been conducted with air in a small-scale blowdown wind tunnel facility to study the interaction between two compressible free shear layers, see Fig. 5. The test section width and height are 50.8 mm and 101.6 mm, respectively, and the step height is 25.4 mm. The approach Mach number, unit Reynolds number, stagnation pressure, and stagnation temperature were 2.07, 5.85×10^7 m^{-1}, 457.3 kPa, and 295 K, respectively, for the upper flow, and 1.50, 3.37×10^7 m^{-1}, 233.8 kPa, and 295 K, respectively, for the lower flow. After expansion at the step, the Mach and unit Reynolds numbers of the external freestream flows were 2.56 and 3.98×10^7 m^{-1}, respectively, for the upper shear layer and 2.23 and 2.72×10^7 m^{-1} for the lower shear layer. The freestream conditions for the upper flow after separation were designed to be similar to those of the ramp reattachment experiment of Fig. 3(a) and the backstep reattachment experiment of Fig. 3(b) for purposes of comparison.

The velocity vector field for this investigation is plotted in Fig. 6, showing the expansion and turning of the shear layers at the backstep separation point and their eventual realignment to an approximately horizontal direction downstream from the reattachment region. For ease of presentation of the results, the dashed line in Fig. 6, which is drawn approximately through the minimum velocity point for each transverse profile, is used to separate the upper and lower flows. The u velocity component direction is defined to correspond to the local freestream flow direction; it is parallel to the x coordinate for the incoming boundary layer flows, rotated 12.4° clockwise relative to the x coordinate for the upper shear flow, and rotated 18.5° counterclockwise for the lower shear layer. In all cases, the v velocity component is defined to be orthogonal to the corresponding u component.

Two-Dimensionality of the Flowfield

All of the LDV data to be presented below were obtained in the spanwise midplane of the wind tunnel. However, the uniformity of the mean flow and turbulence field across the tunnel was checked by additional measurements at z=±10 mm from the midplane at x=28, 36, and 46 mm. The deviations of the data from the centerline values were largest near the sonic line at x=28 and 38 mm, where the turbulence fluctuations were high, as was the statistical uncertainty due to limited sample size. The maximum spanwise variation of the data for the mean velocity, streamwise turbulence intensity, and kinematic turbulent shear stress were ±1.9%, ±2.8%, and ±2.5%, respectively. These variations were within the statistical uncertainty for the finite sample sizes used in the present experiments. Since LDV measurements further off-center were not possible due to reflections of the laser light from the glass windows of the wind tunnel, it can only be concluded that the flow was two-dimensional within ±10 mm of the wind tunnel midplane.

Approach Boundary Layers

Two-component LDV measurements have been made in the approach boundary layers to within 1 mm of the wall of the backstep, with one-component measurements required for locations closer than this due to beam blockage. The boundary layer and momentum thicknesses were measured to be δ=2.26 mm and θ=0.18 mm for the M=2.07 boundary layer flow and δ=1.59 mm and θ=0.14 mm for the M=1.50 boundary layer. The ratio of momentum thickness to boundary layer thickness measured for the upper and lower boundary layers is in good agreement with the values predicted by the method of Maise and McDonald[21], being only 5% and 1%, respectively, higher than the predicted values. The boundary layer mean velocity profiles are also found to be in good agreement with the correlation curve of Maise and McDonald. As with the δ/θ ratio, the M=1.50 boundary layer velocity profile shows better agreement with the curve than does the M=2.07 profile. This suggests that the predictions of Maise and McDonald may be in better agreement with experimental results at lower Mach numbers. The skin friction coefficients used in determining the velocity profiles were found from the wall-wake law and were C_f=0.00176 and 0.00247 for the upper and lower boundary layers, respectively. These values are in the range reported by Laderman[22] for comparable Mach and Reynolds numbers.

The streamwise turbulence intensity measurements for both boundary layers show consistently higher values than for the incompressible boundary layer results of Klebanoff[23], but are in relatively good agreement with the data of Dimotakis et al.[24] at comparable Mach numbers. The boundary layer shear stress measurements follow closely Sandborn's[25] "best estimate" for equilibrium compressible boundary layers. In addition, the streamwise component of the skewness and flatness factors peak sharply at the outer edge of the boundary layers for both cases, and then decline rapidly for the M=2.07 boundary layer and more gradually for the M=1.50 boundary layer. The Mach 2.85 turbulent boundary layers of Hayakawa et al.[26] and the Mach 2.43 results of Petrie et al.[2] show skewness profiles similar to those of the M=2.07 boundary layer of the present study.

Mean Flowfield

The mean u component velocity profiles for each measurement station, including the boundary layer profiles, are shown in Fig. 7, where the u component direction is as defined previously. The velocities of the higher and lower Mach number flows have been nondimensionalized with respect to the boundary layer freestream velocities before separation, $u_{\infty 1}$ and $u_{\infty 2}$, respectively. The abscissa shows the station numbers, the vertical dashed lines mark the location of zero velocity for each station, and the numbers above each dashed line give the axial location of each station in millimeters. Also shown are the dashed line used to separate the upper and lower flows for presentation purposes and the horizontal scale of the parameter plotted in the figure, i.e. $u/u_{\infty 1,2}$=1.0 in this case. The turbulence measurements to be discussed below will be presented in this same general format and are also nondimensionalized by $u_{\infty 1}$ and $u_{\infty 2}$ for the upper and lower shear layers, respectively.

The mean velocity profiles for the two flows show generally similar characteristics with large velocity gradients across the shear layers, reverse flow in the separated region, formation of a wake-like velocity profile near the reattachment point at x=35 mm, and rapid "filling out" of the mean velocity

profile in the downstream redevelopment region. At the last three measurement stations, the rate of profile development appears to be faster for the lower Mach number flow. This rapid development in the mean velocity profile has also been observed in redeveloping boundary layers[6]. Schlieren photographs of the present flowfield and earlier experiments[6] have shown the existence of large eddies stretched in the streamwise direction that seem to cause enhanced mixing in the redeveloping regions. This matter will be discussed further in the presentation of the turbulence field results.

Turbulence Field

The streamwise turbulence intensity profiles for this flow are presented in Fig. 8. The maximum turbulence intensity at each axial location occurs very near the sonic line for both shear layers. This is in agreement with earlier LDV results for supersonic shear layers[2,4,6], but disagrees with the hot wire results of Hayakawa et al.[27] that located the maximum in the supersonic portion of the shear flow. For stations 3-7 in the reattachment region, the maximum turbulence intensity for the lower M flow is larger than that for the higher M shear layer and also shows a faster streamwise growth rate. This could possibly be the result of the well-known stabilizing influence of compressibility, i.e. reduced shear layer growth rates at higher Mach numbers and/or due to differences in the scales of the coherent large-scale motions, which are one of the contributors to the measured fluctuations. For locations 4-10, the maximum turbulence intensity for each flow diffuses across the shear layer and also decays in the streamwise direction. An almost uniform turbulence intensity profile across the redeveloping layer at the last measurement station confirms the existence of enhanced mixing in this region, which agrees with the rapid development of the mean velocity profiles shown in Fig. 7.

The distributions of the transverse turbulence intensity are shown in Fig. 9. For the first two stations after separation at the step, the maximum transverse intensity occurs near the sonic line in the shear layers, which is similar to the result for the streamwise turbulence intensity. However, starting in the reattachment region the peak transverse intensity occurs near the interface between the two flows, which suggests a high rate of turbulence momentum exchange between the flows. The anisotropy ratio, σ_u/σ_v, is also found to peak near the sonic line for both shear layers but decays rapidly toward an isotropic value of unity at the interface between the flows.

The kinematic turbulent shear stress profiles are presented in Fig. 10. In many respects, the general trends are similar to those for the streamwise turbulence intensity evolution, with maximum stresses near the sonic line in each shear layer, very large shear stresses in the recompression and reattachment region, and larger absolute shear stresses in the lower Mach number flow than in the higher M flow. In contrast, the turbulent shear stress at the interface between the two flows is quite small, which is similar to the results for subsonic flow behind airfoils and blunt bodies. Streamwise growth of the maximum shear stress in both free shear layers and the existence of large shear stresses near the reattachment point between the two flows in this study are consistent with earlier measurements[4,6] where free shear layers attached onto solid surfaces. This seems to indicate that the imposition of the v=0 boundary condition by the solid wall in the reattachment region does not affect the turbulence intensity or scale in compressible reattaching shear flows. In contrast, for incompressible reattaching shear layers[28], this restriction is believed to be the cause of significant turbulence intensity and scale decay in the reattachment region. The convective velocity of large-scale structures in supersonic shear flows may be higher than the local speed of sound, such that these structures are unaware of the presence of the walls before reattachment. Thus, the breaking-up process of the eddies could only occur at or after reattachment in these cases. This could be the cause for the differences in behavior between subsonic and supersonic reattaching free shear flows in the presence of solid walls.

Axial distributions of the maximum turbulence intensities and kinematic shear stresses are shown plotted in Fig. 11. The general trends are qualitatively similar for each shear layer and are also similar to previous results for reattaching compressible shear layers[4,6]. A plateau in the maximum turbulence intensities occurs in the reattachment region, while the same type of plateau has been observed in incompressible flow about one step height before reattachment. The rate of increase of the turbulence intensity and shear stress is higher for the lower Mach number shear layer. In addition, the growth rate of these compressible shear layers is approximately a factor of 2 or more less than the average incompressible results. For compressible shear flows, previous results have shown that the growth rate is inversely proportional to the Mach number[29], which is consistent with the present measurements. Another possible cause of the higher turbulence levels in the lower Mach number shear layer could be the larger distortion of the turbulence field passing through the 18.5° expansion at the step for the lower M flow in comparison to the 12.4° expansion for the higher M shear layer.

The ratio of the kinematic turbulent shear stress to the turbulent kinetic energy is shown plotted in Fig. 12 for this flowfield, where the total turbulent kinetic energy, k, is estimated to be $3/4(\sigma_u{}^2+\sigma_v{}^2)$. This turbulence "structure parameter" has been examined by Harsha and Lee[30] for boundary layers, two-dimensional and axisymmetric jets, and wakes in incompressible flow. They concluded that a value of 0.3 is reasonable for computing these incompressible flows. Bradshaw and Ferriss[31] also assumed a value of 0.3 for this parameter in their compressible boundary layer calculations. Generally, this structure parameter does not vary significantly through a flowfield. Although the mean value of this parameter is approximately 0.3 for the present flow, Fig. 12, large variations also occur, thereby confirming that significant turbulence structural variations occur in this relatively complicated flowfield. This conclusion has also been reinforced by examination of the shear stress correlation coefficient, which is also used by some investigators as a turbulence "structure parameter."

The evolution of two components of the turbulence triple products are presented in Figs. 13 and 14. The results are similar to those for the streamwise turbulence intensity and kinematic shear stress, with maximum values near the sonic locations in the free shear layers, significant increases in magnitude near reattachment, and decay in the redeveloping region. The large triple product values in the recompression and interaction region are most likely indicative of increases in the turbulence scale in this area, which is similar to results obtained in free shear layers reattaching onto a solid wall. It may therefore be inferred that solid boundaries in the reattachment region do not have a significant damping effect on the turbulence scale and intensities in supersonic reattaching shear layers. This is in contrast to speculation about the significant effects of solid walls on the turbulence characteristics in subsonic reattaching flows[28]. As previously discussed, the high convective velocities of the large-scale structures in supersonic shear flows could be a cause for these fundamental differences.

Two components of the turbulent triple products, $\langle(v')^2u'\rangle$, Fig. 13, and $\langle(u')^3\rangle$ (not shown), demonstrate behavior in the transverse direction similar to that for incompressible shear flows[28]. This suggests similar mechanisms for streamwise turbulence diffusion in incompressible and compressible shear layers. However, significant differences between incompressible and compressible shear flows occur in the distributions of the $\langle(u')^2v'\rangle$, Fig. 14, and $\langle(v')^3\rangle$ (not shown) triple product components, which are related to the transverse diffusion of turbulence. In the compressible shear layers of this study, Fig. 14, the turbulence diffusion is inward (toward the wind tunnel centerline) on the inner edges of both shear flows and also in the interaction region, while it is outward (away from the wind tunnel

centerline) on the outer edges of both shear layers. This is opposite to the results for incompressible shear flow cases and seems to be a fundamental structural difference.

Figure 15 shows the profiles of kinematic turbulence production for this flow, which is defined as the nondimensionalized product of the kinematic turbulent shear stress and the mean velocity gradient. This definition excludes significant density changes through the recompression and reattachment regions. Clearly, the turbulence production is high in the developing free shear layers, which is similar to the results for subsonic reattaching shear flows[28] and previously examined compressible reattaching shear layers[4]. However, the high levels of production seen in this flow in the recompression and reattachment regions have not been observed in incompressible flows. The pronounced decay of the turbulence production in the redevelopment region is caused by the rapid development of the mean velocity profiles in this region due to enhanced mixing and is consistent with the results discussed earlier.

Conclusions

An overview of a long-term experimental research program directed at understanding the detailed fluid dynamic mechanisms and interactions that occur in high-speed separated flows has been presented. Four series of experiments have been completed or are in progress as part of this program, including: development of constant pressure shear layers, reattachment processes for compressible shear layers, oblique shock wave/turbulent boundary layer interactions in a compression corner, and the interaction of two compressible shear layers originally separated by a finite thickness base. These flows contain the fundamental flow mechanisms of importance in missile base flows. Several other related investigations are also in progress, such as high-temperature two-stream mixing, normal shock wave/turbulent boundary layer interactions in a constant area duct ("shock train"), and two-stream plume-induced separation. The results of these studies will be reported at a later time.

The primary tool used in these detailed studies of high-speed flow interactions has been a two-component laser Doppler velocimeter. A summary of the LDV system setup and experimental procedures employed has been given with special emphasis on the difficulties and constraints that occur for supersonic separated flows.

In addition, the results of one of the recent experiments concerning the interaction between two compressible free shear layers have been presented. The general trends for both shear layers are the same and are also similar to those of compressible shear layers reattaching onto solid surfaces. Therefore, in contrast to incompressible reattaching shear layers, the proximity of a solid surface appears not to decrease significantly the turbulence scale and intensities for compressible reattaching shear flows. The results have also confirmed earlier findings of fundamental structural differences between compressible and incompressible shear flows, especially in terms of the diffusion of turbulence energy in the transverse direction. The turbulence intensity levels and its rate of streamwise increase in the shear layer with the lower Mach number were found to be higher. This agrees with previous studies which show a reduction in shear layer mixing and entrainment with increased Mach number.

Acknowledgments

The authors would like to thank the following Ph.D. students whose dedicated effort brought the research described herein to successful fruition: Dr. Howard L. Petrie, who is now a Research Associate at the Applied Research Laboratory, Pennsylvania State University; Dr. David W. Kuntz, a Member of the Technical Staff at Sandia National Laboratories; and Mr. Vincent A. Amatucci, currently completing his Ph.D. thesis research in the Department of Mechanical and Industrial Engineering at the University of Illinois at Urbana-Champaign.

This research was supported by the U.S. Army Research Office under Contracts DAAG 29-83-K-0043 and DAAL 03-87-K-0010. Dr. Robert E. Singleton and Dr. Thomas L. Doligalski served as Contract Monitors.

References

1. Petrie, H. L., "A Study of Compressible Turbulent Free Shear Layers Using Laser Doppler Velocimetry," Ph.D. thesis, Department of Mechanical and Industrial Engineering, University of Illinois at Urbana-Champaign, 1984.

2. Petrie, H. L., Samimy, M., and Addy, A. L., "Compressible Separated Flows," AIAA Journal, Vol. 24, No. 12, pp. 1971-1978, December 1986.

3. Samimy, M., "An Experimental Study of Compressible Turbulent Reattaching Free Shear Layers," Ph.D. thesis, Department of Mechanical and Industrial Engineering, University of Illinois at Urbana-Champaign, 1984.

4. Samimy, M., Petrie, H. L., and Addy, A. L., "A Study of Compressible Turbulent Reattaching Free Shear Layers," AIAA Journal, Vol. 24, No. 2, pp. 261-267, February 1986.

5. Samimy, M. and Addy, A. L., "Effects of Expansion at the Step on Turbulence Characteristics of Compressible Free Shear Layers," paper presented at the 63rd Supersonic Tunnel Association Meeting, April 1985.

6. Samimy, M., Petrie, H. L., and Addy, A. L., "Reattachment and Redevelopment of Compressible Turbulent Free Shear Layers," ASME International Symposium on Laser Anemometry, FED-Vol. 33, pp. 159-166, November 1985.

7. Kuntz, D. W., "An Experimental Investigation of the Shock Wave-Turbulent Boundary Layer Interaction," Ph.D. thesis, Department of Mechanical and Industrial Engineering, University of Illinois at Urbana-Champaign, 1985.

8. Kuntz, D. W., Amatucci, V. A., and Addy, A. L., "An Experimental Study of the Shock Wave-Turbulent Boundary Layer Interaction," ASME International Symposium on Laser Anemometry, FED-Vol. 33, pp. 173-178, November 1985.

9. Kuntz, D. W., Amatucci, V. A., and Addy, A. L., "Turbulent Boundary Layer Properties Downstream of the Shock Wave/Boundary Layer Interaction," AIAA Journal, Vol. 25, No. 5, pp. 668-675, May 1987.

10. Samimy, M. and Addy, A. L., "Interaction Between Two Compressible, Turbulent Free Shear Layers," AIAA Journal, Vol. 24, No. 12, pp. 1918-1923, December 1986.

11. Amatucci, V. A., Ph.D. thesis research, Department of Mechanical and Industrial Engineering, University of Illinois at Urbana-Champaign, in progress.

12. Walsh, M. J., "Influence of Particle Drag Coefficient on Particle Motion in High-Speed Flow with Typical Laser Velocimetry Applications," NASA TN D-8120, February 1978.

13. Box, G. E., Hunter, W. G., and Hunter, J. S., Statistics for Experimenters, John Wiley & Sons, New York, 1978.

14. Karpuk, M. E. and Tiederman, W. G., Jr., "Effect of Finite Size Probe Volume upon Laser Doppler Anemometer Measurements," AIAA Journal, Vol. 14, No. 8, pp. 1099-1105, August 1976.

15. Erdmann, J. C. and Tropea, C., "Turbulent Induced Statistical Bias in Laser Anemometry," Proceedings of the Seventh Symposium on Turbulence, University of Missouri-Rolla, pp. 129-138, September 1981.

16. Erdmann, J. C. and Tropea, C., "Statistical Bias of the Velocity Distribution Function in Laser Anemometry," Paper 16.2, International Symposium on Applications of Laser Doppler Anemometry to Fluid Mechanics, Lisbon, Portugal, July 1982.

17. McLaughlin, D. K. and Tiederman, W. G., Jr., "Biasing Correction for Individual Realization of Laser Anemometer Measurements in Turbulent Flow," The Physics of Fluids, Vol. 16, No. 12, pp. 2082-2088, 1973.

18. Petrie, H. L., Samimy, M., and Addy, A. L., "Laser Doppler Velocity Bias in Separated Turbulent Flows," to be published in Experiments in Fluids, 1987.

19. Edwards, R. V. (Editor), "Report of the Special Panel on Statistical Particle Bias Problems in Laser Anemometry," Journal of Fluids Engineering, Vol. 109, No. 2, pp. 89-93, June 1987.

20. Buchave, P., "Biasing Errors in Individual Particle Measurements with the LDA-Counter Signal Processor," Proceedings of LDV Symposium, Copenhagen, Denmark, pp. 258-278, 1975.

21. Maise, G. and McDonald, H., "Mixing Length and Kinematic Eddy Viscosity in a Compressible Boundary Layer," AIAA Journal, Vol. 6, pp. 73-80, January 1968.

22. Laderman, A. J., "Adverse Pressure Gradient on Supersonic Boundary Layer Turbulence," AIAA Journal, Vol. 18, pp. 1186-1195, October 1980.

23. Klebanoff, D. S., "Characteristics of Turbulence in a Boundary Layer with Zero Pressure Gradient," NACA Report 1247, 1955.

24. Dimotakis, P. E., Collins, D. J., and Lang, D. B., "Laser Doppler Measurements in Subsonic, Transonic, and Supersonic Turbulent Layers," Laser Velocimetry and Particle Sizing, edited by H. D. Thompson and W. H. Stevenson, Hemisphere Publishing Co., New York, pp. 208-219, 1979.

25. Sandborn, V. A., "A Review of Turbulence Measurements in Compressible Flow," NASA TM X-62-337, March 1974.

26. Hayakawa, K., Smits, A. J., and Bogdonoff, S. M., "Hot-Wire Investigation of an Unseparated Shock-Wave/Turbulent Boundary Layer Interaction," AIAA Journal, Vol. 22, pp. 579-585, May 1984.

27. Hayakawa, K., Smits, A. J., and Bogdonoff, S. M., "Turbulence Measurements in a Compressible Reattaching Shear Layer," AIAA Journal, Vol. 22, pp. 889-895, July 1984.

28. Chandrsuda, C. and Bradshaw, P., "Turbulence Structure of a Reattaching Mixing Layer," Journal of Fluid Mechanics, Vol. 110, pp. 171-194, 1981.

29. Birch, S. F. and Eggers, J. M., "A Critical Review of the Experimental Data for Developed Free Turbulent Shear Layers," Free Turbulent Shear Flows, Vol. 1, NASA SP-321, 1972.

30. Harsha, P. T. and Lee, S. C., "Correlation Between Turbulent Shear Stress and Turbulent Kinetic Energy," AIAA Journal, Vol. 8, pp. 1508-1510, August 1970.

31. Bradshaw, P. and Ferriss, D. H., "Calculation of Boundary Layer Development Using the Turbulent Energy Equation: Compressible Flow on Adiabatic Walls," Journal of Fluid Mechanics, Vol. 46, Pt. 1, pp. 83-110, 1971.

Authors

J. Craig Dutton is currently an Associate Professor in the Department of Mechanical and Industrial Engineering at the University of Illinois at Urbana-Champaign (UIUC). He received his B.S.M.E. degree in 1973 from the University of Washington, his M.S. from Oregon State University in 1975, and his Ph.D. from UIUC in 1979, all in Mechanical Engineering. A. L. "Tad" Addy is a Professor and currently serves as Head of the Department of Mechanical and Industrial Engineering at UIUC. He received his B.S. in Mechanical Engineering in 1958 from the South Dakota School of Mines and Technology, his M.S. in 1960 in Theoretical and Applied Mechanics from the University of Cincinnati, and his Ph.D. in Mechanical Engineering from UIUC in 1963. Mohammad Samimy is now an Assistant Professor in the Mechanical Engineering Department at Ohio State University. He received his B.S. from Arya-Mehr University of Technology, Tehran, Iran, in 1978 and his M.S. and Ph.D. degrees from UIUC in 1981 and 1984, respectively, all in Mechanical Engineering. The research interests of all three center on various analytical, numerical, and experimental aspects of high-speed compressible flows.

Figures

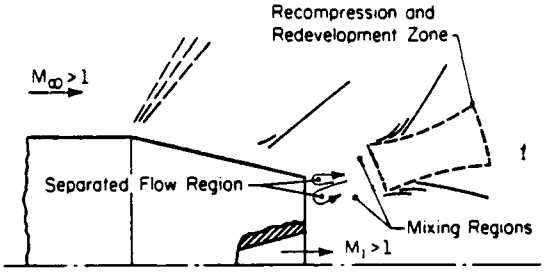

(a) Power-on supersonic base flowfield

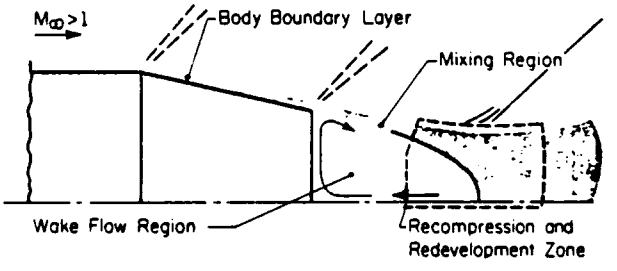

(b) Power-off supersonic base flowfield

Fig. 1 Schematics of missile base flowfields

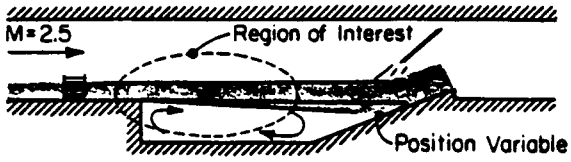

(a) Constant pressure shear layer with recirculation

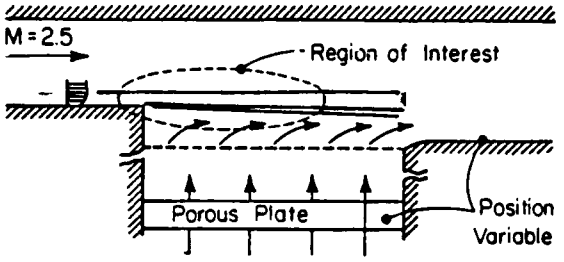

(b) Constant pressure shear layer with mass injection

Fig. 2 Constant pressure shear layer development experiments

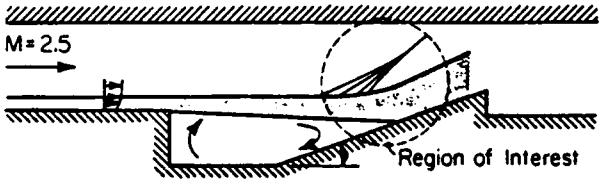

(a) Reattachment of a developed free shear layer

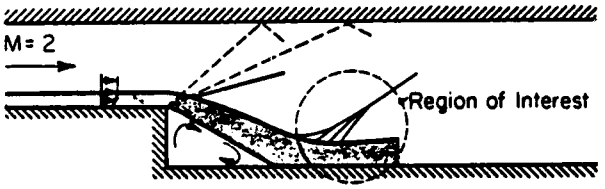

(b) Reattachment of a developing free shear layer

Fig. 3 Configurations for reattachment experiments

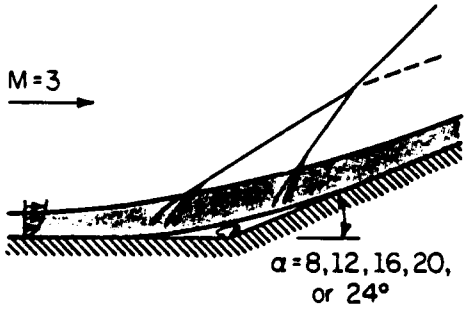

Fig. 4 Supersonic compression corner experiments

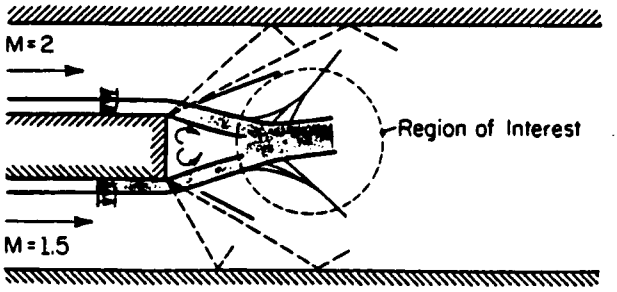

Fig. 5 Experimental configuration for interaction of two free shear layers

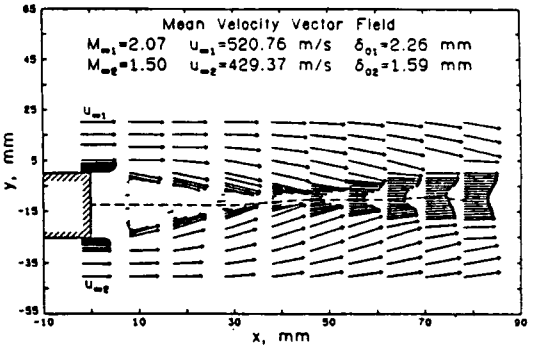

Fig. 6 Mean velocity vector field

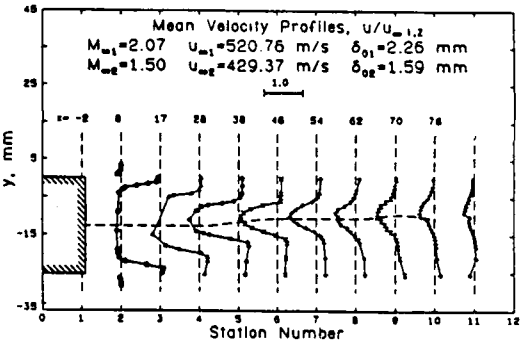

Fig. 7 Streamwise mean velocity profiles ($u_{\infty 1,2}$ means $u_{\infty 1}$ for the higher and $u_{\infty 2}$ for the lower Mach number flows)

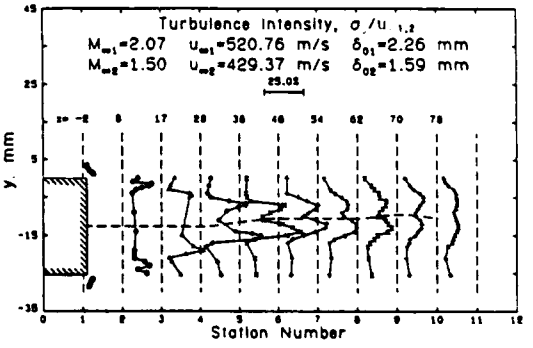

Fig. 8 Streamwise turbulence intensity profiles

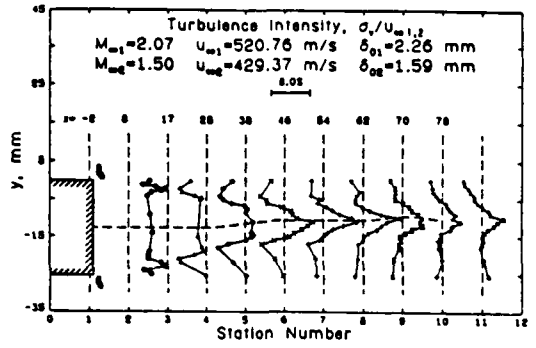

Fig. 9 Transverse turbulence intensity profiles

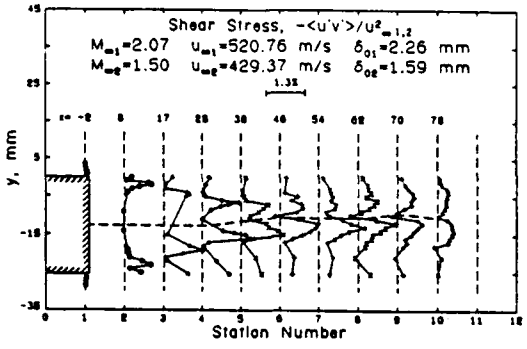

Fig. 10 Evolutionary kinematic shear stress profiles

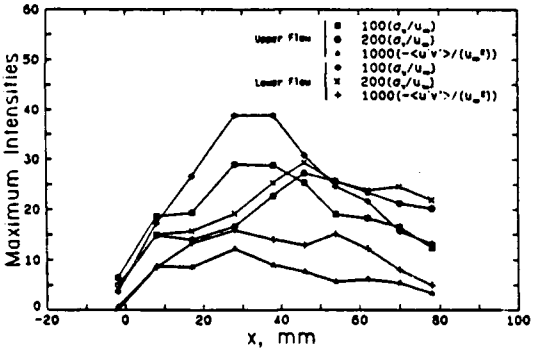

Fig. 11 Axial distribution of maximum turbulence intensities and shear stresses

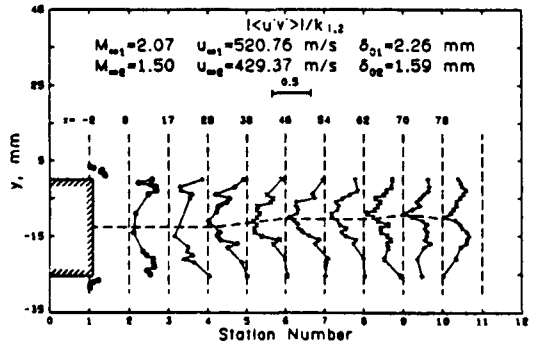

Fig. 12 Turbulence "structure parameter" profiles

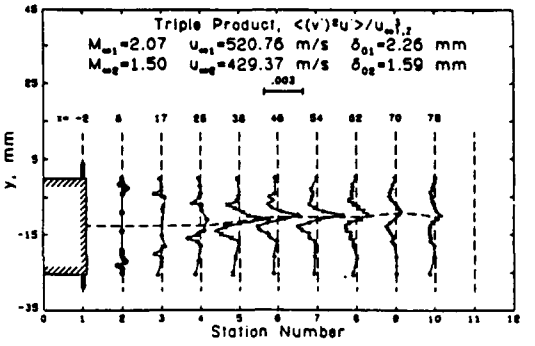

Fig. 13 Profiles of $\langle(v')^2u'\rangle$ turbulent triple product

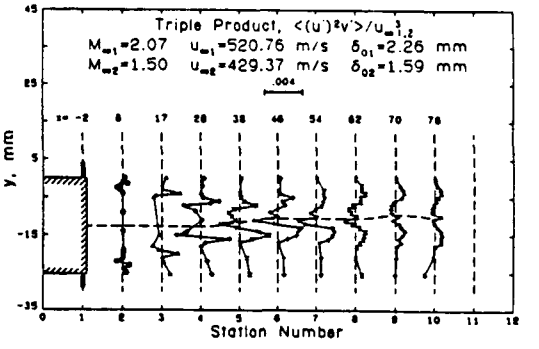

Fig. 14 Profiles of $\langle(u')^2v'\rangle$ turbulent triple product

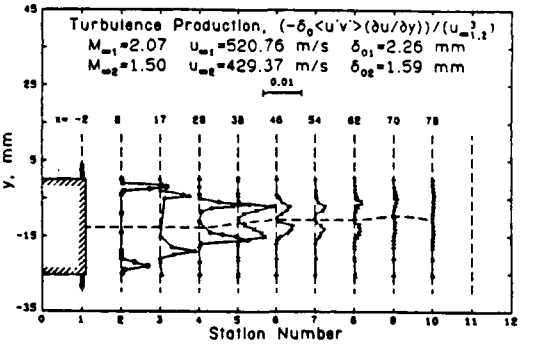

Fig. 15 Turbulence production profiles

SECTION B.6

UNSTEADY REATTACHMENT OF SUPERSONIC FLOW PAST A BACKWARD-FACING STEP

M.S. Thesis

Department of Mechanical and Industrial Engineering

University of Illinois at Urbana-Champaign

December 1987

by

K. Taghavi

UNSTEADY REATTACHMENT OF SUPERSONIC FLOW PAST A BACKWARD-FACING STEP

Kaveh Taghavi, M.S. Thesis
Department of Mechanical and Industrial Engineering
University of Illinois at Urbana-Champaign

ABSTRACT

An experimental investigation was conducted to study the effect of the initial boundary layer thickness prior to separation on the compressible, two-dimensional reattaching free shear layer formed by geometrical separation of a turbulent boundary layer over a backward-facing step. Two small scale full nozzle configurations were constructed to produce a uniform supersonic flow with a freestream Mach number of 2.0. One nozzle set produced an equilibrium turbulent boundary layer with a visually measured thickness of 5 mm and the other nozzle set produced a 2.5 mm boundary layer thickness prior to the geometric corner. Two operating conditions were studied for each nozzle set, incipient and complete reattachment. The incipient reattachment condition was defined as the condition where the shear layers attached to the wall and a normal shock was present within a few boundary layer thicknesses of the reattachment region, while the complete reattachment condition was defined as the case where the realignment compression waves had coalesced into an oblique shock downstream of the reattachment region. A detailed survey of the flow was made utilizing surface static probes, Schlieren photography, and fast response, flush mounted, piezo-resistive pressure transducers. The fast response pressure transducers were placed at locations upstream of separation, in the separated base region, at the reattachment location, and downstream of the reattachment region.

Surface streak pattern measurements indicated highly three-dimensional flow in the separated base and reattachment regions, while upstream of the separation and downstream of the reattachment region no three-dimensionality effects were present. At the condition of complete reattachment, no significant pressure fluctuations were present in the flowfield over the frequency range of 0 to 40 kHz. The incipient reattachment operating condition produced pressure fluctuations at the separated base region, reattachment region, and downstream of the reattachment

region, while only white noise was present upstream of the geometric corner. The oscillating frequency for the incipient reattachment condition at the reattachment region was 60.95 Hz for the 5 mm initial boundary layer and 90.87 Hz for the 2.5 mm initial boundary layer flow. Strong coherence was present between the reattachment region and separated base region flows and the flow downstream of the reattachment region.

Possible sources for the pressure fluctuations are the terminating normal shock in the test section, flapping motion of the shear layers (i.e., reattachment and separation of the shear layers to and from the surface), and back and forth movement of the shear layers across the face of the fast response pressure transducers.

SECTION B.7

LASER DOPPLER VELOCITY BIAS IN SEPARATED TURBULENT FLOWS

Experiments in Fluids

Volume 6, January 1988

Pages 80-88

by

H. L. Petrie, M. Samimy, and A. L. Addy

Experiments in Fluids 6, 80–88 (1988)

Experiments in Fluids

Laser Doppler velocity bias in separated turbulent flows

H. L. Petrie

Applied Research Laboratory, Pennsylvania State University, State College, PA 16804, USA

M. Samimy

Dept. of Mechanical Engineering, Ohio State University, Columbus, OH 43210, USA

A. L. Addy

Dept. of Mechanical and Industrial Engineering, University of Illinois at Urbana-Champaign, Urbana, IL 61801, USA

Abstract. Velocity bias effects on data obtained with a coincident two channel laser Doppler velocimeter in a highly turbulent separated supersonic flow are presented. Probability distributions of the fluctuating velocities were distorted by velocity bias in a manner consistent with theory and a two-dimensional velocity inverse weighting function bias correction produced reasonable appearing velocity probability distributions. The addition of an approximate correction term to account for the effects of the unmeasured third velocity component improved these results but had little effect on the velocity statistics. Experimental factors that could partially compensate or falsely add to the velocity bias, conditions for the bias to occur, and conditions for which the bias may also be observed and corrected for are discussed.

1 Introduction

This study is part of a program investigating supersonic missile base region flows. Features of these base flows include separated regions of recirculating flow bounded by turbulent free shear layers and a recompression zone where the bounding shear layers merge and change direction. The experimental efforts of this investigation have been directed at the detailed study of simpler two-dimensional model flows using laser Doppler velocimetry, Addy et al. (1983).

These model experiment flowfields contain regions of high turbulence intensity and in some cases these high intensities occur where the flow is supersonic. Thus, an extreme dynamic range of velocities is possible and at the outset of experimentation it was expected that LDV velocity and fringe bias could have a substantial statistical effect on the results.

An evaluation of the effect of these biases and the effectiveness and/or need for any corrective actions was felt to be essential to these LDV studies because of the controversial nature of the bias problem and the potential effects on the results. Without such an effort, systematic uncertainties and unanswered questions would exist regarding the quality and accuracy of the experimental results. The purpose of this paper is to present the results of the evaluation of velocity bias effects and the techniques used in the process. This information should be of value to those doing frequency counter based LDV measurements in highly turbulent flows. The problem of fringe bias with coincident two channel frequency shifted LDV systems was studied analytically by Petrie (1984) and Petrie et al. (1986) for the current flows and was reduced or avoided experimentally by frequency shifting.

The data presented below were taken in the model experiment flowfield shown in Fig. 1. A nominal Mach 2.5 flow with a fully developed turbulent approach boundary layer separates at a backward facing step and reattaches onto an inclined ramp downstream of the step. The ramp angle is adjusted to achieve a constant pressure separation at the backstep. This entire flowfield was surveyed from upstream of the backstep to downstream of reattachment with a two color, two-channel coincident frequency shifted laser Doppler velocimeter. Petrie (1984), Petrie et al. (1985, 1986), Samimy et al. (1986), and Samimy (1984) provide further details.

2 Velocity bias

McLaughlin and Tiederman (1973) argued that the LDV individual realization sampling process is biased towards higher velocities in turbulent flows because the volume of fluid and therefore the number of particles swept through the LDV measurement volume is proportional to the quantity being sampled, namely, the velocity. That is:

$$\Delta n = C A V_T \Delta t \tag{1}$$

where Δn is the number of particles sampled in time interval Δt, C is the number density of the particles, A is the cross sectional area of the measurement volume in the plane normal to the velocity vector, and V_T is the total velocity magnitude. If C and A are constant and the probability of signal validation is independent of the velocity magnitude and particle interarrival time, then the data rate and probability of obtaining a sample is directly proportional to the velocity. These preceding assumptions

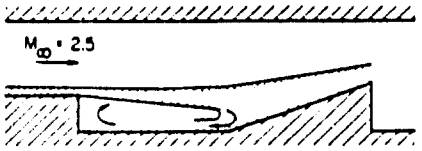

Fig. 1. Configuration of the model experiment flowfield

are never completely true in turbulent flows and are discussed below.

2.1 *Transit time weighting*

The particle transit time across the LDV measurement volume can be used as a weighting function to correct for velocity bias, see McDougall (1980), Buchave (1979), and Hoesel and Rodi (1977). The transit time is, on average, inversely proportional to the velocity. This method of velocity bias correction has the advantage of not producing infinite weights and works just as well for one and two component LDV systems.

The Doppler bursts were processed in the N-cycle mode in the present study. That is, a fixed number of cycles were required and used to determine the frequency of each burst. Transit time information was not available in this mode with the Doppler signal processors used. The N-cycle mode was used because it was less susceptible to noise and produced results superior to the total burst mode due to the difficulty of accurately determining the transit time. Although transit time weighting was not used, many of the procedures and findings discussed below are applicable to transit time weighted data.

2.2 *Interarrival time weighting*

The particle interarrival time may also be an appropriate weighting factor to correct for velocity bias in some cases. A true time average should be approximated closely when the mean sampling rate is of the same order or greater than the highest frequencies of the velocity fluctuations. However, it is sufficient to sample at a frequency which is high compared to the lower frequency energy containing turbulent scales if spectral information is not desired, see Dimotakis (1976). The turbulence frequencies in the supersonic flows of the present work were always large compared to the particle interarrival rate so that the above criterion was not met and this time averaging scheme was therefore not used.

Adams et al. (1984) found that interarrival time weighted velocity statistics were not affected by the data rate. However, these low data rates were achieved by reducing laser power which introduces signal-to-noise ratio effects, see Adams and Eaton (1985). Edwards and Jensen (1983) have statistically modeled sample-and-hold LDV systems and found that when the mean particle arrival rate per turbulence coherent time scale exceeds 10, the measured statistics are nearly those of the flow. When there are fewer than 0.1 particle velocities measured per turbulent time scale, the LDV statistics are those of an individual realization anemometer. In general, the hold time for sample-and-hold and the interarrival times of the particles should be nearly the same. Thus, Edwards and Jensen's (1983) results indicate interarrival time weighting of the data would not correct for velocity bias in the present study.

2.3 *Velocity inverse weighting*

A two-dimensional velocity inverse weighting function, $w_i = 1/(U_i^2 + V_i^2)^{1/2}$, was used in the present study to correct for velocity bias where U_i and V_i are the x and y direction velocities of the ith realization. This is just a natural extension of the one-dimensional velocity inverse weight proposed by McLaughlin and Tiederman (1973) that is possible with a coincident two channel LDV system. The velocity in the (x, y) plane was measured by the LDV with the measurement channels oriented at $\pm 45°$ to the horizontal streamwise direction to avoid fringe bias. The data coordinates were rotated into horizontal and vertical (x, y) for analysis. The z direction velocity component, W, was not measured but was expected to have a mean value of nearly zero in all cases.

A deficiency of this velocity inverse weight is that the weight approaches infinity as the (x, y) plane velocities approach zero and the magnitude of the unmeasured z component becomes an increasingly significant part of the three-dimensional velocity magnitude. Even though this z velocity component had a zero mean value, its mean magnitude was not zero. As a result, the velocity magnitude in Eq. (1) is on average underestimated when the (x, y) plane velocity is small. Thus, small velocity realizations will tend to be overweighted by the two-dimensional velocity inverse correction.

A simple approximate corrective action can be taken to account for the contribution of the z component to the velocity inverse weight. This term will only be significant when $U \cong V \cong 0$. An estimate of the unmeasured z component turbulent intensity based on the measured (x, y) plane values combined with a geometric factor to account for the change in the effective measurement volume cross sectional area normal to the velocity vector can be used to determine an estimated averaged z component velocity magnitude. Nakayama (1985) added an estimated z component term to the velocity inverse weight, w_i, so that:

$$w_i = [U_i^2 + V_i^2 + (a/b)^2 \sigma_w^2]^{-1/2} \tag{2}$$

where a/b is the ratio of the measurement volume diameter to its length; the long axis of the measurement

volume ellipsoid is parallel to the z axis. a/b is also the ratio of the cross sectional area of the measurement volume in the (x, y) plane to that in the (y, z) plane. σ_w is the z component root mean square intensity level, its standard deviation, and is estimated as the average of the measured x and y component values. Since the geometry factor, a/b, is typically smaller than 1/20, the z component term will only be significant when U, and V, are small. Johnson et al. (1982) argued that the simple two-dimensional velocity inverse weight should be sufficiently accurate because the z term contribution is always small but no examination of the effect of including the z term has been made. An appraisal has been made below.

Off-axis light collection, used in the present study, can alter the effective measurement volume geometry and act to increase the effective area ratio $(a/b)_e$, when the photodetector aperture is not large. The effective length of the measurement volume, L_m, was calculated by procedures outlined by TSI Inc. (1980). The effective (y, z) plane cross sectional area of the measurement volume was calculated by assuming a rectangular cross section of dimensions L_m by d_m, where d_m is the measurement volume diameter. With this approach, the effective area ratio for the LDV data discussed below was $(a/b)_e = 0.056$, which is approximately one-third larger than a/b.

3 Results and discussion

With the above details and difficulties in mind, an examination of the effect of the velocity bias and the bias correction was made. The results with the simple two-dimensional bias correction are given the most attention with comparison to the results with the added estimated z term on a limited basis.

Figure 2 shows probability distribution functions, PDF, of the x component velocity, U, taken across the mixing layer for the ramp flowfield in Fig. 1 at $x = 75$ mm downstream of the 25.4 mm backstep. The base of the ramp in Fig. 1 was at $x = 101$ mm and the ramp angle was 19.3°. The freestream velocity was approximately 570 m/s. y^* is the distance from the $U/U_\infty = 0.5$ location and θ is the local mixing layer momentum thickness. 4,096 samples were used to formulate the PDFs for $3 > y^* > -9$. 1,024 samples were used for $y^* > 3$ and 2,048 samples for $y^* > -9$. The horizontal lines at the base of each PDF locate the ordinate and the short vertical lines indicate the mean of the PDF on the abscissa. The biased PDFs were formulated by adding a weighting factor of 1 to the histogram bin accumulator if a velocity realization fell within the range of the bin. The PDFs were normalized by dividing by the sum of these weights, which in this case is the total number of realizations in the sample. Constant bin widths were used at each ordinate location so that normalization does not require division by the bin width for this comparison. The velocity bias corrected PDFs

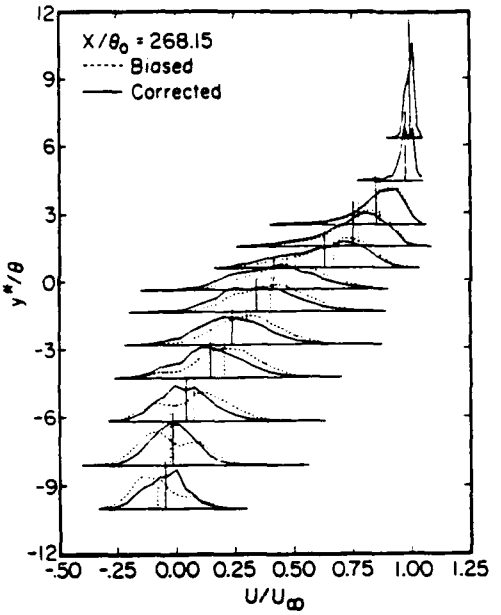

Fig. 2. Biased and corrected U velocity probability distributions across the mixing layer at $x = 75$ mm downstream of the step

were obtained by the same procedure but instead of a unity weighting factor, the simple two-dimensional velocity inverse weighting factor was summed in the bin accumulators. This visualization of the effect of the bias correction on the PDF is informative and simple. It can be applied to examine directly the effect of any weighting function on the PDF including transit and interarrival time weights.

The biased distributions in Fig. 2 exhibit a large decrease in the probability density about the $U = 0$ location in all cases where the probability density is sufficiently large near $U = 0$ to discern such details. This is true of all LDV data taken in this study. This decrease in the U component PDFs is the behavior expected if the velocity bias acts as predicted by Eq. (1). The U component is dominant in this flowfield such that the magnitude of the U velocity component correlates well with the total three-dimensional velocity magnitude. The V velocity component PDFs show no such behavior at $V = 0$ because the event $V = 0$ correlates poorly with a zero three-dimensional velocity magnitude. However, the bias is still present and the V component statistics are affected by it.

There are a number of possible factors other than velocity bias that could contribute to the bimodal character of the PDFs about $U = 0$ in Fig. 2. The time window constraint for the two channel coincidence requirement could cause a bias of similar form. A validated signal must be received from both channels within an adjustable time window to be considered coincident. Differences in light scattering due to wavelength or polarization, differences in measurement volume and fringe visibility between channels, or slight optical misalignment are a few of the possible

factors that may lead to a spatial separation of where a Doppler burst is initiated in one channel with respect to the other channel. Such a spatial separation translates into a temporal separation that is inversely proportional to the velocity. Thus, a time window bias against lower velocity realizations potentially exists. The electronic circuit performing the coincidence test may also be limited in speed and accuracy.

Comparisons of unweighted velocity biased and corrected U components PDFs were made at a fixed point in the mixing layer of the flowfield shown in Fig. 1 for coincidence time windows of 0.5 to 10 μs in duration, see Fig 3. 4.096 samples were taken for each PDF. An appreciable distortion of both biased and corrected PDFs due to the coincidence window size occurred only for time windows smaller than 2.5 μs. The data shown in Fig. 3 were taken at a location with a small mean velocity so that the probability of $U \cong 0$ would be large to maximize the sensitivity to the coincidence requirement for the purpose of this comparison. This also maximizes the effect of the velocity bias which cannot be made to vanish by increasing time window size. The time windows used in this study were sufficiently large to avoid such a bias.

The possibility that the flow was actually bimodal as observed must also be considered. Data taken in this flow support that both the reattachment of the shear layer onto the ramp and the recirculating flow have characteristics indicative of larger scale motions. Petrie et al. (1986). The magnitude of the oscillation in the U velocity, as indicated by the bimodal PDFs, does not change appreciably with distance from the step. However, the velocity magnitudes and turbulence levels in the recirculation zone diminish noticeably as the step is approached from maximum levels which occur at the base of the ramp. Also, the recirculating flow is not bimodal although typical mean velocities in this zone are comparable to half of the magnitude of the oscillation suggested by the bimodal PDFs. Thus, the bimodal switching would have to be localized in the transverse direction to the low speed edge of the mixing layer and yet span the length of the shear layer unaltered significantly in magnitude in the x direction. This is not felt to be plausible. Also, the results below show that probability density contours in the velocity plane actually wrap around the origin, $U = V = 0$. Such behavior is entirely consistent with a velocity bias but is difficult to attribute to a bimodal switching of the flow. Finally, true bimodal behavior in the flow will not be erased by a bias correction when the overweighting near zero velocities is not large compared to the effects of any bimodal switching. A stagnation point in the recirculating flow, for instance, was found to be weakly bimodal after bias correction.

A decrease in the particle number density across the mixing layer from the freestream into the recirculation zone could also result in a bias against the lower velocity realizations. This may have occurred because only the wind tunnel plenum chamber was seeded. The particles present in the recirculating flow were those that diffused across the discriminating streamline prior to reattachment. The ratio of the mean data rate to the local mean of the velocity magnitude, $\langle n \rangle / \bar{V}_{2D}$, was examined to determine whether such particle concentration effects were present. The mean magnitude, $\bar{V}_{2D} = \overline{(U_i^2 + V_i^2)^{1/2}}$, does not equal the magnitude of the mean velocity, $(\bar{U}^2 + \bar{V}^2)^{1/2}$, when negative velocities occur. The mean magnitude of the velocity properly reflects the amount of fluid volume swept through the measurement volume, on average, since this does not depend on the sign of the instantaneous velocities. The results indicate that the data ratios on the low speed side of the mixing layer are comparable or slightly higher than on the high speed side and no offsetting particle concentration effects occurred.

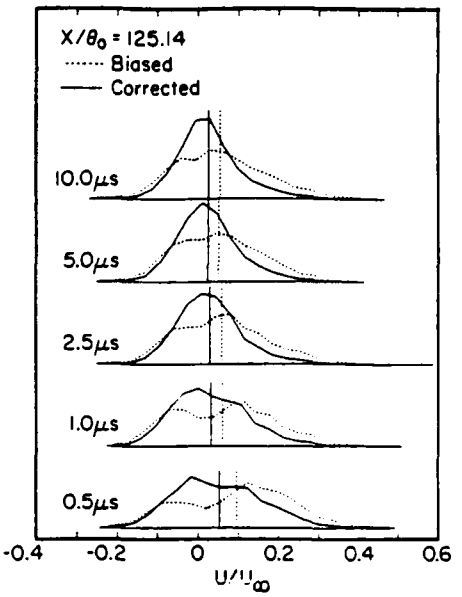

Fig. 3. Comparison of coincidence time window size effects on the U velocity PDFs; 4.096 samples were used for each PDF

The biased distributions of Fig. 2 are distinctly and unrealistically bimodal. That is not to say that a bimodal velocity PDF is always unrealistic but that velocity bias acts to create or exaggerate the bimodal character. The velocity inverse correction eliminates or reduces this bimodal character reasonably well; however, a tendency to overweight near the zero velocity occurs in a few cases in Fig. 2 and elsewhere in the flowfield. The fact that the biased probabilities were not zero at $U = 0$ results from both the finite size of the histogram bins used to formulate the PDF and the fact that the y and z component velocity magnitudes were not on average zero when the U velocity was zero.

The biased, simple two-dimensional corected, and estimated z term corrected U velocity component PDFs are compared in Fig. 4 at one of the measurement locations

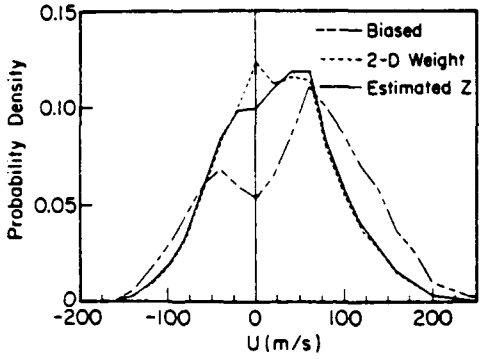

Fig. 4. Comparison of biased, 2-D velocity inverse, and velocity inverse with Z term corrected U velocity PDFs at $y^*/\theta = -6.56$, $x = 75$ mm

shown in Fig. 2. The estimated z term has a noticeable effect near $U = 0$ only, as expected, and appears effective in eliminating the overweighting seen in the simple two-dimensional inverse corrected results.

The probability density contours of Fig. 5, which are the results for the data at $y^*/\theta = -6.56$ in Fig. 2, provide a more detailed view of the effect of the bias. These joint PDFs were formulated and normalized following the procedures outlined for the one-dimensional PDFs above. The probability density increment between contour levels was constant and the same probability density levels were contoured in each part of Fig. 5. The contour levels increase monotonically from the outermost curve, which is at the lowest probability density level, to the innermost curves at higher levels. The uncorrected biased contours in Fig. 5 a follow the circles centered at the origin of the velocity plane closely indicating the expected dependence on the velocity magnitude and a nearly constant z component effect at small (x, y) plane velocities. The corrected result in Fig. 5 b does not show these bias effects but the contours indicate overweighting near $U = 0$ as seen in the one-dimensional PDFs of Fig. 2 at this y^*/θ location. The addition of the estimated z term to the weight reduces the gradient near the origin and no overweighting is apparent in Fig. 5 c. The corrected distributions do not wrap around the origin as the biased data did in Fig. 5 a.

Another way of examining the bias that avoids the complications of contouring but uses all of the velocity magnitude information is to formulate PDFs of the measured two-dimensional velocity magnitude, V_{2D}. This is shown in Fig. 6 for the data at $y^*/\theta = -6.56$ in Fig. 2. Each of the histogram bins used to formulate these PDFs had a constant width, $\Delta V_{2D} = 10$ m/s. The histogram bin accumulators contain the sum of the weights for all of the data between concentric circles centered at the origin in the velocity plane with a difference in radii of ΔV_{2D} and an outer radius at the upper velocity limit of the histogram bin. PDF normalization requires division by the product of the sum of all the weights in the sample with

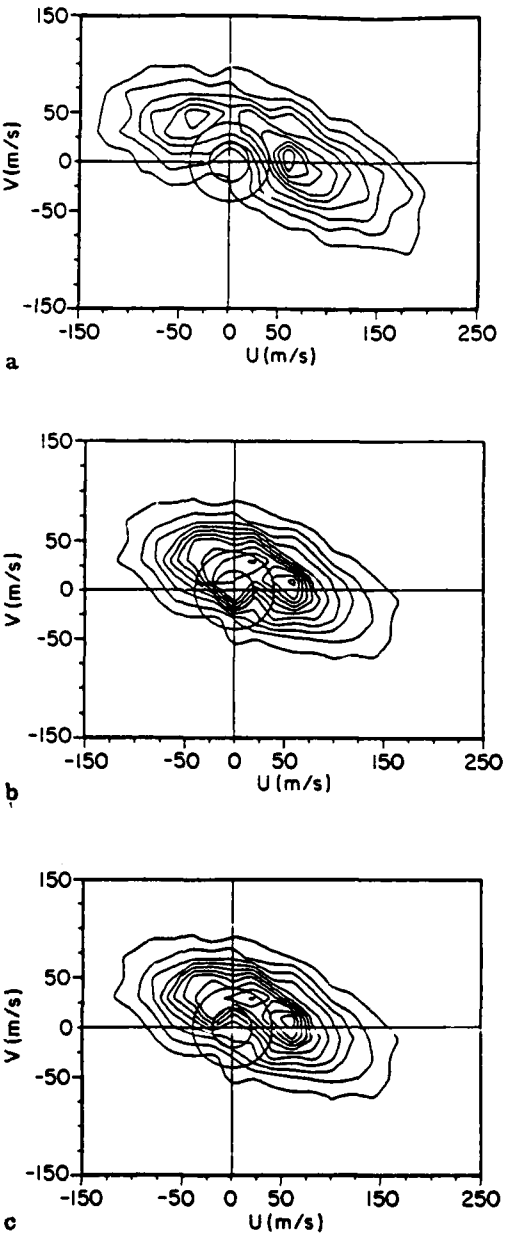

Fig. 5 a–c. Probability density contours for a biased, b 2-D velocity inverse corrected, and c velocity inverse with Z term corrected data at $y^*/\theta = -6.56$, $x = 75$ mm

the area of the current bin between the concentric circles in the velocity plane. The midpoints of each histogram bin in Fig. 6 are connected by straight line segments.

As shown in Fig. 6, the addition of the z term significantly reduces the maximum weight where the simple two-dimensional correction overweights appreciably, near the zero velocity magnitude. The expected form of the unbiased velocity magnitude PDF is not known but a smooth curve with a probability density near zero that is approximately equal to that found an equal distance on

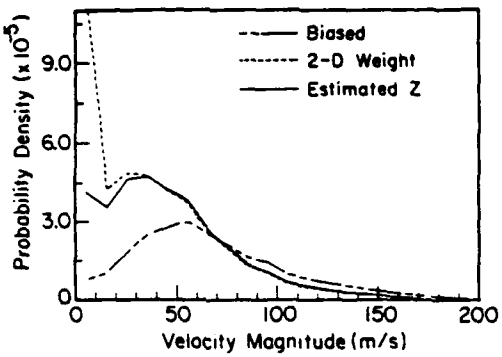

Fig. 6. Comparison of biased and corrected velocity magnitude PDFs at $y^*/\theta = -6.56$, $x = 75$ mm

the opposite side of the maximum probability density location is expected. The exception to this would be the case where the most probable magnitude is zero. No appreciable offsetting compensation for the velocity bias due to improvement of signal quality at lower velocity magnitudes, as discussed by Durao and Whitelaw (1979), is indicated by the results shown in Fig. 6. The range of such a compensation may be too small to notice in this flowfield. Also, Adams and Eaton (1985) indicate this compensation may not occur if the signal-to-noise ratios are sufficiently large. If such an effect were significant, an increase in the biased PDFs with decreasing velocity magnitude to values comparable to the z term corrected results at the lowest velocity magnitudes would be required.

The measured U and V velocity components appear to provide sufficient information to both observe the bias and correct for it reasonably well in the present study. However, this two-dimensional information may not be sufficient in a highly three-dimensional flow where no single velocity component dominates or in a situation where the dominant component is not measured or only partially measured. In such cases, an accurate z term estimate would be unlikely, the data will not show the bias as distinctly, if at all, and the correction will not work as desired. The bias may be entirely present in these situations but the data does not contain sufficiently complete velocity magnitude information to observe or correct for it. For an example of such a situation, consider a study of secondary flows in a corner, say the juncture of a wing with a fuselage, and the large chordwise velocity component is not measured.

Erdmann and Tropea (1981, 1982) have statistically modeled the LDV sampling process for normal and Ricean distribution turbulent flows. The analysis predicts a shift from fully velocity biased to bias free results as the sampling process changes from free running processor to processor controlled. A free running processor is defined as one that is able to process and transfer the data from every particle that generates a validated signal. In this case, the flow determines when particles are sampled. If the processor maximum sampling rate is much less than the validated particle data rate, the processor samples at its constant maximum rate since a validated particle occurs almost immediately after the processor status is ready for more data. In this case, the results are predicted to be unbiased and the processor controls the sampling process.

The reduction of the bias between free running and processor controlled sampling has been observed experimentally, see Johnson et al. (1982), Craig et al. (1984), and Stevenson et al. (1982), and it appears that if the sampling rate is on the order of 50 times less than the validated particle data rate, the data is unbiased. Conversely, the mean validated particle data rate must be significantly smaller than the processor sampling rate for the data to be completely biased. The processor sampling rate exceeded the mean validated data rate by a factor of 30 or more in the current study and free running processor conditions were felt to have been closely approximated.

Erdmann and Tropea (1981, 1982) use three time scales in their analysis of the bias. A turbulence frequency based on integral time scales, f_t, the processors maximum sampling rate, f_s, and the particle arrival rate, f_p, are used. Typical values near the half velocity location in the free shear layer of the flow data presented herein are $f_t = 50.000$ Hz, $f_s = 83.000$ Hz, and $f_p = 1.000$ Hz. Erdmann and Tropea state that a free running processor occurs if $f_t/f_s \ll 1$. Thus by this criterion the processor in the current study was not free running but controlled since $f_t/f_s = 0.6$, approximately. The controlled processor case with a small reduced data rate, $f_p/f_t = 0.02$, is also considered theoretically by Erdmann and Tropea (1981). Using the present conditions, a 43% reduction in the bias is predicted for a controlled processor. However, this is not supported by the data shown in Fig. 7 which is discussed below. The data are completely biased up to a 30% intensity level which occurs at the flow location of this comparison. The criterion that $f_t/f_s \ll 1$ for a free running processor is inconsistent with the physical description that a free running processor is one that is able to sample virtually every particle. It is felt that the condition $f_p/f_s \ll 1$ is a requirement of a free running processor since the turbulent time scale has nothing to do with the processors ability to keep up with the data. Adams et al. (1984), and Adams and Eaton (1985) also discuss the importance of f_p/f_s. The influence of these time scales deserves further study.

The analyses of Erdmann and Tropea (1981, 1982) predict that for a free running processor, in the limit as the turbulent intensity goes to zero, the velocity bias of the mean is equal to the turbulence intensity squared, or:

$$\frac{\bar{U}_{BIASED} - \bar{U}_{TRUE}}{\bar{U}_{TRUE}} = \left(\frac{\sigma_u}{V_{LOCAL}}\right)^2 \tag{3}$$

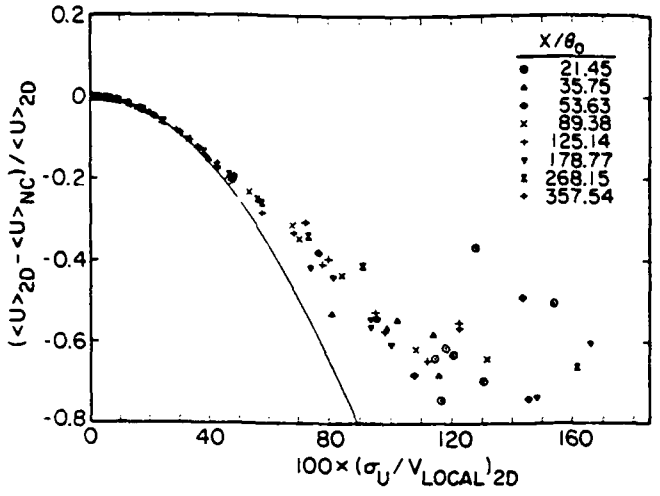

Fig. 7. Velocity bias of the mean U velocity vs. the turbulent intensity based on the magnitude of the local mean velocity (NC indicates no bias correction and 2D indicates the velocity inverse correction was applied)

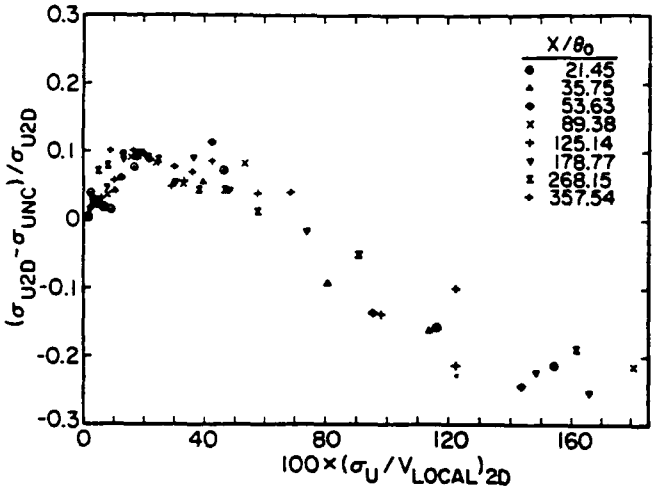

Fig. 8. Velocity bias of the U velocity fluctuation standard deviation vs. the local turbulent intensity

where σ_u is the U component standard deviation and V_{LOCAL} is the magnitude of the mean velocity at the data location. The negative of eq. (3) is shown in Fig. 7 with the U velocity mixing layer and recirculating flow data. The simple two-dimensional velocity inverse corrected results were taken as the true results for the comparison with theory. The statistical prediction and the corrected results are in good agreement up to 40% intensity levels. The low speed data of Johnson et al. (1982) are similar. The turbulence intensity based on the local mean velocity magnitude was 30%–35% at $y^* = 0$, the middle of the mixing layer. The z term correction changed the mean velocity by less than 2% of the simple velocity inverse corrected values; only the data at $x = 75$ mm was examined, however.

The bias errors as a fraction of the freestream velocity, $(\bar{U}_{BIASED} - \bar{U}_{TRUE})/\bar{U}_\infty$, had a maximum value of $6 \pm 0.5\%$ near the location where $\bar{U}_{BIASED}/\bar{U}_\infty = 0.30$ in the mixing layer. These figures agree well with the subsonic results of Adams et al. (1984) and Adams and Eaton (1985). The freestream normalized bias error goes to zero with the mean velocity. Adams et al. (1984) and Adams and Eaton (1985) found experimentally that:

$$\frac{\bar{U}_{BIASED} - \bar{U}_{TRUE}}{\bar{U}_\infty} = \frac{\sigma_u^2/\bar{U}_\infty}{\bar{U}_{BIASED}/\bar{U}_\infty}, \quad \sigma_u < \bar{U}_{BIASED}, \quad (4\,a)$$

$$\frac{\bar{U}_{BIASED}/\bar{U}_\infty}{}, \quad \sigma_u > \bar{U}_{BIASED}. \quad (4\,b)$$

Equation (4 a) was reasonably accurate up to 60% local turbulence intensities in the current study. Equation (4 b) was found to overpredict the freestream normalized bias substantially.

The effect of the bias on the standard deviations of the U velocity components is shown in Fig. 8. A similar non-monotonic trend occurs in the V component results also. Generally, the effect of the velocity bias on these turbulence normal stresses is not large, less than 10% for most of the flow, and the effect on the V component was smaller than the U component by as much as a factor of two in parts of the flow. Given the small effect of the z term correction on the mean velocity, it is expected to have a negligible effect on these standard deviations but this was not investigated. Figure 9 compares the corrected and biased Reynolds shear stress term, $\langle u'v' \rangle$. The bias in the shear stress, as indicated by the correction, may be as large as 20% for turbulence intensities as low as 10%.

Figure 2 provides some insight into the behavior of the bias observed in Figs. 8 and 9. At the freestream edge of the mixing layer, the U velocity PDF develops a long flat tail on the low speed side of the mean. These large negative fluctuations reduce the velocity magnitude and are therefore given larger velocity inverse weights than the rest of the data in the sample. This results in the initial increase in the bias corrected U component standard deviation with respect to the uncorrected result. The higher probability densities given these weighted large negative fluctuations can be seen in Fig. 2 for $0 < y^*/\theta < 3$. As the mean velocity magnitude decreases in a traverse across the mixing layer, the more heavily weighted near zero velocities occur with greater frequency and are closer to the decreasing mean. This results in a decrease of the size of the corrected standard deviation with respect to the uncorrected values. At the highest local turbulence intensities in Fig. 8, the mean velocity is near zero and the bias correction weights the data near the mean the most heavily. This leads to the decrease of the corrected standard deviations to values 20% less than the biased result. Thus, both the mean value and the form of the PDF determine the fractional bias in the second order central moments of the flow.

The greater sensitivity of the Reynolds stress to the effects of the bias is indicative of a basic difference between the

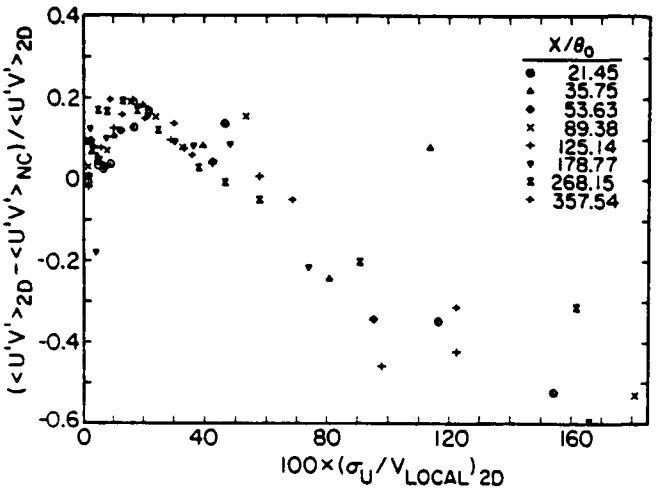

Fig. 9. Velocity bias of the averaged Reynolds stress term, $\langle u'v' \rangle$, vs. the local turbulent intensity

Reynolds stress and the normal stresses. Turbulent boundary layer studies have found the distribution of the Reynolds stress term, uv, to be highly skewed and flat with a most probable value of zero, see Gupta and Kaplan (1972) and Willmarth and Lu (1972). These features are indicative of an intermittent process. Although these characteristics have not been examined in the current study or in free shear flows in general, it is likely that the Reynolds stress distributions at the high and low speed edges of the mixing layer are similar and that the largest deviations from the most probable value, $uv = 0$, contribute most significantly to the Reynolds stress. These larger fluctuations are also most effected by bias and therefore the bias correction.

4 Conclusions

Comparisons between velocity biased and biased corrected statistics for data obtained with a coincident two component LDV system were presented and discussed. The effect of velocity bias on the velocity probability distribution function can be substantial and a two-dimensional velocity inverse bias correction worked reasonably well in compensating for the effects of the bias. The velocity bias changed the mean velocity and Reynolds shear stress term, $\langle u'v' \rangle$, appreciably in many cases but the effect on the root mean square velocity fluctuation level was not as substantial. The two-dimensional velocity inverse correction for velocity bias was improved by the addition of an estimated z velocity component term but the effects of this z term correction on the mean velocities was small and is expected to be negligible for turbulent intensity and shear stress statistics. The ability to observe and correct for velocity bias depends on obtaining sufficiently complete velocity magnitude information and therefore these procedures are limited to two-dimensional flowfields if accurate estimates of the flowfield statistics are to be made. Highly three-dimensional flows require a three-component velocimeter and appropriate accounting for the measurement volume effective cross sectional area variation with vector direction in addition to velocity bias considerations. The effect of the various possible weighting functions on the probability distributions of the velocity components, the velocity magnitude, or even a covariance term like the Reynolds stress can be visualized easily. Such techniques show that overly restrictive coincidence tests can distort velocity PDFs similar to velocity bias at near zero velocities. The bias of the mean velocity in the current experiment was equal to that predicted for a free running processor even though the processor was controlled according to the theoretical criterion. The reduction in the bias predicted for a controlled processor operating with a small reduced data rate was not observed. The decision on how or whether to correct for velocity bias is not trivial and requires careful consideration of the many factors involved as well as close examination of the results.

Acknowledgements

This research was supported by the U.S. Army Research Office under contracts DAAG 29-79-C-0184 and DAAG 29-83-K-0043. Dr. R. E. Singleton served as the Contract Monitor.

References

Adams, E. W.; Eaton, J. K.; Johnston, J. P. 1984: An examination of velocity bias in a highly turbulent separated flow. Presented at the 2nd Symp. on Applications of Laser Doppler Anemometry to Fluid Mechanics, Lisbon, Portugal

Adams, E. W.; Eaton, J. K. 1985: An LDA study of backward-facing step flow, including the effects of velocity bias. International Symposium on Laser Anemometry, New York, ASME FED Vol. 33

Addy, A. L.; Amatucci, V. A.; Kuntz, D. W.; Petrie, H. L.; Samimy, M. 1983: Base flow and related model experiments. Proc. Symp. on Rocket/Plume Fluid Dynamic Interactions (ed. Bertin, J.) Vol. 3. University of Texas at Austin, Report 83–104

Buchave, P. 1979: The measurement of turbulence with burst type laser Doppler anemometer-errors and correction methods. Report TRL-196. State University of New York at Buffalo

Craig, R. R.; Nejad, A. S.; Hahn, E. Y.; Schwartzkopf, K. G. 1984: A general approach for obtaining unbiased LDV data in highly turbulent non-reacting and reacting flows. AIAA Paper 84-0366, presented at AIAA 2nd Aerospace Science Meeting, Reno, Nevada

Dimotakis, P. E. 1976: Single scattering particle laser Doppler measurements of turbulence. AGARD CP-193

Durao, D. F. G.; Whitelaw, J. H. 1979: Relationship between velocity and signal quality in laser Doppler anemometry. J. Phys. E 12, 47–50

Edwards, R. V.; Jensen, A. S. 1983: Particle sampling statistics in laser anemometers: sample-and-hold systems and saturable systems. J. Fluid Mech. 133, 397–411

Erdmann, J. C.; Tropea, C. 1981: Turbulence induced statistical bias in laser anemometry. Proc. 7th Symp. on Turbulence, University of Missouri-Rolla, pp. 129–138

Erdmann, J. C.; Tropea, C. 1982: Statistical bias of the velocity distribution function in laser anemometry. Int. Symp. on Application of Laser Anemometry to Fluid Mechanics, Lisbon, Portugal, Paper 16.2

Gupta, A. K.; Kaplan, R. E. 1972: Statistical characteristics of the Reynolds stress in a turbulent boundary layer. Phys. Fluids 15, 981–985

Hoesel, W.; Rodi, W. 1977: New biasing elimination method for laser Doppler velocimetry counter processing. Rev. Sci. Instr. 48, 910–919

Johnson, D. A.; Moddarress, D.; Owen, F. 1982: An experimental verification of laser velocimeter sampling bias and its correction. In: Engineering applications of laser velocimetry, pp. 153–162. New York: ASME

McDougall, T. J. 1980: Bias correction for individual realization LDA measurements. J. Phys. E. 13, 53–60

McLaughlin, D. K.; Tiedermann, W. G., Jr. 1973: Biasing correction for individual realization of laser anemometer measurements in turbulent flow. Phys. Fluids 16, 2082–2088

Nakayama, A. 1985: Measurements of separating boundary layer and wake of an airfoil using laser Doppler velocimetry. AIAA Paper 85-0181, presented at AIAA 23rd Aerospace Sciences Meeting, Reno, Nevada

Petrie, H. L. 1984: A study of compressible turbulent free shear layers using laser Doppler velocimetry. Ph.D. Thesis, University of Illinois at Urbana-Champaign, Department of Mechanical and Industrial Engineering

Petrie, H. L.; Samimy, M.; Addy, A. L. 1986: Compressible separated flows. AIAA J. 24, 1971–1978

Petrie, H. L.; Samimy, M.; Addy, A. L. 1985: An evaluation of LDV velocity and fringe bias effects in separated high speed turbulent flows. *Proc. of the 11th Int. Congress on Instrumentation for Aerospace Simulation Facilities*, ICIASF Record '85, pp. 297–308. New York: IEEE Publication

Samimy, M. 1984: An experimental study of compressible reattaching turbulent free shear layers. Ph.D. Thesis, University of Illinois at Urbana-Champaign, Department of Mechanical and Industrial Engineering

Samimy, M.; Petrie, H. L.; Addy, A. L. 1986: An experimental study of compressible reattaching free shear layers. AIAA J. 24, 261–267

Stevenson, W. H.; Thompson, H. D.; Roesler, T. C. 1982: Direct measurement of laser velocimeter bias errors in a turbulent flow. AIAA J. 20, 1720–1723

Laser Doppler velocimeter systems. St. Paul/MN: TSI Inc., Technical Data Section

Willmarth, W. W.; Lu, S. S. 1972: Structure of the Reynolds stress near the wall. J. Fluid Mech. 55, 65–92

Received March 27, 1987

SECTION B.8

AN EXPERIMENTAL INVESTIGATION OF THE EFFECTS OF A BASE CAVITY ON THE NEAR-WAKE FLOWFIELD OF A BODY AT SUBSONIC AND TRANSONIC SPEEDS

M.S. Thesis

Department of Mechanical and Industrial Engineering

University of Illinois at Urbana-Champaign

August 1988

by

R. W. Kruiswyk

AN EXPERIMENTAL INVESTIGATION OF THE EFFECTS OF A BASE CAVITY ON THE NEAR-WAKE FLOWFIELD OF A BODY AT SUBSONIC AND TRANSONIC SPEEDS

Richard W. Kruiswyk, M.S. Thesis
Department of Mechanical and Industrial Engineering
University of Illinois at Urbana-Champaign

ABSTRACT

An experimental investigation was conducted to study the effects of a base cavity on the near-wake flowfield of a slender, two-dimensional body in the subsonic and transonic speed ranges. Three base configurations were investigated and compared: a blunt base, a shallow rectangular cavity base of depth equal to one-half the base height, and a deep rectangular cavity base of depth equal to one base height. The models were mounted in a small scale transonic wind tunnel with slotted upper and lower walls to allow testing into the transonic range and to minimize the effects of tunnel wall interference. Each base configuration was tested at three freestream Mach numbers, ranging from the low to high subsonic range, to give a total of nine experimental conditions. The objectives of the investigation were to explain the cavity's drag reducing mechanism, to attain a greater understanding of the phenomena of vortex formation and shedding, and to resolve some of the conflicts that have arisen between the numerical and experimental work on base cavities to date. Schlieren photography, surface oil flow visualization, tuft visualization, and wake static pressure traverses were used to examine the details of the wake vortex structure. Static base pressure measurements were used to measure the drag reduction effect and high-speed near-wake static pressure measurements were employed to determine the effect of the cavity on the vortex shedding frequency.

Schlieren photographs revealed that the basic qualitative structure of the vortex street was unmodified by the presence of a base cavity. However, the vortex street was weakened by the base cavity, apparently due to fluid mixing occurring at the entrance to the cavity. The weaker vortex street yielded higher pressures in the near-wake for the cavity bases relative to the blunt-based configuration, and the higher pressures caused the vortex formation position to be displaced

slightly further downstream for the cavity bases as compared to the blunt base. As a result, no strong recirculatory motion was observed in the cavity at all. The base cavity configurations produced increases in the base pressure coefficients on the order of 10 to 14% relative to the blunt-based configuration, and increases in the shedding frequencies on the order of 4 to 6%. The majority of the changes observed occurred in going from the blunt base to the shallow cavity base, with little additional benefit resulting from increasing the depth of the cavity from one-half to one base height.

SECTION B.9

AN EXPERIMENTAL INVESTIGATION OF THE EFFECTS OF A BASE CAVITY ON THE NEAR-WAKE FLOWFIELD OF A BODY AT SUBSONIC AND TRANSONIC SPEEDS

AIAA Paper No. 89-0210

Presented at the AIAA 27th Aerospace Sciences Meeting

Reno, Nevada

January, 1989

by

R. W. Kruiswyk and J. C. Dutton

AIAA '89

AIAA-89-0210

An Experimental Investigation of the Effects of a Base Cavity on the Near-Wake Flowfield of a Body at Subsonic and Transonic Speeds

R. W. Kruiswyk and J. C. Dutton
Department of Mechanical and Industrial Engineering
University of Illinois at Urbana-Champaign
Urbana, IL 61801

27th Aerospace Sciences Meeting
January 9–12, 1989/Reno, Nevada

AN EXPERIMENTAL INVESTIGATION OF THE EFFECTS OF A BASE CAVITY ON THE NEAR-WAKE FLOWFIELD OF A BODY AT SUBSONIC AND TRANSONIC SPEEDS

R. W. Kruiswyk* and J. C. Dutton**

Department of Mechanical and Industrial Engineering
University of Illinois at Urbana-Champaign
Urbana, Illinois 61801

ABSTRACT

An experimental investigation has been conducted to study the effects of a base cavity on the near-wake flowfield of a slender, two-dimensional body in the subsonic and transonic speed ranges. Three base configurations were investigated and compared: a blunt base, a shallow rectangular cavity base of depth equal to one-half the base height, and a deep rectangular cavity base of depth equal to one base height. Each configuration was studied at three freestream Mach numbers, ranging from the low to high subsonic range. Schlieren photographs revealed that the basic qualitative structure of the vortex street was unmodified by the presence of a base cavity. However, the vortex street was weakened by the base cavity, apparently due to enhanced fluid mixing occurring at the entrance of the cavity. The weaker vortex street yielded higher pressures in the near-wake for the cavity bases, increases in the base pressure coefficients on the order of 10-14%, and increases in the shedding frequencies on the order of 4-6% relative to the blunt-based configuration. The majority of the observed changes occurred in going from the blunt base to the shallow cavity base.

NOMENCLATURE

C_p	=	coefficient of pressure, $C_p \equiv (P-P_{ref})/(1/2\rho_{ref}U_{ref}^2)$
d	=	cavity depth
f	=	frequency
G_{xx}	=	power spectral density function
h	=	base height
M	=	Mach number
P	=	pressure
Re	=	Reynolds number, $Re \equiv \rho_{ref}U_{ref}h/\mu_{ref}$
St	=	Strouhal number, $St \equiv fh/U_{ref}$
U	=	freestream velocity
x	=	streamwise coordinate measured from the trailing edge plane
μ	=	absolute viscosity
ρ	=	density

Subscripts

base	=	base location
ref	=	reference location
∞	=	freestream conditions

INTRODUCTION

The near-wake of a two-dimensional bluff body at subsonic and transonic Mach numbers and sufficiently high Reynolds numbers (greater than 50 based on freestream conditions and body thickness) is dominated by the periodic and alternate shedding of vortices known as the von Karman vortex street. When these vortices form near the leeward side or base of the body, the low pressure of the vortex centers is communicated to the base, producing a low base pressure. This combines with the momentum loss associated with the concentrations of vorticity to yield an especially high base drag. The von Karman vortex street occurs frequently in engineering applications, and has even been observed behind such slender bodies as turbine blades of just three percent thickness ratio.[1] Because the base drag (often the dominant drag component) of both bluff and slender two-dimensional bodies is affected by the strength and proximity of the vortex street, any attempts at base drag reduction must be aimed at weakening the vortex shedding or at displacing the vortex formation position further downstream.

The present investigation focuses on the use of a base cavity as a drag reducing mechanism, and on the effect of such a cavity on the near-wake flowfield of a two-dimensional slender body in the subsonic and transonic speed ranges, Fig. 1. The base cavity has proven effective in reducing drag in several past investigations. However, the precise mechanism of this drag reduction is still unknown. Therefore, the present study is aimed at investigating the interaction between the cavity and the separated flow, and the effect of this interaction on the fluid dynamic mechanisms in the near-wake. The specific objectives of the investigation are to explain the drag reducing effect of the base cavity, to improve understanding of the phenomena of vortex formation and shedding, and to resolve some of the conflicts that have arisen between the numerical and experimental work on base cavities to date.

Experimental investigations of the base cavity have been conducted by Nash *et al.*,[2] Pollock,[3] and Clements[4] among others. They have studied cavity depths of from zero to two base heights on slender, two-dimensional bodies. Generally, they have found base drag reductions of 15-20% in the subsonic speed range, and no effect into the supersonic speed range. The lack of any effect at supersonic speeds is evidence that the cavity acts on the vortex street, since vortex shedding ceases at Mach numbers just beyond 1.0. Clements investigated cavities of various depths and reported base pressure increases for increasing cavity depths up to 1/2 base height, beyond which no further increases in base pressure were observed. Clements also measured a rise in the Strouhal number (*i.e.*, vortex shedding frequency) for increasing cavity depth up to 1/2 base height. While Nash *et al.* hypothesized that the walls of the cavity may constrain the upstream part of the vortices and thus improve wake stability, his Schlieren photographs did not appear to show any vortex motion extending into the base cavity.

Two important computational efforts on the effects of base cavities have been carried out by Clements[4] and Rudy[5]. Clements employed an inviscid discrete vortex method, while Rudy used an explicit, Navier-Stokes, finite-difference scheme at freestream Mach numbers of 0.4 and 0.6 with laminar Reynolds numbers (based on freestream conditions and the base height) of 700 and 962, respectively. Both investigators studied the effects of a rectangular cavity in the base of a slender, two-dimensional body at subsonic speeds. Clements and Rudy both found that the vortices penetrate partially into the cavity for at least a portion of the shedding cycle. Rudy reported that the pressure rises in the low velocity region between the first vortex and the back of the cavity, yielding a higher base pressure for the cavity base as compared to the blunt base. Because of this result, Rudy hypothesized that the drag reducing effect of the base cavity is similar to that of splitter plates and base bleed,[6-11] *i.e.* it is due to the increased distance between the base of the body and the vortex formation location. Interestingly, both Clements and Rudy computed a continuous *decrease* in the

---

*Formerly Graduate Research Assistant; Currently Mechanical Engineer, Caterpillar, Inc., Peoria, Illinois.

** Associate Professor. Member AIAA.

Strouhal number with increasing cavity depth, in direct contrast to the experimental results of Clements. Rudy attributed the decrease in shedding frequency to the increase in interaction between the vortices in the presence of a cavity. As mentioned previously, one of the objectives of this study is to address the discrepancies between previous numerical and experimental investigations of base cavity flows.

There have been a limited number of studies of the effect of a base cavity on an axisymmetric blunt-based body, such as a missile or projectile.[12-15] However, since the vortex shedding is much weaker from an axisymmetric body than a two-dimensional body at both subsonic and supersonic speeds, the base cavity would be expected to have less of a drag reducing effect. This expectation has been borne out in the previous experimental studies of axisymmetric geometries where base drag reductions on the order of 4-10% have been obtained, even for optimized configurations.

EXPERIMENTAL SETUP

Wind Tunnel Facilities and Model

A previously fabricated two-dimensional transonic wind tunnel was used in this investigation. This tunnel has a 101.6 mm x 101.6 mm test section, and was built based on a NASA design by Little and Cubbage.[16] The sidewalls of the tunnel are solid, while the upper and lower walls are slotted to relieve the blockage effect of the model and to allow experimentation through the transonic speed range. A pair of round windows may be mounted in the sidewalls to allow visualization of the flow over the aft end of the model and in the near-wake. Solid aluminum inserts may also be used in place of the windows for the wake static pressure traverses and shedding frequency measurements to be described below. The results of tunnel-empty calibrations at Mach numbers from the low subsonic through transonic speed ranges demonstrated that this tunnel produces remarkably uniform flow.

Compressed, dried, filtered air was supplied to the tunnel by two compressors, an Ingersoll-Rand which delivered 41 kg/min at 960 kPa and a Gardner-Denver which delivered 20 kg/min at 760 kPa. The compressed air was stored in a tank farm with a capacity of approximately 140 m^3, then delivered to the facility stagnation chamber and test section before exiting via a silencer system to the atmosphere. The stagnation pressure of the test section was regulated by way of a pneumatically operated Fisher-Governor control valve in conjunction with an electronic feedback controller.

To accomplish the objectives of this study the two-dimensional model illustrated in Fig. 1 was constructed. The model has a wedge-shaped forebody, a constant 10% thick afterbody, and three interchangeable base geometries (Fig. 2): a blunt base, a shallow rectangular cavity base with depth equal to one-half the base height, and a deep rectangular cavity base with depth equal to one base height. This model is similar to that used in the experiments of Nash *et al.*[2] and is identical to the computational geometry used by Rudy[5], except that Rudy's cavity heights were 90% of the base height and those of the current experiments were 80% of the base height to ensure structural rigidity of the extended portions of the base.

The size of the model relative to the tunnel is the most important factor in determining wall interference effects in transonic wind tunnel testing. The maximum blockage of the model in this study was 15% (see Fig. 1), which is a bit high by transonic tunnel standards. This model size was chosen as a compromise between being as small as possible to minimize blockage effects but being large enough to adequately instrument the base with pressure taps and so that the flowfield could be adequately resolved with the available measurement techniques. In addition, larger than normal interference effects were deemed acceptable in light of the objectives of this investigation to investigate the physical *mechanisms* of the flowfield and the *trends* that the data exhibit with either increasing cavity depth or increasing Mach number. These mechanisms and trends should be accurately reflected in the current measurements even if small errors in the absolute values of the data occur due to interference effects. Also, the basic structure of the vortex street, which is of prime importance here, should not be strongly affected by the 15% blockage of the model. As evidence, El-Sherbiny and Modi[17] found that the lateral and longitudinal spacings of the vortices in the wakes behind inclined flat plates were independent of blockage ratios up to 20%.

Measurement Techniques

Black and white Schlieren photography was used to visualize the structure of the vortex streets behind the model and to determine to what degree the vortex motions extended into the cavities. The Schlieren system used was a standard Toepler arrangement, with the sending and receiving optics located off-axis in the familiar "z" pattern and with parabolic mirrors directing the parallel light beam through the test section. A straight knife-edge in the cut-off plane provided exposure and sensitivity control and was set parallel to the flow direction (*i.e.*, horizontally) to allow visualization of the separating shear layers. The light source was a Xenon model 457 flash lamp with a flash duration of 1.4 microseconds. Processing of large numbers of photographs was accomplished via a 35 mm format camera and Kodak Panatomic-X (ASA 32) roll film.

Surface oil flow visualization was utilized to ascertain flow directions within the cavities and on the model and to examine the streakline patterns formed on the sidewalls by the vortex streets. A mixture of lampblack and a 90 weight viscous oil was used for this purpose. This mixture was either spread evenly on the surface of interest with a paint brush or applied as discrete dots of oil to yield highly defined surface streakline patterns.

Tuft visualization was used to further examine the air motions within the cavities and to complement the results of the surface flow studies. Short strands of a lightweight white thread were fixed with small dots of rubber cement to the trailing edge of the deep cavity, while several others were suspended from the upper cavity wall at depths of 1/3, 1/2, and 2/3 base heights from the entrance.

Base pressure measurements were made to determine the effect of cavity depth on base drag. A set of fifteen static pressure taps was distributed across each base so as to reveal any variations in pressure across the span or height of the base. These taps were connected via flexible nylon tubing to a Pressure Systems Incorporated model DPT 6400 electronic pressure scanner. The output from the PSI system was directed to an HP-9000 mini-computer for data analysis and storage.

Vortex shedding frequency measurements were made to determine the effect of the cavities on the shedding frequency in the hope of resolving the previously mentioned conflict between numerical and experimental results. The shedding frequencies were determined from a Fourier analysis of the signal from fast response pressure transducers. The transducers used were Endevco model 8506B-15 piezo-resistive pressure transducers, which have a 2.31 mm face diameter and a resonant frequency of 130 kHz. The data from the transducers was collected with a DEC PDP 11/73 micro-computer using a Data Translation model DT2752 high-speed, 12 bit, 8 channel, A/D converter. This A/D board is capable of sampling single channel data at up to 100 kHz. A sixth-order anti-aliasing Butterworth analog filter with a cutoff frequency of 8000 Hz was placed prior to the A/D board to eliminate false signals due to aliasing. Data was transferred from the PDP 11/73 to the HP-9000 for reduction and analysis.

Static pressure surveys of the wake were performed in an attempt to define the position of vortex formation for each of the base configurations. This method has been employed in previous investigations by Nash *et al.*[2] and Roshko[6] who state that the location of a low pressure trough in the wake behind a body coincides with the position of vortex formation. Since static pressure measurements in a vortex street wake can only provide a time-averaging effect of an unsteady phenomenon, the results must be considered qualitative rather than quantitative. Four different 3.175 mm diameter static probes were used, with the static holes ranging in distances from 3.175 to 12.5 mm from the tip of the probe. Four static holes were located around the circumference of each probe so as to effectively average the

static pressure at the location of the holes. Each probe was bent at a ninety degree angle approximately 41.28 mm back from the probe tip to exit the test section through the solid insert in the sidewall. Eight exit holes were drilled in the insert at intervals of 7.62 mm (1/2 base height), and in conjunction with the four probes, these gave up to 32 possible pressure measurement locations from the base of the body to a distance of four base heights downstream. Data gathering and reduction followed the same procedures as described previously for the base pressure measurements.

Further details concerning the experimental apparatus, instrumentation, and measurement and data reduction procedures may be found in Ref. 18.

EXPERIMENTAL RESULTS

Experimental Conditions

The experimental results for the three base geometries shown in Fig. 2 are presented in this section. For each model experiments were conducted at three different Mach numbers, ranging from the low to the high subsonic range, to give a total of nine different experimental conditions. These conditions are as follows:

Base Type	Ref. Mach No.	Ref. Reynolds No.
Blunt Base	0.485	1.62×10^5
	0.720	2.32×10^5
	0.880	2.78×10^5
Shallow Cavity	0.485	1.62×10^5
	0.720	2.32×10^5
	0.880	2.78×10^5
Deep Cavity	0.485	1.62×10^5
	0.720	2.32×10^5
	0.880	2.78×10^5

Rather than try to apply a freestream Mach number correction to account for the effects of model blockage, it was decided to specify a reference Mach number *as measured* in the tunnel, *i.e.* without correction factors, that would be most relevant to the flowfield region of greatest interest, namely the vortex street and near-wake. Thus, the reference Mach number was chosen to be that outside the boundary layer over the aft end of the model just prior to separation. The three values of the reference Mach number shown in the table above were chosen to correspond approximately to freestream flows at Mach 0.4, 0.6, and 0.8. The reference of 0.880 was chosen by matching the Schlieren photo at that condition to the Schlieren of Nash *et al.*[2] of a freestream Mach 0.8 flow over the same model geometry in a much larger tunnel with essentially interference-free conditions. The reference of 0.720 was chosen via Rudy's[5] computations, which indicate that at a freestream Mach number of 0.6 the Mach number over the aft end of the body is 0.720. Finally, the reference of 0.485 was chosen simply by setting the upstream Mach number in the tunnel to 0.4, as it was known that interference effects would be relatively small at the lower Mach number.

The Reynolds numbers listed in the table are based on conditions at the reference location and the base height. Boundary layer trips (0.25 mm diameter hypodermic tubing) were placed at the ten percent chord location to fix the transition points. Thus, the boundary layers at separation from the base were turbulent in all cases. The boundary layer thickness at separation for each case was estimated to be 1.5 mm from enlarged Schlieren photographs.

Schlieren Photographs

Schlieren photography was used to visualize the structure of the vortices behind the models and to reveal any qualitative differences that may exist in the near-wakes of the flows for the different base configurations and Mach numbers. Figure 3a depicts the flow over the model fitted with the blunt base at a reference Mach number of 0.485 (the screw visible in the photograph was used for focusing purposes and is outside the tunnel). In this case the vortex shed from the upper surface of the body has apparently reached the fully-formed condition, while the shear layer separating from the lower surface is just beginning to roll up. It is clear from this figure that the vortices form right at the base of the body and that in the fully-formed condition the vortices extend over the majority of the thickness of the base. Figures 3b and 3c show the flowfield over the blunt-based model at reference Mach numbers of 0.720 and 0.880, respectively. The basic features of the near-wake flowfield for these cases are similar to the Mach 0.485 flowfield, except that the vortex street becomes more obscured by turbulence at the higher Mach numbers and at Mach 0.880 pressure waves generated from the vortex shedding are evident at the base of the model. Comparison of these Schlieren photographs with Rudy's[5] computed vorticity contour plots for a freestream Mach 0.6 flow over the same blunt-based configuration indicates excellent qualitative agreement for the near-wake structure, particularly in terms of the proximity of the vortex formation location to the base. Some minor differences, such as more rapid diffusion of the vortices in the experiments, may be attributed to the fact that the boundary layers at separation are turbulent in the experiments and laminar in the computations.

Figures 4a and 4b are Schlieren photos of the flow over the model fitted with the shallow cavity base at reference Mach numbers of 0.485 and 0.720, respectively. The basic structure of the vortex street appears unchanged in comparison to the blunt-based configuration discussed above. By comparing Schlieren pictures of the flow for the two geometries at similar points in the shedding cycle, the spacing of the vortices and the spread rate of the vortex street in the early part of the wake appear virtually identical, as though the base cavity does not influence the vortex formation and shedding process at all. However, a closer examination shows that for the cavity base the vortices may form slightly farther downstream of the trailing edge plane, although this is impossible to confirm from a single still photograph. This point will be discussed further in light of other experimental results to be presented in the sections to follow. The main difference between the various Mach number conditions for the shallow cavity base is again the presence of more turbulence at the higher Mach numbers resulting in greater diffusion of the vortices. Comparison of Rudy's[5] computed vorticity plots with these Schlieren photos for the shallow cavity base show that the experimental and computational results are *not* in agreement for this case. The Schlieren pictures (including many others not shown here) indicate clearly that the vortices do not extend into the cavity during any portion of the shedding cycle, while Rudy's computational results (as well as those of Clements[4]) indicate that the vortices form at least partially within the cavity throughout the shedding cycle. This discrepancy between experiments and computations for base cavity flows was also reported by Clements. Further discussion of this point will follow the presentation of the remainder of the experimental results.

Figures 5a and 5b depict the flow over the model fitted with the deep cavity base at M_{ref}=0.485 and 0.720, respectively. Again the basic structure of the vortex street wake appears unchanged in comparison to the wakes of the two base configurations discussed above. In fact, Figs. 4b and 5b at M_{ref}=0.720 look virtually identical except for the geometry of the base itself. For the deep cavity base, as for the shallow one, it appears that the vortices may form slightly further downstream of the trailing edge plane than they did for the blunt-based configuration. Comparing the Schlieren photos of Figure 5 with Rudy's[5] constant vorticity lines for the Mach 0.6 computations of the deep cavity configuration indicate the same discrepancy between the computational and experimental results noted above: the Schlieren photographs show no vortex motion extending into the cavity whatsoever, while the computations show the vortices extending well into the cavity throughout the shedding cycle. As mentioned, this point will be discussed further below.

Surface Oil Flow Patterns .

The surface oil flow visualization results presented here are intended to answer several important questions regarding the qualitative nature of the flowfield: first, to ascertain that the flow in the tunnel is satisfactorily two-dimensional; second, to determine whether any significant fluid motion occurs within the base cavities; and finally, to help determine if the vortices form farther downstream from the trailing edge plane for the cavity bases in comparison to the blunt-based model, as was hinted at by the Schlieren stills.

The oil flow patterns across the span of the upper surface of all three models and for all three reference Mach numbers indicated that the flow was appropriately two-dimensional, *i.e.* the streaklines were extremely straight and in the streamwise direction with no recirculatory regions even very near the sidewalls. For the blunt-based model essentially vertical streak patterns on the base were formed from a series of oil dots placed across the span of the base midway between the upper and lower trailing edges. Apparently, the mean effect of the vortices shed from alternate trailing edges was to push some of the oil to the upper trailing edge and some to the lower trailing edge. The clarity and rapidity with which these streak patterns formed indicates that the vortices do indeed form immediately adjacent to the base for the blunt-based model, as was evident in the Schlieren photos of Fig. 3.

In order to determine the surface flow patterns on the internal cavity surfaces of the two cavity configurations, oil was spread on all cavity surfaces, and even as discrete dots very near the lip of the cavity. However, no streak patterns were formed on any of these internal cavity surfaces. This indicates that there is no strong vortex motion extending into the cavity, and that apparently no significant recirculatory motion occurs in the cavity at all. The specifics of the air motions, if any, in the cavities will be discussed in some of the results to follow.

Figures 6a-c are reproductions of the oil streak patterns that were formed on the wind tunnel sidewalls for each base configuration with a scale placed so as to indicate the distance of the oil "vortices" from the trailing edge plane. The reference Mach number for these figures is 0.485, although similar patterns were formed for all three reference Mach number conditions. These streak patterns simply represent the mean effect of the unsteady vortex street wake phenomenon. The centers of the "vortices" of oil that formed on the sidewall are considered to represent the correct *relative* position of vortex formation for the three base configurations. In other words, while the absolute position of vortex formation relative to the trailing edge plane may not be correctly represented due to the presence of the sidewall boundary layer, the position of vortex formation for one base geometry relative to the other bases should be approximately correct, assuming that the sidewall boundary layer affects the oil streaks for all three base configurations approximately equally. These photographs indicate an oil vortex formation position of about 3/16 in. (4.76 mm or 0.31 base heights) from the trailing edge for the blunt base and about 1/4 in. (6.35 mm or 0.42 base heights) for the two cavity bases, a difference of approximately 1/16 in. (1.59 mm). Similar results were found at reference Mach number conditions of 0.720 and 0.880. While these photos may not indicate the true and absolute position of vortex formation for the vortex streets, they do indicate the qualitative fact that the vortex formation position for the cavity bases is further downstream from the trailing edge plane *relative* to that for the blunt base configuration. Further support for this argument is presented in the section discussing the wake static pressure traverses.

Tuft Visualizations

The fact that the surface oil flow patterns showed no significant recirculatory flow in the cavity revealed the need for a more sensitive measurement technique to determine if any fluid motion occurs in the cavity. To this end the tuft visualization experiments described earlier were performed with several lightweight tufts attached to the trailing edge of the deep cavity, as well as from the upper cavity wall at several depths from the cavity entrance. The tufts at the trailing edge plane were extremely active, rotating rapidly back and forth in the streamwise direction in a 75 to 80 degree arc, nearly 45 degrees in the downstream direction and roughly 30 to 35 degrees back upstream into the cavity. Some spanwise motion was also observed, though to a much lesser extent. This high degree of activity is not unexpected; since the vortices form close to the trailing edge plane even for the deep cavity, the tufts there are subjected to a rapid periodic pressure variation. For the tufts suspended further back in the cavity the motion was similar, but the level of activity decreased gradually from the trailing edge to the back of the cavity. These results suggest that the periodic pressure pulses from the shedding vortices set the air in the cavity into a rapid vibratory motion, but without any strong net flow direction as would be sensed by the surface oil coatings.

Wake Static Pressure Traverses

The static pressure traverses of the near-wake region, along the centerline of the body and away from the sidewall boundary layers, were performed to help confirm the apparent observation that the vortices form farther downstream in the presence of a base cavity. Because these measurements were time-consuming and because the sidewall surface streaklines indicated similar trends in the vortex formation location for all three reference Mach numbers, these measurements were made at M_{ref}=0.485 only.

The streamwise variation of the near-wake static pressure coefficient, $C_p \equiv (P-P_{ref})/(1/2\rho_{ref}U_{ref}^2)$, for the three base geometries is shown in Fig. 7. The plots display the characteristic features of the vortex street wake as described by Nash *et al.*[2] and Roshko,[6] namely a low pressure trough in the near-wake at the vortex formation position followed by a gradual rise in pressure to an essentially constant value further downstream. This figure shows clearly that the location of vortex formation has indeed been displaced slightly farther downstream from the trailing edge plane in the presence of a base cavity. In addition, the plots for the shallow cavity base and the deep cavity base overlap each other quite closely except for some data scatter between two and four base heights downstream of the trailing edge. This result agrees with the sidewall oil flow visualizations and suggests that increasing the cavity depth beyond 1/2 base height has no further effect in pushing the vortex formation position downstream. The results in this figure may be compared to those in Fig. 8 which has been adapted from the computational study of Rudy[5] for a freestream Mach number of 0.4 (the curves in Fig. 8 have been obtained by averaging the instantaneous pressures at eight different times in the shedding cycle). Note that Rudy's pressure coefficients are based on freestream conditions. The agreement between the experimental and computational results for the vortex formation location is excellent for the blunt-based configuration, but not for the cavity bases where the computations indicate that the vortex formation position moves *upstream*. These results then follow the same trends seen earlier in comparing the Schlieren photos of the present study to Rudy's vorticity plots, as would be expected.

Comparing Fig. 7 to Fig. 6 reveals that the vortex formation positions as indicated by the sidewall oil streak patterns are approximately 0.3 base heights closer to the model trailing edge than the vortex formation positions as indicated by the wake static pressure traverses. As mentioned, this may be attributed to the effects of the sidewall boundary layers on the streaklines or to errors in the static pressure measurements. Again, it should be emphasized that the absolute position of vortex formation is of less importance to this discussion than the *relative* formation position for the cavity bases compared to the blunt base. In this regard, note that both the sidewall oil streak patterns and the wake static pressure traverses indicate a downstream displacement of the vortex formation position of approximately 1/10 base height for the cavity bases relative to the blunt base.

The experimental results in Fig. 7 also reveal that the static pressure within the cavities remains essentially constant. This is again in contrast with the computations but confirms the experimental observations made earlier that there is no

significant recirculatory motion in the cavities. Note in Fig. 8 that the computations indicate a rapid rise in pressure from the trailing edge plane to about midway back in the cavities as a result of the vortices extending partially into the cavity. A final observation on the measurements in Fig. 7 is that the cavity bases cause an increase not only in the base pressure coefficient but also in the values of the pressure coefficient in the near-wake within roughly 5/8 base heights of the trailing edge plane. This point will be considered further in the discussion below.

Base Pressure Measurements

As mentioned above, fifteen static pressure taps were distributed across the base of each model to determine if any significant transverse or spanwise base pressure variations were present. For most of the Mach number-base geometry configurations, the base pressure distributions were quite uniform, though there was a tendency for the pressures near the sidewalls to be slightly higher than at the midplane (maximum variations were generally less than two percent). The average of the pressures at the fifteen taps was taken as the base pressure for the results to be presented here.

The variation of the base pressure coefficient with cavity depth and reference Mach number is plotted in Fig. 9. The percentage increases in the base pressure coefficient for the cavity bases relative to the blunt base are as follows:

Ref. Mach No.	Shallow Cavity	Deep Cavity
0.485	+14.1%	+14.4%
0.720	9.8	11.9
0.880	10.3	11.5

These percentage increases are of the same order as those found by Rudy[5] for his freestream Mach 0.6 case. Figure 9 illustrates quite clearly that the majority of the base pressure increase occurs with a cavity depth equal to 1/2 base height, and that increasing the cavity depth to one base height yields only slightly greater drag reducing benefits. This was precisely the conclusion arrived at in the computational results of both Clements[4] and Rudy. It is quite possible that the majority of the base pressure coefficient increase occurs for an even shallower cavity depth such as 1/4 or 1/3 base height, but this is impossible to confirm from these results. Note that although the beneficial effects drop off slightly between reference Mach numbers of 0.485 and 0.720, there is no significant change between M_{ref}=0.720 and 0.880. It would seem, as reported by Nash *et al.*,[2] that the base cavity will be effective as long as vortex shedding is present, which means through Mach one.

Shedding Frequency Measurements

As discussed previously, the vortex shedding frequencies were determined through a power spectral density analysis of the signal from a fast response piezo-resistive pressure transducer. The collected time domain measurements were transformed into the frequency domain via a fast Fourier routine, and the output was then analyzed to determine the frequency composition. For all results presented herein, the transducer was located in the tunnel sidewall and downstream of one of the trailing edges. It is realized that the frequency measurements obtained at this location could possibly be distorted by the presence of the sidewall boundary layer. However, comparison of measurements obtained for the blunt-based geometry with the transducer located in the base and in the sidewall showed less than a 4% difference in the value of the shedding frequency. It was felt that this difference was small enough that the more convenient sidewall location could be used. In addition, the fluctuating pressure signal for the cavity bases is stronger at the sidewall location than at the rear cavity wall location.

The power spectral density function, G_{xx}, is plotted as a function of frequency for the blunt-based model at M_{ref}=0.485 in Fig. 10, with similar results obtained for the other eight base geometry-Mach number combinations. For all cases, a strong peak occurs at the shedding frequency, with a second smaller peak apparent at twice the shedding frequency. The relatively broad nature of the peaks in the spectral density plots is due at least partly to the fact that the vortex street is superimposed on a random turbulent flowfield, resulting in the diffusion or feeding of some of the discrete energy (from the vortex shedding) to the continuous (turbulent) portion of the spectra. The shedding frequencies and Strouhal numbers, $St \equiv fh/U_{ref}$, for each of the experimental cases are as follows:

Ref. Mach No.	Base Type	Shedding Freq.	Strouhal No.
0.485	Blunt	2539.1 Hz	0.2375
	Shallow	2705.1	0.2530
	Deep	2690.4	0.2517
0.720	Blunt	3730.5	0.2414
	Shallow	3867.2	0.2502
	Deep	3881.8	0.2511
0.880	Blunt	4379.9	0.2372
	Shallow	4492.2	0.2433
	Deep	4501.9	0.2438

Note that these Strouhal numbers are based on the velocity measured at the reference location, *i.e.* over the aft end of the model just prior to separation.

The Strouhal numbers are plotted versus cavity depth and reference Mach number in Fig. 11. The results of Nash *et al.*[2] for a similar blunt-based model indicate that for slender, two-dimensional models the Strouhal number should remain constant from low subsonic speeds up to a freestream Mach number of about 0.9. The results in Fig. 11 agree reasonably well with this observation except for the drop in Strouhal number that occurs for the two cavity bases at the reference Mach number of 0.880. The reason for this drop is unclear. It could be due to the increase in wall interference effects that occurs as the flow approaches Mach 1.0, but that does not explain why a similar decrease did not occur for the blunt-based configuration at the higher Mach number. What is obvious from Fig. 11 is that the effect of the cavity is to *increase* the shedding frequency, in agreement with the experimental observations of Clements[4] but again in disagreement with the computational results of both Clements and Rudy.[5] Also, note that the deep cavity again produces virtually no change beyond that which was achieved with the shallower cavity, a trend that has been evident in all of the experimental results presented so far. Further discussion of some of these observations will be given is the following section.

SUMMARY AND DISCUSSION

The common thread among all of the experimental results is that increasing the depth of the cavity from 1/2 to 1 base height does not have any significant effect on the parameter being observed; the majority of the changes occur in going from the blunt base to the shallow cavity, and may in fact occur for an even shallower cavity of, say, 1/4 or 1/3 base height in depth, though this was not investigated here. This result was also evident in the computational results of both Rudy[5] and Clements[4] and suggests that, whatever the mechanism is that causes the drag reduction for the cavity bases, it is little affected by depth once the cavity has reached some critical, rather shallow, depth.

It is evident in the Schlieren photographs that the basic structure of the vortex street is relatively unmodified by the presence of a base cavity and that the vortex motions do not extend into the cavity at all. In fact, the vortex formation position is pushed slightly further downstream with a base cavity as compared to a blunt base. This is perhaps somewhat surprising; since the vortices form immediately adjacent to the base for the blunt geometry, one might expect the vortices to move partially into the cavity when the solid boundary of the blunt base is replaced with the compliant fluid boundary of the cavity base. That this does not occur refutes the hypothesis of

Nash *et al.*[2] that the cavity walls improve wake stability and decrease drag by constraining the upstream part of the vortices.

The fact that the present results show that the vortices do not extend into the cavity also accounts for the discrepancy between the experiments and computations regarding the effect of a base cavity on the shedding frequency. In the computations, the cavity was found to increase the interaction between the vortices and thereby decrease the shedding frequency.† In the experiments, the interaction between the vortices is apparently *not* facilitated by the presence of the base cavity and so the shedding frequency does not decrease. The observation that the shedding frequency actually *increases* with a base cavity may be due to the fact that the vortices form slightly further downstream in this case so that the distance between the separated shear layers is less at the start of vortex formation.†† This seems plausible: in Bearman's[7,9] splitter plate and base bleed experiments the vortex formation position was moved downstream approximately one base height and the Strouhal number increased by roughly 33%; in this investigation the vortex formation position was moved downstream approximately 1/10 base height due to the cavities and the Strouhal number increased by roughly 4-6%.

The fact that the drag reducing mechanism of the base cavity is different than that of either the splitter plate or base bleed is evidenced by the very different degrees of displacement of the vortex formation position for these geometries relative to a plain blunt-based configuration. For the base cavity there are no structural or fluid elements to interfere with the interaction between the separating shear layers as for splitter plates and base bleed. The effect of the cavity on the vortex street is apparently of a more subtle nature. The results of the present surface flow experiments seem to refute even Compton's[13] theory that the recirculating flow in the cavity forms a steady co-flowing stream on the inner edges of the separated shear layers thereby decreasing mixing and increasing the base pressure. If any significant recirculating flows were present in the cavity, they would most likely have left some directional indication in the oil coatings, and as reported earlier this was not found to be the case in the experiments reported herein.

A clue as to what is happening in the near-wakes of the cavity configurations comes from the results of the wake static pressure traverses. Figure 7 shows that the cavity base increases not only the base pressure coefficient but also the pressure coefficient in the near-wake within roughly 5/8 base heights of the trailing edge. Nash *et al.*[2] have stated that the value of the pressure coefficient in the low pressure trough in the wake of a bluff body decreases with an increasing degree of bluffness of the body and hence with increasing strength of the vortex street. In Fig. 7 it is apparent that the low pressure troughs of the cavity bases do not reach as low a minimum as for the blunt base, and this suggests that the vortex streets of the cavity bases are somewhat weaker than the vortex street of the blunt-based configuration. The weaker vortex street results in the higher pressure at the base and in the near-wake, and the higher pressure, in turn, may then move the vortex formation position to a location slightly further downstream of the trailing edge as compared to the blunt base geometry.

The question then becomes what causes the weakening of the vortex street; there are no interference elements in the wake, there is no constraint of the upstream part of the vortices by the cavity walls, and there is apparently no significant steady recirculating flow causing the formation of a co-flowing stream. The only difference between the blunt base and the cavity bases is that the forming vortices see a solid boundary at the trailing edge plane in the one case and a compliant fluid boundary in the other. It is quite possible that enhanced fluid mixing at the trailing edge of the base cavity causes a greater loss of vorticity than does the solid wall friction at the trailing edge of the blunt base. The tuft experiments have shown that the air at the cavity entrance is in a state of unsteady pulsatile motion as it is forced first one way by the vortex shedding from the upper trailing edge and then the other way by the vortex shedding from the lower trailing edge. These unsteady, oscillating air motions could increase the fluid mixing at the trailing edge plane to such a degree that the forming vortices are weakened. If this is indeed the case, then the shape or geometry of the cavity would seem to be unimportant; the cavity should be effective as long as it is deep enough to completely replace the fluid-solid wall interaction for the blunt base with a purely fluid interaction for the cavity base, and as long as the cavity is of such a height to cover the majority of the base. This was, in fact, evident in the results of Pollock,[3] who found that the drag reducing effect of a special cusp cavity, whose shape was chosen on theoretical grounds, was essentially identical to that of the simple rectangular cavity of Nash *et al.*[2] Furthermore, the results reported herein, as well as the experimental results of Clements,[4] have indeed shown cavity depth to be unimportant once the cavity has reached a somewhat shallow, critical depth.

Having discussed several points of disagreement between the present experimental results and the computational results of Rudy[5] and Clements,[4] it is important to reiterate the differences in the relevant flowfield conditions of these investigations in an attempt to explain why these disagreements may exist. One obvious difference is that the computations model a perfectly two-dimensional flowfield while the experiments can never be completely free from three-dimensional effects. In fact, Nash[20] has stated that over no part of the Reynolds number range is the vortex street strictly two-dimensional, due to the presence of spanwise periodic structures and/or random turbulent fluctuations. Considering the relatively small scale of the wind tunnel used in this investigation, some effects of three-dimensionality are inevitable, despite the two-dimensional indications of the surface oil flow patterns and the base pressure measurements. Apparently, however, the effects of any three-dimensionalities are primarily confined to the interactions of the vortices with the base cavities, as the results for the blunt-based model in these experiments showed excellent agreement with the corresponding results from Rudy's computations. The fact that the tufts suspended in the base cavities did show a degree of spanwise as well as streamwise motion lends support to the argument that three-dimensional effects in the base cavity may affect the interactions with the vortices in the near-wake region.

A second major difference between the conditions of the present experiments and the computational results is the Reynolds numbers. For Rudy's[5] computations the Reynolds numbers based on freestream conditions and base height were 700 for the M_∞=0.4 condition and 962 for the M_∞=0.6 case. Furthermore, the boundary layers at separation were laminar. Clements'[4] computations, on the other hand, were inviscid. In the current experiments the Reynolds numbers based on the reference conditions and base height were between 1.62×10^5 and 2.78×10^5 and the boundary layers at separation were turbulent. In his study of vortex street wakes behind circular cylinders, Roshko[21] observed that the development and characteristics of the vortex street are very dependent on where the transition point is located, and that very different trends are displayed depending on whether the separating shear layers are laminar or turbulent. Thus, it is quite possible that the behavior of a vortex street in the presence of a base cavity will likewise depend on the state of the separating boundary layers. Rudy recognized this and suggested that computations be performed at higher Reynolds numbers using appropriate turbulence models in order to better match experimental conditions.

Another point to be considered is that the computations model an unconstrained freestream while the experiments reflect the blockage effects of the wind tunnel walls. Keeping in mind the relatively large blockage ratio (15%) used in this investigation, it is recognized that some of the observations reported herein may have been influenced by wall interference effects. However, as discussed earlier, it is felt that while wall

† Devices such as splitter plates and base bleed which decrease interaction between the vortices have been found to yield an increase in the shedding frequency.[7-11]

†† Fage and Johansen[19] have found that the vortex shedding frequency is inversely proportional to the distance between the separated shear layers.

interference may have somewhat affected the absolute values of the various measured flow parameters, the effects on the basic structure of the vortex street and the trends of the data with increasing Mach number or cavity depth are probably small. Therefore, the blockage effects are probably less likely to be the cause of the observed discrepancies between the computational and experimental results than the three-dimensional and Reynolds number effects discussed above.

A final point to consider is that the cavity geometries for this investigation were not identical in every detail to those used in Rudy's[5] computations; the cavities in the current experiments covered 80% of the base height, while Rudy's cavities spanned 90% of the base height. It seems doubtful, however, that this difference could be responsible for the discrepancies reported herein.

ACKNOWLEDGMENTS

This research was supported by the U.S. Army Research Office under Contract No. DAAL03-87-K-0010 with Dr. Thomas L. Doligalski and Dr. Robert E. Singleton as Contract Monitors.

REFERENCES

1. Heinemann, H. J., Lawaczeck, O., and Butefisch, K. A., "Von Karman Vortices and their Frequency Determination in the Wakes of Profiles in the Sub- and Transonic Regimes," *IUTAM Symposium Transsonicum II*, Oswatitsch, K. and Rues, D., eds., Springer Verlag, New York, 1978, pp. 75-82.

2. Nash, J. F., Quincey, V. G., and Callinan, J., "Experiments on Two-Dimensional Base Flow at Subsonic and Transonic Speeds," ARC R&M No. 3427, Jan. 1963.

3. Pollock, N., "Some Effects of Base Geometry on Two-Dimensional Base Drag at Subsonic and Transonic Speeds," Australian A.R.L., Aerodynamics Note 316, Oct. 1969.

4. Clements, R. R., "Computer Models of Separated Flows Behind Two-Dimensional Bluff Bodies," Ph.D. Dissertation, Cambridge University, July 1973.

5. Rudy, D. H., "A Numerical Study of Unsteady Two-Dimensional Subsonic Compressible Base Flow," Ph.D. Dissertation, Department of Mechanical and Industrial Engineering, University of Illinois at Urbana-Champaign, May 1987.

6. Roshko, A., "On the Drag and Shedding Frequency of Two-Dimensional Bluff Bodies," NACA TN 3169, July 1954.

7. Bearman, P. W., "Investigation of the Flow Behind a Two-Dimensional Model with a Blunt Trailing Edge and Fitted with Splitter Plates," *Journal of Fluid Mechanics*, Vol. 21, Feb. 1965, pp. 241-255.

8. Nash, J. F., "A Discussion of Two-Dimensional Turbulent Base Flows," ARC R&M No. 3468, July 1965.

9. Bearman, P. W., "The Effect of Base Bleed on the Flow Behind a Two-Dimensional Model with a Blunt Trailing Edge," *Aeronautical Quarterly*, Vol. 18, Aug. 1967, pp. 207-224.

10. Wood, C. J., "The Effect of Base Bleed on a Periodic Wake," *Journal of the Royal Aeronautical Society*, Vol. 68, July 1964, pp. 477-482.

11. Wood, C. J., "Visualization of an Incompressible Wake with Base Bleed," *Journal of Fluid Mechanics*, Vol. 29, Aug. 1967, pp. 259-272.

12. Goodyer, M. J., "Some Experimental Investigations into the Drag Effects of Modifications to the Blunt Base of a Body of Revolution," ISAV Report No. 150, University of Southampton, July 1966.

13. Compton, W. B., "Effect on Base Drag of Recessing the Bases of Conical Afterbodies at Subsonic and Transonic Speeds," NASA TN D-4821, Oct. 1968.

14. Morel, T., "Effect of Base Cavities on the Aerodynamic Drag of an Axisymmetric Cylinder," *Aeronautical Quarterly*, Vol. 30, May 1979, pp. 400-412.

15. Tanner, M., "Base Cavity at Angles of Incidence," *AIAA Journal*, Vol. 26, March 1988, pp. 376-377.

16. Little, B. H., Jr. and Cubbage, J. M., Jr., "The Development of an 8-Inch by 8-Inch Slotted Tunnel for Mach Numbers up to 1.28," NASA TN D-908, Aug. 1961.

17. El-Sherbiny, S. E. and Modi, V. J., "Blockage Effect on Vortex Shedding from Bluff Bodies," *Arabian Journal for Science and Engineering*, Vol. 8, Jan. 1983, pp. 61-66.

18. Kruiswyk, R. W., "An Experimental Investigation of the Effects of a Base Cavity on the Near-Wake Flowfield of a Body at Subsonic and Transonic Speeds," M.S. Thesis, Department of Mechanical and Industrial Engineering, University of Illinois at Urbana-Champaign, Aug. 1988.

19. Fage, A. and Johansen, F. C., "The Structure of Vortex Sheets," ARC R&M No. 1143, Aug. 1927.

20. Nash, J. F., "A Review of Research on Two-Dimensional Base Flow," ARC R&M No. 3323, March 1962.

21. Roshko, A., "On the Development of Turbulent Wakes from Vortex Streets," NACA TN 2913, March 1953.

FIGURES

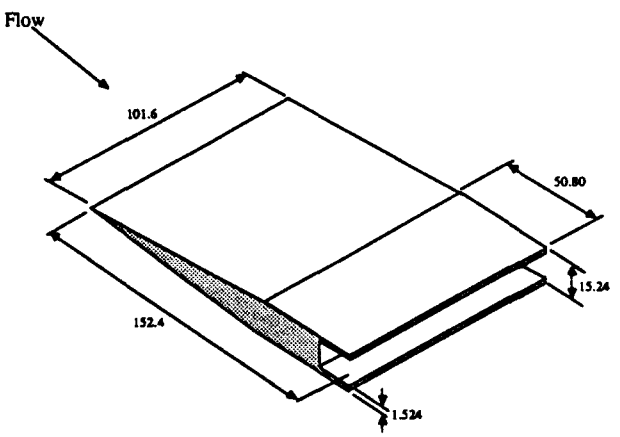

Fig. 1 Schematic of model (dimensions in mm).

(a) Blunt base

(b) Shallow cavity base, depth = 1/2 base height

(c) Deep cavity base, depth = 1 base height

Fig. 2 Model configurations under investigation: (a) blunt base; (b) shallow cavity base, depth=1/2 base height; (c) deep cavity base, depth=1 base height.

(a) M_{ref}=0.485

(b) M_{ref}=0.720

(c) M_{ref}=0.880

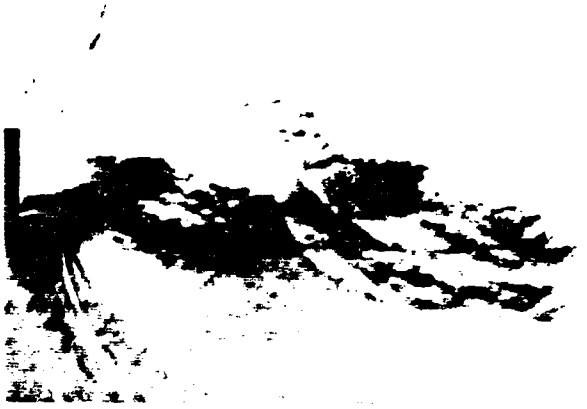

Fig. 3 Schlieren photographs of the near-wake flowfield for the blunt base configuration: (a) M_{ref}=0.485; (b) M_{ref}=0.720; (c) M_{ref}=0.880.

(a) M_{ref}=0.485

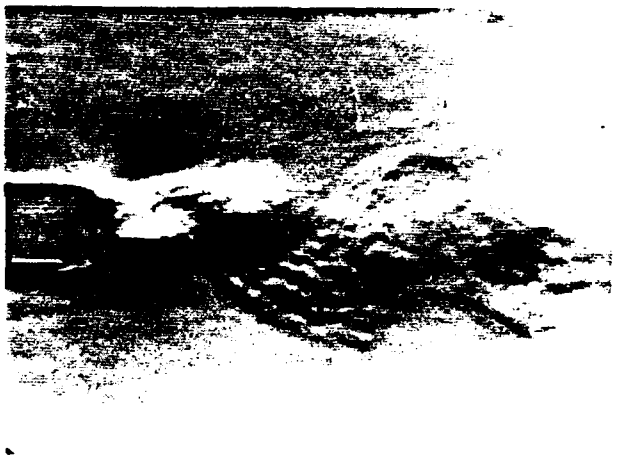

(b) M_{ref}=0.720

Fig. 4 Schlieren photographs of the near-wake flowfield for the shallow cavity base configuration: (a) M_{ref}=0.485; (b) M_{ref}=0.720.

(a) M_{ref}=0.485

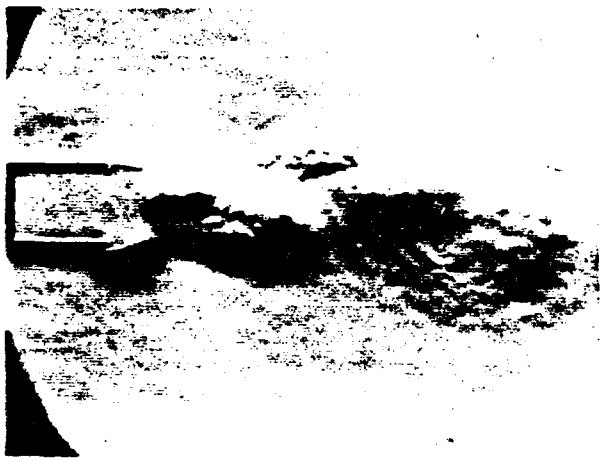

(b) M_{ref}=0.720

Fig. 5 Schlieren photographs of the near-wake flowfield for the deep cavity base configuration: (a) M_{ref}=0.485; (b) M_{ref}=0.720.

(b) Shallow cavity base

(c) Deep cavity base

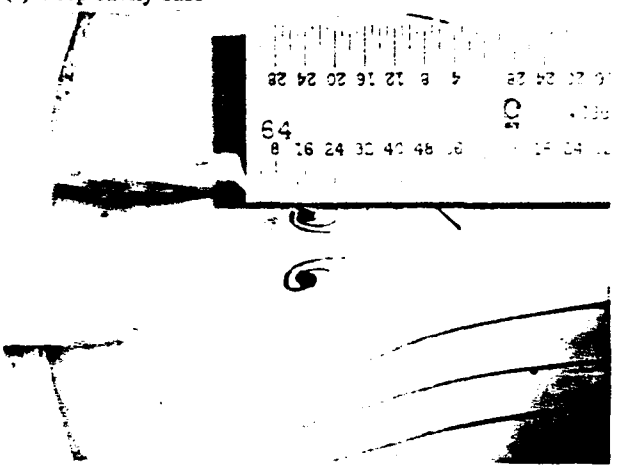

Fig. 6 Oil streak patterns on sidewall for M_{ref}=0.485: (a) blunt base configuration; (b) shallow cavity base configuration; (c) deep cavity base configuration.

(a) Blunt base

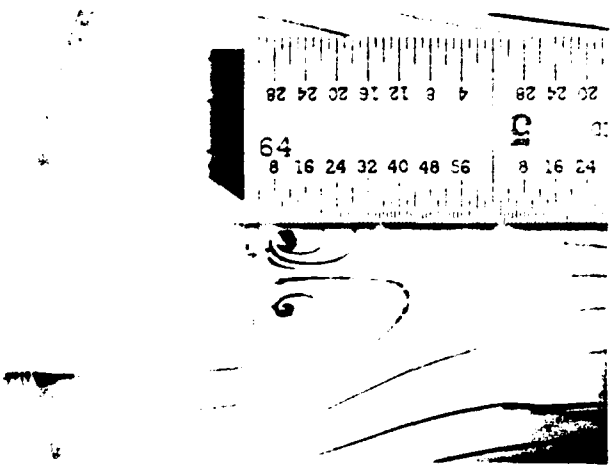

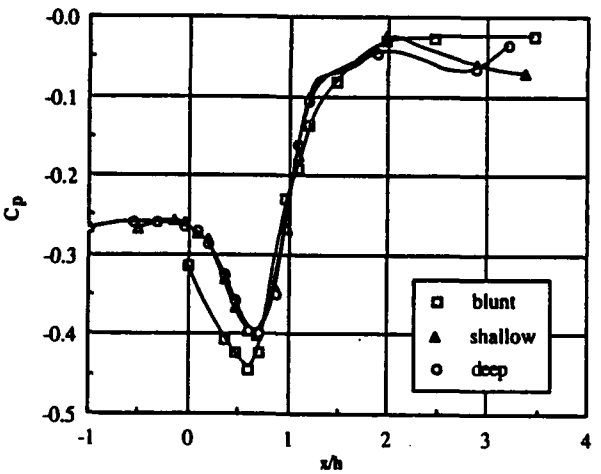

Fig. 7 Near-wake static pressure coefficient at M_{ref}=0.485.

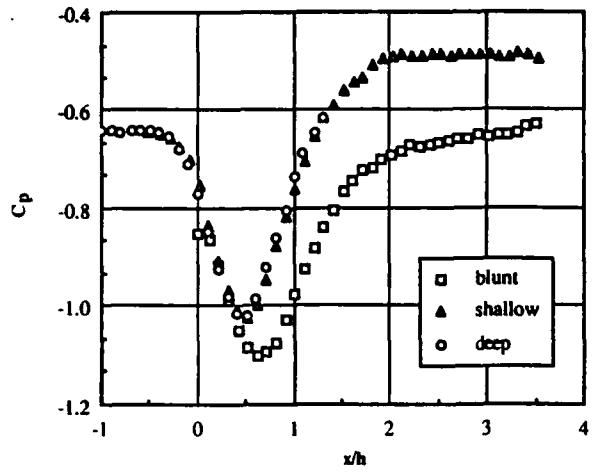

Fig. 8 Near-wake static pressure coefficient at M_{∞}=0.4 from Rudy's computations.[5]

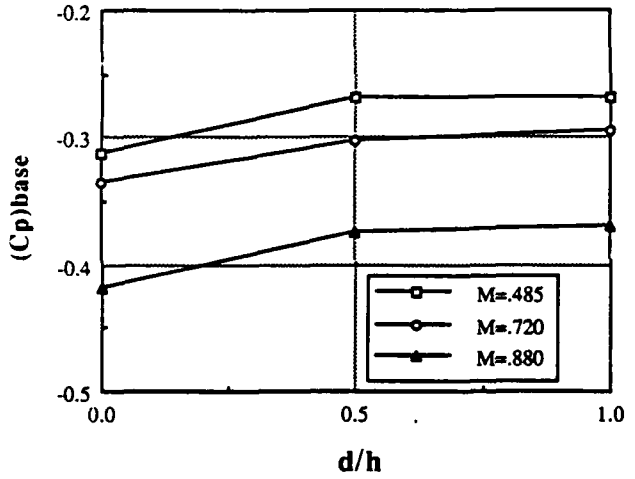

Fig. 9 Base pressure coefficient versus cavity depth and reference Mach number.

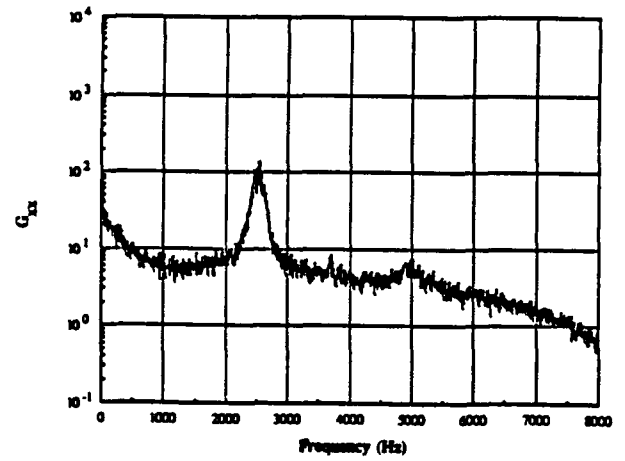

Fig. 10 Power spectral density function versus frequency for blunt base configuration, M_{ref}=0.485.

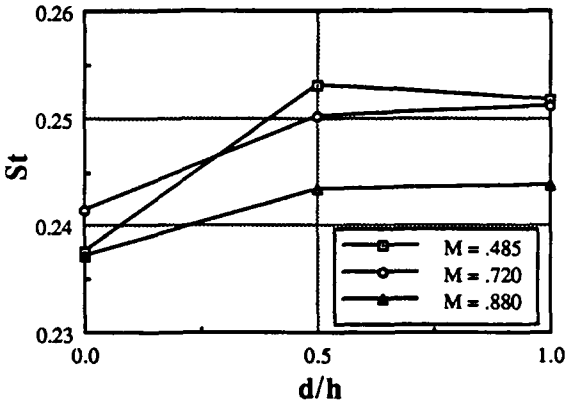

Fig. 11 Strouhal number versus cavity depth and reference Mach number.

SECTION B.10

DESIGN OF AN AXISYMMETRIC SUPERSONIC WIND TUNNEL AND EXPERIMENTAL STUDY OF SUPERSONIC, POWER-OFF BASE FLOW PHENOMENA

M.S. Thesis

Department of Mechanical and Industrial Engineering

University of Illinois at Urbana-Champaign

March 1989

by

J. M. Sauter

DESIGN OF AN AXISYMMETRIC SUPERSONIC WIND TUNNEL AND EXPERIMENTAL STUDY OF SUPERSONIC, POWER-OFF BASE FLOW PHENOMENA

Jeanne M. Sauter, M.S. Thesis
Department of Mechanical and Industrial Engineering
University of Illinois at Urbana-Champaign

ABSTRACT

A small-scale, supersonic, axisymmetric wind tunnel has been designed and constructed to realistically investigate the flow field behind a body of revolution. The annular nozzle design consists of three interchangeable diverging nozzles, a common converging nozzle, and two interchangeable central stings. Design Mach numbers of 2.0, 2.0 and 2.5 are produced for stings with diameters of 2.0, 2.5 and 2.5 inches, respectively. Cylindrical and boattailed afterbodies can be connected to the end of the sting. To eliminate disturbances in the flow, the stings are supported upstream of the nozzle and test section, and the pressure tap leads from the base of the sting are accessed through its hollow center. The tunnel operates in the blowdown mode, and for a stagnation pressure of 60 psia, the run time is 20 seconds. For power-on experiments, central nozzles which operate at Mach 1.0 to 3.8, and are fed through the center of the hollow sting, can be attached to the base of the afterbody. Pitot probe traverses demonstrated that the flow produced by the wind tunnel was very uniform. Static pressure measurements around the periphery of the nozzle indicated that the Mach number at the exit plane varied by approximately 1%.

Several investigations were made of the separated flow region behind the base of a cylindrical, 2.5 inch diameter, power-off model at M=2.0. Schlieren photographs of the near-wake region indicated that an expansion fan emanating from the exit lip of the nozzle impinged upon the separated base flow region. A series of experiments, including varying the stagnation pressure and bleeding air into the test section, was performed in an attempt to reduce the interference effects. Although the strength of the expansion fan was reduced, the wake behind the model opened up, i.e. a closed recirculation region was not formed and no recompression occurred. The precise effects of the interference and the cause of the open wake are unknown;

however, limitations of available facilities prevented further study of these phenomena. A mixture of lampblack and oil applied to the base proved to be highly sensitive to sting positioning and is, therefore, suggested as a criterion for the alignment of axisymmetric models in a supersonic stream.

SECTION B.11

AN EXPERIMENTAL INVESTIGATION OF THE SHOCK WAVE-TURBULENT BOUNDARY LAYER INTERACTION

Manuscript Submitted to the ASME Journal of Fluids Engineering

March 1989

by

D. W. Kuntz, V. A. Amatucci, and A. L. Addy

AN EXPERIMENTAL INVESTIGATION OF THE SHOCK WAVE - TURBULENT BOUNDARY LAYER INTERACTION

D. W. Kuntz

Member of Technical Staff
Aerothermodynamics Division
Sandia National Laboratories
Albuquerque, New Mexico

V. A. Amatucci

Graduate Research Assistant
Department of Mechanical and Industrial Engineering
University of Illinois at Urbana-Champaign
Urbana, Illinois

A. L. Addy

Professor and Head
Department of Mechanical and Industrial Engineering
University of Illinois at Urbana-Champaign
Urbana, Illinois

Abstract

An experimental investigation was conducted to study the interaction between a shock wave and a turbulent boundary layer. The boundary layer was formed on the floor of a wind tunnel operating with a freestream Mach number of 2.94 and a Reynolds number based on boundary layer thickness of 3.1×10^5. A compression corner model having a ramp angle of 20 degrees was used to generate the interaction flowfield. Measurement techniques used in this investigation included Schlieren photography, surface static pressure measurement, surface streak pattern measurement, and laser Doppler velocimetry (LDV). The LDV system was the primary tool and was used to make two-color, two-component coincident velocity measurements in the undisturbed upstream boundary layer and within the redeveloping boundary layer downstream of the interaction. The results of the LDV measurements indicated that both the mean and turbulent flow properties of the boundary layer were significantly altered by the interaction. The mean velocity profiles in

the redeveloping boundary layer exhibited wake-like properties, experiencing a rapid "filling out" downstream of reattachment due most likely to enhanced turbulent mixing via large scale eddies. Large increases in streamwise and vertical turbulence intensity as well as Reynolds stresses confirm the enhanced mixing and alteration of the flowfield turbulence due to the interaction with the shock wave.

Nomenclature

C_f	=	skin friction coefficient
M	=	Mach number
P	=	pressure
Re_δ	=	Reynolds number based on boundary layer thickness
u	=	mean velocity component parallel to the wind tunnel floor or ramp surface
u_τ	=	friction velocity, $(\tau_w/\rho_w)^{1/2}$
u^*	=	Van Driest generalized velocity
v	=	mean velocity component perpendicular to the wind tunnel floor or ramp surface
X	=	longitudinal coordinate parallel to wind tunnel floor
X^+	=	longitudinal coordinate parallel to the ramp surface
Y	=	vertical coordinate
Y^*	=	displaced vertical coordinate
α	=	ramp angle
δ	=	boundary layer thickness, $u_e = 0.99\ u_\infty$
δ^*	=	boundary layer displacement thickness, $\delta^* = \int_0^\delta (1 - \rho u/\rho_e u_e)\, dY$
δ_0	=	undisturbed boundary layer thickness at X = 0

θ = boundary layer momentum thickness,

$$\theta = \int_0^{\delta} [\rho u/\rho_e u_e] (1 - u/u_e)\, dY$$

ν = kinematic viscosity

Π = wake strength parameter

ρ = density

τ = shear stress

$< >$ = root-mean-square quantity

Subscripts

e = boundary layer edge condition

MAX = maximum value

w = wall location

∞ = freestream condition, upstream of the shock wave

Superscripts

$(\overline{\ })$ = ensemble average

$(\ )'$ = fluctuation from the mean value

Introduction

The interaction between a shock wave and a turbulent boundary layer occurs frequently in high speed flight. Interactions of this type are common within supersonic inlets in which a ramp or a spike is used to generate the shock wave as the first step in the diffusion process. Shock wave-turbulent boundary layer interaction flowfields are also typically found in the vicinity of a deflected control surface of an aircraft in the supersonic flight regime. A thorough understanding of the effects of the interaction on the growth and

redevelopment of the downstream boundary layer is essential if flows of this nature are to be predicted accurately. The purpose of the current investigation was to make accurate, reliable, and well-documented measurements within the redeveloping boundary layer downstream of a shock wave-turbulent boundary layer interaction, compare that data with similar measurements made in the undisturbed boundary layer ahead of the shock wave, and thus aid in understanding the fundamental nature of these highly complex flowfields.

The shock wave-turbulent boundary layer interaction in this investigation was generated by a compression corner, or ramp, mounted directly on the floor of a small-scale supersonic wind tunnel. Flowfields of this type can contain a separated region near the corner location, depending upon the ramp angle and the other flow properties. The principal features of the separated compression corner flowfield are shown in Fig. 1. The incoming boundary layer separates upstream of the corner, with the separation shock wave originating deep within the boundary layer near the separation point and extending up into the freestream. The upstream boundary layer becomes a free shear layer as a result of the separation process and subsequently reattaches on the ramp surface. The shock structure generated by the reattachment process coalesces with the separation shock to form the single oblique shock wave associated with a sudden change in flow direction in supersonic flow. Downstream of reattachment, the boundary layer redevelops into an equilibrium turbulent boundary layer.

A review of the literature published in this area of research indicates that there has been a consistent need for detailed measurements within shock wave-turbulent boundary layer interaction flowfields [1]* . A great deal of effort has been dedicated to determining mean properties within these flowfields [2-9], and some investigations have measured turbulent flowfield properties [10-16]. Unfortunately, the few investigations which have used hot-wire or laser Doppler velocimeter (LDV) systems to study these flowfields have

* Numbers in brackets refer to entries in REFERENCES.

been limited to *single*-component measurements, and thus have presented a rather limited amount of information. The numerical simulations of these flowfields have achieved some degree of success, but shortcomings exist in the available turbulence models. Advances in turbulence modeling await a better understanding of the nature of the turbulence itself. The current investigation was conducted with a *two*-component LDV system, and thus has produced new information concerning the details of the turbulence in the shock wave-turbulent boundary layer interaction.

The objective of the present investigation was to make detailed turbulence measurements within the redeveloping boundary layer downstream of a shock wave-turbulent boundary layer interaction and compare the properties of the redeveloping boundary layer with the properties of the undisturbed boundary layer. A compression corner angle of 20 degrees was used to generate a flowfield with a relatively large separated flow region. Surface static pressure measurements, Schlieren photographs, and surface flow visualization techniques were used to determine some of the mean flowfield characteristics. A two-color, two-component coincident laser Doppler velocimeter system was used to make instantaneous velocity measurements within this highly complex flowfield, from which data mean flow and turbulent flow information could be obtained.

Experimental Facilities

The wind tunnel used in this investigation was part of the wind tunnel facility located in the Mechanical Engineering Laboratory of the University of Illinois at Urbana-Champaign. Clean, dry compressed air at approximately 965 kPa was available from a storage facility connected to the wind tunnel stagnation chamber through a piping network. The pressure in the stagnation chamber was regulated by means of a pneumatically operated control valve which maintained a constant stagnation pressure with an accuracy of $\pm$ 1.5 percent during data acquisition. The test section within the wind tunnel had a square cross section 101.6 mm on a side. A solid aluminum converging-diverging nozzle produced a

Mach number of 2.94 with a maximum deviation of less than 1 percent in the test section. Additional details of the wind tunnel facility can be found in Reference 1.

A stagnation pressure level of 482.6 kPa was used during the course of this investigation and the wind tunnel was operated in the blowdown mode. This stagnation pressure level was high enough to ensure that the flow within the freestream of the wind tunnel was completely supersonic, yet was low enough to allow wind tunnel operating times of approximately 90 seconds. The flowfield stagnation temperature was close to the ambient temperature within the laboratory, thus yielding nearly adiabatic conditions within the wind tunnel boundary layers.

A schematic of the compression corner model used in this investigation is shown in Fig. 2, along with the coordinate system used in the presentation of the experimental results. The 20 degree compression corner model consisted of a ramp mounted on a ramp support, with the forward part of the ramp support forming the lower wind tunnel wall upstream of the corner. The section of the model downstream of the ramp sloped gradually back down to the floor level to reduce the disturbances within the wind tunnel test section caused by the presence of the model during the experiment. The ramp and ramp support were fabricated of aluminum and anodized flat black to reduce laser light reflections during the LDV measurements. The model support was sealed with linear o-ring material both along the side walls and upstream of the corner where the support mated with the wind tunnel floor. The corner was sealed with a gasket sealing compound. Static pressure taps were 0.57 mm in diameter and were located every 2.54 mm longitudinally on the surface of the ramp and on the model support upstream of the corner.

The compression corner model used in this investigation spanned the full 101.6 mm width of the test section. It may have proved beneficial to have used a narrower ramp model with splitter plates located along the sides to eliminate the effects of the side wall boundary layers on the interaction region, similar to those used in other investigations [6-8, 10-13, 17-19]. However, the side wall splitter plates would have denied optical access to

the interaction region, and thus would have made LDV measurements impossible. As a result, full span models were used and the extent of the side wall boundary layer interference was determined using surface flow pattern measurements.

Measurement Techniques

The primary measurement technique employed in the current investigation was laser Doppler velocimetry. The LDV system was used to make detailed flowfield measurements within the upstream and redeveloping turbulent boundary layers, and the majority of information presented here is a result of this measurement technique. To complete the investigation of this flowfield, surface static pressure measurements, surface streak pattern measurements, and Schlieren photographs were also made. The pressure measurements were used to determine the location of the beginning of the interaction, and to ensure that the ramp models were long enough to achieve a complete pressure rise. The surface streak patterns were used to check for regions of three-dimensionality within the flowfield, to determine the existence of separation, and to determine the separation and reattachment locations. The Schlieren photographs were used to qualitatively describe the flowfield, to determine a spatial grid for subsequent LDV measurements, and to look for any gross flowfield unsteadiness.

The laser Doppler velocimeter used in this investigation was a two-color, two-component coincident system utilizing optical and electronic components manufactured by Thermal Systems Incorporated (TSI). A Spectra-Physics 5-watt Argon-ion laser operating in the multi-line mode was used to provide the necessary laser light. The beam from the laser was split into its principal components using a dispersion prism, and the two most powerful beams, the green beam with wavelength of 514.5 nm and the blue beam with wavelength of 488.0 nm, were used in these experiments. Each of these beams was split into two equal intensity parallel beams, and one of each of the pairs of beams was then passed through a Bragg cell which shifted the frequency by 40 MHz. A 350 mm focal

length lens was used to redirect the four parallel beams, causing them to cross at a single point within the wind tunnel to form the measurement volume, which is roughly ellipsoidal in shape. A measurement volume diameter of 0.18 mm and a measurement volume length of approximately 6 mm were obtained with this optical arrangement. The fringe spacing was approximately 8.5 μm, and the fringe velocity (due to frequency shifting) was approximately 340 m/sec. The laser and transmitting optics were mounted on a traversing table which could be moved manually in three orthogonal directions by means of threaded rod arrangements with an accuracy of approximately ± 0.1 mm. In this manner the LDV measurement volume could be positioned at any spatial location within the wind tunnel test section.

The collection optics were located on the opposite side of the wind tunnel test section, and consisted of a 250 mm focal length lens to collect the scattered green and blue light and a dichroic mirror and filter arrangement to separate the two color signals. These optical components were oriented 10 degrees off the transmitting optical axis in order to simplify alignment procedures, improve signal-to-noise ratio, and to reduce the "effective" measurement volume length to less than 2 mm. Photomultipliers converted the scattered light signals to analog voltage signals, and TSI frequency counters were used to determine the frequencies of these signals as well as perform validation checks to reject erroneous data. The output data from the counters were stored directly in the memory of a Digital Equipment Corporation PDP 11-03 minicomputer for initial conversion of these data into velocities and then serially transferred to a Hewlett-Packard 9000 Series 500 computer for thorough analysis.

The seed particles for the LDV measurements in this investigation were generated by using a standard TSI six-jet atomizer to atomize silicon oil. The oil droplets were introduced in the stagnation chamber upstream of the wind tunnel test section. A series of experiments was conducted to determine the size of these seed particles. In these experiments, two-component velocity measurements were made downstream of an oblique

shock wave generated by an 8 degree compression corner in the Mach 2.94 flowfield. The particle response was compared to the predicted response of particles of various sizes. The results of this investigation indicated that the silicone oil droplets had an effective mean diameter of 1.5 to 2 μm. Particles of this size have been shown to have a sufficient frequency response to track large scale velocity fluctuations found downstream of shock wave-turbulent boundary layer interactions [1]. Some particle lag was measured in the regions immediately downstream of the shock wave due to the large velocity gradient generated by the shock wave. The measurements reported in this investigation were confined to regions relatively far downstream from the shock wave in a conscious effort to minimize the effects of particle lag on the data.

LDV measurements obtained at a particular spatial location involve inherent uncertainties due to the finite sample size. A statistical analysis can be used to determine the level of certainty which can be attained when using the mean of a finite size sample to represent an overall population mean. The statistical uncertainty involved in determining mean velocities from individual velocity measurements in turbulent flowfields is a function of the sample size and the local turbulence intensity. The sample size in this investigation was increased as local turbulence intensity increased, with 1024 samples collected when the local turbulence intensity was less than 15 percent, 2048 samples collected when the local turbulence intensity was between 15 and 25 percent, 3072 samples collected when the local turbulence intensity was between 25 and 30 percent, and 4096 samples collected when the local turbulence intensity exceeded 30 percent. Using a statistical analysis which assumes a normal velocity distribution, the uncertainty in mean velocity was found to be less than 2 percent for all velocity profiles. The statistical uncertainty in turbulence intensity can be shown to be a function of sample size only, and was found to be less than 3.6 percent for the measurements of the redeveloping boundary layer downstream of the 20 degree compression corner.

Mean and turbulent flow properties computed from LDV data have been shown in the literature to be affected by certain biasing errors [20,21], most notably velocity biasing [22-24] and fringe biasing [25,26]. Velocity biasing results from the fact that in a turbulent flow with uniformly distributed seed particles, a larger volume of fluid passes through the measurement volume during periods when the velocity is higher than the mean, than when the velocity is lower than the mean. Thus, a simple arithmetic average of the individual velocity measurements is biased towards higher velocities. Fringe biasing arises from the requirement that a particle must cross a pre-selected number of fringes within the measurement volume for its velocity to be measured. Thus, particles traveling in a direction parallel to the fringe plane are not "seen" by the LDV and this results in a bias in favor of particles traveling perpendicular to the fringe plane. The effects of velocity biasing were essentially eliminated from the results of this investigation by weighting the velocity measurements with the two-dimensional velocity bias correction factor, $1/(u^2 + v^2)^{1/2}$ [1]. The effects of fringe biasing were significantly reduced by frequency shifting such that the fringes moved in a direction opposite to that of the mean flow, and also by orienting the set of fringe planes at $\pm$ 45 degrees relative to the wind tunnel floor for the upstream boundary layer surveys, and at $\pm$ 45 degrees relative to the ramp surface for the downstream boundary layer surveys. A comparison between the two-dimensional velocity bias corrected mean velocities and mean velocities corrected with both the two-dimensional velocity bias correction and a fringe bias correction based on the study of Buchhave [25,26] yielded differences of 1.7 percent or less. Thus, in this investigation the effects of fringe bias were not significant in comparison to the effects of velocity bias, and the results presented here were corrected with the velocity bias correction only.

The particle lag, statistical uncertainty, and biasing effects described above constitute the major sources of errors in this investigation. Other less significant sources of errors include optical alignment accuracy, inaccuracies due to counter clock resolution, and inaccuracies in the frequency shifting components. Alignment accuracy with the LDV is

believed to be quite good due to the ability to project the beams over large distances and thus make accurate measurements of small angles. The largest source of alignment error is in the orientation of the two fringe planes (green and blue) perpendicular to each other. In this investigation the fringes were aligned within 1 degree of perpendicularity, and thus the error in velocity as a result of alignment errors is of the order of 1 percent. The counter clock resolution errors result from the 1 nanosecond resolution of the clock which measures the time required for a particle to pass through the required eight fringes. The amount of this error is a direct function of velocity, and decreases from 1.2 percent at a streamwise velocity measurement of 630 m/sec to 0.6 percent at a streamwise velocity of 100 m/sec. Thus, this source of error is most significant in the high velocity regions of the flowfield, in which the turbulence intensity is low and the other sources of error such as statistical uncertainty and biasing effects are at a minimum. Errors caused by the frequency shifting components include slight changes in beam angles caused by the necessary optics, and small inaccuracies in the 40 MHz shifting frequency. A comparison between measurements made with and without frequency shifting in flowfields which were similar, but not necessarily identical, indicates that these errors are of the order of 1.5 percent, although one point indicated a difference of 2.3 percent.

Experimental Results

Undisturbed Boundary Layer

Detailed boundary layer surveys were made using the LDV system in the turbulent boundary layer which formed on the floor of the wind tunnel test section in the absence of the compression corner model. These surveys were made on the wind tunnel centerline at four streamwise stations within the test section. Two-component velocity measurements were made within the boundary layer to a point 1.5 mm ($Y/\delta_0 = 0.18$) above the wind tunnel floor at which point blockage of the two lower laser beams began to occur. The boundary layer surveys were completed with single-component LDV measurements down

to a point 0.25 mm (Y/δ_0 = 0.03) above the surface. In these measurements of the undisturbed boundary layer, frequency shifting proved unnecessary due to the relatively low turbulence intensities and lack of any reverse flows.

The boundary layer thickness at X = 0 in the center of the test section was determined to be 8.27 mm ($u_e = 0.99\ u_\infty$). The displacement and momentum thicknesses were determined by numerical integration of the velocity profiles, accounting for compressibility effects, and had values of $\delta^* = 3.11$ mm and $\theta = 0.57$ mm, respectively. The Reynolds number within the test section based on the boundary layer thickness, Re_δ, was 3.1×10^5. The freestream velocity measured at X = 0 using the LDV system was within 0.2 percent of the velocity predicted from the measured pressure distribution.

Further insight into the details of the undisturbed boundary layer can be obtained using the transformed wall-wake law of Maise and McDonald [27]. A curve fit of the data of the current investigation to the wall-wake law can be used to obtain estimates of the wake strength parameter, Π, and the skin friction coefficient, C_f. The profile of the undisturbed boundary layer in wall-wake coordinates is shown in Fig. 3 for both the measured LDV data and the least-squares curve fit. The quantity u^* is the Van Driest generalized velocity [27] and the quantity u_τ is the friction velocity, defined as $(\tau_w/\rho_w)^{1/2}$. From this curve fit, the wake strength parameter, Π , was determined to be equal to 0.977 and the skin friction coefficient, C_f, was found to be 0.00114. Although the wake strength parameter value of 0.977 is somewhat higher than the values reported in some of the literature, Samimy [28-31] and Sturek and Danberg [32,33] report comparable results. The value for the skin friction coefficient agrees very well with the data of Settles [5] and Sturek and Danberg [32,33].

The streamwise component turbulence intensity measured with the LDV system for the undisturbed boundary layer is shown in Fig. 4. The data measured at four stations within the test section fall within a very narrow band and compare well with other experimental data. The measured turbulence intensities at the edge of the boundary layer

and the freestream are probably higher than the actual levels which exist within the flowfield due to the limitations of the 1 nanosecond counter clock resolution factor previously discussed. The turbulence intensities of this investigation are somewhat higher than the hot-wire data of Kistler [34] and Rose [35]. This difference can be attributed to the counter clock resolution in the outer regions of the boundary layer, and possibly to difficulties in hot-wire calibration and interpretation in the lower velocity regions of the inner boundary layer. The turbulence intensities of the current investigation compare well with the LDV data of Petrie [36-38], Samimy [28-30], and Johnson [39], as seen in Fig. 4.

The turbulent shear stress distribution determined from the "D" measurements within the undisturbed boundary layer at X = 0 is shown in Fig. 5, along with the data of Samimy [28-30], Petrie [36-38], and Johnson [39]. The air density at each measurement location was calculated assuming adiabatic conditions within the boundary layer. Although there is a good deal of scatter in the data, the data of the current investigation agree reasonably well with those of the other three investigations. There is a tendency for the shear stress of the current investigation to reach a peak within the boundary layer and then decrease as the wall is approached. Similar shear stress behavior can be seen in data reported in other boundary layer studies using both LDV systems [40-42] and slanted hot-wire systems [12,13]. Yanta and Lee [40] and Johnson and Rose [41] have suggested that this is the result of other turbulent shear stress terms, such as $\overline{\rho' u' v'}$, becoming significant in the lower regions of the boundary layer. However, Dimotakis, Collins, and Lang [42] suggest that this is the result of particle dynamics near solid walls which influence LDV measurements. This latter theory does not explain the decrease in shear stress near the wall that has been measured by hot-wire probes, and further study of this phenomenon is necessary.

20 Degree Compression Corner Flowfield

The Schlieren system was used to view the 20 degree compression corner flowfield during the initial phases of this investigation. The freestream flow was observed to be

completely supersonic and some unsteadiness was observed in the separation shock structure similar to that reported in the literature for a number of compression corner studies using 16, 20, and 24 degree ramps [17-19, 43]. Surface streak patterns were used to determine the separation and reattachment locations, and to determine the extent of the influence of the side wall boundary layers on the flowfield. Separation was found to take place a distance of 1.63 δ_0 upstream of the corner. The separation line was relatively straight and spanned the center 50 mm of the wind tunnel. Reattachment occurred a distance of 0.52 δ_0 downstream of the corner on the ramp face, with the reattachment line spanning the center 70 mm of the wind tunnel. Some three-dimensional effects were seen in the streak lines within the separated region near the wind tunnel side walls, but these effects did not disturb the centerline flow downstream of reattachment.

The mean surface static pressure distribution is shown in Fig. 6. The solid line to the right of the experimental data (at approximately $P/P_\infty = 3.7$) represents the theoretical downstream pressure determined from oblique shock wave theory. The data in this figure illustrate that the pressure rise began well upstream of the corner, more than 15 mm before $X = 0$, due to the presence of the separated region. The pressure distribution exhibits the "kink," or triple inflection point characteristic which is typical of separated compression corner flowfields [8]. The static pressure on the ramp face rose gradually and reached a plateau level within 5.5 percent of the theoretical value.

The mean streamwise velocity profiles upstream and downstream of the shock wave-turbulent boundary layer interaction are shown in Fig. 7. The profiles downsteam of the interaction exhibit wake-like properties, similar to those observed by other investigators downstream of separated compression corners [8], and downstream of reattaching free shear layers [28-31]. These wake-like profiles resulted from the shear layer velocity profile which formed the initial condition for the redeveloping boundary layer. The shear layer formed from the upstream boundary layer separation process and developed its wake-like characteristics from interaction with the separated region in the compression corner. The

velocity profiles downstream of reattachment experienced a rapid "filling out," which can also be seen in Fig. 7. This rapid change in the boundary layer profiles was most likely caused by enhanced turbulent mixing due to the formation of large scale eddies, and further adds to the wake-like appearance of the boundary layer profiles. The decrease in the measured streamwise velocity with X, which can be seen in the outer regions of the boundary layers downstream of the corner, was caused by a combination of two effects. The surface static pressure distribution, shown in Fig. 6, indicates that the pressure was still rising at the streamwise locations where the velocity profiles shown in Fig. 7 were measured. Thus, the flow in this region was still turning and decelerating in the final stages of the compression process. Also, it is possible that the effects of particle lag may have contributed slightly to the decrease of u with X, and the specific extent to which particle lag is affecting the results is uncertain.

The mean vertical velocity profiles for the compression corner flowfield are presented in Fig. 8. The decrease in negative vertical velocities with distance downstream in the outer regions of the boundary layers is further indication that the change in flow direction during the recompression process takes place gradually. The small positive vertical velocities seen in the lower regions of the last two stations in Fig. 8 accompany the rapid "filling out" of the streamwise profiles seen in Fig. 7, and are a result of the severe changes which are taking place within the boundary layer as the wake-like characteristics diminish.

The streamwise turbulence intensity data, <u'>, nondimensionalized with the freestream velocity upstream of the shock wave, u_{∞}, are shown in Fig. 9. The turbulence intensity in the upstream boundary layer is also included for comparison, and once again the data in this figure illustrate that the level of turbulence was significantly increased by the interaction between the shock wave and the boundary layer. The turbulence intensity profiles reach a maximum value within the central regions of the boundary layer, and decrease as both the freestream and the wall are approached. The turbulence can be seen

spreading vertically with the profiles becoming flatter in the downstream stations. A gradual decrease in the peak turbulence intensity accompanies this diffusion process, from a $(\langle u' \rangle / u_\infty)_{MAX}$ value of approximately 0.19 for the X = 15 mm traverse to a value of approximately 0.155 for the traverse at X = 40 mm. This once again indicates the gradual process that the boundary layer experiences as it recovers from the effects of the interaction with the shock wave. The relatively severe changes in turbulence intensity level due to the passage of the boundary layer through the shock wave can be observed in Fig. 9 by comparing the profile at X = 40 mm with the profile of the upstream boundary layer.

The vertical turbulence intensity data, $\langle v' \rangle$, nondimensionalized by u_∞, are presented in Fig. 10. The vertical turbulence intensity, like the streamwise turbulence intensity, was significantly amplified by the interaction with the shock wave. However, unlike the streamwise turbulence intensity, the vertical turbulence intensity shows very little dependence on distance above the ramp surface, Y^*, and is nearly constant throughout the redeveloping boundary layer and within the freestream downstream of the shock wave. There is a slight tendency for $\langle v' \rangle / u_\infty$ to reach a maximum near the edge of the boundary layer, but this characteristic is not found in all the profiles. It can also be seen in Fig. 10 that the vertical turbulence intensity was significantly increased in the regions outside the boundary layer. These data, in conjunction with other turbulence statistics obtained in this investigation, such as turbulence triple products and skewness and flatness factors, indicated that there was a significant alteration of the freestream turbulence structure caused by the presence of the oblique shock wave. While it is mildly possible that this effect is caused by particle lag, this is considered very unlikely because the effects of particle lag diminish rapidly as the distance from the shock wave to the measuring point increases, while the large freestream values of $\langle v' \rangle / u_\infty$ persist to the most downstream measurement stations with very little sign of dissipation.

The kinematic Reynolds stress data, $-\overline{(u'v')}$, nondimensionalized with the square of the undisturbed freestream velocity, u_∞^2, are presented in Fig. 11. The data show that

the Reynolds stress, like the streamwise turbulence intensity, was significantly increased by the interaction with the shock wave. The large magnitude of the Reynolds stress is further indication of the existence of large scale turbulent structures within the redeveloping boundary layer. The Reynolds stress profiles reach maximum values in the central regions of the boundary layers, with the maximum value in each profile decreasing as the flow proceeds downstream. The Reynolds stress, like the streamwise turbulence intensity, diffuses outward through the boundary layer as the effects of the interaction begin to diminish.

The trends in the Reynolds stresses of this investigation agree quite well with those found by Muck and Smits [13] in their investigation of a 20 degree compression corner flowfield with similar initial flow conditions. The tendency for the Reynolds stress to reach a maximum in the central regions of the boundary layer, the gradual decay in Reynolds stress with X downstream of the interaction, and the vertical diffusion of the Reynolds stress in the boundary layer can all be seen in their hot wire results. However, the magnitudes of the quantity $-\overline{(u'v')}/u_\infty^2$ reported by Muck and Smits [13] are significantly lower than the results of the current investigation, with the maximum values differing by factors greater than 2. This large discrepancy is most likely caused by calibration problems associated with the slanted hot wire technique used by these authors. Muck and Smits [13] state that the hot wire calibration is only valid in regions in which the Mach number component normal to the wire exceeds 1.2. Taking into account the 30 degree yaw angle of the slanted hot wires, this yields a lower Mach number limit of 1.39. The local Mach numbers at the regions of maximum Reynolds stress in the current investigation were all below 1.39. In addition to these low mean Mach numbers, the high turbulence intensities in these regions indicate that the local Mach number frequently drops far below the calibration limits, and these occurrences of low Mach number contribute significantly to the magnitude of $-\overline{(u'v')}$. Considering these factors, it is not surprising that a discrepancy exists between Reynolds stresses measured with slanted hot wires, and those

measured with two-component LDV systems in highly turbulent flowfields. An investigation in which *both* techniques are used to make measurements in the *same* flowfield would be extremely useful in understanding and resolving these discrepancies.

Conclusions

The interaction between the shock wave and the turbulent boundary layer in this 20 degree compression corner flowfield, with the resultant separated region, caused significant changes in both the mean and the turbulent properties of the boundary layer. The LDV system yielded accurate and reliable velocity data in the undisturbed upstream boundary layer and the ramp boundary layer profiles downstream of the shock wave which compared well with data of other researchers. The mean velocity profiles downstream of the interaction appear very wake-like as a result of the separation and reattachment processes, and experience a very rapid "filling out" as the flow proceeds downstream. The streamwise turbulence intensity profiles reach maximum values within the central regions of the boundary layer and show the large amplification in freestream turbulence structure due to the interaction with the shock wave. The large magnitudes of the Reynolds stress data further indicate the existence of large scale turbulent structures within the redeveloping boundary layer. Some serious differences in magnitude of the Reynolds stress values between these LDV measurements and other researchers' hot wire measurements seem associated with hot wire calibration problems in highly turbulent supersonic flow, and further study is necessary.

Acknowledgements

Support for this research was provided by the U.S. Army Research Office through contract monitor Dr. Robert E. Singleton under Research Grant DAAG 29-79-C-0184 and Research Grant DAAG 29-83-K-0043; and the Department of Mechanical and Industrial Engineering at the University of Illinois at Urbana-Champaign.

References

1. Kuntz, D. W., "An Experimental Investigation of the Shock Wave-Turbulent Boundary Layer Interaction," Ph.D. Thesis, Department of Mechanical and Industrial Engineering, University of Illinois at Urbana-Champaign, Urbana, Illinois, 1985.
2. Chapman, D. R., Kuehn, D. M., and Larson, H. K., "Investigation of Separated Flows in Supersonic and Subsonic Streams with Emphasis on the Effect of Transition," NACA TN-3869, March 1957.
3. Spaid, F. W. and Frishett, J. C., "Incipient Separation of a Supersonic, Turbulent Boundary Layer, Including Effects of Heat Transfer," *AIAA Journal*, Vol. 10, No. 7, July 1972, pp. 915-922.
4. Elfstrom, G. M., "Turbulent Hypersonic Flow at a Wedge-Compression Corner," *Journal of Fluid Mechanics*, Vol. 53, Part 1, 1972, pp. 113-127.
5. Settles, G. S., "An Experimental Study of Compressible Turbulent Boundary Layer Separation at High Reynolds Numbers," Ph.D. Thesis, Princeton University, Princeton, New Jersey, 1975.
6. Settles, G. S., Bogdonoff, S. M., and Vas, I. E., "Incipient Separation of a Supersonic Turbulent Boundary Layer at High Reynolds Numbers," *AIAA Journal*, Vol. 14, No. 1, January 1976, pp. 50-56.
7. Settles, G. S., Vas, I. E., and Bogdonoff, S. M., "Details of a Shock-Separated Turbulent Boundary Layer at a Compression Corner," *AIAA Journal*, Vol. 14, No. 12, December 1976, pp. 1709-1715.
8. Settles, G. S., Fitzpatrick, T. J., and Bogdonoff, S. M., "Detailed Study of Attached and Separated Compression Corner Flowfields in High Reynolds Number Supersonic Flow," *AIAA Journal*, Vol. 17, No. 6, June 1979, pp. 579-585.

9. Law, C. H., "Supersonic Shock Wave Turbulent Boundary-Layer Interactions," *AIAA Journal*, Vol. 14, No. 6, June 1976, pp. 730-734.

10. Hayakawa, K., Smits, A. J., and Bogdonoff, S. M., "Hot-wire Investigation of an Unseparated Shock-Wave/Turbulent Boundary Layer Interaction," AIAA Paper 82-0985, June 1982.

11. Jayaram, M. and Smits, A. J., "The Distortion of a Supersonic Turbulent Boundary Layer by Bulk Compression and Surface Curvature," AIAA Paper 85-0299, January 1985.

12. Muck, K. C. and Smits, A. J., "The Behavior of a Compressible Turbulent Boundary Layer Under Incipient Separation Conditions," 4th Symposium on Turbulent Shear Flows, Karlsruhe, West Germany, September 1983.

13. Muck, K. C. and Smits, A. J., "Behavior of a Turbulent Boundary Layer Subjected to a Shock-Induced Separation," AIAA Paper 84-0097, January 1984.

14. Rose, W. C. and Johnson, D. A., "Turbulence in a Shock-Wave Boundary-Layer Interaction," *AIAA Journal*, Vol. 13, No. 7, July 1975, pp. 884-889.

15. Modarress, D. and Johnson, D. A., "Investigation of Turbulent Boundary-Layer Separation Using Laser Velocimetry," *AIAA Journal*, Vol. 17, No. 7, July 1979, pp. 747-752.

16. Ardonceau, P. L., "The Structure of Turbulence in a Supersonic Shock-Wave/ Boundary-Layer Interaction," *AIAA Journal*, Vol. 22, No. 9, September 1984, pp. 1254-1262.

17. Dolling, D. S. and Murphy, M., "Wall Pressure Fluctuations in a Supersonic Separated Compression Ramp Flowfield," AIAA Paper 82-0986, June 1982.

18. Muck, K. C., Dussauge, J.-P., and Bogdonoff, S. M., "Structure of the Wall Pressure Fluctuations in a Shock-Induced Separated Turbulent Flow," AIAA Paper 85-0179, January 1985.

19. Andreopoulos, J. and Muck, K. C., "Some New Aspects of the Shock Wave Boundary Layer Interaction in Compression Ramp Flows," AIAA Paper 86-0342, January 1986.

20. Edwards, R. V., "Report of the Special Panel on Statistical Particle Bias Problems in Laser Anemometry," *Transactions of the ASME: Journal of Fluids Engineering*, Vol. 109, No. 2, June 1987, pp. 89-93.

21. Petrie, H. L., Samimy, M., and Addy, A. L., "An Evaluation of LDV Velocity and Fringe Bias Effects in Separated High Speed Turbulent Flows," Proceedings of the International Congress on Instrumentation in Aerospace Simulation Facilities (ICIASF '85), August 26-28, 1985, pp. 297-308. [Also IEEE Publication 85CH2210-3].

22. McLaughlin, D. K. and Tiederman, W. G., "Biasing Correction for Individual Realization of Laser Anemometer Measurements in Turbulent Flows," *The Physics of Fluids*, Vol. 16, No. 12, 1973, pp. 2082-2088.

23. Stevenson, W. H., Thompson, H. D., and Roesler, T. C., "Direct Measurements of Laser Velocimeter Bias Errors in a Turbulent Flow," *AIAA Journal*, Vol. 20, No. 12, December 1982, pp. 1720-1723.

24. Petrie, H. L., Samimy, M., and Addy, A. L., "Laser Doppler Velocity Bias in Separated Turbulent Flows," *Experiments in Fluids*, Vol. 6, No. 2, 1988, pp. 80-88.

25. Buchhave, P., "Biasing Errors in Individual Particle Measurements with the LDA-Counter Signal Processor," Proceedings of the LDA-Symposium, Copenhagen, Denmark, 1975.

26. Buchhave, P., George, W. K., and Lumley, J. L., "The Measurement of Turbulence with the Laser-Doppler Anemometer," *Annual Review of Fluid Mechanics*, Vol. 11, pp. 443-503, 1979.

27. Maise, G. and McDonald, H., "Mixing Length and Kinematic Eddy Viscosity

in a Compressible Boundary Layer," *AIAA Journal*, Vol. 6, No. 1, January 1968, pp. 73-80.

28. Samimy, M., "An Experimental Study of Compressible Turbulent Reattaching Free Shear Layers," Ph.D. Thesis, Department of Mechanical and Industrial Engineering, University of Illinois at Urbana-Champaign, Urbana, Illinois, 1984.
29. Samimy, M., Petrie, H. L., and Addy, A. L., "A Study of Compressible Turbulent Reattaching Free Shear Layers," *AIAA Journal*, Vol. 24, No. 2, February 1986, pp. 261-267.
30. Samimy, M., Petrie, H. L., and Addy, A. L., "Reattachment and Redevelopment of Compressible Turbulent Free Shear Layers," ASME International Symposium on Laser Anemometry, November 17-21, 1985, FED-Vol. 33, pp. 159-166.
31. Samimy, M. and Addy, A. L., "Interaction Between Two Compressible, Turbulent Free Shear Layers," *AIAA Journal*, Vol. 24, No. 12, December 1986, pp. 1918-1923.
32. Sturek, W. B. and Danberg, J. E., "Supersonic Turbulent Boundary Layer in Adverse Pressure Gradient. Part I: The Experiment," *AIAA Journal*, Vol. 10, No. 4, April 1972, pp. 475-480.
33. Sturek, W. B. and Danberg, J. E., "Supersonic Turbulent Boundary Layer in Adverse Pressure Gradient. Part II: Data Analysis," *AIAA Journal*, Vol. 10, No. 5, May 1972, pp. 630-635.
34. Kistler, A. L., "Fluctuation Measurements in a Supersonic Turbulent Boundary Layer," *The Physics of Fluids*, Vol. 2, No. 3, May-June 1959, pp. 290-296.
35. Rose, W. C., "Turbulence Measurements in a Compressible Boundary Layer," *AIAA Journal*, Vol. 12, No. 8, August 1974, pp. 1060-1064.

36. Petrie, H. L., "A Study of Compressible Turbulent Free Shear Layers Using Laser Doppler Velocimetry," Ph.D. Thesis, Department of Mechanical and Industrial Engineering, University of Illinois at Urbana-Champaign, Urbana, Illinois, 1984.

37. Petrie, H. L., Samimy, M., and Addy, A. L., "A Study of Compressible Turbulent Free Shear Layers Using Laser Doppler Velocimetry," AIAA Paper 85-0177, January 1985.

38. Petrie, H. L., Samimy, M., and Addy, A. L., "Compressible Separated Flows," *AIAA Journal*, Vol. 24, No. 12, December 1986, pp. 1971-1978.

39. Johnson, D. A., "Turbulence Measurements in a Mach 2.9 Boundary Layer Using Laser Velocimetry," *AIAA Journal*, Vol. 12, No. 5, May 1974, pp. 711-714.

40. Yanta, W. J. and Lee, R. E., "Measurements of Mach 3 Turbulent Transport Properties on a Nozzle Wall," *AIAA Journal*, Vol. 14, No. 6, June 1976, pp. 725-729.

41. Johnson, D. A. and Rose, W. C., "Turbulence Measurements in Supersonic Boundary Layer Flows Using Laser Velocimetry," Proceedings of the Second International Workshop on Laser Velocimetry, Vol. 2, Purdue University, West Lafayette, Indiana, March 1974.

42. Dimotakis, P. E., Collins, D. J., and Lang, D. B., "Laser Doppler Velocity Measurements in Subsonic, Transonic, and Supersonic Turbulent Boundary Layers," Laser Velocimetry and Particle Sizing, edited by H. D. Thompson and W. H. Stevenson, Hemisphere Publishing, New York, 1979, pp.208-219.

43. Tran, T. T. and Bogdonoff, S. M., "A Study of Unsteadiness of Shock Wave/ Turbulent Boundary Layer Interactions from Fluctuating Wall Pressure Measurements," AIAA Paper 87-0552, January 1987.

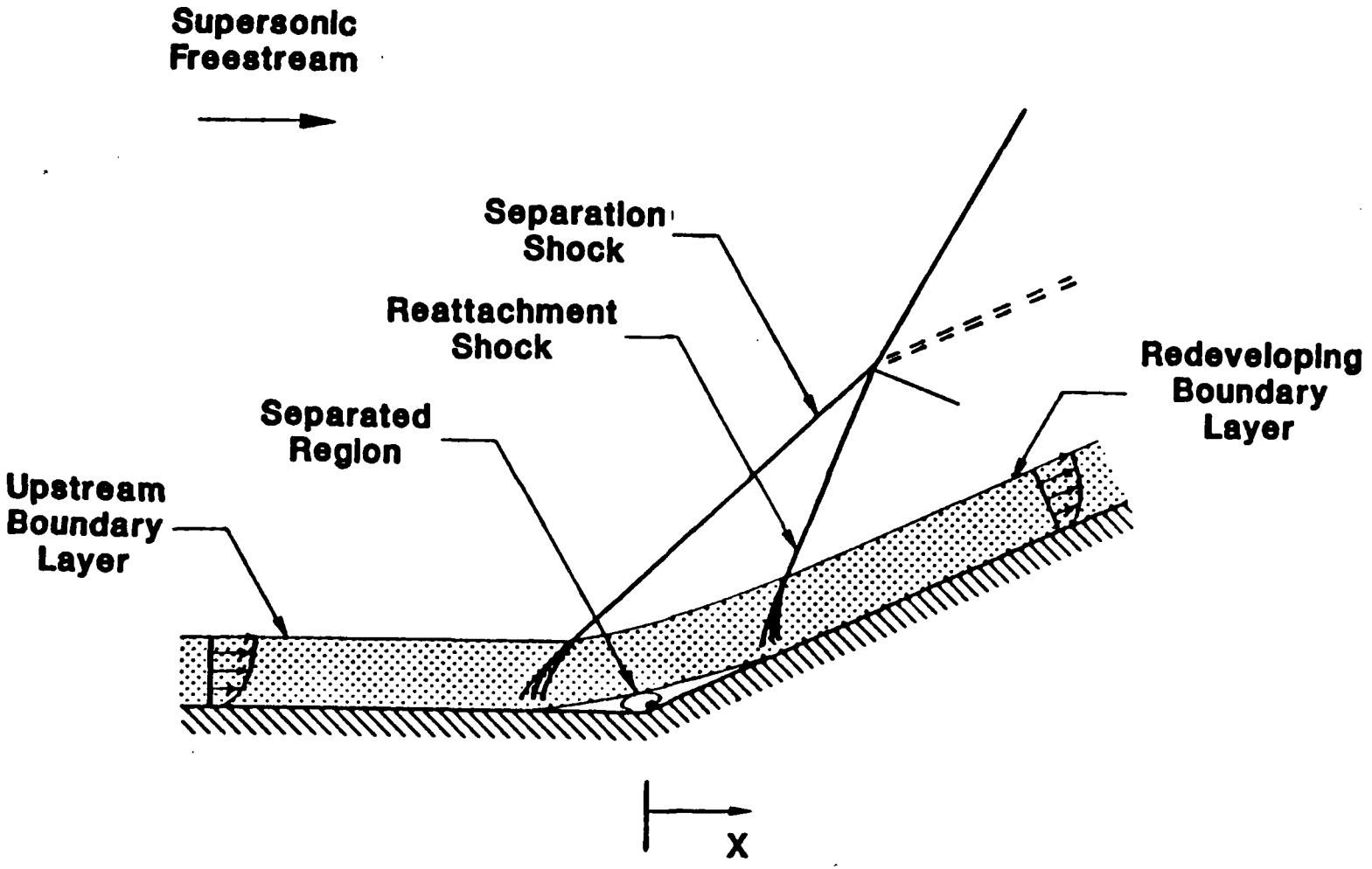

Figure 1 Separated compression corner flowfield

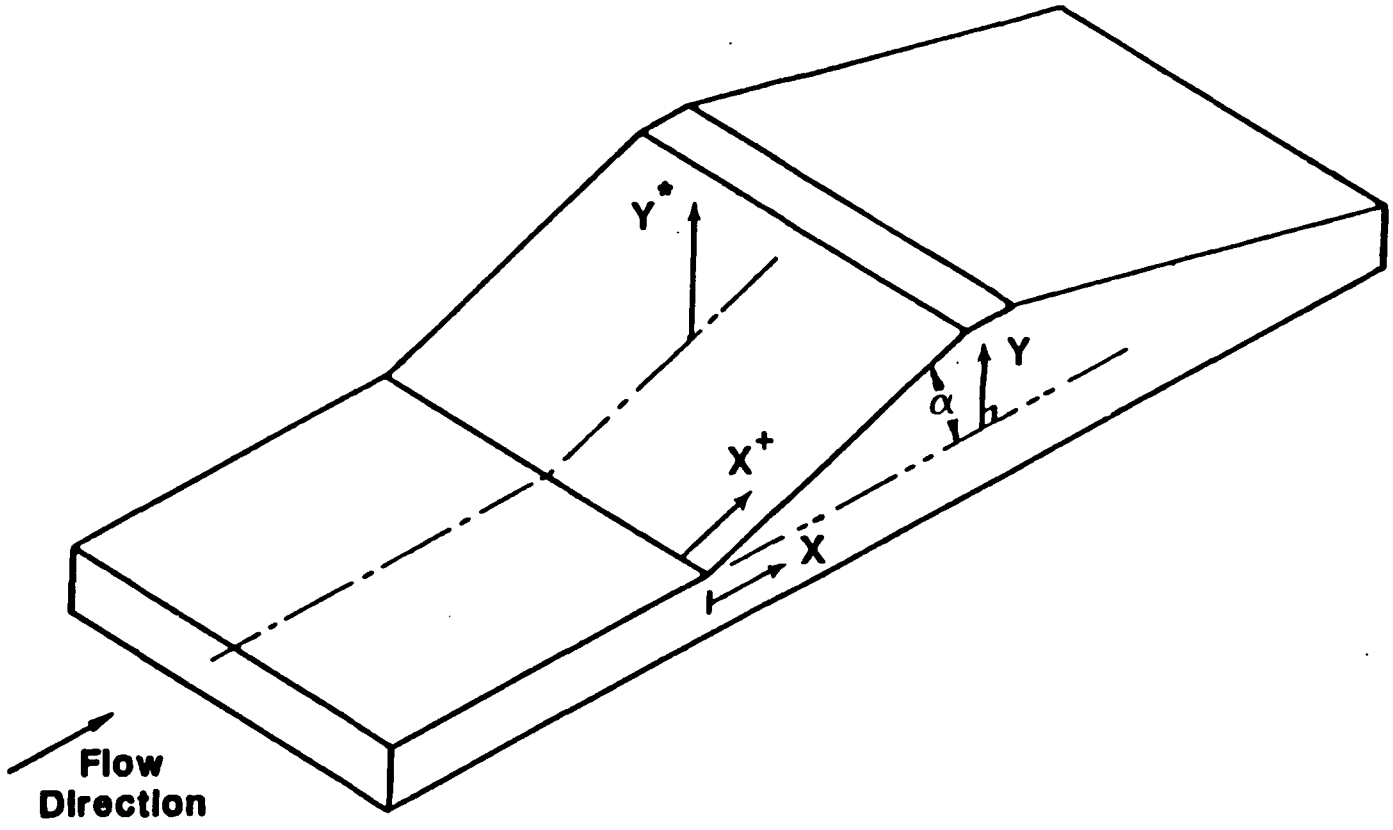

Figure 2 Compression corner model and coordinate system

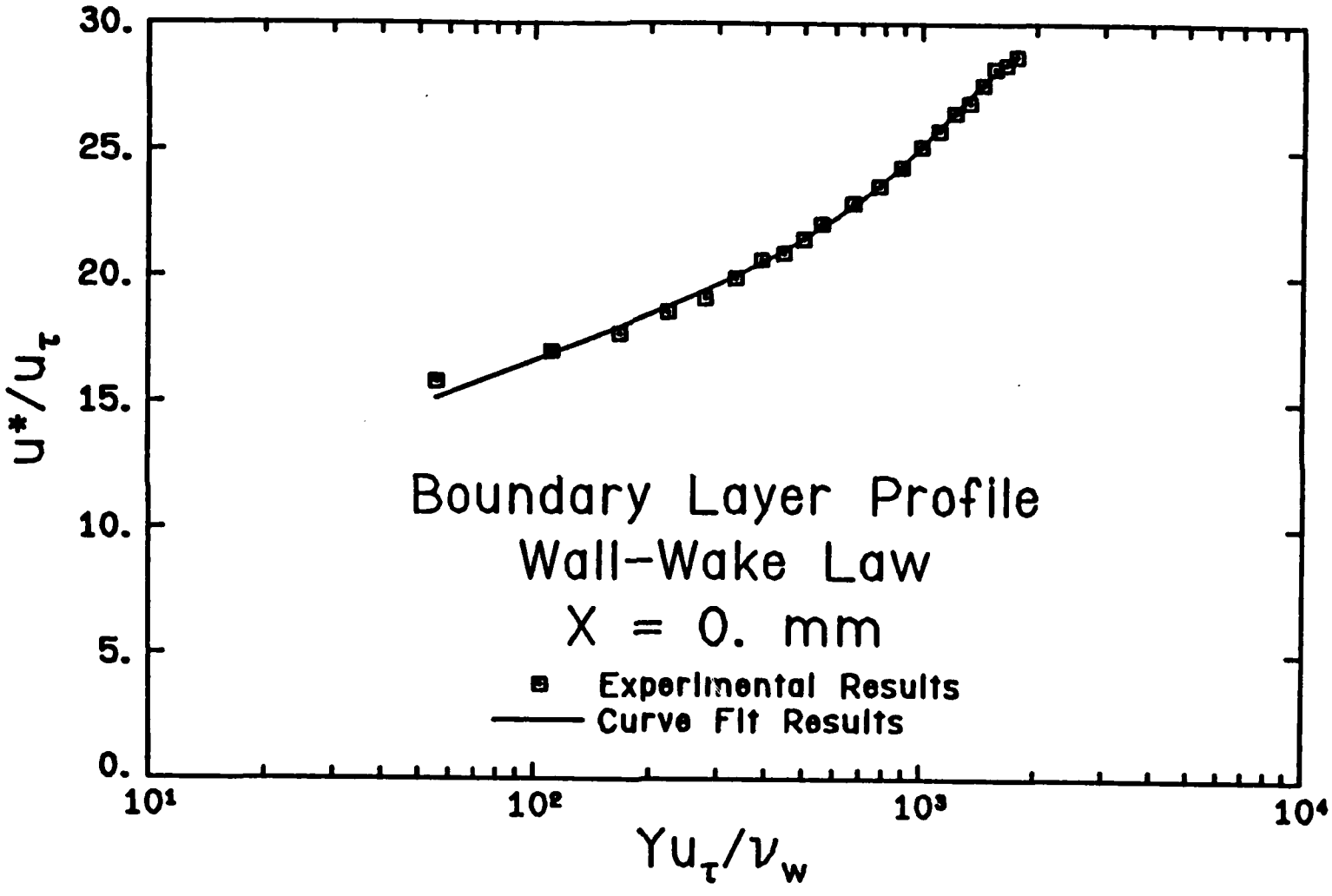

Figure 3 Undisturbed boundary layer profile in wall-wake coordinates

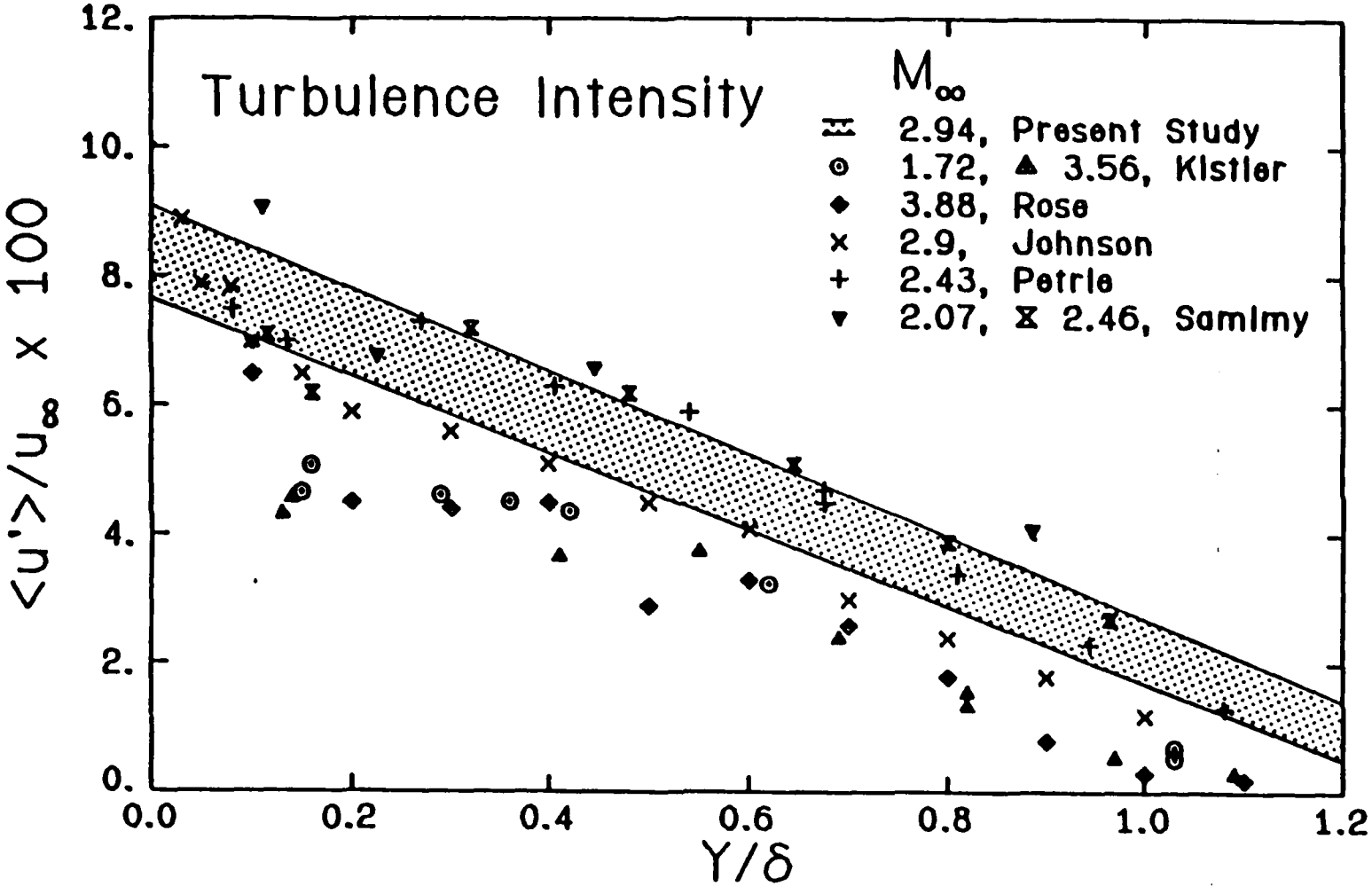

Figure 4 Undisturbed boundary layer streamwise turbulence intensity measurements

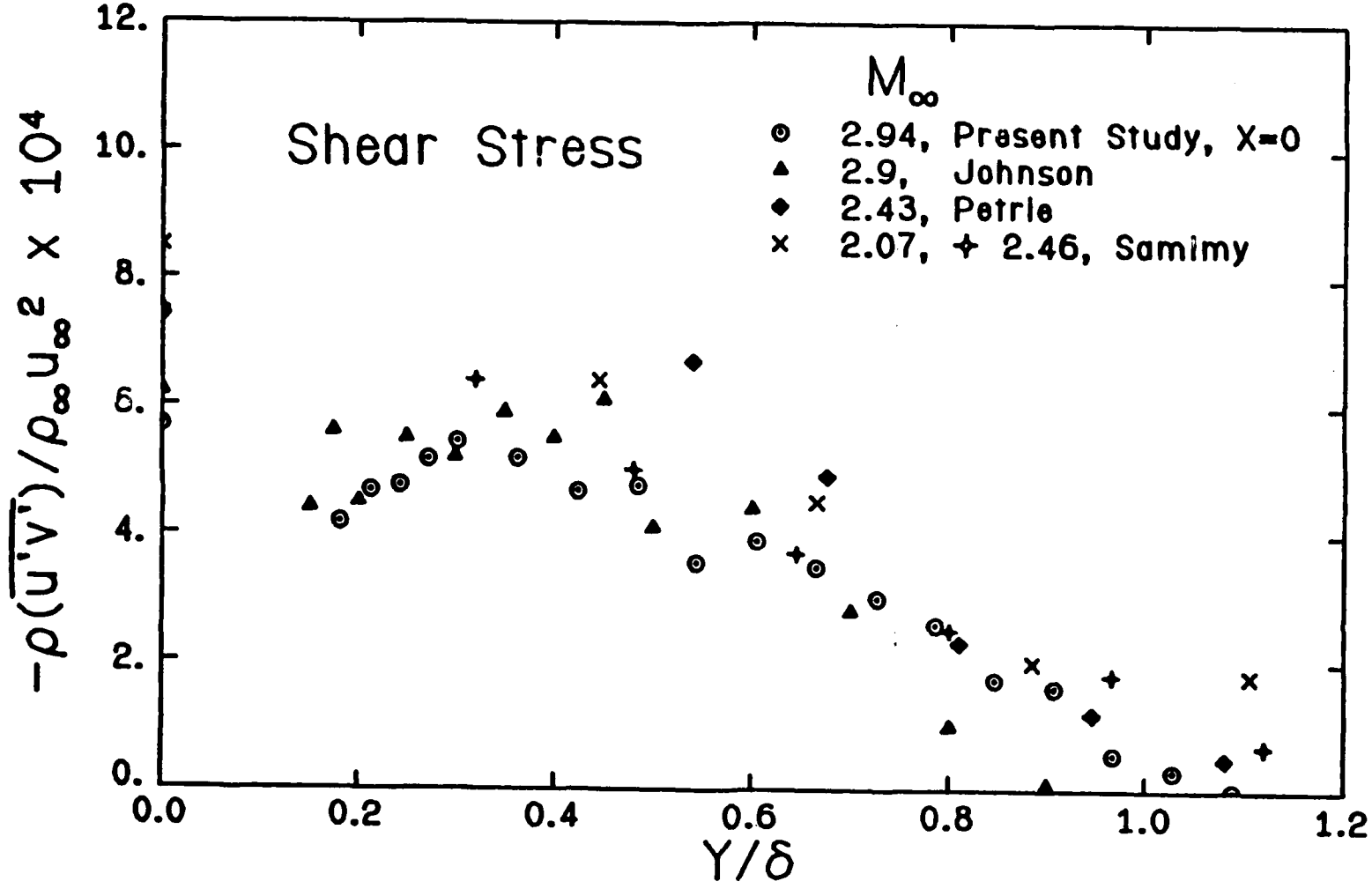

Figure 5 Undisturbed boundary layer shear stress measurements

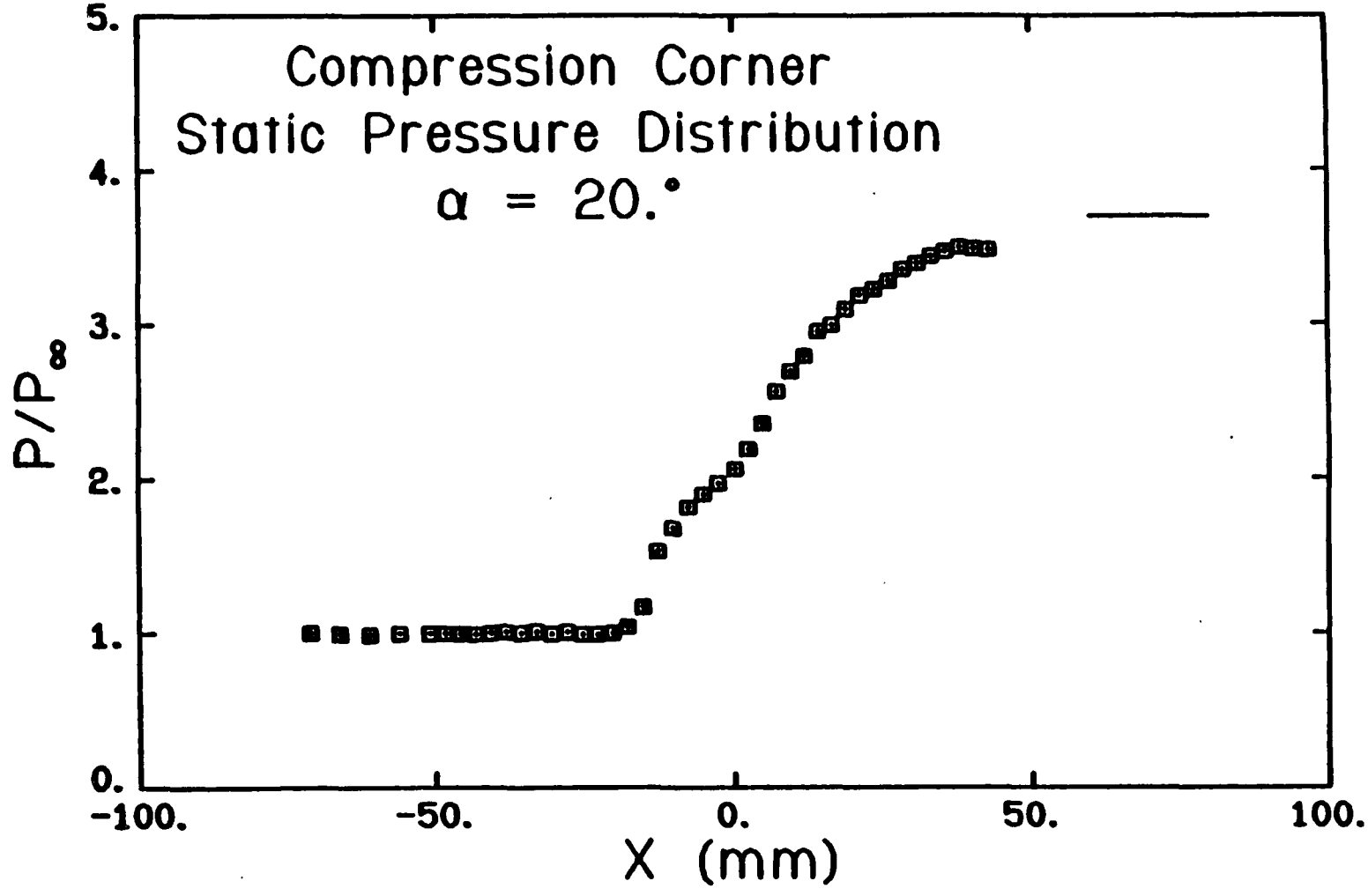

Figure 6 Mean surface static pressure distribution

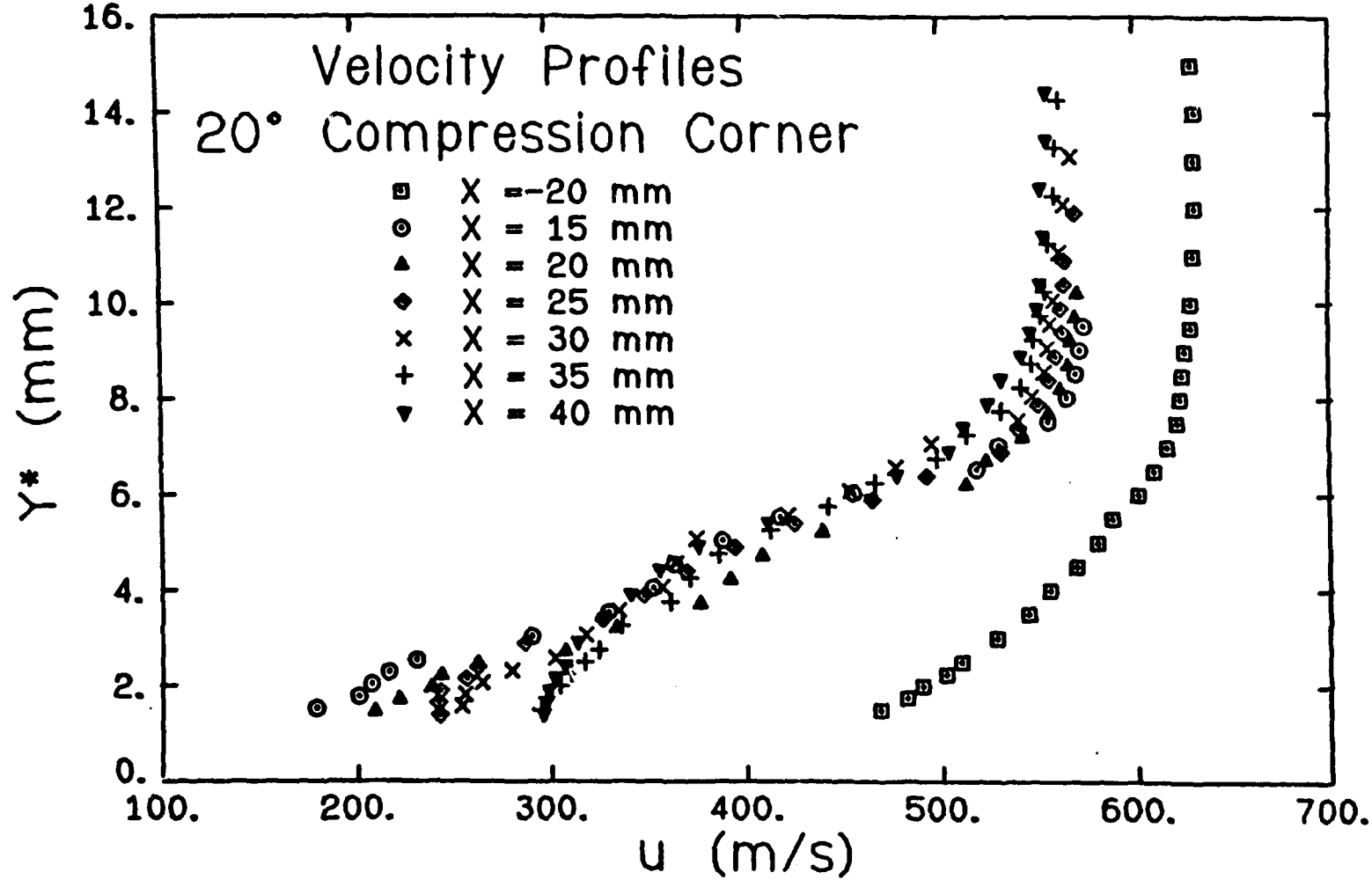

Figure 7 Mean streamwise velocity profiles

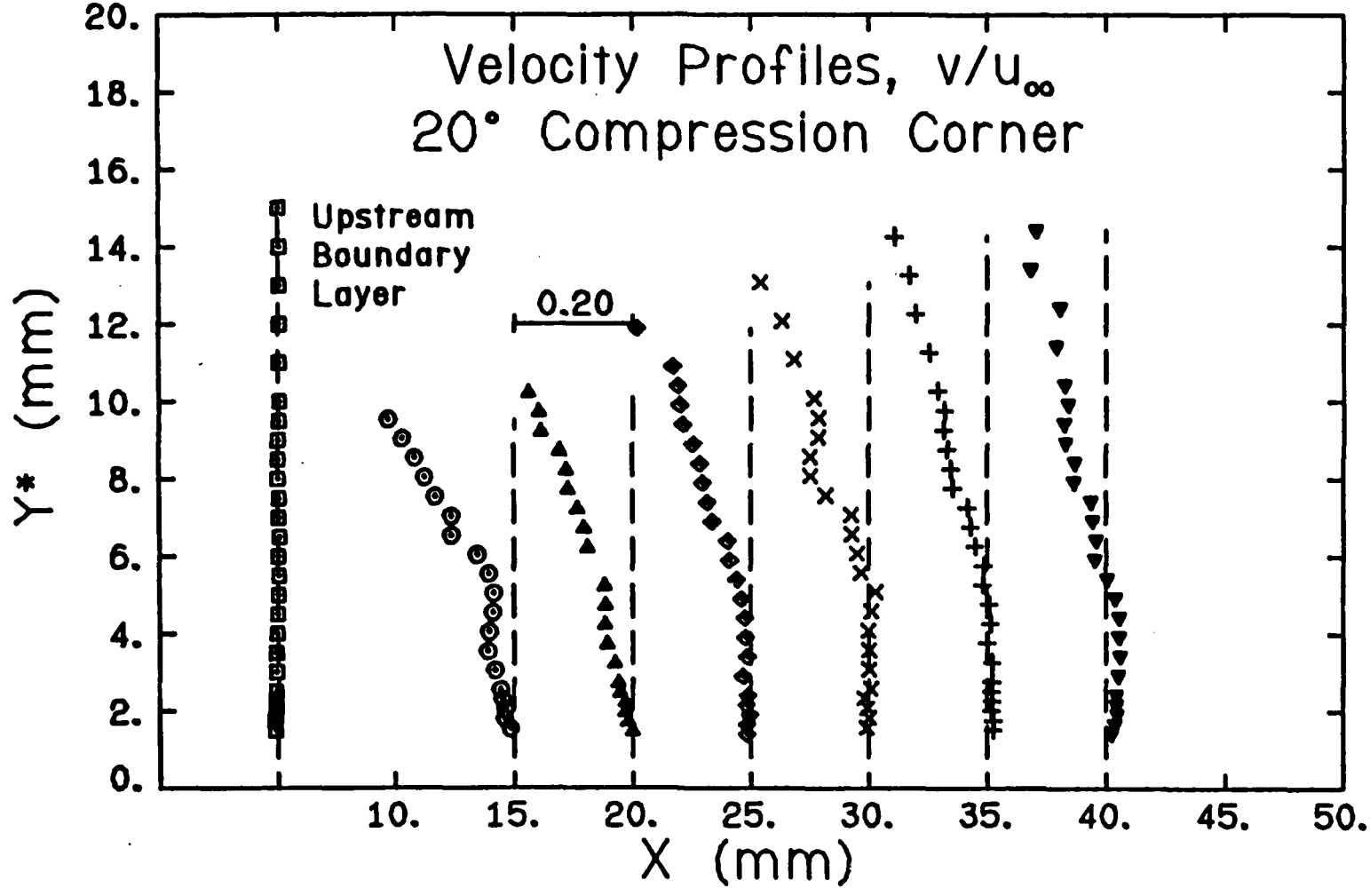

Figure 8 Mean vertical velocity profiles

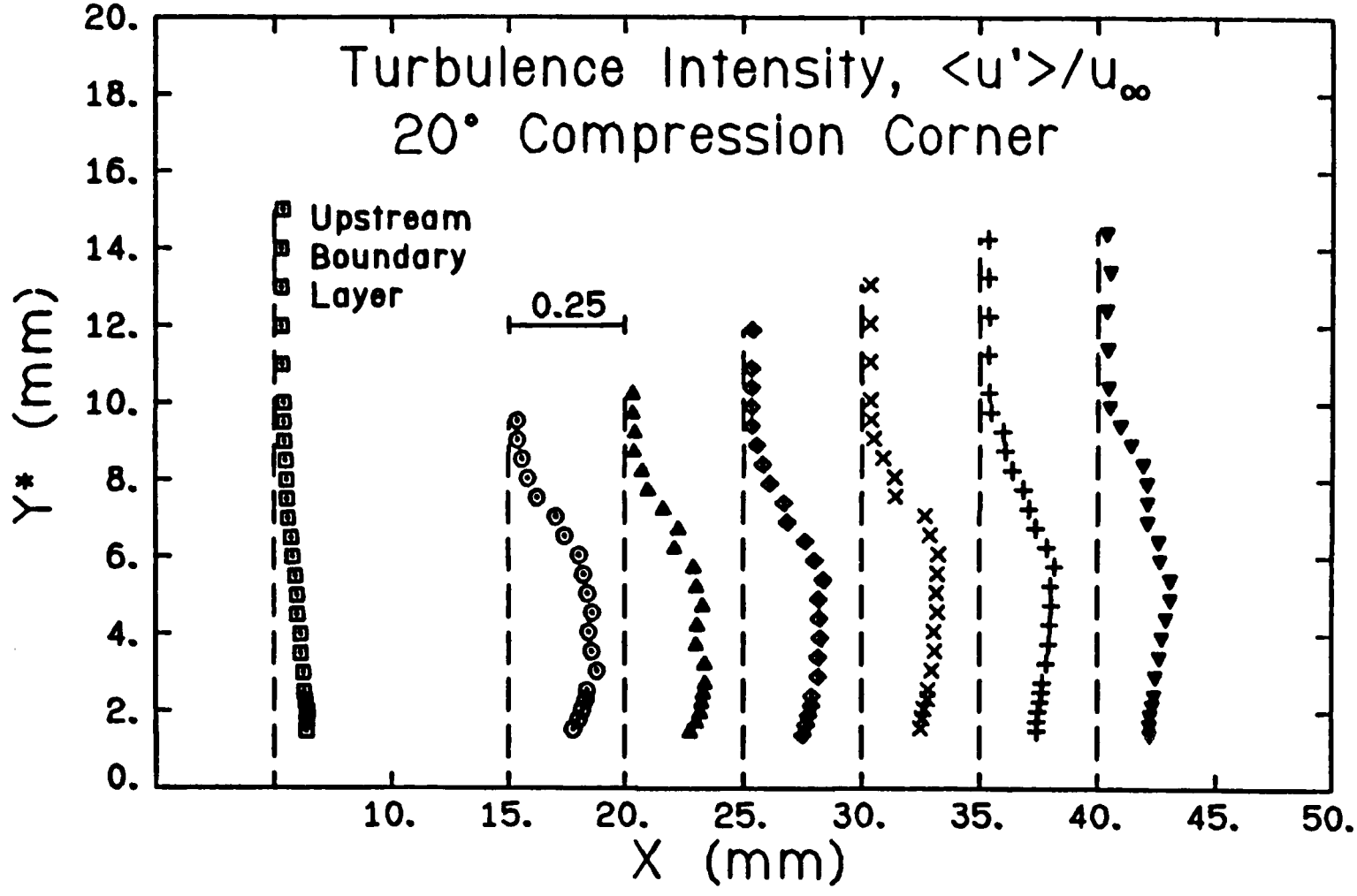

Figure 9 Streamwise turbulence intensity profiles

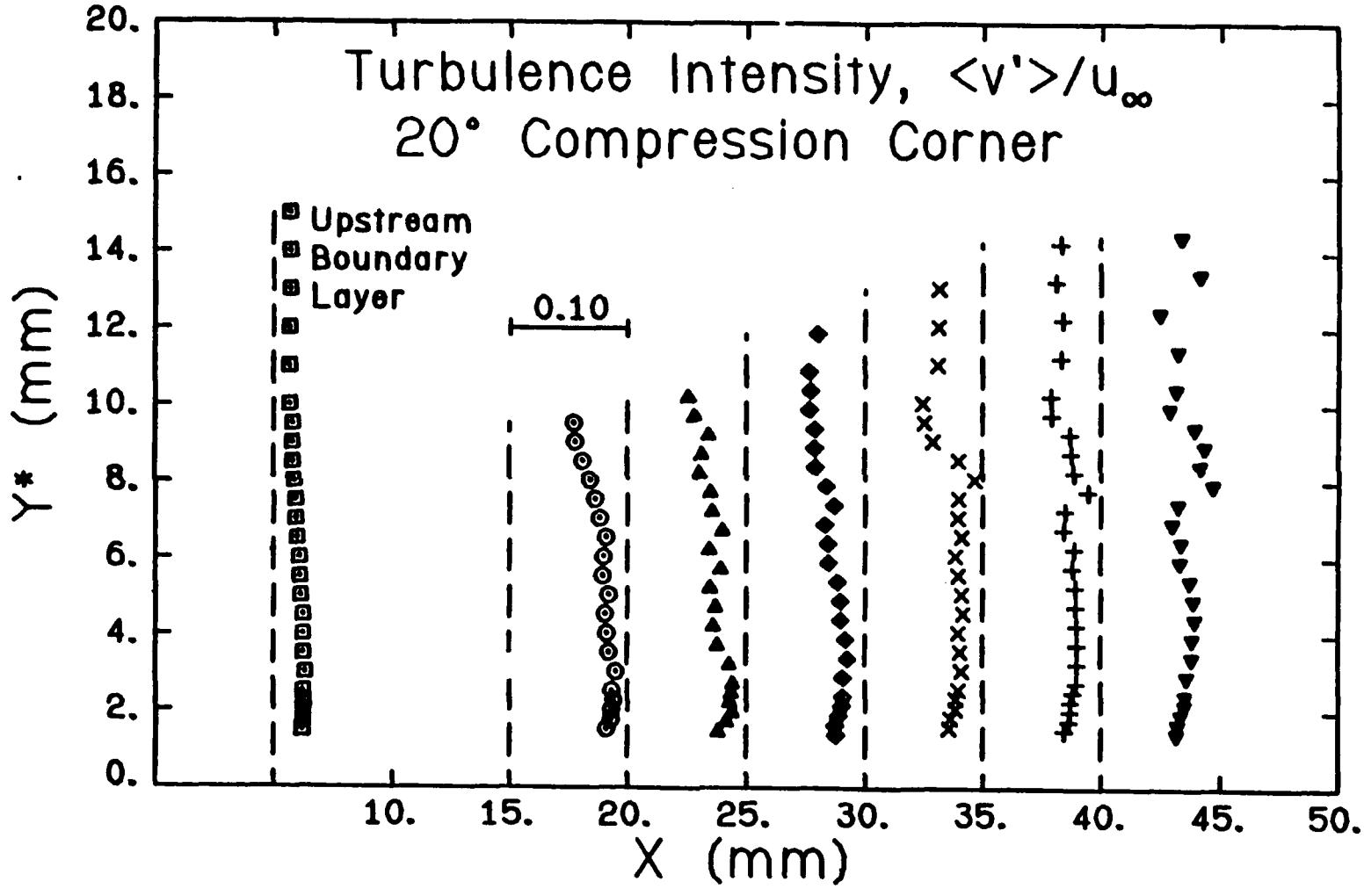

Figure 10 Vertical turbulence intensity profiles

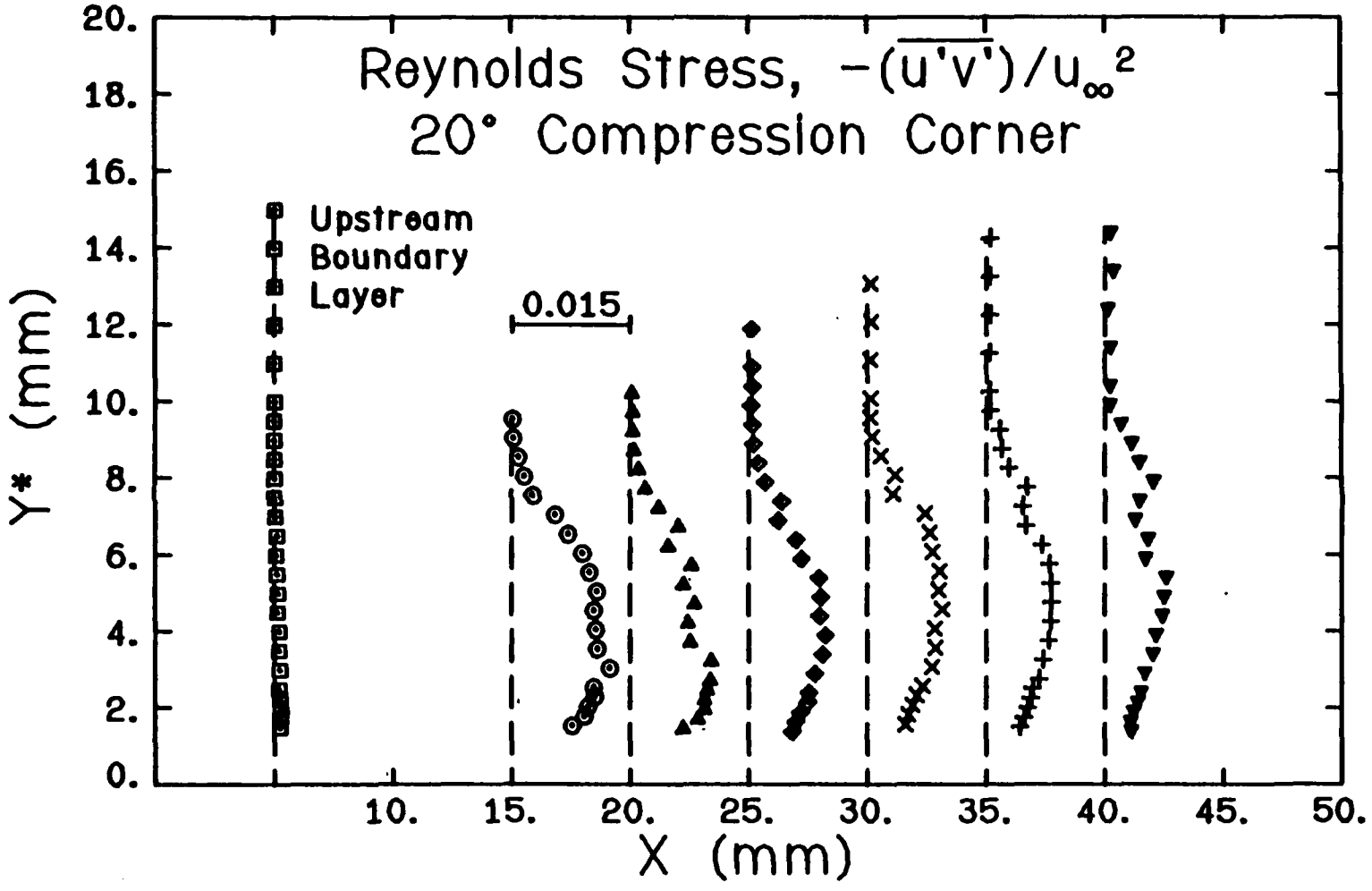

Figure 11 Reynolds stress profiles

SECTION B.12

AN EXPERIMENTAL INVESTIGATION OF THE TWO-STREAM, SUPERSONIC, NEAR-WAKE FLOWFIELD BEHIND A FINITE-THICKNESS BASE

Ph.D. Thesis

Department of Mechanical and Industrial Engineering

University of Illinois at Urbana-Champaign

December 1989

by

V. A. Amatucci

AN EXPERIMENTAL INVESTIGATION OF THE TWO-STREAM, SUPERSONIC, NEAR-WAKE FLOWFIELD BEHIND A FINITE-THICKNESS BASE

Vincent A. Amatucci, Ph.D. Thesis
Department of Mechanical and Industrial Engineering
University of Illinois at Urbana-Champaign

ABSTRACT

The complex interaction region generated by the separation of two supersonic streams past a finite-thickness base occurs frequently in high-speed flight and is characteristic of the aft-end flowfield of a powered missile in the supersonic flight regime. In an effort to examine the fundamental fluid dynamic mechanisms and interactions ongoing in this near-wake region, an experimental investigation was conducted to obtain mean and turbulence data by making measurements in a small-scale wind tunnel. The two-dimensional test section produced a Mach 2.56 upper stream and a Mach 2.05 lower stream which both undergo geometric separation past a finite-thickness splitter plate and experience strong expansion and shear layer mixing processes before eventual recompression, reattachment, and redevelopment of the wake flow. This flowfield immediately behind the base in the near-wake is characterized by strong velocity and density gradients, energetic viscous interactions, high turbulence intensity levels, and a relatively energetic recirculation region with large-magnitude reverse flow.

The experimental data for the near-wake interaction flowfield was obtained using Schlieren photographs, stagnation and sidewall static pressure measurements, and laser Doppler velocimeter (LDV) measurements. The primary tool was a two-color, two-component LDV system which provided instantaneous velocity data from which mean and turbulence quantities were extracted. The qualitative and quantitative information for this flowfield was analyzed in a component style approach consistent with the Chapman-Korst model of the near-wake region. The strong dependence of the component model on empirical coefficients defines a need for detailed experimental data, while more recent computational efforts to predict the near-wake flowfield similarly require turbulence data for validation and improvement of turbulence modeling.

The dynamic interactions in the near-wake of the finite-thickness base after separation of the Mach 2.56 and Mach 2.05 streams correctly modeled the flowfield at the aft-end of a powered missile in supersonic flight. The flow regions included strong Prandtl-Meyer expansions, shear layer mixing and recompression, recirculation, and downstream wake redevelopment. The shear layer mixing regions were characterized by constant-pressure mixing along the initial two-thirds of their length, by an evolution of velocity profiles from truncated forms of the boundary layer shapes to more wake-like profiles farther downstream, and by relatively high levels of turbulence as compared to the levels existing in the turbulent boundary layers prior to separation. While relative self-similarity of the mean velocity data was achieved, the turbulence field exhibited evidence of progression toward self-similarity but did not reach that state before recompression of the shear layers began. The separated flow region was characterized by vigorous recirculation, large negative velocities reaching 23 percent of the Mach 2.56 freestream value, and strong turbulent interaction with the low-velocity regions of both shear layers. Turbulence intensities, kinematic Reynolds stresses, and turbulent triple products were increased greatly in the latter portions of the two shear layers and in the recompression/reattachment region, seeming to indicate the presence of large-scale turbulent structures. The turbulence field in the region of reattachment was strongly anisotropic, and the transverse diffusion of turbulence energy by exchange of the kinematic Reynolds stress for turbulent kinetic energy seems in agreement with existing correlations. Recovery of the mean velocity field in the redeveloping wake flow occurred relatively quickly, while the turbulence field remained perturbed to the furthest streamwise location in the range of measurements. The data obtained for the two-stream interaction flowfield should prove quite valuable for use in validation and improvement of computational schemes aimed at prediction of the mean and turbulence profiles for the near-wake behind a finite-thickness base.